



HAL
open science

Development of an innovative permeable and cool pavement solution

Khaled Seifeddine

► **To cite this version:**

Khaled Seifeddine. Development of an innovative permeable and cool pavement solution. Civil Engineering. Université Clermont Auvergne, 2022. English. NNT : 2022UCFAC068 . tel-04098444

HAL Id: tel-04098444

<https://theses.hal.science/tel-04098444v1>

Submitted on 16 May 2023

HAL is a multi-disciplinary open access archive for the deposit and dissemination of scientific research documents, whether they are published or not. The documents may come from teaching and research institutions in France or abroad, or from public or private research centers.

L'archive ouverte pluridisciplinaire **HAL**, est destinée au dépôt et à la diffusion de documents scientifiques de niveau recherche, publiés ou non, émanant des établissements d'enseignement et de recherche français ou étrangers, des laboratoires publics ou privés.

Université Clermont Auvergne

École Doctorale

SCIENCES POUR L'INGÉNIEUR DE CLERMONT-FERRAND

THÈSE

Présentée par

Khaled SEIFEDDINE

Pour obtenir le grade de

DOCTEUR D'UNIVERSITÉ

Spécialité : Génie Civil - Matériaux

Titre de la thèse :

**Mise au point d'une solution innovante de revêtements
drainants et à effet rafraichissant**

Thèse dirigée par :

Prof. Amziane Sofiane & Prof. Toussaint Evelyne

Soutenu publiquement le 30 septembre 2022 devant le jury composé de :

M. Petit Christophe, professeur, Université de Limoge (rapporteur)

M. Bernardin Frederic, MCF HDR, Cerema (rapporteur)

Mme. Ghorbel Elhem, Professeure, Université de Cergy-Pontoise (examinatrice)

M. Fabbri Antonin, Directeur de recherche, ENTPE (examinateur)

M. Amziane Sofiane, Professeur, Université Clermont Auvergne INP (directeur de thèse)

Mme. Toussaint Evelyne, Professeure, Université Clermont Auvergne INP (directrice de thèse)

REMERCIEMENTS

Tout d'abord je remercie la Région AURA Auvergne Rhône-Alpes pour le soutien financier du projet de recherche.

J'adresse mes sincères remerciements à mon directeur de thèse Monsieur Sofiane AMZIANE, qui m'a transmis sa passion pour ce sujet et a permis l'aboutissement heureux de ce travail. Je le remercie pour ses immenses compétences scientifiques, ses conseils « en or » et ses corrections qui ont beaucoup apporté à mon travail. Sans lui, cette thèse n'aurait jamais vu le jour. J'exprime toute ma gratitude à Madame Evelyne TOUSSAINT, qui, en tant que Directrice de thèse, s'est toujours montrée à l'écoute et disponible au cours de la réalisation de la thèse. Son œil critique m'a été très précieux pour structurer le travail pendant ma thèse et pour améliorer la qualité de rédaction de ce mémoire. Je remercie également mes directeurs pour leur disponibilité tout au long de cette période. Je n'oublie pas leurs encouragements permanents et leur grand professionnalisme ainsi que leurs consignes sur le plan professionnel et personnel.

Je souhaite exprimer mes remerciements les plus respectueux aux membres du Jury qui ont accepté d'évaluer mon travail de thèse. Je voudrais remercier M. Frederic BERNARDIN et M. Christophe PETIT, de m'avoir fait l'honneur d'accepter de juger les travaux de ce mémoire. Je tiens également à remercier et M. Antonin FABBRI d'avoir accepté d'examiner ce travail. Je n'oublie pas de remercier Mme. Elhem GHORBEL d'avoir accepté d'examiner ce travail et d'avoir présidé le jury de cette thèse.

Je remercie également tous les enseignants du département Génie Civil de Polytech de m'avoir accordé leur confiance et l'opportunité de connaître mes premières expériences d'enseignement pendant ces trois ans.

Non, je ne les ai pas oubliés, mes compagnons de galère ! Durant ces trois années de thèse, j'ai été bien entourée. Je n'oublierai jamais la salle des doctorants qui a formé une vraie famille internationale de doctorants. Mes remerciements les plus sincères à mes amis. La thèse vous fait prendre conscience à quel point il est important et primordial de les avoir dans votre vie. Ils sont là pour vous faire rire, vous faire décompresser ! Merci à mon amie d'enfance, Rime, qui a été à mes côtés toutes ces années. Tu étais plus qu'une amie pour moi, tu étais une sœur. Hisham, l'ami fidèle, loyal, aimant, je ne t'oublierai jamais même si tu es dans un autre pays. Caroline qui était toujours à mes côtés quand j'avais besoin d'elle. Phan, mon cher ami avec qui je bois le café tous les matins. Mouhammed amine, merci pour tous les conseils que tu m'as donnés tu étais un grand frère pour moi surtout quand je suis stressé. Arthur mon cher ami cultivé qui aide tout le monde sans hésitation. Merci à Bilal, Arnauld, Martian, Esther, Fengdong et Arnoul pour tous ces moments agréables. Je n'oublierai jamais tous les moments que j'ai partagés avec vous. Vous avez été d'une aide si précieuse durant cette aventure. Vous étiez à mes côtés dans les plus merveilleux.

Je souhaite également m'adresser à ma famille. Pour ma mère Sanaa : ton admiration m'a donné tant de courage. Pour mon père Jamal : ta fierté me poussait au-delà de mes retranchements. Merci beaucoup, c'est grâce à vous que je suis là où je suis aujourd'hui. Vous m'avez porté à bout de bras pour être l'homme que je suis aujourd'hui, je vous en serai éternellement reconnaissant. Pour mon frère mohammed : tu es un homme doux et attentionné qui m'a donné beaucoup de forces durant cette aventure ! Je remercie aussi mon frère mahmoud et mes sœurs Ihsan et Zaynab qui n'ont cessé d'être derrière moi et de me soutenir.

RESUME

Les chaussées imperméables conventionnelles ont remplacé les sols naturels en raison de la croissance rapide de l'urbanisation, ce qui entraîne des irrégularités dans l'écosystème naturel et l'évaporation de l'eau et rend la gestion des eaux pluviales compliquée. De plus, ces chaussées ont généralement une surface sombre et une grande inertie thermique. Pendant l'été, elles ont tendance à absorber et à stocker le rayonnement solaire et empêchent le refroidissement par évaporation. Ces chaussées engendrent divers problèmes, notamment les îlots de chaleur urbains et les inondations. Le béton drainant à base de ciment (BD) est un type particulier de béton dont la structure des pores est fortement interconnectée. La structure poreuse et l'interconnexion des pores permettent un drainage efficace de l'eau à travers sa matrice et peuvent offrir des solutions de drainage durables. Le remplacement des chaussées conventionnelles par des chaussées en BD présente donc un grand potentiel pour la modernisation et la durabilité environnementale, et contribuent simultanément à limiter les inondations urbaines et à atténuer les îlots de chaleur urbains via le refroidissement par évaporation.

L'objectif principal de cette thèse est d'étudier le comportement thermique du BD, de mesurer et de quantifier son pouvoir rafraichissant afin de réduire les effets d'îlots de chaleurs urbains. La thèse est constituée de deux parties dont la première est composée de 3 articles de revue qui visent à examiner de manière synthétique les avancées récentes de la recherche concernant les propriétés mécaniques, hydrauliques du BD ainsi que les propriétés thermiques des chaussées rafraichissantes. Des modèles ont été établis afin de prédire avec précision les propriétés fondamentales du BD telles que la densité, la perméabilité et la résistance mécanique. La deuxième partie est composée également de 3 articles qui visent à comprendre les facteurs qui influent sur le taux d'évaporation des revêtements perméables et d'étudier le comportement thermique du BD en condition sèche et humide via une étude analytique et expérimentale. Un dispositif expérimental innovant a été conçu et mis en place au laboratoire. Ce dispositif est équipé de plusieurs appareils permettant d'étudier le comportement thermique des revêtements perméables en condition sèche et humide dans des conditions climatiques contrôlées en laboratoire.

Mots-clés : îlots de chaleur urbains, béton drainant, porosité, perméabilité, taux d'évaporation, effet rafraichissant.

ABSTRACT

Conventional impervious pavements have replaced natural soils due to the rapid growth of urbanization, which causes irregularities in the natural ecosystem and water evaporation and makes stormwater management complicated. In addition, these pavements usually have a dark surface and high thermal inertia. During the summer, they tend to absorb and store solar radiation and cancel out cooling by evaporation. These pavements cause a variety of urban problems, including urban heat islands and urban flooding. Pervious cement-based concrete (PC) is a special type of concrete with a highly interconnected pore structure. The porous structure and interconnectedness of the pores allow for efficient drainage of water through its matrix and can provide sustainable drainage solutions. The replacement of conventional pavements with PC pavements therefore has great potential for modernization and environmental sustainability, and simultaneously contributes to mitigating urban flooding and urban heat islands via evaporative cooling.

The main objective of this thesis is to study the thermal behavior of PC and to measure and quantify its cooling performance in order to reduce urban heat island effects. The thesis is separated in two parts, the first one is composed of 3 review papers which aim to examine in a synthetic way the recent research advances concerning the mechanical, hydraulic and thermal properties of cool pavements. Models have been established to accurately predict the fundamental properties of PC such as density, permeability and mechanical strength. The second part is also composed of 3 papers that aim to understand the factors that influence the evaporation rate of permeable pavements and to study the thermal behavior of PC in dry and wet conditions via an analytical and experimental study. An innovative experimental bench has been designed and set up at Polytech Clermont-Ferrand. This bench is equipped with several devices allowing to study the thermal behavior of permeable pavements in dry and wet conditions under controlled climatic conditions in laboratory.

Keywords: urban heat islands, pervious concrete, porosity, permeability, evaporation rate, cooling effect.

Table of contents

Part 1. State of the art - Bibliographic synthesis

Chapter I Review on thermal behavior of cool pavements

Highlights	16
Keywords.....	16
1. Introduction.....	16
2. Urban heat islands	17
2.1. Definition of Urban heat islands	17
2.2. Impact of urban heat islands	18
2.3. Causes of urban heat islands	18
3. Cool pavements to mitigate UHIs.....	19
3.1. Definition of cool pavements.....	19
3.2. Reflective pavements	20
3.2.1. Definition and method of measuring albedo	20
3.2.2. Reflective asphalt and concrete pavements.....	20
3.2.3. Aging of reflective pavements	24
3.3. Evaporative pavements.....	25
3.3.1. Porous vegetated pavers.....	26
3.3.2. Impermeable pavers with permeable joints.....	26
3.3.3. Permeable pavements	27
3.3.4. Water-retaining pavements	32
3.4. Pavements that modify their heat storage	35
3.4.1. Cool pavements containing phase-change materials	35
3.4.2 High-conductivity pavements	37
3.4.3. Pavements with energy harvesting systems	38
4. Overview and discussion.....	40
5. Conclusion	42
Acknowledgements	43
Bibliography.....	43

Chapter II State of the art on the mechanical properties of pervious concrete

Highlights	55
Keywords.....	55
1. Introduction.....	55
2. Pervious concrete and pervious paving slabs.....	56
2.1. Composition and method of formulation.....	56
2.2. Porosity of pervious concrete.....	60
2.3. Permeability of pervious concrete.....	65
3. Mechanical characteristics	66
3.1. Compressive strength of natural aggregate-based pervious concrete.....	66
3.1.1. Relationship between porosity and compressive strength.....	66
3.1.2. Influence of aggregate size.....	67
3.1.3. Influence of the water/cement ratio	69
3.1.4. Influence of thickness of cement paste	69
3.1.5. Influence of the aggregate/cement ratio (A/C).....	70
3.1.6. Empirical equations for predicting compressive strength	72
3.2. Tensile strength.....	75
3.3. Simple flexural strength.....	77
Conclusions and avenues for future research.....	78
Bibliography.....	80
 Chapter III State of the art on the hydraulic properties of pervious concrete	
Highlights:	90
Keywords:	90
1. Introduction.....	90
2. Composition and formulation method for pervious concrete	91
2.1. Cementitious materials or binder	91
2.2. Coarse Aggregates	92
2.3. Fine Aggregates	92
2.4. Water and additives.....	92
2.5. Fibers.....	92
3. Characterization of physical properties.....	93
4. Hydraulic characteristics of pervious concrete.....	96
4.1. Methods of measuring permeability in the laboratory.....	96
4.2. Comparison of laboratory permeability measurement methods.....	98
4.3. Field permeability measurement methods	98

5. Factors influencing the permeability of pervious concrete	100
5.1. Relationship between open porosity and permeability	100
5.2. Influence of aggregate size and pore size on permeability	102
5.3. Influence of aggregate shape and water/cement ratio on permeability	103
5.4. Influence of cement paste thickness on permeability	105
5.5. Influence of the aggregate/cement ratio on permeability	105
6. Permeability prediction models	107
6.1. Empirical models for permeability prediction	107
6.2. Modified Kozeny-Carman model.....	107
6.3. Modified Katz-Thompson model.....	109
6.4. Comparison between different permeability prediction models	111
Conclusions	112
Bibliography.....	113

Part 2. Thermal behaviour of permeable pavements

Chapter IV Experimental investigation of physical characteristics to improve the cooling effect of permeable pavements

Highlights	124
Keywords.....	124
1. Introduction.....	124
2. Experimental study	125
2.1. Materials	125
2.2. Dosages and sample preparation	129
2.3. Methodologies and measuring devices	129
2.3.1. Open porosity measurement.....	129
2.3.2. Albedo measurement	130
2.3.3. Permeability measurement	131
2.3.4. Thermal conductivity measurement	131
2.3.5. Capillary rise height measurement	131
2.3.6. Bulk density measurement	131
2.3.7. Water-absorption coefficient measurement	131
2.3.8. Evaporation rate measurement	132
3. Results and discussion.....	134
3.1. Meteorological data evolution over time	134
3.2. Evolution of the amount of water evaporated during the experiment	136

3.3. Study of the cooling effect of permeable pavements based on recycled tire aggregates and pozzolan	138
3.3.1. Evolution of surface temperature	138
3.3.2. Evolution of evaporation rate and latent heat flux.....	139
3.4. Study of the cooling effect of aggregate porous pavements: sand and natural gravel.....	143
3.4.1. Evolution of surface temperature	143
3.4.2. Evolution of evaporation rate and latent heat flux.....	144
3.4.3. The influence of capillary rise.....	145
3.5. Study of the cooling effect of pozzolan porous pavements	147
3.5.1. Evolution of surface temperature	147
3.5.2. Evolution of evaporation rate and latent heat flux.....	148
3.6. Effect of open porosity and permeability on evaporation rate	149
3.7. Effect of water depth in samples on evaporation rate.....	150
4. Conclusion and prospects	152
Acknowledgements	153
Appendix A. Albedo measurement method	153
Bibliography	155
 Chapter V Thermal behavior of pervious concrete in dry conditions	
Highlights	160
Keywords.....	160
1. Introduction.....	160
2. Energy balance at the pavement surface – Analytical method and physical concepts	161
3. Materials and methods.....	165
3.1. Dosage and sample preparation	165
ASTM C29 [53].....	166
3.2. Porosity of pervious concrete.....	167
3.3. Mechanical and hydraulic properties.....	168
3.3.1. Compressive strength.....	168
3.3.2. Permeability	168
3.4. Thermophysical properties	168
3.4.1. Albedo measurement	168
3.4.2. Emissivity measurement	169
3.4.3. Thermal conductivity measurement	170
4. General presentation of the experimental bench.....	170

4.1. Two-compartment bin	170
4.2. Infrared lamps/heating	171
4.3. Temperature sensors	171
4.3.1. Thermocouples in bins	171
4.3.2. Surface temperature measurement	171
4.4. Pyranometer and pyrgeometer	171
4.5. Data acquisition system	171
4.6. Experimental setup	172
5. Results and analysis	172
5.1. Prediction of surface temperature of pervious concrete and ordinary concrete	172
5.2. Experimental validation	175
6. Discussion	176
6.1. Distribution of energy fluxes	176
6.2. Sensitivity analysis	178
Appendix A. Experimental bench	184
Appendix B. Experimental setup.....	186
 Chapter VI Thermal behaviour of pervious concrete in wet conditions	
Highlights	192
Keywords.....	192
1 Introduction	192
2. Materials and methods.....	193
2.1. Materials	193
2.2. Experimental methods	194
2.2.1. Dosage and sample preparation.....	194
2.2.2. Porosity measurement.....	195
2.2.3. Strength and permeability tests	196
2.2.4. Tests to determine thermophysical properties	196
2.2.5. Water absorption test	197
2.2.6. Experimental setup to study the thermal behavior of pervious concrete	198
3. Results and discussions	200
3.1. Physical properties	200
3.2. Water-absorption properties	202
3.3. Thermal behavior of PC pavements in dry conditions	204
3.4. Thermal behavior of PC pavements in wet conditions	205
3.4.1. Variation in albedo and evaporation rate	205

3.4.2. Variation in surface temperature	207
3.4.3. Energy distribution	209
4. Conclusion	210
Acknowledgements	211
Appendix A. Experimental bench	212

INTRODUCTION GÉNÉRALE

L'urbanisation continue en raison de la croissance de la population et du développement socio-économique joue un rôle essentiel dans le changement climatique et environnemental mondial. On estime que les zones urbaines sont responsables d'environ 70 % des émissions mondiales de carbone [1]. Parallèlement, le processus d'urbanisation a également donné lieu à l'effet d'îlot de chaleur urbain (ICU), un phénomène selon lequel les zones urbaines sont souvent plus chaudes que leur environnement rural, en particulier pendant les saisons chaudes [2].

L'effet d'îlot thermique urbain a été reconnu pour la première fois par le météorologue britannique Luke Howard au début du 19e siècle [3]. Ce phénomène est causé par de nombreux facteurs, dont les plus importants sont l'utilisation de matériaux de construction, la géométrie complexe de l'environnement urbain, la réduction de la couverture végétale et les émissions de chaleur anthropiques [4]–[6]. En particulier, les chaussées conventionnelles imperméables denses et à albédo relativement faible absorbent une grande quantité de rayonnement solaire incident et peuvent être plus chaudes que la végétation naturelle, à la fois durant la journée et la nuit. L'effet d'ICU a des impacts significatifs sur la consommation d'énergie des bâtiments, la qualité de l'air, la consommation d'eau des habitations et les émissions de gaz à effet de serre pendant les saisons chaudes, comme le soulignent de nombreuses études [4], [7]–[10]. De plus, la température élevée due à l'ICU expose les habitants des villes à un risque plus élevé de maladies et de décès liés à la chaleur, en particulier pendant les vagues de chaleur extrême [11]–[13]. Pour rendre les villes plus habitables, avec une meilleure qualité environnementale et des modes de consommation d'énergie durables, il est indispensable de faire face à ces effets négatifs par des stratégies d'atténuation de l'ICU.

Au cours des dernières décennies, des efforts de recherche ont été consacrés au développement et à l'évaluation de diverses stratégies d'atténuation de l'ICU par le biais de mesures, de techniques de télédétection et de simulations numériques. Les stratégies d'atténuation de l'ICU les plus largement étudiées comprennent l'infrastructure verte (par ex, les arbres et l'herbe) [14]–[16], les toitures rafraîchissantes [17]–[19], les stratégies liées aux chaussées [20]–[23], les stratégies liées à l'eau (irrigation) [24]–[26], et les conceptions de la morphologie urbaine et de la géométrie des bâtiments [27]–[29]. Les stratégies d'atténuation de l'ICU liées aux chaussées sont souvent appelées chaussées rafraîchissantes [20], [30]. Ces chaussées présentent généralement une température de surface inférieure à celle des chaussées conventionnelles telles que l'asphalte imperméable [31]. Comme les chaussées constituent 30 à 45 % de la surface totale des villes [32], l'utilisation de chaussées rafraîchissantes pour atténuer les ICU est une stratégie intéressante dans le monde actuel. Il existe plusieurs types de chaussées rafraîchissantes telles que les chaussées réfléchissantes [33], [34], les chaussées modifiant le stockage de la chaleur [35]–[37] et les chaussées perméables évaporatives [38], [39].

Le béton drainant à base de ciment fait partie des chaussées perméables les plus utilisées, c'est un type particulier de béton qui contient pas ou peu de sable [40]. En plus de sa contribution à l'atténuation des effets des îlots de chaleur urbains en tant que chaussée évaporative, il répond également à d'autres problématiques telles que la gestion des eaux pluviales. Le béton drainant présente une porosité élevée par rapport au béton imperméable. Ses avantages

environnementaux comprennent : le contrôle du ruissellement des eaux pluviales [41], l'amélioration de la qualité de l'eau [42], [43], la recharge des nappes phréatiques et la réduction du bruit acoustique des routes [44], [45].

L'objectif principal de cette thèse est d'étudier le comportement thermique du béton drainant et d'identifier les différents facteurs qui influent sa température de surface en condition sèche et humide. Un banc expérimental innovant a été conçu pour étudier le comportement thermique du béton drainant dans des conditions climatiques contrôlées en laboratoire. Il est équipé par plusieurs appareils qui permettent d'établir un bilan énergétique complet d'une chaussée. Ce banc a permis aussi de valider les résultats analytiques.

Organisation du manuscrit

Le manuscrit est organisé en une succession de 6 chapitres. Chaque chapitre est un article qui a été soumis ou publié dans une revue internationale de rang A. Ce manuscrit est composé de deux parties organisées de la manière suivante :

La première partie est composée de 3 chapitres qui constituent une étude bibliographique sur le comportement mécanique, hydraulique et thermique du béton drainant :

- Chapitre 1 « Review on thermal behavior of cool pavements » : L'objectif de cette étude est d'examiner de manière critique les études disponibles sur la performance de refroidissement de plusieurs types de chaussées rafraichissantes, afin de comprendre leurs caractéristiques, leur comportement thermique et leur efficacité dans l'atténuation des effets d'îlots de chaleur urbains. L'accent a été mis sur les technologies récentes dans le domaine des chaussées rafraichissantes. L'effet de refroidissement de ces types de chaussées a été analysé et comparé, et les différents facteurs influençant cet effet de refroidissement ont été identifiés. Des pistes de recherches futures ont été proposées.
- Chapitre 2 « State of the art on the mechanical properties of pervious concrete » : l'objectif de cette étude est d'examiner de manière approfondie les études disponibles sur les propriétés mécaniques du béton drainant. Elle vise à présenter la composition et la méthode de formulation du béton drainant, à identifier les différents facteurs influençant la porosité et à établir une relation entre la porosité et la densité et entre la porosité et la résistance à la compression du béton drainant à base de ciment et de granulats naturels résultant de divers travaux de recherche. Des modèles permettant de prédire la résistance à la flexion et à la traction du béton drainant ont aussi été établis
- Chapitre 3 « State of the art on the hydraulic properties of pervious concrete » : l'objectif de cette étude est de faire une analyse critique des études disponibles sur les propriétés hydrauliques du béton drainant. Elle vise à présenter les méthodes de mesure de perméabilité, les facteurs qui influencent les caractéristiques hydrauliques et à établir des modèles permettant de prédire avec précision la perméabilité du béton drainant. Les résultats des modèles ont été comparés aux différentes équations et modèles présents

dans la littérature. Les comparaisons et les analyses des résultats obtenus ont été discutées.

La deuxième partie est composée de 3 chapitres sur l'effet rafraichissant des revêtements perméables :

- Chapitre 4 « Experimental investigation of physical characteristics to improve the cooling effect of permeable pavements » : l'objectif principal de cette étude est de quantifier et de comparer le taux d'évaporation de neuf formulations de chaussées perméables dans des conditions extérieures. Ces formulations se répartissent en deux catégories : les revêtements perméables à base de granulats de pneus recyclés et de pouzzolane locale, et les revêtements poreux à base de granulats. L'objectif est de trouver les facteurs de premier ordre qui influencent le taux d'évaporation, en mettant en évidence l'influence de la porosité ouverte sur l'effet de refroidissement par évaporation. Il est donc indispensable d'étudier le taux d'évaporation de plusieurs types de chaussées perméables ayant des propriétés physiques différentes.
- Chapitre 5 « Thermal behavior of pervious concrete in dry conditions » : l'objectif de cette étude est d'examiner le comportement thermique du béton drainant en vue de réduire sa température de surface en conditions sèches. Cette étude se concentre sur l'influence des propriétés thermophysiques sur la température de surface, afin de concevoir du béton drainant qui peut réduire de façon permanente sa température de surface en conditions sèches. Pour ce faire, la température de surface du béton drainant et du béton ordinaire a été calculée analytiquement, sur la base des lois physiques et du bilan énergétique à la surface de la chaussée. Les résultats analytiques ont été validés expérimentalement à l'aide d'un banc d'essai innovant conçu pour réaliser l'étude dans des conditions climatiques contrôlées en laboratoire. L'influence des facteurs thermo physiques sur la température de surface du béton drainant a été étudiée. La sensibilité de la température de surface aux différents facteurs d'influence a été calculée par une étude de sensibilité.
- Chapitre 6 « Thermal behavior of pervious concrete in wet conditions » : Dans cette étude, le comportement thermique du béton drainant à base de pouzzolane a été comparé à celui du béton drainant conventionnel à base de granulats denses dans des conditions sèches et humides en laboratoire. Il s'agit de la première étude qui examine l'amélioration de l'effet de refroidissement par évaporation du béton drainant en utilisant des agrégats légers à base de pouzzolane. Ces agrégats sont caractérisés par un coefficient d'absorption d'eau élevé et pourront améliorer les propriétés d'absorption et l'effet de refroidissement du béton drainant. Les facteurs affectant le taux d'évaporation et l'effet de refroidissement par évaporation ont été étudiés.

Chapter I Review on thermal behavior of cool pavements

Article soumis au journal : Urban Climate



Résumé et objectif

Le terme "îlots de chaleur urbains" (ICU) désigne un phénomène de température élevée localisé dans les zones urbaines par rapport aux zones rurales environnantes. L'augmentation de la population urbaine dans le monde entier a entraîné une augmentation significative des activités anthropiques et le remplacement de la végétation par des revêtements imperméables qui ont une surface sombre et une forte inertie thermique. Ces chaussées absorbent et stockent le rayonnement solaire, empêchent le refroidissement par évaporation et contribuent au développement des ICU. Comme les chaussées représentent une fraction importante des zones urbaines, l'idée d'utiliser des chaussées rafraîchissantes est une solution intéressante pour réduire les effets des ICU. Cet article offre une synthèse des avancées récentes de la recherche concernant l'utilisation de plusieurs types de chaussées rafraîchissantes (chaussées réfléchissantes, chaussées perméables évaporatives et les chaussées qui changent leur stockage de chaleur) pour atténuer les ICU. Le comportement thermique et les principaux facteurs qui influencent l'effet de refroidissement de ces chaussées ont été analysés. Les performances de refroidissement de ces chaussées ont été comparées entre elles. Les limites et les facteurs qui affectent leur durabilité ont été identifiés.

Il a été déduit de ce travail de synthèse que l'utilisation de revêtements réfléchissants est une stratégie efficace pour atténuer les ICU et améliorer le microclimat. La réflectivité des revêtements traditionnels peut être augmentée par l'application d'un revêtement réfléchissant blanc, d'un revêtement thermochromique ou d'un revêtement rétro réfléchissant, d'un revêtement coloré à haute réflectivité ou d'un liant approprié. L'application de ces techniques doit tenir compte de la rentabilité, du vieillissement et de l'adhérence de la chaussée. Des recherches supplémentaires sont nécessaires pour évaluer l'éblouissement et la pollution lumineuse potentielle. En outre, les performances globales de réflexion de ces techniques doivent être évaluées plus en détail pour garantir le confort thermique et la sécurité de conduite dans les applications pratiques. Cependant, il n'y a pas encore de normes en place pour les performances des revêtements réfléchissants.

Tous les types de chaussées évaporatives : les pavés poreux végétalisés, les pavés imperméables avec joints perméables, le béton drainant, les chaussées en asphalte perméable et les chaussées à structure réservoir, sont capables de réduire leur température de surface pendant le jour et la nuit. La disponibilité de l'eau près de la surface, le temps d'arrosage, le coefficient d'absorption de l'eau, la capacité de rétention de l'eau et la remontée capillaire sont les principaux facteurs

qui influencent les performances de refroidissement par évaporation des chaussées. La disponibilité de l'eau est donc une condition primordiale qui détermine les performances thermiques de ces chaussées. Ces revêtements doivent être arrosés régulièrement pour garantir un effet de refroidissement significatif sur une période prolongée. En conditions sèches, les chaussées perméables peuvent avoir une température de surface plus élevée que les chaussées denses conventionnelles imperméables. Il a été constaté que l'utilisation de chaussées perméables doit être évitée dans les pays où les étés sont secs et où l'arrosage est compliqué à mettre en œuvre.

L'augmentation de la conductivité thermique des chaussées assure une température plus basse pendant la journée, mais conduit à une température plus élevée pendant la nuit lorsque la chaleur stockée est libérée par diffusion. Cette observation peut aggraver le problème des îlots de chaleur urbains nocturnes. Les chaussées qui contiennent des matériaux à changement de phase et les chaussées à récupération d'énergie peuvent améliorer le microclimat urbain. Ils nécessitent un coût initial plus élevé et des procédures de construction plus complexes que les revêtements évaporatifs et réfléchissants. Des recherches supplémentaires sont nécessaires pour améliorer l'efficacité de ces revêtements afin de justifier l'investissement initial élevé.

Des efforts supplémentaires sont nécessaires pour remédier aux limitations liées à l'utilisation des chaussées rafraichissantes, ce qui sera essentiel pour traiter efficacement les impacts négatifs des ICU et promouvoir une utilisation plus durable de l'énergie urbaine.

L'influence de la porosité sur le comportement mécanique et hydraulique des chaussées perméables a été largement étudiée dans la littérature. Les études futures doivent se concentrer sur l'examen de l'effet des caractéristiques des pores sur le comportement thermique des chaussées perméables. Ces études conduiront à la conception de chaussées présentant de bonnes performances mécaniques, hydrauliques et de refroidissement. En outre, il est nécessaire de développer des chaussées qui combinent plusieurs technologies de chaussées rafraichissantes comme, par exemple, une chaussée réfléchissante et perméable, ayant une conductivité thermique élevée afin de maximiser l'effet de refroidissement.

Dans ce chapitre les études disponibles sur les propriétés thermiques du béton drainant ont été examinées afin d'étudier leur performance dans la réduction des effets des îlots de chaleur urbains. Cependant, le béton drainant doit résister aux sollicitations pour remplir ses fonctions. Dans le chapitre suivant, les propriétés physiques et mécaniques du béton drainant ont été étudiées en détail, des modèles de prédiction ont été élaborés pour prédire les propriétés mécaniques (résistance à la compression, à la flexion et à la traction) et les différents facteurs qui influencent ses propriétés ont été identifiés.

Khaled Seifeddine^a, Sofiane Amziane^a, Evelyne Toussaint^a, Salah-Eddine Ouldboukhitine^a

^a Université Clermont Auvergne, CNRS, SIGMA Clermont, Institut Pascal, F-63000 Clermont-Ferrand, France.

Highlights

- A complete review of the different cool pavement technologies was carried out.
- Factors influencing the cooling performance of cool pavements were identified.
- Recent developments to improve the performance of cool pavements were presented.
- Limitations and opportunities for future developments in cool pavements were discussed.

Keywords

Urban heat islands; Heat mitigation strategies; Cool pavements; Thermal properties; Road engineering.

1. Introduction

Climate change has now become a reality, and its impacts are evident in the environment (ecosystems, air quality), human health and the evolution of lifestyles [1]. Global warming will increase in the coming decades due to greenhouse gas emissions and human activities. As human activities are concentrated in urban areas, cities contribute directly to climate change. In 1995, the heatwave that hit Chicago killed between 550 and 800 people [2]. Similarly, the heatwave in Europe in the summer of 2003 contributed to the deaths of about 30,000 people, including 15,000 in France [3]. Another study on the impact of ambient temperature on mortality in the Netherlands [4] shows that each degree above the optimal temperature value leads to a 2.72% increase in mortality.

Along with climate change, a particular phenomenon occurs in cities, known as an urban heat island (UHI), which aggravates the situation [5]–[7]. UHIs observed in cities, causing a further increase in air temperature, will amplify the phenomenon for urban populations [8], [9]. This phenomenon is caused by many factors; the most important include the use of building materials, the complex geometry of the urban environment, anthropogenic heat emissions and the reduction of vegetation cover [10]–[12], and in particular, the use of traditional impermeable pavements (such as asphalt). These pavements absorb a large amount of solar radiation during the day, and since there is no evaporation, the temperature of the ground surface is significantly higher than that of the overlying atmosphere. This high surface temperature then causes a heat exchange between the surface and the atmosphere, resulting in an increase in air temperature in the urban area [13].

In addition, these pavements absorb and store a significant part of the incident solar radiation during the day, owing to the high absorption factor and the high thermal capacity that is characteristic of them. The energy stored in the form of sensible heat is then released during the night, increasing the temperature of the urban air [14], [15]. This heat exchange causes so-called nocturnal UHIs [16]. These pavement materials have also made stormwater management more difficult, and have consequently increased the frequency and severity of floods, and lowered

the level of the water table. This has resulted in a disruption of the natural water cycle [17], a degradation of the natural environment and an increase in localized pollution at discharge points such as wastewater treatment plants [18].

Today, cities around the world are seeking solutions to limit the impacts of global warming and heatwaves during hot weather. Among these solutions, cool pavements have been developed to mitigate urban heat islands; in general, these are pavements designed to limit their surface temperature compared to traditional pavements [19].

There are several techniques that can be used to create a cooler pavement. In the beginning, these were mainly made of white or light-colored pavements and materials [20], [21]. Later on, reflective pavements were developed with various innovative techniques, in order to decrease their surface temperature [22]–[26].

To address the issues of stormwater management and UHIs, several studies have been conducted to evaluate and/or improve the evaporative cooling performance of several types of permeable pavements [27]–[31]. Through evaporation, part of the net radiation received is converted into latent heat, which helps mitigate UHIs.

Other technologies have been developed to combat UHIs, such as pavements that modify their heat storage such as high conductive pavements [14], or pavements that contain phase-change materials [32]–[34], which have proved significantly effective in decreasing the surface temperature of pavements, in order to improve thermal comfort.

The objective of this review is to critically examine the available studies on the cooling performance of several types of pavements, in order to understand their characteristics, their thermal behavior and their effectiveness in UHI mitigation. The focus was on recent technologies in the field of cool pavements. The cooling effect of these types of pavements was analyzed and compared, and the different factors influencing this cooling effect were identified. Avenues for future research were proposed.

2. Urban heat islands

2.1. Definition of Urban heat islands

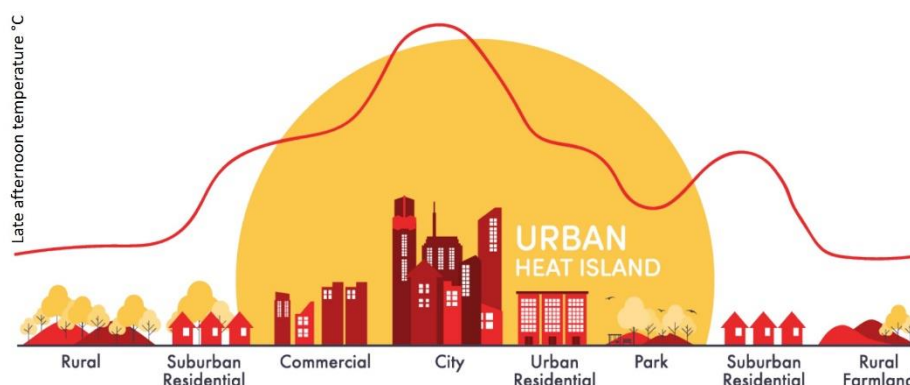


Fig. 1. Variation in air temperature in a cross-section of an urbanized area, illustrating the UHI phenomenon [35].

UHIs are the result of many factors that can be controlled. These include anthropogenic heat, the composition and structure of buildings, and green spaces. Other factors are uncontrollable and result from natural conditions, such as wind speed, season, cloud cover, etc. [36].

2.2. Impact of urban heat islands

UHIs have negative impacts on population health, the economy and the environment [12], [37]. Regarding health, UHIs increase the frequency, intensity and duration of extreme heatwaves, which can lead to public health risks by creating heat stress in humans [11], [38], [39]. Therefore, there is a need to ensure thermal comfort by reducing individual vulnerability. Defining a fixed state of thermal comfort for an entire population is complicated, because it depends on the requirements and feelings of each individual. In Fanger et al.'s [40] analysis of thermal comfort, most people participating in the study mention comfort criteria in a temperature range between 20 and 27°C with a humidity level between 35 and 60%.

UHIs can also impact water and energy consumption. Indeed, they increase the use of potable water through the creation of cool areas such as water features, swimming pools and watering of vegetated areas [41]. UHIs can also cause an increase in energy consumption, by increasing the uptake and use of air-conditioning systems. A temperature rise of 2°C caused by heat islands increases energy consumption by up to 5% [42]. The study by Chen et al. [43] shows that the total economic loss caused by heatwaves in Nanjing in 2013 was 27.49 billion yuan, which represents 3.43% of the city's GDP for 2013.

From a health perspective, UHIs can exacerbate the dangerous effects of smog on the health of the population, as increasing temperatures increase pollution in the atmosphere [42], [44]–[47]. UHIs can also have adverse impacts on the environment. Indeed, they worsen the quality of outdoor air by diffusion of pollution, and thus contribute to the formation of smog which is composed of fine particles and tropospheric ozone, formed after a reaction between sunlight, heat and pollutants [21]. In addition, UHIs help molds and bacteria to thrive, degrading indoor air quality and affecting the surrounding aquatic ecosystems [48].

2.3. Causes of urban heat islands

The terms used for the UHI phenomenon suggest that it is related to urbanization and urban activities. It is estimated that over 55% of the world's population lived in urban areas in 2018 [49]. Stempihar et al. [50] estimate that by 2030, up to 61% of the world's population will live in urban areas. The foremost cause of UHI is the fact that urbanization increases the impervious surfaces and reduces natural vegetation [21], [45], [51]. These surfaces have low albedo and high absorption of solar radiation, which increases urban temperature, especially during the night [52], [53]. Ordinary asphalt can be up to 20°C warmer than grass [45]. In our cities, the amount of vegetation is decreasing and pavements now cover an increasingly high proportion of our cities, contributing to the heat island phenomenon [41], [54].

One of the contributing factors is the use of engineering materials in cities, which have low reflectivity and high heat storage capacity. It should also be noted that the hydraulic, radiative, and thermal properties of materials used in modern construction are completely different to those of natural soil and rocks [55]–[57]. These materials create new surface and atmospheric conditions, which alter the exchange of energy and water, as well as air flow. For example, urban buildings are densely packed. They also reduce cooling by reflection because their albedo

is low [47]. In addition, their height affects the view of the sky, the wind speed and direction, and the radiative balance of the waves. These factors all aggravate the UHI effect [58], [59].

Anthropogenic heat emission also leads to UHIs. The main anthropogenic sources of heat are industrial activity [60], air conditioning [61], heating [62], transportation [46], and human activity. These heat emissions are added to the ambient heat in the environment [38], [60].

As pavements cover large areas in urban cities around the world, replacing traditional pavements with cool pavements is today an interesting solution to mitigate the formation of UHIs. In the next section, the definition, physical mechanisms and cooling techniques of cool pavements to mitigate UHIs are presented.

3. Cool pavements to mitigate UHIs

3.1. Definition of cool pavements

Although there is no official standard definition of cool pavements, the United States Environmental Protection Agency (USEPA) points to "cool pavements that have a range of established technologies that communities are exploring as part of their heat island reduction efforts" [26]. Cool pavements must therefore maintain a lower surface temperature than conventional pavements. They have the potential to limit sensible heat emissions.

Studies in the literature show that the maximum surface temperature, $T_{S_{max}}$, occurs at around 15:00 [27], [28]. The maximum pavement temperature is the focus of many works of research. Diefenderfer et al. [63] developed a model to predict the daily maximum $T_{p_{max}}$ (°C) and minimum $T_{p_{min}}$ (°C) pavement temperature by knowing the maximum $T_{a_{max}}$ (°C) and minimum $T_{a_{min}}$ (°C) ambient air temperatures, the depth from the surface P_d (m), the solar irradiance R_s (kJ/m²) and other empirical coefficients (**Eq.** (1a) and (1b)). This model has the particularity of forecasting the future temperature of the pavements, and determining the duration for which they should be used, on the basis of the evolution of ambient temperature from previous records.

$$T_{p_{max}} = 2.78752 + 0.6861T_{a_{max}} + 5.6736 \times 10^{-4} R_s - 27.8739P_d \quad (1a)$$

$$T_{p_{min}} = 1.2097 + 0.6754T_{a_{min}} + 3.7642 \times 10^{-4} R_s - 7.2043P_d \quad (1b)$$

The previous model (**Eq.** (1)) does not include the thermal properties of the pavement. However, the theoretical model presented in **Eq.** (2) includes these properties [26].

$$T_{S_{max}} = \Gamma \frac{(1-\alpha)I_0}{\eta\sqrt{\omega}} + T_0 \quad (2)$$

where Γ = percentage of absorption compared to thermal conduction; α = albedo (dimensionless); I_0 = daily zenithal irradiation (w/m²); $\eta = \sqrt{\lambda c \rho}$ (J.m⁻².K⁻¹.s^{-1/2}) = thermal inertia of the pavement; λ (W.m⁻¹.K⁻¹), c (j.kg⁻¹.K⁻¹) and ρ (kg.m⁻³) are, respectively, the

thermal conductivity, specific heat capacity, and density; ω = angular frequency equal to $2\pi/(24 \times 3600)$ (1/s); T_0 = regressive constant ($^{\circ}\text{C}$).

From **Eq. (2)**, three properties of cool pavements that help to decrease maximum surface temperature can be deduced. The first is increased albedo. Pavements with a low absorption reduce the heat absorptivity by reflecting the solar radiation towards the sky (as is the case with a reflective pavement). The second is increased thermal inertia of the pavement, which reduces the surface temperature by increasing the thermal conductivity (as is the case with a highly conductive pavement). The third is a reduced factor Γ , for example by promoting evaporation, which increases the release of latent heat (as is the case with wet permeable pavement).

3.2. Reflective pavements

3.2.1. Definition and method of measuring albedo

The reflectivity or albedo determines a surface's ability to reflect the incident solar radiation, with the value ranging between 0 and 1. If we take a pavement with a high albedo of 0.7, for example, this pavement reflects a large majority of the incident radiation. This factor reflects the ability of a material to diffuse energy. The part of the energy which is not reflected increases the temperature of the surface [41].

Two approaches are possible to measure the albedo: the first one is field measurement according to the ASTM E1918-06 standard [64]. The principle consists of measuring the incident solar flux with a pyranometer and then turning it 180° to measure the reflected flux. This method is essential for measuring the albedo of heterogeneous surfaces in the field, such as soils or ground vegetation. The second is a laboratory approach consisting of measuring the reflectance for all wavelengths involved in solar radiation [22].

Several studies in the literature have investigated pavement albedo and its influence on surface temperature and heat transfer [22], [65], [66]. Dumais et al. [66] created a model based on albedo to calculate pavement surface temperatures in permafrost regions. This model was validated using data from a test section constructed in Yukon, Canada. The model inputs are surface albedo, air temperature, wind speed and solar radiation, which can be daily, weekly, monthly or seasonal average values. With this model, they found that high-albedo surfaces can be used to mitigate permafrost degradation.

Albedo is a property which should be measured with great accuracy. It represents a very important parameter in the equation of the energy balance on the surface of a pavement. The intensity of solar radiation, the angle of incidence and the environment have a remarkable effect on the albedo value measured in the field [22].

3.2.2. Reflective asphalt and concrete pavements

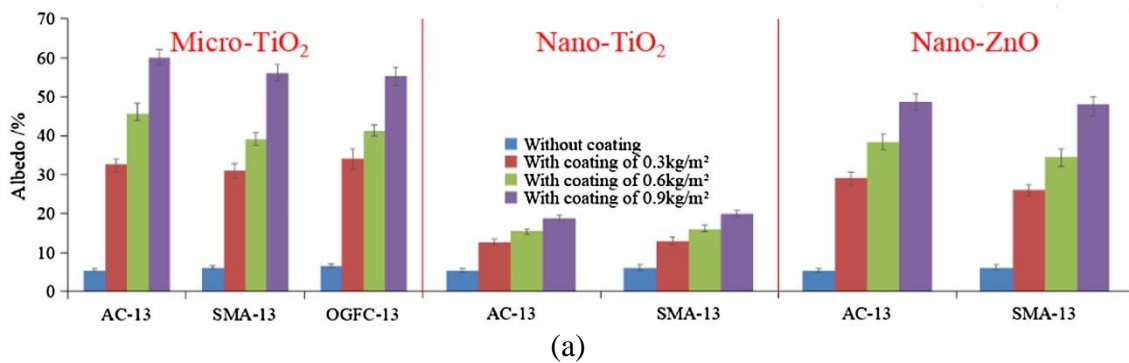
The albedo of pavements is strongly influenced by the color and roughness of the surface [22], [54]. There are techniques to increase the albedo of concrete pavements and make them highly reflective, such as mixing concrete with whitish cementitious materials and light-colored aggregates [26]. Marceau et al. [67] tested 135 concrete samples from 45 concrete mixtures to determine which combinations of concrete constituents meet the LEED-NC (Leadership in Energy and Environmental Design for New Construction) solar reflectance index requirements

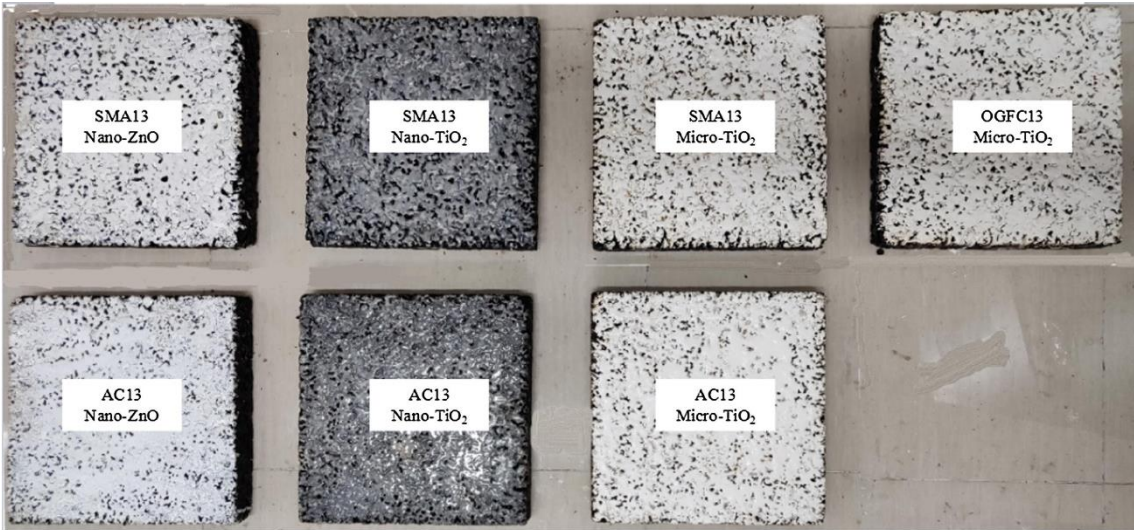
to reduce heat islands. This study shows that the solar reflectance of cement had more effect on the solar reflectance of concrete than did that of any other constituent material.

Levinson et al. [68] found that the albedo of concrete develops as the hydration reaction of the cement progresses, and stabilizes within six weeks of pouring. as cement is the most important constituent in determining the reflectance of concrete, Boriboonsomsin et al. [69] whitened their concrete by focusing on the cement. They replaced cement with whiter constituents – fly ash and slag, which are environmentally friendly and readily available.

The results of this study show that compared to a conventional concrete mix, concrete mixes containing fly ash have a lower albedo while concrete mixes containing slag have a high albedo. A mix with 70% slag as a cement replacement achieves an albedo of 0.582, which is 71% higher than that of the conventional concrete mix. This mix has several advantages: better compressive strength, a reduction in energy consumption of 43.5%, and production of 20 to 60% less pollutants and greenhouse gases [69]. These results are in accordance with those found by Marceau et al. [70] that the use of slag in the concrete mix is a better solution than fly ash in terms of increasing albedo.

The study of Chen et al. [22] shows that reflective pavement coated in a solvent based on transparent epoxy glue in which products such as Nano-TiO₂ (nano-titanium dioxide), Micro-TiO₂ and Nano-ZnO (nano-zinc oxide) are integrated considerably increases the albedo and decreases the temperature of the asphalt mixture (Fig. 2). Such pigments are interesting because they have high reflectivity of infrared radiation and therefore they reflect less visible light. Indeed, the reflection of visible light by reflective pavements can cause glare and esthetic problems [26]. However, there have been few studies considering the adverse environmental effect of more reflective pavements and their contribution to glare, thermal comfort and human health of residents [45].





(b)

Fig. 2. Measured albedo of asphalt slabs: (a), asphalt slabs coated with three types of surfacing materials with the use of 0.9 kg/m²; (b), with AC: asphalt concrete, SMA: Stone matrix asphalt, OGFC: open graded friction course [22].

Thermochromic materials tend to be used where it is desirable to have a pavement with a high reflectance in summer but a low reflectance in winter to retain the heat. These materials change their albedo with temperature variation. A study [71] shows that the incorporation of thermochromic pigments in cement paste caused a temperature decrease of 4 to 6°C during hot weather, and a temperature increase of 2 to 3°C during cold weather. Zhang et al. [72] found that the recommended thermochromic powder content for asphalt concrete mixtures is 4%. This addition can improve the ageing resistance of bituminous binders. There are also other techniques to increase the albedo of asphalt pavements, such as light-colored painting or micro-surfacing with light-colored materials [73].

Table 1 presents a review of several techniques used to make conventional asphalt and concrete pavements more reflective. It shows the thermal properties of the materials used and their influence on the temperature of conventional pavements.

Table 1
Different techniques used to make conventional pavements more reflective

Reference	Materials and strategy	Thermal properties	Results
Miao et al., 2022 [74]	A crosslinkable heat-absorbing waterborne polyurethane has been used to prepare a reflective coating for asphalt pavements	Increases the solar reflectance of asphalt up to 0.298	Reduces the inner temperature of conventional asphalt by 7–11°C
Zhu et al., 2019 [75]	Covering the surface of conventional concrete with a mixture of cement mortar containing "cool cold" black pigments of sand and TiO ₂	Increases near infrared reflectance of ordinary concrete from 0.28 to 0.40	Decreases surface temperature of ordinary concrete by 20°C

Kyriakodis and Santamouris, 2018 [76]	Covering asphalt pavements with a thin yellow coating	<i>Materials</i>	α		ΔT_{mean} compared to conventional pavements	
		Light yellow asphalt	0.35			7.5°C
	Replacing grey concrete pavements with white concrete pavements mixed with TiO ₂ pigments	Conventional asphalt	0.04		6.1°C	
		White concrete	0.66			
		Conventional grey concrete	-			
Sha et al., 2017 [77]	Applying a reflective coating based on resin and TiO ₂ pigment to the surface of asphalt pavements	Increases the solar reflectance of the pavement			Decreases pavement surface temperature by 10 ± 2.5°C	
Rosso et al., 2017 [78]	Innovative concrete elements (pavements, building facades, etc.) with infrared-reflective (IRR) pigments	Increases solar reflectance up to 15.8% compared to standard concrete prototypes			Decreases surface temperature up to 10.6°C	
Guntor et al., 2014 [25]	Covering asphalt pavements with waste tile coating	<i>Materials</i>	α	$\varepsilon^{(1)}$	Decreases surface temperature of asphalt pavements to 4.4°C	
		Coated surface	0.09	0.94		
		Uncoated surface	0.52	0.93		
Carnielo and Zinzi, 2013 [24]	Colored coating applied to asphalt pavements	<i>Color</i>	$\rho_e^{(2)}$		ΔT_{max} (°C) compared to conventional asphalt pavements	
		Control	0.05			0
		Off-white	0.66			19.3
		Grey	0.40			10.0
		Green	0.36			7.8
		Blue	0.25			7.9
		Red	0.28			6.2
Wan and Hien, 2012 [79]	PerfectCool: dark-colored coating with high albedo applied on asphalt pavements	Reflects up to 81% of near infrared red waves, thermal conductivity = 0.252 W. m ⁻¹ .K ⁻¹ , high emissivity = 0.828			Reduces the temperature by up to 17°C, compared to a normal asphalt surface without PerfectCool	

Synnefa et al., 2011 [23]	Covering existing asphalt pavements with thin layers of colored asphalt	<i>Color</i>	ρ_e	ΔT_{\max} (°C) compared to conventional asphalt pavements
		Control	0.04	0
		Off-white	0.55	11.9
		Beige	0.45	7.9
		Green	0.27	4.8
		Red	0.27	4.1
		Yellow	0.44	9.2
Karlessi et al., 2009 [80]	Application of 11 different colored thermochromic coatings with or without TiO ₂ on the concrete surface	Increases solar reflectance: $0.51 \leq \rho_e \leq 0.81$		Reduces surface temperature from 5.4 to 10°C

⁽¹⁾ = emissivity.

⁽²⁾ = solar reflectance.

3.2.3. Aging of reflective pavements

Conventional cement-based concrete pavements have an albedo between 0.35 and 0.4, but as the concrete ages, it becomes progressively darker due to dirt and tire wear [45], which decreases its albedo to values between 0.2 and 0.3 [26]. Therefore, future studies should focus on the albedo variation of traditional concrete pavements and those of pervious pavements, to accurately measure its reflectivity and thus to better estimate its influence in mitigating urban heat islands in the long term.

Alchapar et al. [81] studied 38 frequently used pedestrian pavements in the local urban environment. The pavements were classified into four compositions: mono-layer such as concrete and natural stone, and bi-layer such as concrete-stone and limestone concrete, and having several different shapes and colors (Fig. 3).


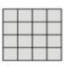
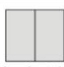

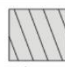



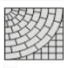


LAYER	COMPOSITION	COLOR	TEXTURE	SHAPE					
Mono	Concrete 	Red Yellow	Gray Black	Rustic	Straight				
	Natural Stone 	Travertine Red-multicolor	Gray-multicolor Black-withe	Smooth					
Bi	Concrete-stone 	Bordeau Jade Green	Black-multicolor Murcia Black	Rustic Smooth	Circular				Flat
	Concrete-calcareous 	Red Yellow	Black	Smooth					

Fig. 3. Classification of materials by composition, color and texture (a), and by shape (b) [81].

The results show that 74% of pedestrian pavements tend to decrease in solar reflectance index due to wear and tear produced by outdoor conditions and dirt accumulation. However, one

group of materials showed an improvement in classification: monolayer composition, straight shape and black or black-white color.

Unlike conventional concrete pavements, new asphalt concrete pavements with an initial albedo of 0.04 to 0.1 lighten as the binder oxidizes and the aggregate becomes more worn. Aged asphalt pavements have exposed aggregates and brighten with an albedo of 0.1 to 0.15 [26]. Table 2 shows some typical albedo values for new and old asphalt pavements based on the literature.

Table 2

Typical values of asphalt pavement surface albedo.

Pavement type	Albedo	References
New asphalt concrete	0.08-0.09	[82]
	0.04-0.06	[83]
	0.04-0.05	[84]
	0.05	[24]
Aged asphalt concrete	0.1-0.15	[85]
	0.12-0.15	[86]
	0.14	[82]

Sen and Roesler [87] established a model which shows that the albedo of asphalt concrete increases and quickly reaches a nearly constant value after one year according to **Eq. (3)**.

$$\alpha = 0.1214 + 0.1056 N^{0.0152} \quad (3)$$

where N = age of construction (years).

3.3. Evaporative pavements

Evaporative pavements reduce UHIs by means of evaporative cooling [1], [41], [45], [51]. Evaporative cooling could reduce both pavement temperature and air temperature due to the latent heat absorbed to change the phase of water from liquid to gas. This strategy therefore requires the presence of water in the pavement structure or in the underlying soil. The use of this type of pavement is particularly suitable in countries with high summer rainfall. Otherwise, the pavements must be artificially watered.

Evaporative pavements are among the most common cool pavements. These types of pavements are generally permeable. There are several types of permeable evaporative pavements: porous pavers, impermeable pavers with permeable joints, permeable pavements and water retentive pavements. These pavements can also offer many environmental benefits such as stormwater management [88], [89], water quality improvement [90], groundwater replenishment [91], pollution reduction and vehicle noise reduction [91]–[94].

3.3.1. Porous vegetated pavers

This type of structure allows grassing; it has alveolar shapes that allow soil vegetation and ensure water infiltration (Fig. 4). It is also capable of supporting heavy loads, such as parking lots [41]. In general, this type of porous pavement includes reinforced turf or grass, and plastic geo-cells with grass.

When soil or gravel is used as fill, the cooling effect is slight. In this case, the system is thermally similar to a concrete pavement. When grass is used as infill, it promotes transpiration, with its roots transporting moisture from the soil to the surface to evaporate and cool the sidewalks. For vegetated porous pavements, it is only during the day that the atmosphere is heated by the sensible heat released from the pavement surface. After sunset, the temperature of the pavement surface decreases rapidly and quickly becomes lower than that of the atmosphere, and the surface begins to cool the atmosphere [13], thus reducing the effect of UHIs. In addition, this system is highly reflective, and has a compressive strength of up to 40 MPa [95].



Fig. 4. Reinforced porous grass pavers [95].

A similar technique was used in Japan to compare asphalt parking areas and grass-covered parking areas. The surface temperature of both was calculated from a thermal image captured by an infrared camera. The results show that the sensible heat flux from the grassy areas is 100-150 W/m² lower during the day period and about 50 W.m⁻² lower during the night compared to the asphalt concrete parking areas [96]. The disadvantages of these pavements are their high cost and the problems of winter maintenance at all levels [95].

3.3.2. Impermeable pavers with permeable joints

This type of pavement is constructed by placing impervious pavers against each other, which allows water not to pass directly through the pavement to the base but allows water to percolate through the permeable joints [41]. These joints, which represent small openings, provide a channel for the evaporation of water stored in the surface layer or in the lower layers. These joints represent a surface ratio of between 8 and 20% [26]. This design exhibits very good filtration of sediments from stormwater runoff, though the progressive accumulation of sediments leads to a reduction in permeability. Luck and Beecham [97] show that this design retains satisfactory filtration performance even after 8 years of operation.

As to the thermal properties, Li et al. [28] showed that the surface temperature of this type of pavement is up to 20°C lower than that of an asphalt pavement in dry conditions. These results are in agreement with those found by Thomson et al. [98].

In wet conditions, Andersen et al. [99] found that the average daily evaporation of this type of pavement ranges from 0.09 to 0.22 mm. In order to achieve a significant evaporative cooling effect, Liu et al. [100] developed a new innovative permeable structure by introducing capillary columns to move water up to the pavement surface by the capillary effect (Fig. 5). The results of this study show that this type of pavement improves the evaporation rate and has a surface temperature up to 9.4°C lower than that of a conventional permeable pavement without capillary columns. In a later study, Liu et al. [101] show that this innovative permeable pavement type reduces the overall volume of stormwater by 90.6% in an area with a high water table. In addition, during summer, it has a surface temperature up to 15.3°C lower than conventional impermeable concrete with a cooling time of more than one week.

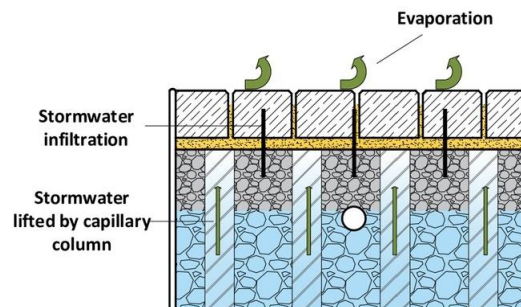


Fig. 5. Innovative permeable pavers [101].

3.3.3. Permeable pavements

Pervious concrete and permeable asphalt pavements are among the most common permeable pavements. They allow water to pass directly through their structures due to an interconnected network of pores [10]. These permeable pavements have various uses: they are used in low traffic pavements, parking areas, bicycle paths, etc.

These two types of permeable pavements are presented below, with an emphasis on their hydraulic, mechanical and thermal characteristics in dry and wet conditions.

a) *Pervious concrete*

Pervious concrete (PC) is a composite material. It is made up of the same components as conventional concrete: water, cement and aggregates. The only difference is that there are almost no fine particles to fill the voids between the coarse aggregates, which leads to the creation of interconnected voids, allowing water to pass through the PC [102]. This permeable pavement has a total porosity ranging from 15 to 40%, and an open porosity ranging from 15 to 35% [102]–[106].

Several studies in the literature have highlighted the mechanical and hydraulic properties of PC [107]–[113]. However, to date, there have been few studies on the thermal properties of these pavements and their contribution to UHI mitigation [27], [29].

Hydraulic conductivity or permeability is an essential factor that determines its performance in relation to its primary function: stormwater management. A wide range of permeability values can be found in the literature: 0.2 to 1.2 cm/s [114], 0.025 to 0.61 cm/s [115], 0.22 to 0.54 cm/s [116], 0.076 to 3.5 cm/s [117], and 0.2 to 0.6 cm/s [118]. The permeability value should be adjusted according to the local rainfall. The permeability of the PC must be higher than 0.0054 cm/s to be qualified as draining [119], and higher than 0.1 cm/s to avoid the risk of clogging [120].

The mechanical strength of PC is lower than that of conventional impermeable concrete due to its high porosity, attributable to the thin layer of cement paste that binds the aggregates together [121]. The compressive strength of PC mixtures can vary from 3.5 to 28 MPa [125]. It should have a compressive strength greater than 17 MPa for use as a low-traffic pavement [126] and greater than 14 MPa for use in parking areas [127].

Porosity (P) is a key factor that controls the mechanical and hydraulic properties of PC [128]. This factor also affects its thermal properties. Zhang et al. [122] show that the albedo decreases linearly with increasing porosity of PC. Moreover, its albedo is 0.05 to 0.15 lower than that of conventional impermeable concrete. Chen et al. [123] show that the thermal conductivity also decreases linearly with increasing porosity. The results of these experiments and the prediction models obtained are presented in Fig. 6.

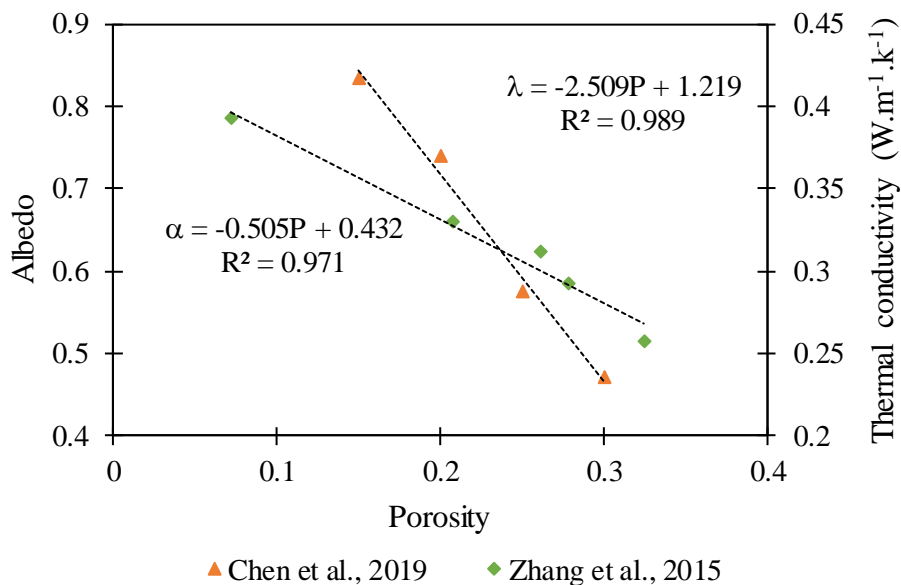


Fig. 6. Variation in albedo and thermal conductivity of PC as a function of porosity.

Regarding the thermal behavior of PC in dry conditions, the laboratory study of Chen et al. [14] shows that PC ($\rho = 1819.8 \text{ kg.m}^{-3}$, $\lambda = 0.59 \text{ W.m}^{-1}.\text{K}^{-1}$, $P = 26.8\%$) has a surface temperature up to 5.75°C higher than that of conventional impermeable concrete ($\rho = 2291.4 \text{ kg.m}^{-3}$, $\lambda = 1.42 \text{ W.m}^{-1}.\text{K}^{-1}$) during the heating period (infrared lamp on). During the cooling period (infrared lamp off), the conventional impermeable concrete cools down faster than the PC. These results are in agreement with those found numerically by Qin & Hiller [27].

During the daytime, the relatively low thermal conductivity of PC limits conductive heat transfer to the interior of the material due to the presence of pores. In addition, its low albedo leads to higher absorption of incident short-wave radiation, making it warmer than conventional

concrete during the day. On the other hand, during the night, due to its low thermal inertia, PC is less resistant to temperature drop and therefore becomes cooler than conventional concrete.

In wet conditions, Qin & Hiller [27] show that PC has a surface temperature up to 10°C lower than conventional concrete when it is saturated with water. This evaporative cooling effect lasts from 12 to 24 hours. After saturation (water content $\theta = 100\%$), the evaporation flux decreases from 500 W/m² to a value of less than 75 W/m² after 24 hours ($\theta \cong 60\%$). This study also shows that PC can be cooler than conventional concrete permanently if it is watered periodically every 24 hours; the best wetting time to achieve a better evaporative cooling effect is around noon.

Bulk evaporative resistance r (s/m) is a key factor affecting PC evaporation. This resistance is divided into aerodynamic resistance r_a (s/m) which represents the resistance to moisture transport from the pores into the ambient air [124], and surface resistance r_s (s/m) [125]. Syrrakou et al. [126] show that the bulk evaporative resistance of PC decreases exponentially from 2000 to 200 s/m when the water content decreases from 100 to 70% (Fig. 7). Thus, high water content favors evaporation and, if it is lower than 70%, evaporation becomes negligible.

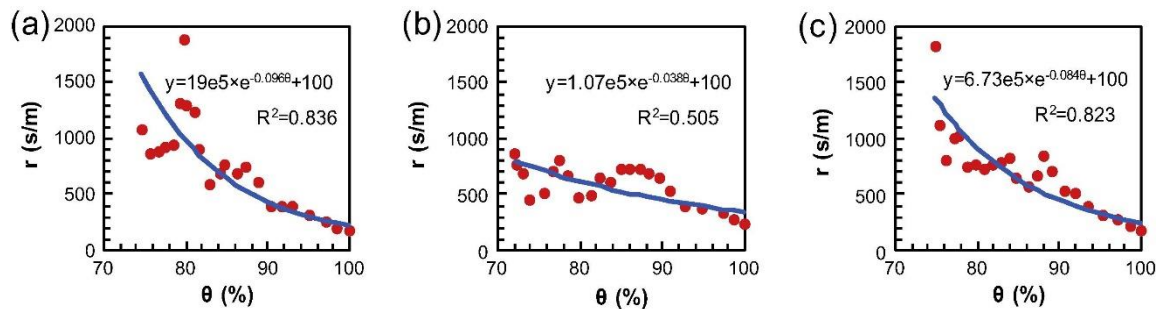


Fig. 7. Variation in evaporation resistance as a function of moisture content during June (a), July (b), and August (c) [27], [126].

Several researchers in the literature have indicated the importance of the presence of water near the surface to promote evaporation [27], [125]–[132]. Nemirovsky et al. [31] experimentally tested evaporation in PC using artificial solar radiation. The structure consisted of a 152 mm-thick PC layer on a 914 mm aggregate layer. Then, different water levels were considered: 0, 25, 76 and 151 mm in order to simulate the influence of the water level on the cooling effect. The results of this experiment show that if water is present near the surface (0-25 mm), the maximum evaporation rate is high – it is between 16.8 and 25 mm/day. On the other hand, the maximum evaporation rate corresponding to deeper water levels (76-152 mm) is less: it is between 6.7 and 9.3 mm/day. In this case, the evaporative fluxes contribute much less to the cooling effect.

b) Permeable asphalt pavements

Permeable asphalt pavements (PAPs) are characterized by high porosity and permeability, allowing rainwater to infiltrate more rapidly through their porous structure [133]. As with pervious concrete, these pavements play an essential role in stormwater management. They also offer several benefits such as improved skid resistance in wet conditions, improved road safety and reduced vehicle noise [134]–[138].

Several experimental studies [139]–[143] in the field and in the laboratory show that the permeability of asphalt mixes can vary by 6 orders of magnitude (10^{-7} to 10^{-1} cm/s) for samples whose porosity ranges from 3 to 26%. Moreover, the permeability of dense and semi-dense asphalt mixes (10^{-6} to 10^{-2} cm/s) is lower than that of discontinuous and porous asphalt mixes (10^{-2} to 10^{-1} cm/s) which have a porosity higher than 12%. The 4 types of asphalt mixes are shown in Fig. 8.

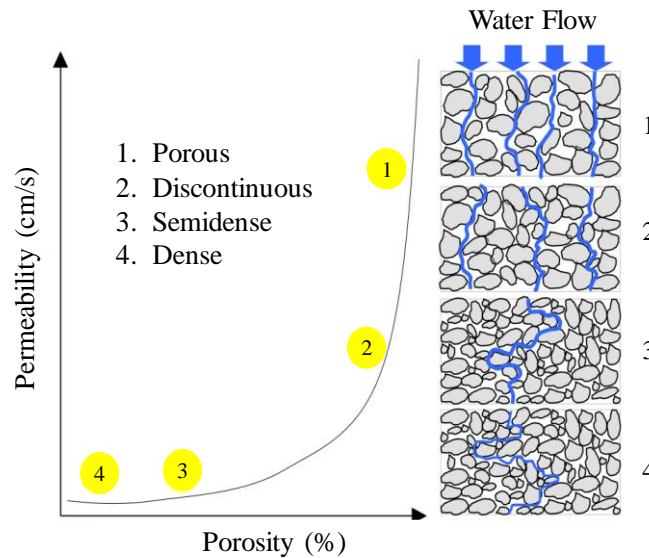


Fig. 8. Diagrammatic representation of the relationship between permeability and porosity in asphalt mixtures with different pore structures [144].

PAP has lower mechanical strength than dense impermeable asphalt pavement (IAP) due to the weak adhesion between the aggregates [145]. To improve the performance of PAP, it is important to select a high-quality binder, aggregates, and additives that are suitable for traffic conditions. Although it has environmental benefits, it can suffer from problems that can affect both its performance and service life. The high porosity exposes a large surface area to the effects of water and air, resulting in rapid aging of the binder [146]. In addition, pore clogging can influence its functionality [147].

As to the thermal behavior of PAP in dry conditions, the rate of air voids present in its structure affects some of its physical properties, such as specific heat capacity and thermal conductivity, and consequently affects its surface temperature [148]. In wet conditions, the surface temperature of PAP is significantly reduced by the energy used for water evaporation. This is because as the PAP temperature increases, water evaporates, which reduces the pavement’s surface temperature [149]. Table 3 shows the influence of several factors on the thermal behavior of different PAP mixtures under dry and/or wet conditions.

Table 3
Thermal behavior of PAPs in dry and wet conditions.

Reference	Factor studied	Thermal properties	Results
-----------	----------------	--------------------	---------

Gao et al., 2019 [150]	The influence of porosity on the convective heat transfer coefficient and on the temperature of PAP	P (%)	λ (W.m ⁻¹ .K ⁻¹)	c (j.kg ⁻¹ .K ⁻¹)	$k^{(1)}$ ($\times 10^{-7}$ m ² .s ⁻¹)	In windless conditions, the surface temperature of PAPs increases with increasing porosity. The phenomenon is reversed under windy conditions. The convective heat transfer coefficient increases with increasing porosity
		16.68	1.03	926.88	4.98	
		18.11	0.97	926.09	4.77	
		19.66	0.93	926.09	4.69	
		20.79	0.88	925.3	4.49	
		23.05	0.8	915.82	4.18	
Sreedhar and Biligiri, 2016 [151]	The influence of specific heat capacity and thermal conductivity on the surface temperature of several conventional and modified asphalt mixtures under dry conditions	<i>Materials</i>	P	λ	c	The surface temperature increases as the specific heat capacity increases and the thermal conductivity decreases
		Asphalt-rubber open graded	18	0.51	664	
		Asphalt-rubber gap graded	8	0.77	863	
		Conventional dense graded	4	0.88	933	
		Conventional dense graded	7	0.96	1039	
Hassn et al., 2016 [152]	The influence of the porosity of PAPs on their temperature in dry and wet conditions	P	λ	c	In dry conditions, samples with higher porosity exhibit a higher rate of temperature rise.	
		5.0	1.16	963.70		
		13.2	0.96	957.77		
		14.4	0.92	953.03	In wet conditions, the rate of temperature increase decreases with increasing porosity	
		21.5	0.90	947.11		
		25.3	0.82	945.92		
Garcia et al., 2015 [148]	The influence of PAP porosity on the evaporation rate	P	λ	c	The maximum evaporation rate in PAPs increases with increasing porosity. This factor is strongly related to the complex interaction of several geometric properties such as the percentage and diameter of air voids, tortuosity and Euler number	
		5.6	1.16	963.70		
		9.9	1.04	961.33		
		13.2	0.96	957.77		
		17.4	0.92	953.03		
		21.5	0.90	947.11		
		25.3	0.82	945.92		
		<i>Materials</i>	α	In dry conditions, the maximum surface temperature of the PAP		

Li et al., 2013 [28]	The influence of watering on the thermal behavior of PAP	IAP		0.07		during the daytime is 5°C higher than that of the IAP. In wet conditions, the maximum surface temperature of the PAP is 30°C lower than the IAP at the beginning of watering and 5°C 24 hours after watering
		PAP		0.055		
Stempihar et al., 2012 [50]	The thermal behavior of PAP and IAP during daytime and nighttime with different albedos	<i>Materials</i>	α	λ	c	For the same albedo value, the PAP temperature over several depths is higher than the IAP temperature during the daytime. However, this phenomenon is reversed during the night
		IAP	0.05–0.2	1.2	921	
		PAP	0.05–0.2	0.4	800	

⁽¹⁾ = thermal diffusivity.

3.3.4. Water-retaining pavements

Water-retaining pavements (WRPs) are designed to retain water primarily in the upper layers for a relatively long period of time [153]. They can retain more water than permeable pavements for evaporative cooling [26]. Generally, they are composed of an impermeable bottom surface and a permeable top layer. This can also be achieved by injecting permeable fillers with high capillarity into the pores [154]. This type of pavement can be asphalt or cement-based. Such pavements are used in public or private areas: streets, parking lots, roads and sidewalks, etc.

Qin et al. [155] conducted an experiment to evaluate the cooling performance of reservoir-structured pavements: WRP compared to PC and conventional impermeable concrete pavement (Fig. 9).

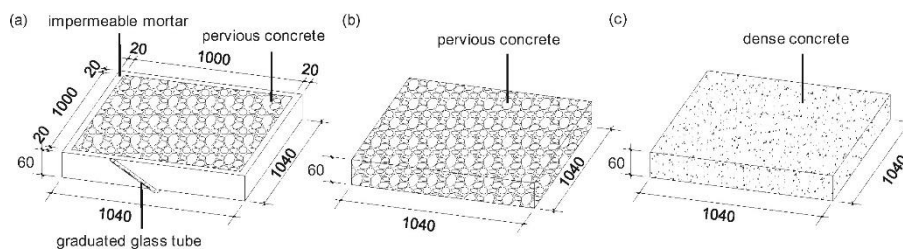


Fig. 9. The prepared pavements: WRP (a), PC (b), and dense impermeable concrete (c) [155].

WRP and PC have the same composition. However, WRP has better water storage capacity, as it retains water in the pavement by sealing the bottom and sides of the pavement with an impermeable mortar material. The results of the experiment show that this pavement can retain about 9.5 L/m². The temperature of the WRP was 2 to 10°C lower than that of the PC and dense impermeable concrete. This proves that the evaporative cooling of WR is more efficient than other pavements in UHI mitigation.

Qin et al. [155] show that sealing the bottom and sides of a permeable pavement block can retain a significant amount of water. However, this leads to overflow in the event of heavy rainfall. To avoid this problem, Bao et al. [156] developed a new WRP that can retain water to

reduce UHIs and also quickly drain excess water during heavy rainfall. This type of WRP contains tubes filled with pervious concrete with a height of 1 cm less than the thickness of the pavement, which allows water to flow out of the WPR when the level of water retained exceeds the height of the tubes (Fig. 10).

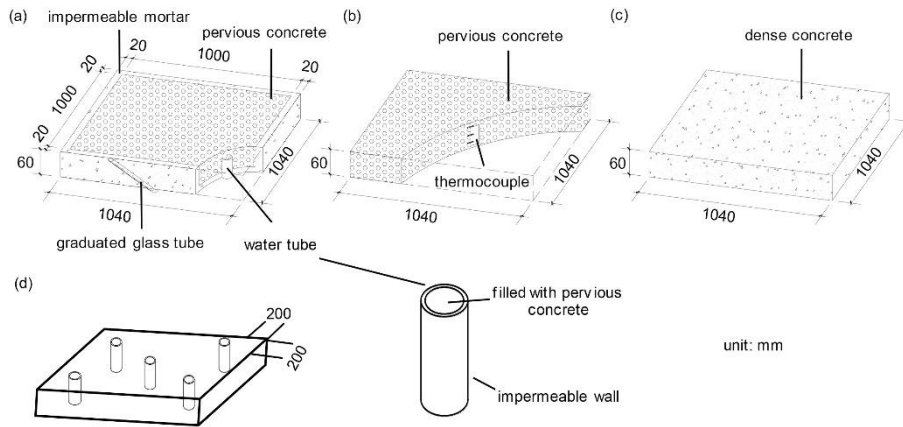


Fig. 10. WRP (a), PC (b), dense waterproof concrete (c), and water tube configuration (d) [156].

The results of this study show that after watering, the temperature of the new WPR is reduced by a maximum of 13°C during the daytime and 3°C during the nighttime. Moreover, during the day, it has a temperature up to 10.15°C and 11.5°C lower than that of PC and conventional dense concrete, respectively, during the day.

One of the solutions to improve the cooling effect of permeable pavements is to optimize the design of the porous structure, but the performance is still limited by the hydraulic and mechanical properties. On the other hand, the addition of water-retentive filler is considered a more feasible strategy. Several materials have been used to improve the water absorption capacity of WRP, such as blast-furnace slag [157], [158], porous geopolymers [159], allophane and vermiculite materials [160], and steel by-products based on a silica compound [157]. Tan et al. [161] studied the thermal behavior of PC containing biochar particles as hygroscopic filler. This study shows that the use of 5% pulverized biochar as an admixture in the PC mixture increases the total water absorption from $100 \pm 2 \text{ kg/m}^3$ to $117 \pm 8 \text{ kg/m}^3$. In addition, the PC containing biochar has a surface temperature of 3 to 6°C cooler compared to conventional PC without biochar, with an additional cooling period of 6 hours.

Besides concrete-based WRP, there are other types of pavements with different materials and structures that function as a water retaining pavement. These pavements have different properties and exhibit significant evaporative cooling performance. Table 4 summarizes examples of the implementation of these types of WRPs reported in several recent studies.

Table 4

Cooling performance of several types of WRP, based on a number of recent studies.

Reference	WRP Type	Objective	Pavement properties			Results
	Self-locking block pavements	Study the effect of WRP	Materials	ρ_e	$WRC^{(1)}$ ($\text{kg}\cdot\text{m}^{-3}$)	WRP significantly reduces surface temperature by up to 13.5°C and human

Shimazaki et al. 2022 [162]	that use permeable blocks containing fine voids to retain water	implementation with different reflectance values on human health	IAP	0.08	-		thermal loads by up to 61 W/m ² compared to IAP
			WRP13	0.13	9.14		
			WRP25	0.25	8.76		
Seifeddine et al., 2022 [163]	Three types of WRP with different grain sizes based on recycled tire aggregates, pozzolan and polyurethane resin	Compare the thermal behavior of an innovative WRP in wet conditions with that of IAP	<i>Materials</i>	<i>P</i> (%)	α	λ (W.m ⁻¹ .K ⁻¹)	In wet conditions after watering, the surface temperature of the WRPs is 15.6 to 28.1°C lower than that of the IAP during the first day and 0.5 to 8.8°C lower during the second day
			IAP	-	0.08	2.2	
			WRP	23–31	0.063–0.074	0.163–0.317	
Kinoshita et al., 2022 [164]	Self-locking block pavements made of blocks with high water-retention capacity	Study the impact of WRP on the thermal environment	<i>Materials</i>	α		WRC	WRP has a surface temperature 10 to 15°C lower than IAP. They reduce the air temperature at 1 m by 3 to 5°C
			IAP	-		-	
			WRP	0.13	9.14		
Shimazaki et al. 2021 [165]	Reflective and evaporative WRPs made of ceramic (90%) and glass (10%) water retention blocks	Study the influence of WRP and IAP on the thermal environment and thermal comfort	<i>Materials</i>	ρ_e		WRC	WRP has a temperature 9.5°C lower than IAP. They reduce the human thermal loads at a pedestrian height of 1.5 to 22 W/m ²
			IAP	0.085 ± 0.01		-	
			WRP	0.253 ± 0.029		≥ 15 volume %	
Dong et al., 2019 [28]	Semi-flexible water retaining pavement (SFWRP) composed of asphalt and water retention mortar.	Study the thermal behavior of SFWRP in wet and dry conditions	<i>Materials</i>	λ	ρ (j.kg ⁻¹ .K ⁻¹)	ε	In dry conditions, the surface temperature of SFWRP is up to 5°C lower than that of IAP due to its higher reflectivity. In wet conditions, the temperature difference is 17.3°C due to the combined effect of reflection and evaporation
			IAP	1.128	823	0.93	
			SFWRP	1.010	734	0.85	
Wang et al., 2018 [29]	Sintered ceramic pervious brick (CB), pervious concrete brick (PB) and open	Study the influence of the water absorption capacity of WRPs on their	<i>Materials</i>	α	$A_{cap}^{(2)}$ (kg/m ⁻² .s ^{-0.5})	$W_{cap}^{(3)}$ (kg.m ⁻³)	The maximum temperature decrease of wet WRP compared to dry WRP is
			CB	0.22	2.040	121.07	

	graded pervious concrete (PC)	evaporative cooling performance	PB	0.18	0.069	114.17	20°C for CB, 12°C for PB and 2°C for PC
			PC	0.24	0.010	101.36	
Higashiyama et al., 2016 [166]	Water-retaining asphalt pavement with several cement slurry materials poured into the pavement pores: NCZ, NCF, UCZ and UCF ⁽⁴⁾	Identify the best performing mix of WRP with several cement grout materials to mitigate UHIs	The water absorption ratio of the cement-based grouting material ranges from 48.1 to 48.9%. These materials have different colors				When the temperature of conventional PAP is 60°C, the temperature difference is 20.3°C for PAP with UCZ, 12.5°C for PAP with UCF, 14.8°C for PAP with NCZ and 8.9°C for PAP with NCF
Jiang et al., 2016 [167]	Water-retaining asphalt pavement product by incorporating a water-retentive slurry based on fly ash and ground granulated blast furnace slag and calcium hydroxide into the PAP	Compare the thermal behavior of PAP and WRP during outdoor and laboratory tests	The water absorbing capacity varies according to the curing time and dosage of each component of the water-retentive slurry. This capacity can reach 50%				Laboratory tests show that WRP has a surface temperature up to 10°C lower than PAP. Outdoor tests show that the maximum temperature difference is 13°C

⁽¹⁾ = maximum water retention capacity.

⁽²⁾ = water absorption coefficient.

⁽³⁾ = water retention capacity.

⁽⁴⁾ = N for Normal Portland Cement, U for Ultra-fast setting cement, C for Ceramic waste powder, F for Fly ash, and Z for natural Zeolite.

3.4. Pavements that modify their heat storage

3.4.1. Cool pavements containing phase-change materials

Phase-change materials (PCMs) are materials capable of changing their physical state within a restricted temperature range. The most prevalent phase change is melting/solidification [168]. These materials have the ability to store heat and control temperature [169], [170].

PCMs have a wide range of uses. For example, they have been used in thermal energy storage areas, and in various building materials such as wall panels, ceilings and roofs [171]–[178]. They have also been used for thermal management of thermoelectric generators [179], [180], and other electrical appliances [181], in thermal comfort improvement of buildings [182]–[184], for transient thermal management applications with high thermal flux [185], for solar energy systems [186], in air conditioning [187] and positive cold energy storage [188]–[190].

These materials have been used in asphalt and concrete pavements [191], [192]. They exhibit good performance in regulating pavement temperature by absorbing or releasing heat [168]. It is possible to incorporate PCMs into pavements using one of the following methods: incorporation of metal containers/pipes filled with PCM [192], incorporation of mineral fillers impregnated with PCM [193], and partial substitution of aggregates by light materials impregnated with PCM [194]. Table 5 presents the cooling performance of several cool pavements containing PCM.

Table 5

Influence of the addition of PCM on the surface temperature of conventional pavement materials.

Reference	Type of pavement	PCM type	Thermal properties	Maximum surface temperature reduction measured by indoor or/and outdoor tests
Sha et al., 2022 [195]	Asphalt	Polyurethane M_PU5 with 4,4'-diphenylmethane diisocyanate (MDI) as the isocyanate, the molar ratio of MDI and polyethylene glycol being 5	$T_m^{(1)} = 36-48.3^\circ\text{C}$ $\Delta H_m^{(2)} = 93.5 \text{ j}\cdot\text{g}^{-1}$	Outdoor: 4.8°C
Liu et al., 2022 [196]	Asphalt	A new coating with TiO ₂ -2DMts/SA ⁽³⁾	$T_m = 40-85^\circ\text{C}$ $\Delta H_m = 242.37 \text{ j}\cdot\text{g}^{-1}$	Indoor: 24.8°C Outdoor: 7.29°C
BR et al., 2021 [197]	Concrete	Organic mixture 35	$T_m = 35^\circ\text{C}$ $\Delta H_m = 171 \text{ j}\cdot\text{g}^{-1}$	Outdoor: 1.85°C
		Organic Mixture 42	$T_m = 44^\circ\text{C}$ $\Delta H_m = 199 \text{ j}\cdot\text{g}^{-1}$	Outdoor: 2.76°C
Jin et al., 2019 [198]	Asphalt	PCM based on diatomite, stearic and palmitic acid	$T_m = 52.93^\circ\text{C}$ $\Delta H_m = 106.7 \text{ j}\cdot\text{g}^{-1}$	Indoor: 8.11°C
Mizwar et al., 2019 [191]	Asphalt	Paraffin	-	Outdoor: 12°C
Refaa et al., 2018 [193]	Asphalt	Eicosane	$T_m = 36.5^\circ\text{C}$ $\Delta H = 247.3 \text{ j}\cdot\text{g}^{-1}$	Outdoor: 2.7°C
Jin et al., 2018 [199]	Asphalt	Polyethylene glycol	$T_m = 54-60^\circ\text{C}$ $\Delta H_m = 29-50 \text{ j}\cdot\text{g}^{-1}$	Indoor: 9.1°C

Ryms et al., 2015 [194]	Asphalt	Ceresin	$T_m = 42-78^\circ\text{C}$	Indoor: 8.5°C Outdoor: 7°C

⁽¹⁾ = phase-change temperatures.

⁽²⁾ = latent heat-storage capacity.

⁽³⁾ = 2DMTs for two-dimensional montmorillonite nanosheets, SA for stearic acid.

3.4.2 High-conductivity pavements

A second type of pavement that changes its heat storage is high-conductivity pavement. When the thermal conductivity of the pavement increases, it contributes to faster heat transfer from the surface to the interior of the pavement and vice versa. In fact, during the daytime, when the pavement temperature is higher than the ground temperature, there is a heat transfer to the ground, which decreases its surface temperature. The opposite phenomenon is observed during the night.

Although the increase in pavement surface temperature during the night is negligible compared to the benefits it provides during the day, it can contribute to the development of nocturnal UHI. This phenomenon affects the thermal comfort of people at night and leads to increased air-conditioning costs [200], as well as health problems [201]. Therefore, pavements with high thermal conductivity are not recommended for regions with relatively high nighttime temperatures.

It is possible to increase the thermal conductivity of pavements by adding products with high thermal conductivity, such as steel and carbon fibers, graphite, carbon black [202], [203], by adding aggregates with high thermal conductivity (steel slag for example) [204], and by adding metal rods with high thermal conductivity [205]. Table 6 presents several techniques used to increase the thermal conductivity of pavements and their impact on their thermal behavior.

Table 6
Cooling performance of high-conductivity pavements

Reference	Type of pavement	Strategy	Thermal properties			Results
Park et al., 2021 [206]	Pervious concrete	Improving the cooling effect of an ecological PC containing amorphous metallic fiber (AMF)	<i>Materials</i>	$V^{(1)}$ (%)	λ ($\text{W}\cdot\text{m}^{-1}\cdot\text{K}^{-1}$)	The evaporative cooling effect increases up to an additional 2°C with increasing AMF volume fraction
			Conventional PC	0	0.117	
			PC _{5%}	5%	0.170	
			PC _{10%}	10%	0.183	
Yinfei et al., 2021 [207]	Asphalt	Adding curved hook steel fiber (CHSF) to the asphalt mixture	<i>Materials</i>	V	λ	Laboratory tests indicate that using 1% CHSF asphalt mix below the top asphalt layer decreases the
			Asphalt pavement with CHSF	0	1.39	

			Asphalt pavement without CHSF	1%	1.6	temperature at a depth of 4 cm by 1.8°C
Chen et al., 2019 [14]	Pervious concrete	Adding steel fibers to the pervious concrete mix	<i>Materials</i>	V	λ	Decrease of the surface temperature of the PC by 1 to 3°C
			Conventional PC	0	0.59	
			PC _{1.0%}	1.0	0.72	
			PC _{1.5%}	1.5	0.85	
ShengYue et al., 2014 [208]	Asphalt	Developing a new unidirectional heat-transfer asphalt pavement structure (UHT)	<i>Materials</i>		λ	Laboratory measurements show a decrease in surface temperature of 6.2°C (day) and 1.3°C (night) compared to conventional asphalt. Outdoor measurements show a decrease of 3.4°C (day) and 1.2°C (night)
			Conventional asphalt		1.0618	
			UHT	Top layer	1.1428	
				Middle layer	1.2007	
		Bottom layer	1.2544			
Yinfei et al., 2015 [209]	Asphalt	Developing a unidirectional heat-transfer asphalt pavement (UHT) and a bidirectional heat-induced asphalt pavement (BHI)	BHI pavement is obtained by applying a reflective coating on the UHT pavement to reduce the absorbed thermal energy and transfer the absorbed heat into the subsoil			Laboratory measurements show a temperature decrease at a depth of 4 cm of 2.38°C (day) for UHT and 7.76°C (day) for BHI compared to conventional asphalt
Dawson et al. 2012 [210]	Asphalt	Total replacement of limestone aggregates by quartzite	<i>Materials</i>		λ	Decrease of the surface temperature by up to 4°C
			Asphalt with 100% limestone aggregates		1.21	
			Asphalt with 100% quartzite aggregates		2.47	

⁽¹⁾ = volume fraction of materials added in pavements.

3.4.3. Pavements with energy harvesting systems

Energy harvesting is of great interest in a world facing an energy crisis and the depletion of natural resources. The study of road structures in order to capture energy and reuse it for their own needs or for those of their close environment is an avenue of research that is thriving. Energy harvesting involves the following procedure: energy collection, energy storage and energy use. The energy recovered by these systems can be used, for example, to produce electricity, to heat or cool buildings or to de-ice road surfaces.

The insertion of pipes for the circulation of heat transfer fluid, photovoltaic panels and thermoelectric generators are some of the techniques that allow energy capture with road structures and reduce their surface temperature. They are therefore a solution to reduce the risk of UHIs.

a) Pavements with fluid circulation systems

As the fluid circulates through the tubes, it absorbs the energy transferred to the pavement by solar radiation, which increases the temperature of the fluid in the tubes, which can be stored in geothermal systems or in well-insulated tanks [211]. Several numerical models have been developed to study the influence of various parameters on the energy performance of this system, such as the injection temperature of the fluid, the depth and the spacing between the tubes [210]–[215].

Asfour et al. [216] have numerically and experimentally studied a new hydraulic heating and energy harvesting system in a pavement that does not contain tubes (Fig. 11). This system consists of circulating water in a permeable asphalt layer under the wearing course with an undrained base. This study shows that this system, by injecting water during summer, can effectively decrease the surface temperature by up to 23°C [217].

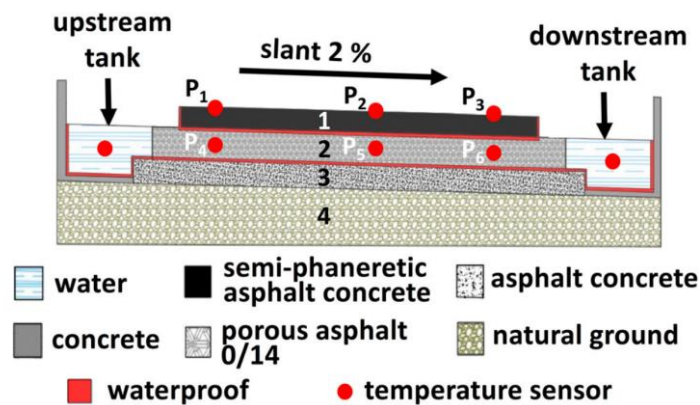


Fig. 11. Diagram of the pavement structure [216].

Several studies have investigated the use of convection-powered airflows to control pavement temperature [218]–[220]. By using air as a fluid instead of liquids, it is possible to dispense with electrical machines for the circulation of the fluid and thus prevent disaster in case of pipe rupture [221]. This system allows both cooling of a hot pavement [218]–[221] and heating of a cold pavement [219]. It can reduce the temperature of asphalt pavements by up to 6°C.

b) Thermoelectric pavements

Thermoelectric generators harvest thermal energy from the thermal gradients of the pavement substructure. This technique can be used to harvest thermal energy from the pavement and transform it into electricity [211]. This transformation into electricity is based on the phenomenon discovered in 1821, called the Seebeck effect [222]. Jiang et al. [223] developed a new road thermoelectric generator system that integrates three modules into the asphalt pavement structure: thermoelectric-conversion, heat-conduction and cold-end cooling. The results show that this system reduces the surface temperature of asphalt pavements by 8 to 9°C during hot weather.

c) Pavements with photovoltaic applications

Photovoltaic pavement coatings lower the surface temperature, whilst also generating large quantities of energy which could be injected into the electricity grid to help meet high demand.

Efthymiou et al. [224] show that the use of photovoltaic coatings decrease the road surface temperature by 2 to 5°C, and also cool the ambient air by 0.5 to 1°C. These results are in keeping with those found by a recent study [225], which shows that this type of material can reduce surface temperature by 3 to 5°C during heatwaves. In addition, these materials generate 11 to 12% less heat in different weather conditions.

4. Overview and discussion

In the present work, several types of cool pavement were presented in a synthetic way. The thermal proprieties and the main factors that influence the cooling effect of these pavements were analyzed. Each technique aims to reduce the temperature of UHIs but the cooling performance varies from a pavement to another.

Fig. 12 presents the maximum surface temperature reduction corresponding to the use of the different types of cool pavements presented above. The temperature reduction presented in Fig. 12 is in comparison to: ⁽¹⁾ conventional concrete pavement; ⁽²⁾ conventional asphalt pavement; ⁽³⁾ pavement in dry conditions; ⁽⁴⁾ permeable asphalt pavement; and ⁽⁵⁾ conventional pervious concrete pavement.

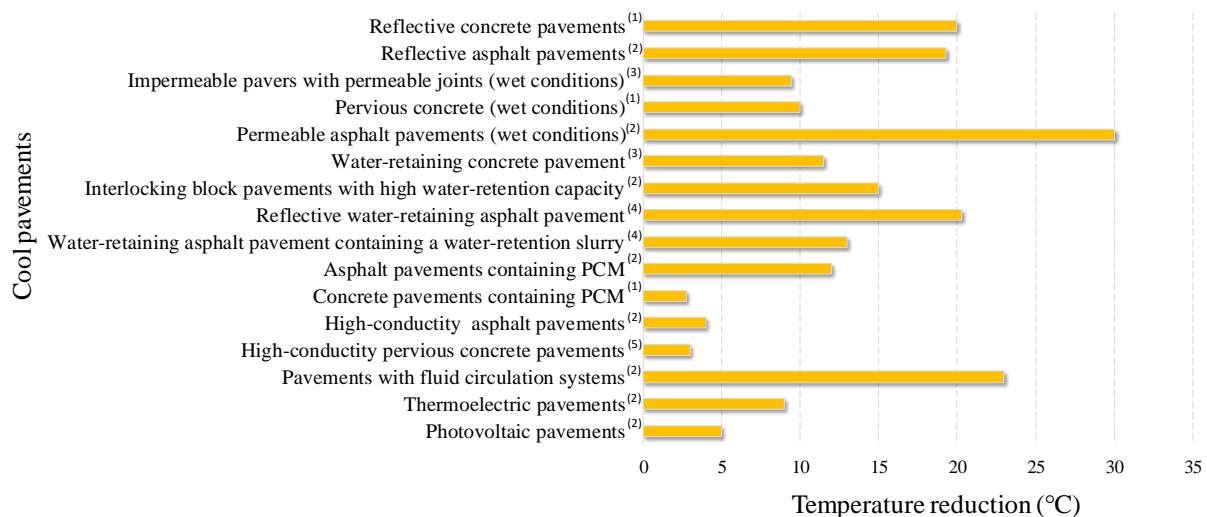


Fig. 12. Cooling performance of different types of cool pavements.

Fig. 12 shows that reflective and evaporative pavements have more influence on the development of cool pavements to mitigate UHIs than pavements with high thermal conductivity. In addition, pavements with high thermal conductivity emit less instantaneous sensible heat during the day, but more during the night. This can affect residents' thermal comfort during the night and aggravate the problem of nocturnal UHIs.

It is important to mention that the cooling performance of several types of pavements shown in Fig. 12 is not always assured, and is dependent upon several factors. Indeed, the cooling performance of evaporative pavements is conditioned by the availability of water near the surface. Periodic watering of these pavements is essential to guarantee a significant cooling effect at all times compared to conventional impermeable pavements. One of the main limitations to the use of evaporative permeable pavements is their low mechanical strength which limits their use in roadways due to their high porosity. Further studies are essential to

design permeable pavements with optimal porosity that provides high mechanical strength, adequate permeability and high cooling performance.

It must be noted that reflective pavements are only effective if the incident radiation is reflected back to the atmosphere, otherwise the reflected radiation may affect the thermal comfort of pedestrians. In addition, the cooling performance of these pavements is limited by pollution, which reduces the albedo and affects durability. Recent developments in the field of reflective pavements should help overcome some of these limitations.

Fig. 12 also shows that asphalt and concrete pavements containing PCM can reduce surface temperature. In general, PCM is introduced into pavements in an encapsulated form, which may break under heavy traffic loads, thus affecting the cooling performance of this type of pavement [194]. In addition, the PCM and the encapsulating medium must be able to withstand the high temperatures of the asphalt mixture during mixing, laying and compaction [226].

At the city level, to reduce the formation of heat islands and improve the quality of life in urban areas, there are solutions that are beneficial to health, the environment and quality of life. One of these solutions is to reduce the emission of anthropogenic heat. Indeed, energy consumption in buildings represents 35% of greenhouse gas emissions (case of Montreal) [42]. In order to reduce energy demand, it is necessary to use energy-efficient appliances and maximize the use of natural light. It is also necessary to favor less polluting public transportation that does not promote smog, and limit the traffic of individual vehicles in city centers. In addition, we can improve our choice of materials. We must also promote passive air conditioning, bioclimatic architecture, promote insulation and limit electric air conditioners.

This article shows that pavements can also be used to mitigate UHIs. First of all, it is necessary to reduce the use of asphalt and concrete with techniques that exist today, such as the promotion of vegetated parking lots, roofs and walls, as well as the vegetation of the sides of buildings and roadsides, in addition to integrating green spaces into development projects. It is also necessary to reduce the impermeabilization of cities, because the return of water to the ground and to storage surfaces helps to cool the air, reduces the UHI effect and improves the thermal comfort of individuals by evapotranspiration. This phenomenon is most significant in cities, especially during periods of high heat that may worsen with climate change. Therefore, it is important to use permeable pavements and choose materials according to their albedo.

Finally, the mechanical strength of pavements can be affected by the incorporation of energy-harvesting system components [227]. Additional techniques must be used to ensure that this type of pavement is able to withstand heavy traffic loads [228]. These energy-harvesting components must be protected and maintained regularly. Maintenance techniques, such as overlaying, milling, and trenching, can also affect the thermal and structural efficiency of this type of pavement [227].

From this review, it appears that it is necessary to choose the type of cool pavement according to the constraints and the climatic and geographical conditions of each city. In order to optimize the choice of cool pavement, future studies should focus on some topics that have not been sufficiently studied in the literature, such as durability and life cycle analysis of cool pavements. Moreover, in order to maximize the cooling effect, it will be useful to study the cooling effect of pavements that combine several cooling pavement technologies (for example, evaporative and reflective pavements). Numerical simulations should also be developed to evaluate the

effectiveness of cool pavements. Since many factors influence their cooling performance which is also affected by the site conditions where they are implemented, these numerical simulations must be validated by field experiments.

5. Conclusion

A great deal of research is being conducted to better document, understand and mitigate urban heat islands. New materials, systems and technologies have been developed and proposed to decrease the sensible heat flux to the atmosphere from various urban structures. In recent years, researchers working on pavement technologies have begun to study their thermal properties with the aim of using them to mitigate urban heat islands. This article reviews the majority of existing cool-pavement technologies. Thermal characteristics, cooling performance and factors affecting this performance, as well as limitations regarding the implementation of these pavements, have been discussed. The following conclusions can be drawn to summarize the basic findings of this review:

The use of reflective pavements is an effective strategy for mitigating UHIs and improving the microclimate. The reflectivity of traditional pavements can be increased by applying either a suitable white reflective coating, thermochromic coating or retroreflective coating materials, colored high-reflectivity coatings, or a suitable binder. The application of these techniques must take account of cost effectiveness, aging, and pavement adhesion. Additional research is needed to evaluate glare and potential light pollution. In addition, the overall reflective performance of these techniques should be further evaluated to ensure thermal comfort and driving safety in practical applications. However, there are no standards in place, as yet, for the performance of reflective pavements.

All types of evaporative pavements: porous vegetated pavers, impermeable pavers with permeable joints, pervious concrete, permeable asphalt pavements, and water-retaining pavements, are capable of reducing their surface temperature during the day and night. The availability of water near the surface, watering time, water absorption coefficient, water retention capacity, and capillary rise are the key factors that influence the evaporative cooling performance of evaporative pavements. The availability of water is therefore a primary condition that determines the thermal performance of these pavements. These pavements must be watered regularly to guarantee a significant cooling effect over an extended period. In dry conditions, permeable pavements can have a higher surface temperature than conventional dense pavements. It has been found that the use of permeable pavements should be avoided in countries with dry summers and where watering is complicated to implement.

Increasing the thermal conductivity of the pavements ensures a lower temperature during the day, but leads to a higher temperature during the night when the stored heat is released by diffusion. This technique can aggravate the problem of nocturnal urban heat islands. Pavements containing phase-change materials and energy-harvesting pavements can improve the urban microclimate. They require a higher initial cost and more complex construction procedures than evaporative and reflective pavements. Further research is needed to improve the efficiency of these pavements to justify the high initial investment.

The influence of porosity on the mechanical and hydraulic behavior of permeable pavements has been extensively studied in the literature. Future studies need to focus on investigating the effect of pore characteristics such as size, distribution, shape and tortuosity on the thermal

behavior of permeable pavements. These studies will lead to the design of pavements with good mechanical, hydraulic and cooling performances. In addition, it is necessary to develop pavements that combine several cooling pavement technologies such as, for example, a reflective and permeable pavement, having thermal conductivity in order to maximize the cooling effect.

Acknowledgements

The authors would like to thank the Auvergne Regional Council (France) and the European ERDF funding program for their financial support of this work through the CPER ECOMAT program.

Bibliography

- [1] J. Fahed, “Etude numérique du potentiel de rafraîchissement des techniques de réduction des îlots de chaleur urbain (ICU) sous climat méditerranéen”, doctoral dissertation, Toulouse, INSA, 2019.
- [2] E. Klinenberg, “Heat wave: A social autopsy of disaster in Chicago”. University of Chicago press, 2015.
- [3] A. Fouillet *et al.*, “Excess mortality related to the August 2003 heat wave in France”, *Int. Arch. Occup. Environ. Health*, vol. 80, no. 1, pp. 16–24, 2006.
- [4] M.-M. Huynen, P. Martens, D. Schram, M. P. Weijenberg, and A. E. Kunst, “The impact of heat waves and cold spells on mortality rates in the Dutch population”, *Environ. Health Perspect.*, vol. 109, no. 5, pp. 463–470, 2001.
- [5] G. B. Anderson and M. L. Bell, “Heat waves in the United States: mortality risk during heat waves and effect modification by heat wave characteristics in 43 US communities”, *Environ. Health Perspect.*, vol. 119, no. 2, pp. 210–218, 2011.
- [6] J. Tan *et al.*, “The urban heat island and its impact on heat waves and human health in Shanghai”, *Int. J. Biometeorol.*, vol. 54, no. 1, pp. 75–84, 2010.
- [7] J. Yang, L. Hu, and C. Wang, “Population dynamics modify urban residents’ exposure to extreme temperatures across the United States”, *Sci. Adv.*, vol. 5, no. 12, p. eaay3452, 2019.
- [8] S. W. Kim and R. D. Brown, “Urban heat island (UHI) intensity and magnitude estimations: A systematic literature review”, *Sci. Total Environ.*, vol. 779, p. 146389, 2021.
- [9] F. Bassani, V. Garbero, D. Poggi, L. Ridolfi, J. von Hardenberg, and M. Milelli, “An innovative approach to select urban-rural sites for Urban Heat Island analysis: the case of Turin (Italy)”, *Urban Clim.*, vol. 42, no. September 2021, p. 101099, 2022, doi: 10.1016/j.uclim.2022.101099.
- [10] C. Wang, Z. H. Wang, K. E. Kaloush, and J. Shacat, “Cool pavements for urban heat island mitigation: A synthetic review”, *Renew. Sustain. Energy Rev.*, vol. 146, no. October 2020, p. 111171, 2021, doi: 10.1016/j.rser.2021.111171.
- [11] P. E. Phelan *et al.*, “Urban heat island: mechanisms, implications, and possible remedies”, *Annu. Rev. Environ. Resour.*, vol. 40, pp. 285–307, 2015.
- [12] H. Akbari and D. Kolokotsa, “Three decades of urban heat islands and mitigation technologies research”, *Energy Build.*, vol. 133, pp. 834–842, 2016.
- [13] T. Asaeda and V. T. Ca, “Characteristics of permeable pavement during hot summer weather and impact on the thermal environment”, *Build. Environ.*, vol. 35, no. 4, pp. 363–375, 2000, doi: 10.1016/S0360-1323(99)00020-7.
- [14] J. Chen, R. Chu, H. Wang, L. Zhang, X. Chen, and Y. Du, “Alleviating urban heat island effect using high-conductivity permeable concrete pavement”, *J. Clean. Prod.*, vol. 237, p. 117722, 2019, doi: 10.1016/j.jclepro.2019.117722.
- [15] T. Asaeda, V. T. Ca, and A. Wake, “Heat storage of pavement and its effect on the lower atmosphere”, *Atmos. Environ.*, vol. 30, no. 3, pp. 413–427, 1996.
- [16] T. Oke “The energetic basis of urban heat island”, *Quarterly Journal of the Royal Meteorological Society*, 1982, vol. 108, no 455, p. 1-24.
- [17] Y. Azzout, S. Barraud, F. N. Cres, and E. Alfakih, “Techniques Alternatives en Assainissement Pluvial”, *Technique et Documentation*. p. 372, 1994.
- [18] J. L. Bertrand-Krajewski, “Cours d’hydrologie urbaine”, INSA Lyon, 2006.
- [19] M. Hendel, “Cool pavements”, *Eco-efficient pavement construction materials*. Woodhead Publishing, 2020. p. 97-125.

- [20] H. Taha, “Urban climates and heat islands: Albedo, evapotranspiration, and anthropogenic heat”, *Energy Build.*, vol. 25, no. 2, pp. 99–103, 1997, doi: 10.1016/s0378-7788(96)00999-1.
- [21] H. Akbari, M. Pomerantz, and H. Taha, “Cool surfaces and shade trees to reduce energy use and improve air quality in urban areas”, *Sol. Energy*, vol. 70, no. 3, pp. 295–310, 2001, doi: 10.1016/S0038-092X(00)00089-X.
- [22] J. Chen, Z. Zhou, J. Wu, S. Hou, and M. Liu, “Field and laboratory measurement of albedo and heat transfer for pavement materials”, *Constr. Build. Mater.*, vol. 202, pp. 46–57, 2019, doi: 10.1016/j.conbuildmat.2019.01.028.
- [23] A. Synnefa, T. Karlessi, N. Gaitani, M. Santamouris, D. N. Assimakopoulos, and C. Papakatsikas, “Experimental testing of cool colored thin layer asphalt and estimation of its potential to improve the urban microclimate”, *Build. Environ.*, vol. 46, no. 1, pp. 38–44, 2011, doi: 10.1016/j.buildenv.2010.06.014.
- [24] E. Carnielo and M. Zinzi, “Optical and thermal characterisation of cool asphalts to mitigate urban temperatures and building cooling demand”, *Build. Environ.*, vol. 60, pp. 56–65, 2013, doi: 10.1016/j.buildenv.2012.11.004.
- [25] N. A. A. Guntor, M. Fadhil, M. Ponraj, and K. Iwao, “Thermal performance of developed coating material as cool pavement material for tropical regions”, *J. Mater. Civ. Eng.*, vol. 26, no. 4, pp. 755–760, 2014, doi: 10.1061/(ASCE)MT.1943-5533.0000859.
- [26] Y. Qin, “A review on the development of cool pavements to mitigate urban heat island effect”, *Renew. Sustain. Energy Rev.*, vol. 52, pp. 445–459, 2015, doi: 10.1016/j.rser.2015.07.177.
- [27] Y. Qin and J. E. Hiller, “Water availability near the surface dominates the evaporation of pervious concrete”, *Constr. Build. Mater.*, vol. 111, pp. 77–84, 2016, doi: 10.1016/j.conbuildmat.2016.02.063.
- [28] H. Li, J. T. Harvey, T. J. Holland, and M. Kayhanian, “Erratum: The use of reflective and permeable pavements as a potential practice for heat island mitigation and stormwater management”, *Environ. Res. Lett.*, vol. 8, no. 4, 2013, doi: 10.1088/1748-9326/8/4/049501.
- [29] J. Wang, Q. Meng, K. Tan, L. Zhang, and Y. Zhang, “Experimental investigation on the influence of evaporative cooling of permeable pavements on outdoor thermal environment”, *Build. Environ.*, vol. 140, no. January, pp. 184–193, 2018, doi: 10.1016/j.buildenv.2018.05.033.
- [30] A. Karasawa, K. Toriiminami, N. Ezumi, and K. Kamaya, “Evaluation of Performance of Water-Retentive Concrete Block Pavements”, *8th Int. Conf. Concr. Block Paving*, pp. 233–242, 2006.
- [31] E. M. Nemirovsky, A. L. Welker, and R. Lee, “Quantifying evaporation from pervious concrete systems: Methodology and hydrologic perspective”, *J. Irrig. Drain. Eng.*, vol. 139, no. 4, pp. 271–277, 2013, doi: 10.1061/(ASCE)IR.1943-4774.0000541.
- [32] M. Z. Chen, J. Hong, S. P. Wu, W. Lu, and G. J. Xu, “Optimization of phase change materials used in asphalt pavement to prevent rutting”, *Adv. Mater. Res.*, vol. 219–220, pp. 1375–1378, 2011, doi: 10.4028/www.scientific.net/AMR.219-220.1375.
- [33] N. P. Sharifi and K. C. Mahboub, “Application of a PCM-rich concrete overlay to control thermal induced curling stresses in concrete pavements”, *Constr. Build. Mater.*, vol. 183, pp. 502–512, 2018, doi: 10.1016/j.conbuildmat.2018.06.179.
- [34] A. Arora, G. Sant, and N. Neithalath, “Numerical simulations to quantify the influence of phase change materials (PCMs) on the early- and later-age thermal response of concrete pavements”, *Cem. Concr. Compos.*, vol. 81, pp. 11–24, 2017, doi: 10.1016/j.cemconcomp.2017.04.006.
- [35] K. FULADLU, M. RİZA, and M. İLKAN, “the Effect of Rapid Urbanization on the Physical Modification of Urban Area”, pp. 1–9, 2018, doi: 10.14621/tna.
- [36] T. Plocoste, “Étude de la dispersion nocturne de polluants atmosphériques issus d’une décharge d’ordures ménagères mise en évidence d’un îlot de chaleur urbain”, doctoral dissertation, Antilles-Guyane, 2013, doi: 10.13140/2.1.4639.7765.
- [37] S. Sangkertadi and R. Syafriny, “New Equation for Estimating Outdoor Thermal Comfort in Humid-Tropical Environment”, *Eur. J. Sustain. Dev.*, vol. 3, no. 4, p. 43, 2014.
- [38] R. Kotharkar, A. Bagade, and A. Ramesh, “Assessing urban drivers of canopy layer urban heat island: A numerical modeling approach”, *Landsc. Urban Plan.*, vol. 190, p. 103586, 2019.
- [39] M. Santamouris, “Cooling the cities—a review of reflective and green roof mitigation technologies to fight heat island and improve comfort in urban environments”, *Sol. energy*, vol. 103, pp. 682–703, 2014.
- [40] K. Nagashima, K. Tokizawa, and S. Marui, “Thermal comfort”, *Handbook of Clinical Neurology*, vol. 156, pp. 249–260, 2018, doi: 10.1016/B978-0-444-63912-7.00015-1.
- [41] M. Giguère, “Mesures de lutte aux îlots de chaleur urbains”, *desLibris*, 2009.
- [42] P. Anquez and A. Herlem, “Les îlots de chaleur dans la région métropolitaine de Montréal : causes , impacts et solutions”, Chaire de responsabilité sociale et de développement durable, UQAM, 2011.
- [43] Y. Xia *et al.*, “Assessment of the economic impacts of heat waves: a case study of Nanjing, China”, *J.*

- Clean. Prod.*, vol. 171, pp. 811–819, 2018.
- [44] A. Abolata, “Vegetation in different street orientations of aspect ratio (H/W 1: 1) to mitigate UHI and reduce buildings’ energy in arid climate”, *Build. Environ.*, vol. 172, p. 106712, 2020.
- [45] A. Mohajerani, J. Bakaric, and T. Jeffrey-Bailey, “The urban heat island effect, its causes, and mitigation, with reference to the thermal properties of asphalt concrete”, *J. Environ. Manage.*, vol. 197, pp. 522–538, 2017, doi: 10.1016/j.jenvman.2017.03.095.
- [46] G. Evola *et al.*, “UHI effects and strategies to improve outdoor thermal comfort in dense and old neighbourhoods”, *Energy Procedia*, vol. 134, pp. 692–701, 2017.
- [47] B.-J. He, “Towards the next generation of green building for urban heat island mitigation: Zero UHI impact building”, *Sustain. Cities Soc.*, vol. 50, p. 101647, 2019.
- [48] Z. Fang, W. Guo, J. Zhang, and X. Lou, “Influence of Heat Events on the Composition of Airborne Bacterial Communities in Urban Ecosystems”, *International journal of environmental research and public health*, 2018, doi: 10.3390/ijerph15102295.
- [49] U. Nations, “World urbanization prospects: The 2014 revision, highlights. department of economic and social affairs”, *Popul. Div. United Nations*, vol. 32, 2014.
- [50] J. J. Stempihar, T. Pourshams-Manzouri, K. E. Kaloush, and M. C. Rodezno, “Porous asphalt pavement temperature effects for urban heat island analysis”, *Transp. Res. Rec.*, vol. 2293, no. 1, pp. 123–130, 2012.
- [51] Y. Yamamoto, “Measures to Mitigate Urban Heat Islands”, *Environ. Energy Res. Unit. Quaterly Rev.*, vol. 18, pp. 65–83, 2005.
- [52] X. He *et al.*, “Observational and modeling study of interactions between urban heat island and heatwave in Beijing”, *J. Clean. Prod.*, vol. 247, p. 119169, 2020.
- [53] M. F. Shahidan, P. J. Jones, J. Gwilliam, and E. Salleh, “An evaluation of outdoor and building environment cooling achieved through combination modification of trees with ground materials”, *Build. Environ.*, vol. 58, pp. 245–257, 2012.
- [54] M. Santamouris, “Using cool pavements as a mitigation strategy to fight urban heat island - A review of the actual developments”, *Renew. Sustain. Energy Rev.*, vol. 26, pp. 224–240, 2013, doi: 10.1016/j.rser.2013.05.047.
- [55] M. Petralli, L. Massetti, G. Brandani, and S. Orlandini, “Urban planning indicators: useful tools to measure the effect of urbanization and vegetation on summer air temperatures”, *Int. J. Climatol.*, vol. 34, no. 4, pp. 1236–1244, 2014.
- [56] L. P. Wong, H. Alias, N. Aghamohammadi, S. Aghazadeh, and N. M. N. Sulaiman, “Urban heat island experience, control measures and health impact: A survey among working community in the city of Kuala Lumpur”, *Sustain. cities Soc.*, vol. 35, pp. 660–668, 2017.
- [57] S. GRIMMOND, “Urbanization and global environmental change: local effects of urban warming”, *The Geographical Journal*, 2007, vol. 173, no 1, p. 83-88.
- [58] R. Giridharan and R. Emmanuel, “The impact of urban compactness, comfort strategies and energy consumption on tropical urban heat island intensity: A review”, *Sustain. cities Soc.*, vol. 40, pp. 677–687, 2018.
- [59] C. Yuan, A. S. Adelia, S. Mei, W. He, X.-X. Li, and L. Norford, “Mitigating intensity of urban heat island by better understanding on urban morphology and anthropogenic heat dispersion”, *Build. Environ.*, vol. 176, p. 106876, 2020.
- [60] R. Kotharkar and M. Surawar, “Land use, land cover, and population density impact on the formation of canopy urban heat islands through traverse survey in the Nagpur urban area, India”, *J. Urban Plan. Dev.*, vol. 142, no. 1, p. 4015003, 2016.
- [61] Y. Hirano and Y. Yoshida, “Assessing the effects of CO2 reduction strategies on heat islands in urban areas”, *Sustain. Cities Soc.*, vol. 26, pp. 383–392, 2016.
- [62] T. R. Oke, “City size and the urban heat island”, *Atmos. Environ.*, vol. 7, no. 8, pp. 769–779, 1973.
- [63] K. A. Birzeit, “Iterative Linear Approach for Nonlinear Nonhomogenous Stochastic Pavement Management Models Iterative Linear Approach for Nonlinear Nonhomogenous”, *J. Transp. Eng.*, vol. 2, no. February 2006, 2006, doi: 10.1061/(ASCE)0733-947X(2006)132.
- [64] F. Praticò, M. Giunta, C. Marino, and A. Attinà, “Pavement albedo and sustainability: An experimental investigation”, *7th Int. Conf. Maint. Rehabil. Pavements Technol. Control. MAIREPAV 2012*, no. August, 2012.
- [65] Y. Qin, “Urban canyon albedo and its implication on the use of reflective cool pavements”, *Energy Build.*, vol. 96, pp. 86–94, 2015, doi: 10.1016/j.enbuild.2015.03.005.
- [66] S. Dumais and G. Doré, “An albedo based model for the calculation of pavement surface temperatures in permafrost regions”, *Cold Reg. Sci. Technol.*, vol. 123, pp. 44–52, 2016, doi: 10.1016/j.coldregions.2015.11.013.

- [67] M. L. Marceau and M. G. Vangeem, “Solar Reflectance of Concretes for LEED Sustainable Sites Credit : Heat Island Effect”, *PCA R&D Ser. No. 2982*, no. 2982, p. 94, 2007.
- [68] R. Levinson and H. Akbari, “Solar Reflectance of Cool Paving Materials Effects of Composition and Exposure on Albedo of Concrete”, *Cem. Concr. Res.*, vol. 32, pp. 2001–2002, 2002.
- [69] K. Boriboonsomsin and F. Reza, “Mix design and benefit evaluation of high solar reflectance concrete for pavements”, *Transp. Res. Rec.*, vol. 2011, no. 1, pp. 11–20, 2007.
- [70] B. Terms, “Solar Reflectance Values for Concrete Intrinsic material properties can minimize the heat island effect”, vol. 2, no. August, pp. 52–58, 2008.
- [71] Y. Ma and B. Zhu, “Research on the preparation of reversibly thermochromic cement based materials at normal temperature”, *Cem. Concr. Res.*, vol. 39, no. 2, pp. 90–94, 2009, doi: 10.1016/j.cemconres.2008.10.006.
- [72] H. Zhang, Z. Chen, G. Xu, and C. Shi, “Physical, rheological and chemical characterization of aging behaviors of thermochromic asphalt binder”, *Fuel*, vol. 211, no. October 2017, pp. 850–858, 2018, doi: 10.1016/j.fuel.2017.09.111.
- [73] N. Tran, B. Powell, H. Marks, R. West, and A. Kvasnak, “Strategies for design and construction of high-reflectance asphalt pavements”, *Transp. Res. Rec.*, no. 2098, pp. 124–130, 2009, doi: 10.3141/2098-13.
- [74] C. Miao *et al.*, “A super-cooling solar reflective coating with waterborne polyurethane for asphalt pavement”, *Prog. Org. Coatings*, vol. 165, p. 106741, 2022.
- [75] C. Zhu *et al.*, “Dark, heat-reflective, anti-ice rain and superhydrophobic cement concrete surfaces”, *Constr. Build. Mater.*, vol. 220, pp. 21–28, 2019.
- [76] G. E. Kyriakodis and M. Santamouris, “Using reflective pavements to mitigate urban heat island in warm climates-Results from a large scale urban mitigation project”, *Urban Clim.*, vol. 24, pp. 326–339, 2018.
- [77] A. Sha, Z. Liu, K. Tang, and P. Li, “Solar heating reflective coating layer (SHRCL) to cool the asphalt pavement surface”, *Constr. Build. Mater.*, vol. 139, pp. 355–364, 2017.
- [78] F. Rosso *et al.*, “New cool concrete for building envelopes and urban paving: Optics-energy and thermal assessment in dynamic conditions”, *Energy Build.*, vol. 151, pp. 381–392, 2017.
- [79] W. Wan and W. Hien, “A study on the effectiveness of heat mitigating pavement coatings in Singapore”, *J. Heat Isl. Inst. Int.*, vol. 7, no. 2, pp. 238–247, 2012.
- [80] T. Karlessi, M. Santamouris, K. Apostolakis, A. Synnefa, and I. Livada, “Development and testing of thermochromic coatings for buildings and urban structures”, *Sol. Energy*, vol. 83, no. 4, pp. 538–551, 2009.
- [81] N. L. Alchapar, E. N. Correa, and M. A. Cantón, “Solar Reflectance Index of Pedestrian Pavements and Their Response to Aging”, *J. Clean Energy Technol.*, vol. 1, no. 4, pp. 281–285, 2013, doi: 10.7763/jocet.2013.v1.64.
- [82] H. Li, J. Harvey, and A. Kendall, “Field measurement of albedo for different land cover materials and effects on thermal performance”, *Build. Environ.*, vol. 59, pp. 536–546, 2013.
- [83] M. Santamouris, A. Synnefa, and T. Karlessi, “Using advanced cool materials in the urban built environment to mitigate heat islands and improve thermal comfort conditions”, *Sol. Energy*, vol. 85, no. 12, pp. 3085–3102, 2011.
- [84] M. Pomerantz, H. Akbari, S.-C. Chang, R. Levinson, and B. Pon, “Examples of cooler reflective streets for urban heat-island mitigation: Portland cement concrete and chip seals”, Lawrence Berkeley National Laboratory, 2003.
- [85] “Albedo: A Measure of Pavement Surface Reflectance”, American Concrete Pavement Association, USA, 2002.
- [86] M. Pomerantz, “The effect of pavements’ temperatures on air temperatures in large cities”, Lawrence Berkeley National Laboratory, Berkeley, CA 94720, 2000.
- [87] S. Sen and J. Roesler, “Aging albedo model for asphalt pavement surfaces”, *J. Clean. Prod.*, vol. 117, pp. 169–175, 2016, doi: 10.1016/j.jclepro.2016.01.019.
- [88] E. Z. Bean, W. F. Hunt, D. A. Bidelspach, and R. J. Burak, “Study on the infiltration rate of permeable pavements”, *Critical transitions in water and environmental resources management 2004*.
- [89] N. Jayasuriya and N. Kadurupokune, “Impact of Pervious Pavements on Drainage Infrastructure”, *Proceedings of 11th ICUD*, Melbourne, 31 August to 5 September 2008.
- [90] J. Faleyeux, “Elements modulaires en beton pour revêtement des ouvrages d’infiltration des eaux pluviales: référentiel technique”, *Epernon, Fr. CERIB*, 2015.
- [91] J. P. Christory and J. Abdo, “Voiries et aménagements urbains en beton-structures reservoirs et aménagements qualitatifs”, *Rev. Gen. des routes*, no. 775, 1999.
- [92] A. Dawson, “Water in road structures: movement, drainage & effects”, vol. 5. Springer Science & Business Media, 2008.

- [93] D. Thorpe and Y. Zhuge, “Advantages and disadvantages in using permeable concrete pavement as a pavement construction material”, *Assoc. Res. Constr. Manag. ARCOM 2010 - Proc. 26th Annu. Conf.*, no. September, pp. 1341–1350, 2010.
- [94] M. Kováč and A. Sičáková, “Pervious concrete as a sustainable solution for pavements in urban areas”, *10th Int. Conf. Environ. Eng. ICEE 2017*, vol. 2017-April, no. April, pp. 27–28, 2017, doi: 10.3846/enviro.2017.031.
- [95] K. W. Lee, V. O. Craver, S. Kohm, and H. Chango, “Cool pavements as a sustainable approach to green streets and highways”, *Green Streets and Highways 2010: An Interactive Conference on the State of the Art and How to Achieve Sustainable Outcomes*. 2010, vol. 389, pp. 235–247, 2010, doi: 10.1061/41148(389)20.
- [96] H. Takebayashi and M. Moriyama, “Study on the urban heat island mitigation effect achieved by converting to grass-covered parking”, *Sol. Energy*, vol. 83, no. 8, pp. 1211–1223, 2009, doi: 10.1016/j.solener.2009.01.019.
- [97] T. Lucke and S. Beecham, “Field investigation of clogging in a permeable pavement system”, *Build. Res. Inf.*, vol. 39, no. 6, pp. 603–615, 2011, doi: 10.1080/09613218.2011.602182.
- [98] M. R. Thompson, B. J. Dempsey, H. Hill, and J. Vogel, “Characterizing Temperature Effects for Pavement Analysis and Design”, *Transportation Research Record*. pp. 14–22, 1987.
- [99] C. T. Andersen, I. D. L. Foster, and C. J. Pratt, “The role of urban surfaces (permeable pavements) in regulating drainage and evaporation: Development of a laboratory simulation experiment”, *Hydrol. Process.*, vol. 13, no. 4, pp. 597–609, 1999, doi: 10.1002/(SICI)1099-1085(199903)13:4<597::AID-HYP756>3.0.CO;2-Q.
- [100] Y. Liu, T. Li, and H. Peng, “A new structure of permeable pavement for mitigating urban heat island”, *Sci. Total Environ.*, vol. 634, pp. 1119–1125, 2018.
- [101] Y. Liu, T. Li, and L. Yu, “Urban heat island mitigation and hydrology performance of innovative permeable pavement: A pilot-scale study”, *J. Clean. Prod.*, vol. 244, p. 118938, 2020, doi: 10.1016/j.jclepro.2019.118938.
- [102] D. H. Nguyen, “Etude du comportement hydromécanique des bétons drainants à base de coproduits coquilliers”, doctoral dissertation, Caen, 2014.
- [103] N. Neithalath, M. S. Sumanasooriya, and O. Deo, “Characterizing pore volume, sizes, and connectivity in pervious concretes for permeability prediction”, *Mater. Charact.*, vol. 61, no. 8, pp. 802–813, 2010, doi: 10.1016/j.matchar.2010.05.004.
- [104] L. K. Crouch, J. Pitt, and R. Hewitt, “Aggregate effects on pervious portland cement concrete static modulus of elasticity”, *J. Mater. Civ. Eng.*, vol. 19, no. 7, pp. 561–568, 2007, doi: 10.1061/(ASCE)0899-1561(2007)19:7(561).
- [105] A. Kia, H. S. Wong, and C. R. Cheeseman, “Clogging in permeable concrete: A review”, *J. Environ. Manage.*, vol. 193, pp. 221–233, 2017, doi: 10.1016/j.jenvman.2017.02.018.
- [106] A. C. I. (American C. Institute), “Report on pervious concrete”, 2010.
- [107] J. Shan, Y. Zhang, S. Wu, Z. Lin, L. Li, and Q. Wu, “Pore characteristics of pervious concrete and their influence on permeability attributes”, *Constr. Build. Mater.*, vol. 327, no. February, p. 126874, 2022, doi: 10.1016/j.conbuildmat.2022.126874.
- [108] L. G. Li *et al.*, “Effects of aggregate bulking and film thicknesses on water permeability and strength of pervious concrete”, *Powder Technol.*, vol. 396, pp. 743–753, 2022, doi: 10.1016/j.powtec.2021.11.019.
- [109] S. Park, S. Ju, H.-K. Kim, Y.-S. Seo, and S. Pyo, “Effect of the rheological properties of fresh binder on the compressive strength of pervious concrete”, *J. Mater. Res. Technol.*, 2022.
- [110] S. K. Pradhan and N. Behera, “Performance assessment of pervious concrete road on strength and permeability by using silica fume”, *Mater. Today Proc.*, 2022.
- [111] H.-Q. Nguyen, B.-V. Tran, and T.-S. Vu, “Numerical approach to predict the flexural damage behavior of pervious concrete”, *Case Stud. Constr. Mater.*, vol. 16, p. e00946, 2022.
- [112] O. AlShareedah and S. Nassiri, “Spherical discrete element model for estimating the hydraulic conductivity and pore clogging of pervious concrete”, *Constr. Build. Mater.*, vol. 305, p. 124749, 2021.
- [113] V.-H. Vu, B.-V. Tran, B.-A. Le, and H.-Q. Nguyen, “Prediction of the relationship between strength and porosity of pervious concrete: A micromechanical investigation”, *Mech. Res. Commun.*, vol. 118, p. 103791, 2021.
- [114] ACI 552R-10, “Report on pervious concrete, American concrete institute”, 2010.
- [115] “Freeze thaw resistance of pervious concrete”, National Ready Mixed Concrete Association, 2004.
- [116] P. D. Tennis, M. L. Leming, and D. J. Akers, “Pervious concrete pavements”, portland cement association, 2004.
- [117] A. K. Chandrappa and K. P. Biligiri, “Comprehensive investigation of permeability characteristics of

- pervious concrete: A hydrodynamic approach”, *Constr. Build. Mater.*, vol. 123, pp. 627–637, 2016, doi: 10.1016/j.conbuildmat.2016.07.035.
- [118] V. R. Schaefer and K. Wang, “Mix design development for pervious concrete in cold weather climates”, Iowa. dept. of transportation, Highway division, 2006.
- [119] Probeton, PTV 122, “Prescriptions techniques pour les pavés et dalles en béton perméables à l’eau”, 3ème édition, 12 p., 2009.
- [120] K. Wang, V. R. Schaefer, J. T. Kevern, and M. T. M. M. T. Suleiman, “Development of Mix Proportion for Functional and Durable Pervious Concrete”, *NRMCA Technol. Forum Focus Pervious Concr.*, no. December, pp. 1–12, 2006.
- [121] Y. Joung and Z. Grasley, “Evaluation and optimization of durable pervious concrete for use in urban areas”, Research report SWUTC/08/167163-1. 82 p., vol. 7, no. 2, p. 82, 2008.
- [122] R. Zhang, G. Jiang, and J. Liang, “The Albedo of Pervious Cement Concrete Linearly Decreases with Porosity”, *Adv. Mater. Sci. Eng.*, vol. 2015, 2015, doi: 10.1155/2015/746592.
- [123] J. Chen, H. Wang, P. Xie, and H. Najm, “Analysis of thermal conductivity of porous concrete using laboratory measurements and microstructure models”, *Constr. Build. Mater.*, vol. 218, pp. 90–98, 2019, doi: 10.1016/j.conbuildmat.2019.05.120.
- [124] S. Liu, L. Lu, D. Mao, and L. Jia, “Evaluating parameterizations of aerodynamic resistance to heat transfer using field measurements”, *Hydrol. Earth Syst. Sci.*, vol. 11, no. 2, pp. 769–783, 2007, doi: 10.5194/hess-11-769-2007.
- [125] P. Starke, P. Göbel, and W. G. Coldewey, “Urban evaporation rates for water-permeable pavements”, *Water Sci. Technol.*, vol. 62, no. 5, pp. 1161–1169, 2010, doi: 10.2166/wst.2010.390.
- [126] C. Syrrakou and G. F. Pinder, “Experimentally determined evaporation rates in pervious concrete systems”, *J. Irrig. Drain. Eng.*, vol. 140, no. 1, pp. 1–6, 2014, doi: 10.1061/(ASCE)IR.1943-4774.0000652.
- [127] J. Wei and J. He, “Numerical simulation for analyzing the thermal improving effect of evaporative cooling urban surfaces on the urban built environment”, *Appl. Therm. Eng.*, vol. 51, no. 1–2, pp. 144–154, 2013, doi: 10.1016/j.applthermaleng.2012.08.064.
- [128] E. M. Nemirovsky, A. L. Welker, and R. G. Traver, “Evaporation from a pervious concrete stormwater control measure: Parameterization, quantifying and evaluation”, *World Environmental and Water Resources Congress 2011: Bearing Knowledge for Sustainability*. 2011. p. 3610-3619.
- [129] H. Li, J. Harvey, and Z. Ge, “Experimental investigation on evaporation rate for enhancing evaporative cooling effect of permeable pavement materials”, *Constr. Build. Mater.*, vol. 65, pp. 367–375, 2014, doi: 10.1016/j.conbuildmat.2014.05.004.
- [130] H. Li, “Chapter 7 - Evaporation Rate and Evaporative Cooling Effect of Pavement Materials”, *Pavement Materials for Heat Island Mitigation*, H. Li, Ed. Boston: Butterworth-Heinemann, 2016, pp. 135–153.
- [131] N. Tziampou, S. J. Coupe, L. A. Sañudo-fontaneda, A. P. Newman, and D. Castro-fresno, “Fluid transport within permeable pavement systems : A review of evaporation processes , moisture loss measurement and the current state of knowledge”, *Constr. Build. Mater.*, vol. 243, p. 118179, 2020, doi: 10.1016/j.conbuildmat.2020.118179.
- [132] P. Göbel, P. Starke, and W. G. Coldewey, “Evaporation measurements on enhanced water-permeable paving in urban areas Keywords”, pp. 1–8, 2008.
- [133] T. Tang, K. Anupam, C. Kasbergen, A. Scarpas, and S. Erkens, “A finite element study of rain intensity on skid resistance for permeable asphalt concrete mixes”, *Constr. Build. Mater.*, vol. 220, pp. 464–475, 2019.
- [134] R. Tanzadeh, J. Tanzadeh, and S. A. Tahami, “Experimental study on the effect of basalt and glass fibers on behavior of open-graded friction course asphalt modified with nano-silica”, *Constr. Build. Mater.*, vol. 212, pp. 467–475, 2019.
- [135] P. Lastra-González, I. Indacoechea-Vega, M. A. Calzada-Pérez, D. Castro-Fresno, and J. Carpio-García, “Analysis of the skid resistance and adherence between layers of asphalt concretes modified by dry way with polymeric waste”, *Constr. Build. Mater.*, vol. 133, pp. 163–170, 2017.
- [136] S. H. A. Ai-min and J. Wei, “Design philosophy and architecture of eco-friendly porous pavement materials”, *China J. Highw. Transp.*, vol. 31, no. 9, p. 1, 2018.
- [137] N. Qian, D. Wang, D. Li, and L. Shi, “Three-dimensional mesoscopic permeability of porous asphalt mixture”, *Constr. Build. Mater.*, vol. 236, p. 117430, 2020.
- [138] M. Kayhanian, H. Li, J. T. Harvey, and X. Liang, “Application of permeable pavements in highways for stormwater runoff management and pollution prevention: California research experiences”, *Int. J. Transp. Sci. Technol.*, vol. 8, no. 4, pp. 358–372, 2019.
- [139] R. J. Charbeneau, J. B. Klenzendorf, and M. E. Barrett, “Methodology for determining laboratory and in

- situ hydraulic conductivity of asphalt permeable friction course”, *J. Hydraul. Eng.*, vol. 137, no. 1, pp. 15–22, 2011.
- [140] J. C. Stormont, J. Hines, R. E. Pease, and D. O’Dowd, “Hydraulic Properties of Asphalt Concrete”, *Geotech. Test. J.*, vol. 33, no. 6, 2010.
- [141] R. A. Tarefder, L. White, and M. Zaman, “Neural network model for asphalt concrete permeability”, *J. Mater. Civ. Eng.*, vol. 17, no. 1, pp. 19–27, 2005.
- [142] R. B. Mallick, L. A. Cooley, M. Teto, and R. Bradbury, “Development of a simple test for evaluation of in-place permeability of asphalt mixes”, *Int. J. Pavement Eng.*, vol. 2, no. 2, pp. 67–83, 2001.
- [143] K. Kanitpong, C. H. Benson, and H. U. Bahia, “Hydraulic conductivity (permeability) of laboratory-compacted asphalt mixtures”, *Transp. Res. Rec.*, vol. 1767, no. 1, pp. 25–32, 2001.
- [144] J. Norambuena-Contreras, E. Asanza Izquierdo, D. Castro-Fresno, M. N. Partl, and Á. Garcia, “A New Model on the Hydraulic Conductivity of Asphalt Mixtures”, *Int. J. Pavement Res. Technol.*, vol. 6, no. 5, 2013.
- [145] J. Hu, T. Ma, and K. Ma, “DEM-CFD simulation on clogging and degradation of air voids in double-layer porous asphalt pavement under rainfall”, *J. Hydrol.*, vol. 595, p. 126028, 2021.
- [146] L. D. Poulikakos *et al.*, “Mechanical properties of porous asphalt, recommendations for standardization”, *recommendations for standardization*, 2006.
- [147] M. Hamzah, N. Abdullah, J. Voskuilen, and G. van Bochove, “Laboratory simulation of the clogging behaviour of single-layer and two-layer porous asphalt”, *Road Mater. pavement Des.*, vol. 14, no. 1, pp. 107–125, 2013.
- [148] A. Garcia, A. Hassn, A. Chiarelli, and A. Dawson, “Multivariable analysis of potential evaporation from moist asphalt mixture”, *Constr. Build. Mater.*, vol. 98, pp. 80–88, 2015.
- [149] N. R. Buyung and A. N. A. Ghani, “Permeable pavements and its contribution to cooling effect of surrounding temperature”, in *AIP Conference Proceedings*, 2017, vol. 1892, no. 1, p. 170003.
- [150] L. Gao, Z. Wang, J. Xie, Y. Liu, and S. Jia, “Simulation of the cooling effect of porous asphalt pavement with different air voids”, *Appl. Sci.*, vol. 9, no. 18, p. 3659, 2019.
- [151] S. Sreedhar and K. P. Biligiri, “Development of pavement temperature predictive models using thermophysical properties to assess urban climates in the built environment”, *Sustain. cities Soc.*, vol. 22, pp. 78–85, 2016.
- [152] A. Hassn, A. Chiarelli, A. Dawson, and A. Garcia, “Thermal properties of asphalt pavements under dry and wet conditions”, *Mater. Des.*, vol. 91, pp. 432–439, 2016.
- [153] C. M. Nwakaire, C. C. Onn, S. P. Yap, C. W. Yuen, and P. D. Onodagu, “Urban Heat Island Studies with emphasis on urban pavements: A review”, *Sustain. Cities Soc.*, vol. 63, p. 102476, 2020.
- [154] B. R. Anupam, U. C. Sahoo, A. K. Chandrappa, and P. Rath, “Emerging technologies in cool pavements: A review”, *Constr. Build. Mater.*, vol. 299, p. 123892, 2021.
- [155] Y. Qin, Y. He, J. E. Hiller, and G. Mei, “A new water-retaining paver block for reducing runoff and cooling pavement”, *J. Clean. Prod.*, vol. 199, pp. 948–956, 2018, doi: 10.1016/j.jclepro.2018.07.250.
- [156] T. Bao, Z. L. Liu, X. Zhang, and Y. He, “A drainable water-retaining paver block for runoff reduction and evaporation cooling”, *J. Clean. Prod.*, vol. 228, pp. 418–424, 2019.
- [157] T. Nakayama and T. Fujita, “Cooling effect of water-holding pavements made of new materials on water and heat budgets in urban areas”, *Landsc. Urban Plan.*, vol. 96, no. 2, pp. 57–67, 2010.
- [158] K. Takahashi and K. Yabuta, “Road temperature mitigation effect of ‘road cool,’ a Water-retentive material using blast furnace slag”, *JFE Tech. Rep.*, vol. 19, pp. 58–62, 2009.
- [159] K. Okada, A. Ooyama, T. Isobe, Y. Kameshima, A. Nakajima, and K. J. D. MacKenzie, “Water retention properties of porous geopolymers for use in cooling applications”, *J. Eur. Ceram. Soc.*, vol. 29, no. 10, pp. 1917–1923, 2009.
- [160] K. Okada, S. Matsui, T. Isobe, Y. Kameshima, and A. Nakajima, “Water-retention properties of porous ceramics prepared from mixtures of allophane and vermiculite for materials to counteract heat island effects”, *Ceram. Int.*, vol. 34, no. 2, pp. 345–350, 2008.
- [161] K. Tan, Y. Qin, T. Du, L. Li, L. Zhang, and J. Wang, “Biochar from waste biomass as hygroscopic filler for pervious concrete to improve evaporative cooling performance”, *Constr. Build. Mater.*, vol. 287, p. 123078, 2021.
- [162] Y. Shimazaki, M. Aoki, K. Karaki, and A. Yoshida, “Improving outdoor human-thermal environment by optimizing the reflectance of water-retaining pavement through subjective field-based measurements”, *Build. Environ.*, vol. 210, p. 108695, 2022.
- [163] K. Seifeddine, E. Toussaint, and S. Amziane, “Experimental investigation on evaporation rate for enhancing evaporative cooling of pervious pavement containing recycled rubber”, *Construction Technologies and Architecture*, 2022, vol. 1, pp. 847–854.

- [164] N. Kinoshita, Y. Shimazaki, J. Yuan, and K. Ichinose, "Influence of water-holding pavement on thermal and acoustic environment on road surface, report 1 - field thermal environment measurement and sound absorption coefficient measurement", in *Journal of the Society of Air-Conditioning and Sanitary Engineers*, Vol. 23, 2022, pp. 9-12.
- [164] N. Kinoshita, Y. Shimazaki, J. Yuan, and Koh Ichinose, "Influence of water-holding pavement on thermal and acoustic environment on road surface", *Journal of the society of air-conditioning and hygiene engineers*, , Vol. 23, 2022, pp. 9-12.
- [165] Y. Shimazaki, M. Aoki, J. Nitta, H. Okajima, and A. Yoshida, "Experimental determination of pedestrian thermal comfort on water-retaining pavement for uhi adaptation strategy", *Atmosphere (Basel)*, vol. 12, no. 2, p. 127, 2021.
- [166] H. Higashiyama, M. Sano, F. Nakanishi, O. Takahashi, and S. Tsukuma, "Field measurements of road surface temperature of several asphalt pavements with temperature rise reducing function", *Case Stud. Constr. Mater.*, vol. 4, pp. 73–80, 2016.
- [167] W. Jiang, A. Sha, J. Xiao, Z. Wang, and A. Apeagyei, "Experimental study on materials composition design and mixture performance of water-retentive asphalt concrete", *Constr. Build. Mater.*, vol. 111, pp. 128–138, 2016.
- [168] M. Guo, M. Liang, Y. Jiao, W. Zhao, Y. Duan, and H. Liu, "A review of phase change materials in asphalt binder and asphalt mixture", *Constr. Build. Mater.*, vol. 258, p. 119565, 2020.
- [169] J. Guo, H. Xiang, Q. Wang, C. Hu, M. Zhu, and L. Li, "Preparation of poly (decaglycerol-co-ethylene glycol) copolymer as phase change material", *Energy Build.*, vol. 48, pp. 206–210, 2012.
- [170] M. Chen, L. Wan, and J. Lin, "Effect of Phase-Change Materials on Thermal and Mechanical Properties of Asphalt Mixtures", *J. Test. Eval.*, vol. 40, no. 5, p. 20120091, 2012, doi: 10.1520/jte20120091.
- [171] V. D. Cao, T. Q. Bui, and A. L. Kjøniksen, "Thermal analysis of multi-layer walls containing geopolymer concrete and phase change materials for building applications", *Energy*, vol. 186, p. 115792, 2019, doi: 10.1016/j.energy.2019.07.122.
- [172] Y. Zhang, K. Lin, Y. Jiang, and G. Zhou, "Thermal storage and nonlinear heat-transfer characteristics of PCM wallboard", *Energy Build.*, vol. 40, no. 9, pp. 1771–1779, 2008, doi: 10.1016/j.enbuild.2008.03.005.
- [173] D. A. Neeper, "Thermal dynamics of wallboard with latent heat storage", *Sol. Energy*, vol. 68, no. 5, pp. 393–403, 2000, doi: 10.1016/S0038-092X(00)00012-8.
- [174] M. Koschenz and B. Lehmann, "Development of a thermally activated ceiling panel with PCM for application in lightweight and retrofitted buildings", *Energy Build.*, vol. 36, no. 6, pp. 567–578, 2004, doi: 10.1016/j.enbuild.2004.01.029.
- [175] P. W. Griffiths and P. C. Eames, "Performance of chilled ceiling panels using phase change material slurries as the heat transport medium", *Appl. Therm. Eng.*, vol. 27, no. 10, pp. 1756–1760, 2007, doi: 10.1016/j.applthermaleng.2006.07.009.
- [176] W. Saman, F. Bruno, and E. Halawa, "Thermal performance of PCM thermal storage unit for a roof integrated solar heating system", *Sol. Energy*, vol. 78, no. 2, pp. 341–349, 2005, doi: 10.1016/j.solener.2004.08.017.
- [177] A. Pasupathy, L. Athanasius, R. Velraj, and R. V. Seeniraj, "Experimental investigation and numerical simulation analysis on the thermal performance of a building roof incorporating phase change material (PCM) for thermal management", *Appl. Therm. Eng.*, vol. 28, no. 5–6, pp. 556–565, 2008, doi: 10.1016/j.applthermaleng.2007.04.016.
- [178] J. Sarkar and S. Bhattacharyya, "Application of graphene and graphene-based materials in clean energy-related devices Minghui", *Arch. Thermodyn.*, vol. 33, no. 4, pp. 23–40, 2012, doi: 10.1002/er.
- [179] X. Luo, Q. Guo, Z. Tao, Y. Liang, and Z. Liu, "Modified phase change materials used for thermal management of a novel solar thermoelectric generator", *Energy Convers. Manag.*, vol. 208, no. December 2019, p. 112459, 2020, doi: 10.1016/j.enconman.2019.112459.
- [180] A. Rezanian, S. A. Atouei, and L. Rosendahl, "Critical parameters in integration of thermoelectric generators and phase change materials by numerical and Taguchi methods", *Mater. Today Energy*, vol. 16, p. 100376, 2020, doi: 10.1016/j.mtener.2019.100376.
- [181] L. Abdolmaleki, S. M. Sadrameli, and A. Pirvaram, "Application of environmental friendly and eutectic phase change materials for the efficiency enhancement of household freezers", *Renew. Energy*, vol. 145, pp. 233–241, 2020, doi: 10.1016/j.renene.2019.06.035.
- [182] S. R. L. da Cunha and J. L. B. de Aguiar, "Phase change materials and energy efficiency of buildings: A review of knowledge", *J. Energy Storage*, vol. 27, no. October 2019, 2020, doi: 10.1016/j.est.2019.101083.
- [183] J. Cheng *et al.*, "Preparation and characterization of carbon nanotube microcapsule phase change materials for improving thermal comfort level of buildings", *Constr. Build. Mater.*, vol. 244, p. 118388, 2020, doi:

- 10.1016/j.conbuildmat.2020.118388.
- [184] C. Veerakumar and A. Sreekumar, “Thermo-physical investigation and experimental discharge characteristics of lauryl alcohol as a potential phase change material for thermal management in buildings”, *Renew. Energy*, vol. 148, pp. 492–503, 2020, doi: 10.1016/j.renene.2019.10.055.
- [185] P. J. Shamberger and N. M. Bruno, “Review of metallic phase change materials for high heat flux transient thermal management applications”, *Appl. Energy*, vol. 258, no. March 2019, p. 113955, 2020, doi: 10.1016/j.apenergy.2019.113955.
- [186] K. B. A. K. Pandey, S. Shahabuddin, M. Samykano, T. M., and R. Saidur, “Phase change materials integrated solar thermal energy systems: Global trends and current practices in experimental approaches”, *J. Energy Storage*, vol. 27, no. August 2019, p. 101118, 2020, doi: 10.1016/j.est.2019.101118.
- [187] S. F. Li, Z. hua Liu, and X. J. Wang, “A comprehensive review on positive cold energy storage technologies and applications in air conditioning with phase change materials”, *Appl. Energy*, vol. 255, no. August, p. 113667, 2019, doi: 10.1016/j.apenergy.2019.113667.
- [188] J. Chen *et al.*, “Effects of different phase change material thermal management strategies on the cooling performance of the power lithium ion batteries: A review”, *J. Power Sources*, vol. 442, no. October, p. 227228, 2019, doi: 10.1016/j.jpowsour.2019.227228.
- [189] S. Lei, Y. Shi, and G. Chen, “A lithium-ion battery-thermal-management design based on phase-change-material thermal storage and spray cooling”, *Appl. Therm. Eng.*, vol. 168, no. August 2019, p. 114792, 2020, doi: 10.1016/j.applthermaleng.2019.114792.
- [190] W. Zhang, J. Qiu, X. Yin, and D. Wang, “A novel heat pipe assisted separation type battery thermal management system based on phase change material”, *Appl. Therm. Eng.*, vol. 165, no. October 2019, p. 114571, 2020, doi: 10.1016/j.applthermaleng.2019.114571.
- [191] I. K. Mizwar, M. Napiyah, and M. H. Sutanto, “Thermal properties of cool asphalt concrete containing phase change material”, *IOP conference series: materials science and engineering*, 2019, vol. 527, no. 1, p. 12049.
- [192] Y. Farnam *et al.*, “Evaluating the use of phase change materials in concrete pavement to melt ice and snow”, *J. Mater. Civ. Eng.*, vol. 28, no. 4, p. 4015161, 2016.
- [193] Z. Refaa, M. R. Kakar, A. Stamatiou, J. Worlitschek, M. N. Partl, and M. Bueno, “Numerical study on the effect of phase change materials on heat transfer in asphalt concrete”, *Int. J. Therm. Sci.*, vol. 133, pp. 140–150, 2018.
- [194] M. Ryms, W. M. Lewandowski, E. Klugmann-Radziemska, H. Denda, and P. Wcisło, “The use of lightweight aggregate saturated with PCM as a temperature stabilizing material for road surfaces”, *Appl. Therm. Eng.*, vol. 81, pp. 313–324, 2015.
- [195] A. Sha, J. Zhang, M. Jia, W. Jiang, and W. Jiao, “Development of polyurethane-based solid-solid phase change materials for cooling asphalt pavements”, *Energy Build.*, p. 111873, 2022.
- [196] Q. Liu *et al.*, “A novel functional coating with 2DMts/SA phase change material as filler and its pavement temperature regulation performance”, *Mater. Lett.*, vol. 306, p. 130905, 2022.
- [197] A. BR, U. C. Sahoo, and P. Rath, “Thermal and mechanical performance of phase change material incorporated concrete pavements”, *Road Mater. Pavement Des.*, pp. 1–18, 2021.
- [198] J. Jin *et al.*, “Preparation and thermal performance of binary fatty acid with diatomite as form-stable composite phase change material for cooling asphalt pavements”, *Constr. Build. Mater.*, vol. 226, pp. 616–624, 2019.
- [199] J. Jin *et al.*, “Preparation and thermal properties of encapsulated ceramsite-supported phase change materials used in asphalt pavements”, *Constr. Build. Mater.*, vol. 190, pp. 235–245, 2018.
- [200] Y. Zhang, A. T. Murray, and B. L. Turner Li, “Optimizing green space locations to reduce daytime and nighttime urban heat island effects in Phoenix, Arizona”, *Landsc. Urban Plan.*, vol. 165, pp. 162–171, 2017.
- [201] P. A. Hancock and I. Vasmatzidis, “Effects of heat stress on cognitive performance: the current state of knowledge”, *Int. J. Hyperth.*, vol. 19, no. 3, pp. 355–372, 2003.
- [202] X. Liu and S. Wu, “Study on the graphite and carbon fiber modified asphalt concrete”, *Constr. Build. Mater.*, vol. 25, no. 4, pp. 1807–1811, 2011.
- [203] S. Wu, L. Mo, Z. Shui, and Z. Chen, “Investigation of the conductivity of asphalt concrete containing conductive fillers”, *Carbon N. Y.*, vol. 43, no. 7, pp. 1358–1363, 2005.
- [204] W. Jiao, A. Sha, Z. Liu, W. Jiang, L. Hu, and X. Li, “Utilization of steel slags to produce thermal conductive asphalt concretes for snow melting pavements”, *J. Clean. Prod.*, vol. 261, p. 121197, 2020.
- [205] Y. Du and S. Wang, “Oriented heat release in asphalt pavement induced by high-thermal-conductivity rods”, *Appl. Therm. Eng.*, vol. 90, pp. 424–431, 2015.
- [206] J. H. Park, Y. U. Kim, J. Jeon, S. Wi, S. J. Chang, and S. Kim, “Effect of eco-friendly pervious concrete

- with amorphous metallic fiber on evaporative cooling performance”, *J. Environ. Manage.*, vol. 297, p. 113269, 2021.
- [207] D. Yinfei, W. Jiacheng, and C. Jiaqi, “Cooling asphalt pavement by increasing thermal conductivity of steel fiber asphalt mixture”, *Sol. Energy*, vol. 217, pp. 308–316, 2021.
- [208] W. ShengYue, Z. QiYang, D. YingNa, and S. PeiDong, “Unidirectional heat-transfer asphalt pavement for mitigating the urban heat island effect”, *J. Mater. Civ. Eng.*, vol. 26, no. 5, pp. 812–821, 2014.
- [209] D. Yinfei, S. Qin, and W. Shengyue, “Bidirectional heat induced structure of asphalt pavement for reducing pavement temperature”, *Appl. Therm. Eng.*, vol. 75, pp. 298–306, 2015.
- [210] A. R. Dawson, P. K. Dehdezi, M. R. Hall, J. Wang, and R. Isola, “Enhancing thermal properties of asphalt materials for heat storage and transfer applications”, *Road Mater. Pavement Des.*, vol. 13, no. 4, pp. 784–803, 2012, doi: 10.1080/14680629.2012.735791.
- [211] G. Wu and X. Yu, “Thermal energy harvesting across pavement structure,” 2012.
- [212] X. Liu, S. J. Rees, and J. D. Spitler, “Modeling snow melting on heated pavement surfaces. Part I: Model development”, *Appl. Therm. Eng.*, vol. 27, no. 5–6, pp. 1115–1124, 2007, doi: 10.1016/j.applthermaleng.2006.06.017.
- [213] Q. Gao, Y. Huang, M. Li, Y. Liu, and Y. Y. Yan, “Experimental study of slab solar collection on the hydronic system of road”, *Solar Energy*, vol. 84, no. 12, pp. 2096–2102, 2010, doi: 10.1016/j.solener.2010.09.008.
- [214] H. Xu and Y. Tan, “Development and testing of heat-and mass-coupled model of snow melting for hydronically heated pavement”, *Transportation Research Record*, no. 2282, pp. 14–21, 2012, doi: 10.3141/2282-02.
- [215] RB. Mallick, B. Chen, S. Bhowmick, and MS. Huken, “Capturing solar energy from asphalt pavements”, *International isap symposium on asphalt pavements and environment*, Zurich, Switzerland, 2008.
- [216] S. Asfour, F. Bernardin, and E. Toussaint, “Experimental validation of 2D hydrothermal modelling of porous pavement for heating and solar energy retrieving applications”, *Road Materials and Pavement Design*. 2018, doi: 10.1080/14680629.2018.1525418.
- [217] S. Asfour, “Récupération d’énergie dans les chaussées pour leur maintien hors gel”, doctoral dissertation, Université Blaise Pascal-Clermont-Ferrand, 2016.
- [218] A. Chiarelli, A. R. Dawson, and A. Garcia, “Parametric analysis of energy harvesting pavements operated by air convection”, *Appl. Energy*, vol. 154, pp. 951–958, 2015.
- [219] A. Chiarelli, A. R. Dawson, and A. Garcia, “Pavement temperature mitigation by the means of geothermally and solar heated air”, *Geothermics*, vol. 68, pp. 9–19, 2017.
- [220] A. Chiarelli, A. Al-Mohammedawi, A. R. Dawson, and A. Garcia, “Construction and configuration of convection-powered asphalt solar collectors for the reduction of urban temperatures”, *Int. J. Therm. Sci.*, vol. 112, pp. 242–251, 2017.
- [221] A. Garcia and M. N. Partl, “How to transform an asphalt concrete pavement into a solar turbine”, *Appl. Energy*, vol. 119, pp. 431–437, 2014.
- [222] S. B. Riffat and X. Ma, “Thermoelectrics: a review of present and potential applications”, *Appl. Therm. Eng.*, vol. 23, no. 8, pp. 913–935, 2003.
- [223] W. Jiang, J. Xiao, D. Yuan, H. Lu, S. Xu, and Y. Huang, “Design and experiment of thermoelectric asphalt pavements with power-generation and temperature-reduction functions”, *Energy Build.*, vol. 169, pp. 39–47, 2018.
- [224] C. Efthymiou, M. Santamouris, D. Kolokotsa, and A. Koras, “Development and testing of photovoltaic pavement for heat island mitigation”, *Sol. Energy*, vol. 130, pp. 148–160, 2016.
- [225] P. Xie and H. Wang, “Potential benefit of photovoltaic pavement for mitigation of urban heat island effect”, *Appl. Therm. Eng.*, vol. 191, p. 116883, 2021.
- [226] B. R. Anupam, U. C. Sahoo, and P. Rath, “Phase change materials for pavement applications: A review”, *Constr. Build. Mater.*, vol. 247, p. 118553, 2020.
- [227] A. Dawson, R. Mallick, A. G. Hernandez, and P. K. Dehdezi, “Energy harvesting from pavements”, in *Climate Change, Energy, Sustainability and Pavements*, Springer, 2014, pp. 481–517.
- [228] A. B. Northmore and S. L. Tighe, “Performance modelling of a solar road panel prototype using finite element analysis”, *Int. J. Pavement Eng.*, vol. 17, no. 5, pp. 449–457, 2016.

Chapter II State of the art on the mechanical properties of pervious concrete

Article publié dans le journal : European Journal of Environmental and Civil Engineering

Seifeddine, K., Amziane, S., & Toussaint, E. (2021). State of the art on the mechanical properties of pervious concrete. *European Journal of Environmental and Civil Engineering*, 1-29.



European Journal
of Environmental
and Civil Engineering

Résumé et Objectif

Le béton drainant peut-être décrit comme un béton poreux qui permet à l'eau de pénétrer à travers un réseau interconnecté de pores. Au cours du siècle dernier, l'industrie de la construction a montré un intérêt croissant pour le béton drainant, qui est un matériau respectueux de l'environnement. Cet article a pour objectif de présenter la composition et la méthode de formulation du béton drainant, d'identifier les différents facteurs influençant la porosité. Il existe une abondante littérature documentant les différentes propriétés mécaniques du béton drainant, mais il manque une étude systématique pour résumer ces propriétés. Ce travail de synthèse consiste non seulement à faire un résumé des résultats présents dans la littérature, mais également à proposer des modèles permettant de prédire les propriétés mécaniques du béton drainant. Une relation entre la porosité et la densité du béton drainant à base de ciment et de granulats naturels a été proposée à partir de divers travaux de recherche. Une autre relation a été établie entre la résistance à la compression du béton drainant conventionnel et sa porosité. L'équation de la courbe obtenue montre que cette résistance est influencée par d'autres paramètres qui n'ont pas été largement étudiés dans la littérature. L'influence de ces facteurs (taille des agrégats, rapport agrégats/ciment A/C, eau/ciment E/C et l'épaisseur de la pâte cimentaire) a été étudiée afin de proposer des solutions permettant d'optimiser la conception du mélange du béton drainant pour maximiser sa résistance mécanique. De plus, dans cette étude, des modèles ont été établis pour prédire la résistance à la traction et la résistance à la flexion à partir de la résistance à la compression, car il n'existe pas de modèles dans la littérature qui permettent de corréliser ces propriétés entre elles.

Les résultats de cette étude montrent que la densité du béton drainant diminue linéairement avec l'augmentation de la porosité. Cette densité dépend d'autres facteurs tels que le type de granulats naturels et leurs propriétés physiques et géométriques, le rapport A/C, la teneur en pâte de ciment et la quantité de granulats fins utilisés. La perméabilité du béton drainant augmente avec la porosité. Le type de porosité et la méthode de mesure de la perméabilité doivent être précisés pour mieux corréliser la perméabilité à la porosité du matériau de revêtement.

Concernant les propriétés mécaniques, la résistance à la compression du béton drainant diminue de façon exponentielle avec l'augmentation de la porosité. La porosité seule ne suffit pas à prédire avec précision cette propriété, qui dépend d'autres facteurs tels que le rapport E/C et A/C, la teneur en pâte de ciment, ainsi que le type et les propriétés mécaniques, physiques et géométriques des granulats. Pour une utilisation structurelle en tant que chaussée à faible trafic,

le béton drainant doit avoir une résistance à la compression supérieure à 17 MPa. Afin de maximiser la résistance à la compression du béton de chaussée d'un point de vue pratique, il devrait être dosé avec un rapport E/C de 0,3 à 3,6 et un rapport A/C de 4,2 à 5, selon les résultats trouvés dans la littérature. En outre, l'utilisation de granulats plus fins permet toujours d'obtenir une résistance à la compression plus élevée. La résistance à la compression peut également être améliorée par l'ajout d'une certaine quantité de sable, jusqu'à un maximum de 10% de la masse des agrégats, et en augmentant le degré de compactage. Cependant, de nombreuses études ne fournissent pas suffisamment de détails sur la méthode et le degré de compactage, ce qui rend la comparaison des indicateurs de performance mécaniques invalide dans certains cas. Ces techniques peuvent avoir un impact négatif sur le taux d'infiltration du béton drainant. Un test de perméabilité est nécessaire pour vérifier que la perméabilité est supérieure à 1 mm.s^{-1} afin que la chaussée continue à remplir sa fonction principale de gestion des eaux pluviales.

Un nombre limité d'études ont développé des équations qui donnent la relation entre les résistances à la traction et à la compression du béton perméable. Il existe des divergences entre les valeurs de la résistance à la traction obtenues à partir de ces modèles. En outre, le modèle de prédiction de la résistance à la traction du béton conventionnel ne peut pas être appliqué au béton drainant. Par contre, le modèle de prédiction de la résistance à la flexion du béton drainant sur la base de sa résistance à la compression, établi à partir des données de diverses études, est quasiment identique à celui du béton conventionnel. Par conséquent, le modèle pour le béton conventionnel peut être utilisé pour prédire les résistances à la flexion des mélanges de béton drainant à partir de leurs résistances à la compression.

Étant donné le nombre important de facteurs qui influencent sur la résistance mécanique du béton drainant, une étude de sensibilité sur un grand ensemble de données, considérant toutes les variables d'influence, est nécessaire. Une telle étude permettrait d'améliorer la conception des mélanges de béton drainant, en aidant à trouver les facteurs les plus influents et le dosage optimal pour maximiser les résistances mécaniques (alors que jusqu'à présent, l'utilisation du béton drainant a été limitée aux aires de stationnement ou aux chaussées à faible trafic). Cette étude doit également prendre en compte l'influence de tous ces facteurs sur la conductivité hydraulique, la gestion des eaux de pluie étant le rôle principal de ces revêtements.

Dans ce chapitre, les propriétés mécaniques du béton drainant ont été étudiées. Cependant, la fonction principale de ce type de matériau est la gestion des eaux pluviales. Pour remplir cette fonction, il doit avoir une perméabilité adéquate, qui doit être ajustée en fonction de l'intensité des précipitations. Le chapitre suivant examine en détail les propriétés hydrauliques du béton drainant. Des modèles de prédiction de la perméabilité ont été développés. Les facteurs qui influencent ses propriétés ainsi que les modèles de prédiction de la perméabilité ont été étudiés.

Khaled Seifeddine ^a, Sofiane Amziane ^a, Evelyne Toussaint ^a

^a Université Clermont Auvergne, CNRS, SIGMA Clermont, Institut Pascal, F-63000 Clermont-Ferrand, France

Highlights

- This paper presents the composition and method for making up pervious concrete based on cement and natural aggregates.
- It lists the factors affecting the porosity of pervious concrete.
- A relation is established between density and porosity and between compressive strength and porosity.
- The factors that influence the compressive strength of pervious concrete are studied.
- The equation for predicting the tensile strength of conventional concrete is not suitable for pervious concrete.
- The equation for predicting the flexural strength of conventional concrete is suitable for pervious concrete.

Keywords

Pervious concrete; Total and effective porosity; Compressive strength; Tensile strength; Flexural strength.

1. Introduction

The development of urbanization and the increase in ground sealing make rainwater management a crucially important task vital. Permeable surfaces become impermeable due to the construction of buildings, parking lots, houses and other structures. This leads to an increase in the frequency and extent of flooding, a lowering of the water table and disruption in the natural water cycle [1]. In addition, waterproofing harms the natural environment and increases local pollution at discharge points (such as wastewater treatment plants) [2]. In view of these issues, sustainable rainwater management is plainly very important in sustainable development for cities, and consequently, developers are increasingly turning to permeable coatings.

Permeable coatings have many environmental benefits, such as reducing flood risk and reducing runoff [3], [4], replenishing groundwater, reducing urban heat islands [5]–[8] and increasing evapotranspiration and evaporative cooling [9]–[12]. They improve water quality [13] and reduce water pollution [14], as well as allowing efficient land use without the need for expensive facilities, such as retention basins [15], and reducing the noise emitted by vehicles to the same degree as roadway and noise barriers do [16]–[20].

Pervious concrete coatings are one of the most common permeable coatings. They are characterized by a porous structure that allows water penetration. The mechanical and hydraulic performances, and durability, of these coatings has been extensively studied [21]–[29]. They have a variety of uses. For example, they can be used in low-traffic pavements, cycle paths, parking lots, sports fields, urban tree perimeters, residential access roads for residents and service vehicles [30], concrete pavement underlayments, water sports centers and zoos, tennis courts, pool decks and walls (including load-bearing walls) [31].

Draining concrete pavements are increasingly used as a “green method” for low-impact development that better manages the impact of infrastructure construction and operation on the

natural environment [32], [33]. Its inferior mechanical strength means pervious concrete is only used to supplement or replace traditional “gray infrastructure”, especially on roads and parking areas intended for low speed, low weight and low traffic [34], [35].

Prior research on the mechanical properties of pervious concrete has focused mainly on the impact of porosity on compressive strength [36], [37], [46]–[49], [38]–[45]. However, there is a lack of studies in the available literature on the different factors influencing the compressive strength of traditional pervious concrete. While compressive strength is important in assessing the quality and durability of pervious concrete, and evaluating its mechanical behavior, tensile strength is also an important parameter in pavement design [50]. There are many equations that correlate tensile strength and compressive strength for conventional concrete [51]–[52], but few that do the same for pervious concrete. Researchers have already compared the tensile and compressive strength of pervious concrete, but very few have developed equations to precisely correlate these two properties. In addition, the flexural strength of pervious concrete in a pavement is very important for its design [31], and there are many equations that correlate the flexural and compressive strength of conventional concrete [53]–[55]. The literature does offer previous studies on pervious concrete which compare the flexural and compressive strength, but do not develop equations to precisely correlate the two properties.

In this context, the purpose of this paper is to critically examine the studies available on pervious concrete. Recent years have seen a considerable upswing in the number of studies on this subject. This review summarizes the work in these different domains in order to gain a fuller understanding of the mechanical characteristics of pervious concrete. This document presents the composition, methods of formulation and mechanical characteristics of pervious concrete (the factors influencing the mechanical characteristics, the minimum strength thresholds, the empirical equations that can be used to predict the compressive strength of pervious concrete, and the models used to predict tensile and flexural strength on the basis of simple compressive strength).

2. Pervious concrete and pervious paving slabs

2.1. Composition and method of formulation

Pervious concrete is a composite material. It is made up of the same ingredients as conventional concrete – namely cement, water and aggregates. The difference between pervious concrete and ordinary concrete is that the former includes very little sand or other fine particles to fill the spaces between the large particles. In addition, traditional impervious concrete uses grains of differing levels of coarseness, the particle size distribution (PSD) of the gravel used in pervious concrete is relatively uniform (Fig. 1). These two major differences create a network of interconnected voids, allowing water to quickly penetrate the concrete [56].

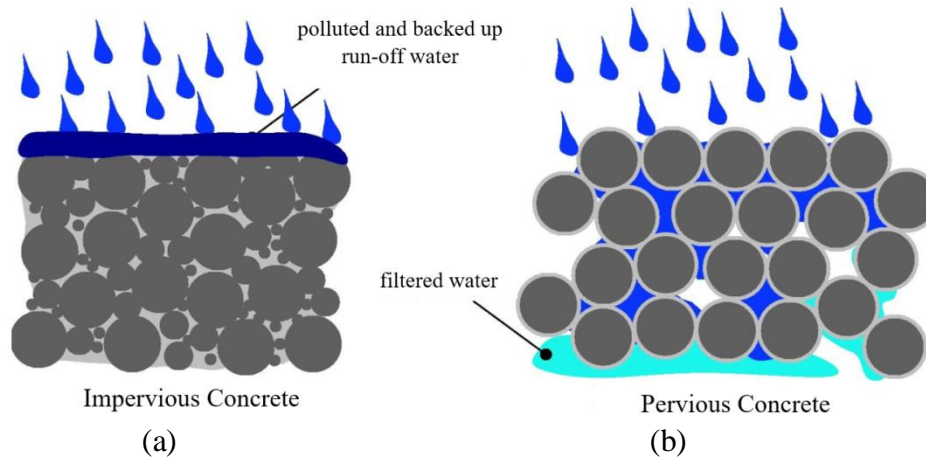


Fig. 1. Comparison of pervious concrete to impervious concrete [57].

The materials used in the manufacture of pervious concrete are:

Cement: Portland cement is used in pervious concrete as a cementitious binder [58]. According to various technical documents [31], [59], [60], the same type of cement can be used for both ordinary concrete and pervious concrete. Examples include Portland cement (CEM I), Portland composite cement (CEM II), blastfurnace slag (CEM III), pozzolanic cement (CEM IV), compound cement (CEM V) and even ecological cement [59], [60]. Matsuo et al. [61] used regular Portland cement and environmentally friendly cement which is made from the ashes of incinerated municipal solid waste and waste materials such as sewage sludge, and found no significant difference between them in terms of performance.

The cement paste content depends on several factors: the gravel particle size, the mechanical strength required and the desired permeability. In general, the mass of cement per m^3 of pervious concrete varies from 270 to 415 kg/m^3 .

Water: The quality of the water used for pervious concrete is subject to the same requirements as for ordinary concrete [59]. Drinking water or recycled water from the concrete industry can be used [31]. Water and its use in pervious concrete are crucial. When the fine particles are removed from the pervious concrete, the strength depends on the bond of the cement paste with the aggregates via the interface. As with traditional concrete, lack of water will result in incomplete hydration of the cement. However, excess water will cause sedimentation of the cement paste in the pervious coating and lead to clogging of the pores. The right amount of water can maximize strength without compromising permeability [62].

Pervious concrete must be dosed with an optimal Water/Cement (W/C) ratio (Fig. 2), which generally varies from 0.26 to 0.4 [59]. Numerous studies have shown that when the W/C ratio is between 0.27 and 0.34, an adjuvant must be used [39], [63]; if the W/C ratio is between 0.34 and 0.4, an adjuvant may not be needed [62], [64], [65].

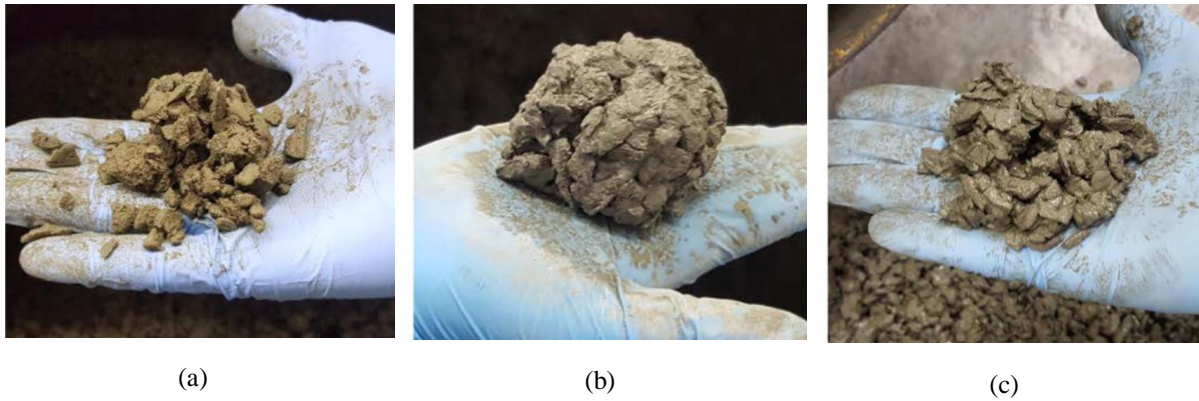


Fig. 2. Samples of pervious concrete with different water contents formed into a ball: (a) very low quantity of water, (b) adequate quantity of water and (c) high quantity of water [66].

Aggregates: The main ingredient by volume in pervious concrete is gravel, which is the chief load-bearing component. The mass of gravel per m^3 of pervious concrete varies between 1190 and 1600 kg/m^3 , and the Aggregate/Cement (A/C) mass ratio is between 4.0 and 4.5 [67].

The physical properties of the aggregates used, such as grain size, shape and distribution, play a major role in determining the mechanical properties, durability and permeability of pervious concrete pavements [68].

It is recommended that coarse aggregates be used to maximize hydraulic conductivity by forming large voids in the concrete, reducing the risk of clogging. In addition, increased aggregate size makes the pavement surface rougher, thus increasing skid resistance, but sharply worsening handling [38], [60], [69]. However, small aggregates are generally used for applications such as low-traffic pavements, walkways, and parking lots, and can also be used for aesthetic reasons [31].

In order to maintain good porosity, pervious concrete is generally composed of aggregates between 9.5 and 19 mm [50]. Other studies have used coarse aggregates, of 2.36 to 9.5 mm, to improve mechanical strength [37], [68], [70].

An increased amount of aggregate leads to a decrease in the cement suspension in the mixture. Consequently, less paste fills the voids, so porosity is increased. In addition, less paste is used for the aggregates, which reduces the compressive strength and modulus of elasticity [70], meaning that the amount of cement must also be calculated relative to the amount of aggregate. It is also necessary to limit materials that affect the bond between the aggregate and the cement paste, such as clay [71].

Fine aggregates tend not to be used in pervious concrete mixes. However, in some studies in the literature, a certain amount of sand is used to improve the product's compressive strength [72], [73]. According to Onstenk et al. [74], the quantity should be no more than 175 kg/m^3 , since multiple studies have shown that any increase beyond this quantity greatly reduces permeability [74], [75].

Bonicelli et al. [76] showed that the addition of 5 to 10% of sand (% aggregate weight) helps improve its mechanical properties (tensile strength by up to +70%, rigidity up to +35%), and reduces subsidence (by up to -40%) due to a thicker coating of cement around the aggregate particles, though porosity and permeability were reduced by 44.2% and 67.1%, respectively. The addition of fine particles can also improve freeze-thaw resistance, thus improving durability [69]. The study by Kevern et al. [24] shows that freeze-thawing of a pervious concrete sample leads to a 19% reduction in mass after 156 cycles. However, when 7% sand is added,

relative to the amount of aggregate in the sample, the mass reduction is limited to 2% after 300 cycles.

Adding sand, therefore, increases mechanical strength and reduces permeability. Some studies in the literature indicate that the optimum amount of sand added to achieve a satisfactory balance between mechanical strength and permeability should be between 5% and 10% (mass ratio between fine and coarse aggregates) [21], [77]–[79].

Fly ash, certain fibers, and other mineral additives (such as natural pozzolan, blastfurnace slag, and silica fume) have been used in a number of studies. These materials are found to alter the setting time, mechanical strength, porosity, permeability and durability of the pervious concrete [21], [42], [80]–[85].

Adjuvants are also used in pervious concrete mixes in order to obtain particular properties, in the same way as they are in traditional concrete. Retarding adjuvants are often used because of the rapid setting of pervious concrete [31], and water reducers are almost always used to ensure workability while maintaining a low W/C ratio. [86].

Therefore, the physical and geometric properties of each component and their amount in the pervious concrete mix will affect its hydraulic and mechanical properties. Below, we study the influence of these factors in order to optimize the design of pervious coatings with respect to their mechanical properties. Table 1 shows the different dosages used in several studies in the literature.

Table 1

Dosages of pervious concrete based on natural aggregates.

Study	Water (W) (kg/m ³)	Cement (C) (kg/m ³)	Fine aggregates (kg/m ³)	Coarse aggregates (A) (kg/m ³)	Ratio (W/C)	Ratio (A/C)
Kevern et al., 2006 [39]	96	356	0	1601	0.27	4.5
	88	326	0	1601	0.27	4.9
	92	343	0	1601	0.27	4.7
	91	339	100	1483	0.27	4.4
Joung & Grasley, 2008 [67]	56	190	0	1565	0.30	8.3
	83	275	50	1396	0.30	5.1
	107	358	99	1227	0.30	3.4
Neithalath et al., 2010 [87]	103	312	0	1559	0.33	5.0
Huang et al., 2011 [88]	130	360	100	1430	0.36	4.0
Sumanasooriya & Neithalath, 2011 [41]	181	560	0	1253	0.32	2.2
	161	492	0	1285	0.33	2.6
	138	414	0	1281	0.33	3.1
	109	345	0	1612	0.32	4.7
	95	297	0	1634	0.32	5.5
	91	216	0	1652	0.42	7.6
Ibrahim et al., 2014 [89]	70	200	0	1600	0.35	8.0
	60	200	0	1600	0.30	8.0
	53	150	0	1800	0.35	12.0

Gesoglu et al., 2014 [90]	122	450	0	1594	0.27	3.5
Anush et al., 2016 [91]	122	487	0	1462	0.25	3.0
	117	391	0	1562	0.30	4.0
	114	326	0	1628	0.35	5.0
Nguyen et al., 2017 [92]	111	301	110	1574	0.37	5.2
Yu et al., 2019 [93]	117	378	0	1703	0.31	4.5
Debnath & Sarkar, 2020 [36]	131	468	77	1110	0.28	2.4
	136	453	77	1110	0.30	2.5
	140	438	77	1110	0.32	2.5
	146	418	77	1111	0.35	2.7
Elango et al., 2020 [94]	144	412	0	1360	0.35	3.3
Vieira et al., 2020 [95]	132	529	0	2117	0.25	4.0
	155	516	0	2063	0.3	4.0
Sandoval et al., 2020 [96]	176	518	0	1367	0.34	2.6
Shahedo et al., 2020 [44]	121	402	0	1612	0.3	4.0
	138	393	0	1574	0.35	4.0
	148	387	0	1590	0.38	4.1
Taheri et al., 2020 [48]	134	335	0	1340	0.4	4
	134	335	107.2	1232.8	0.4	3.68
	100.5	335	107.2	1232.8	0.3	3.68

2.2. Porosity of pervious concrete

A porous material is one composed of a solid matrix in which there are voids, filled with one or more fluids [97]. For example, the pores may be occupied by air or water, and where water completely fills the pores, the medium is considered saturated. The medium is characterized by a saturation value of between 0 and 1 [98]. The characteristics of porous media include:

- Homogeneous porous media: the resistance to the flow of a fluid in a given direction is the same at all points [99].
- Isotropic porous media: the medium's properties, including resistance to the flow of a fluid, are identical in all directions.
- Anisotropic porous media: the properties depend on the direction of observation, as is the case with most natural porous media [99], [100].

The porosity represents the volumetric proportion of the material occupied by the pores. This parameter provides quantitative information on the respective volumes of the two phases [101]. However, in the case of pervious concrete, it is possible to distinguish three types of porosity depending on the degree of interconnection of the pores: pores in the cement paste (0.5 to 1.5 nm); voids in the aggregate, which may or may not be interconnected; and air voids that are either small (10 μm to 1 mm) or large (> 1 mm) [58]:

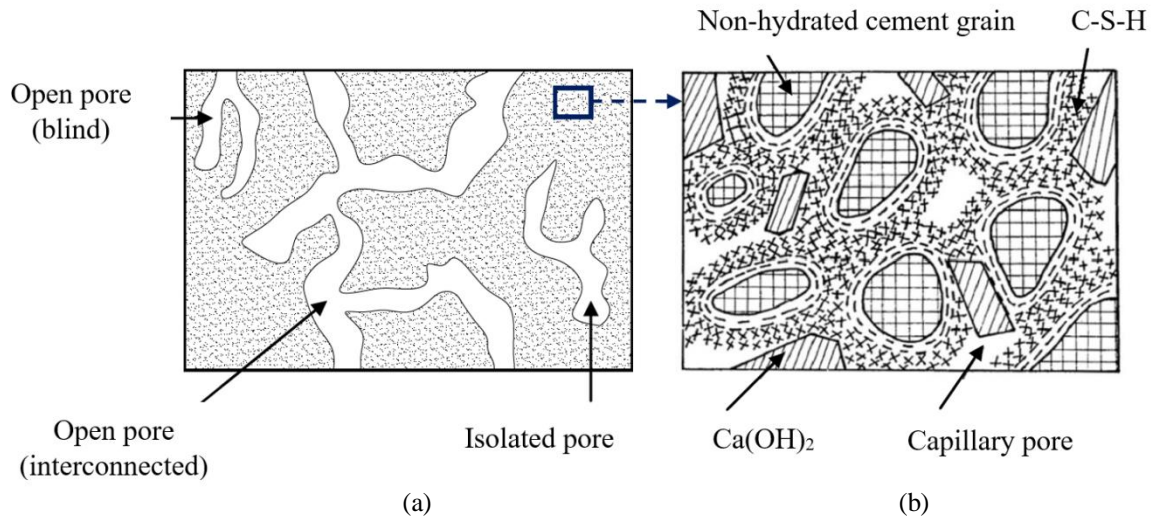


Fig. 3. Different types of pores in pervious concrete. Pores at macroscopic level (a), and capillary pores in the structure of the cement paste [102] (b).

From Fig. 3, we can distinguish the open, effective or continuous porosity P_0 of a pervious concrete. P_0 is the ratio between a) the volume of gravitational water that the porous concrete matrix can contain in its saturated state and then release when fully drained, and b) its total volume. We can examine two types of pores belonging to this family. The first are pores which all water to flow through the material, which are often called interconnected pores [56]. They are also called penetrating pores [103]. The second are blind pores, which are only open at one end, like a dead-end street (see **Eq. (1)**).

$$P_0 = P_{\text{open interconnected}} + P_{\text{open blind}} \quad (1)$$

We can also distinguish the total porosity of the pervious concrete P_t . This includes the volume of interconnected pores plus the isolated pores (closed air pockets) not connected to the external environment, plus the pores not accessible to gravitational water, and its total volume. In this definition, the total porosity includes all types of pores: nanoporosity, capillary porosity and large pores (**Eq. (2)**). As is the case with ordinary concrete, the porosity accessible to water measured in a vacuum is considered to be equal to the total porosity [56].

$$P_t = P_{\text{open interconnected}} + P_{\text{open blind}} + P_{\text{isolated}} + P_{\text{capillary}} + P_{\text{nanometric}} \quad (2)$$

Open porosity is easier to determine in comparison with total porosity [15], and has been the subject of numerous studies [70], [87], [104]–[106]. Lian et al. [80] found a linear relationship between the open porosity and total porosity of pervious concrete, on the basis of experimental data (**Eq. (3a)**). Zhong and Wille [107] also arrived at a similar equation (**Eq. (3b)**):

$$P_t = 0.78P_0 + 14.2 \quad (3a)$$

$$P_t = 0.67P_0 + 12 \quad (3b)$$

The open porosity of pervious concrete is between 15% and 35%, and the total porosity is between 15% and 40% [15], [70], [87], [108], [109]. According to Tennis et al. [31], the ideal open porosity for structural and hydraulic design is 20%. When less than 15%, hydraulic performance is poor, but mechanical strength is good. If the porosity is greater than 35%, the opposite is true.

For pervious concrete, the voids may measure between 2 and 8 mm, depending on the mix proportions. Thus, the characteristics of the aggregates used – namely, the degree of compaction [31], [110], volumetric proportion, typological structure of pores and particle size distribution – are critical parameters which determine the behavior of pervious concrete [111], and its performance [64], [112]. Table 2 offers a summary of the results found in the literature:

Table 2

Factors affecting the porosity of pervious concrete.

Factor	Effect on porosity	Reference
W/C ratio	Increasing the W/C ratio decreases porosity	[64], [113]
	No correlation between W/C ratio and porosity	[114]
Particle size distribution	Porosity increases with larger aggregates	[39], [115]
Compaction energy	Porosity decreases with increased compaction energy	[15], [39]
Cement paste content	Porosity is inversely proportional to cement paste content	[15], [64], [113], [116], [117]
Concrete thickness	Porosity varies throughout the thickness of the concrete	[38], [113], [118], [119]

Table 3 shows the different total porosities of different types of concrete:

Table 3

Total porosities of different types of concrete.

Type of concrete	Pervious concrete	Ordinary concrete	High performance concrete	Very high performance concrete	Ultra high performance fiber-reinforced concrete
Total porosity range (%)	15 – 40%	12 – 16%	9 – 12%	6 – 9%	1.5 – 6%

While there are ASTM standards for measuring the porosity of certain concretes and aggregates, such as the ASTM standard test method for unit weight, yield and (gravimetric) air content of concrete (C138-92), none is specific to pervious concrete.

The total porosity and dry density of the concretes (after vacuum evaporation and drying in an oven at 105°C) are determined by the hydrostatic (underwater) weighing method, in accordance with the NF P18-459 standard (AFNOR, 2010b). The test setup is shown in Fig. 4.



Fig. 4. Device for measuring porosity and apparent density [120].

For pervious concrete, most research is based on Archimedes' principle [21], [24], [39], [105], [121] in measuring open porosity. Samples are dried at 40°C for three days. A sample is then immersed in water for 30 minutes, and both its dry and underwater mass are determined. The open porosity of the sample is calculated using Eq. (4). This measurement method is used to calculate the density in air (40°C).

$$P_0 = \left[1 - \left(\frac{M_s - M_i}{\rho_w \times V_t} \right) \right] \times 100 \quad (4)$$

where:

- P_0 : open porosity (%);
- M_s : mass of the sample on leaving the oven at 40°C (kg);
- M_i : mass of the sample underwater (kg);
- V_t : total volume of the sample (m³);
- ρ_w : density of water (kg/m³).

Open pores allow water to infiltrate the concrete rapidly. Of those open pores, only the interconnected pores allow rapid infiltration of water through the pervious concrete to impart water permeability. Li et al. [122] measured the interconnected and open porosity separately. They measured the weight of pervious concrete samples twice: after 30 seconds of immersion in water and 24 hours after immersion. In the first 30 seconds, the water filled the interconnected pores, and thus the resulting porosity was considered the interconnected porosity. After 24 hours, the water filled in the open pores and therefore the resulting porosity was taken as the open porosity. Montes et al. [105] showed that increasing the immersion time beyond 30 minutes had a negligible impact on the value of the open porosity.

Based on this information, and given that the majority of researchers correlate open porosity with the mechanical properties of pervious concrete, this porosity has been used in this study to establish predictive models for the density and compressive strength of pervious concrete.

The effective porosity of pervious concrete can also be determined by a commonly used procedure, measuring the amount of water required to fill a sample of pervious concrete enclosed in a latex sleeve and converting it to an equivalent volume [72], [110], [123], [124].

Porosity can be statically determined using image analysis (IA), which is time-consuming and difficult to perform [123]. The experimental method of determining porosity is easy to implement, but the IA method may be a better choice because it can also provide other information such as tortuosity, volumes, areas, sizes, shapes, connectivities and pore diffusion [87], [119], [125]–[128]. X-ray tomography and scanners are used to measure porosity by IA [129], [87].

For pervious concrete, the majority of authors have found a linear relationship between open porosity and density. Fig. 5 presents a summary of the results found by the authors cited above. Their studies were similar, and are therefore comparable [21], [22], [116], [121], [130]–[132]. **Eq. (5)** of the resulting curve gives the relationship between density “ ρ (kg/m³)” and open porosity:

$$\rho = -18.505 P_0(\%) + 2370.5 \quad (5)$$

In general, ordinary impermeable concrete is pervious concrete that has zero open porosity. **Eq. (5)** shows that pervious concrete can have a density equal to 2370.5 kg/m³ when $P_0 = 0\%$. This density represents the absolute density of the pervious concrete which is almost equal to the density of ordinary concrete (about 2400 kg/m³ [133]). **Eq. (5)** therefore represents a model to relate the density of ordinary concrete to the density of pervious concrete.

This linear relationship between porosity and density is only valid for samples of cement-based pervious concrete and natural aggregates with no additives used when predicting the density or porosity. It is valid for pervious concrete samples with density between 1557 kg/m³ and 2300 kg/m³ and porosity between 8.8% and 41.8%. However, as mentioned previously, concrete with <15% open porosity exhibits very poor hydraulic performances [31].

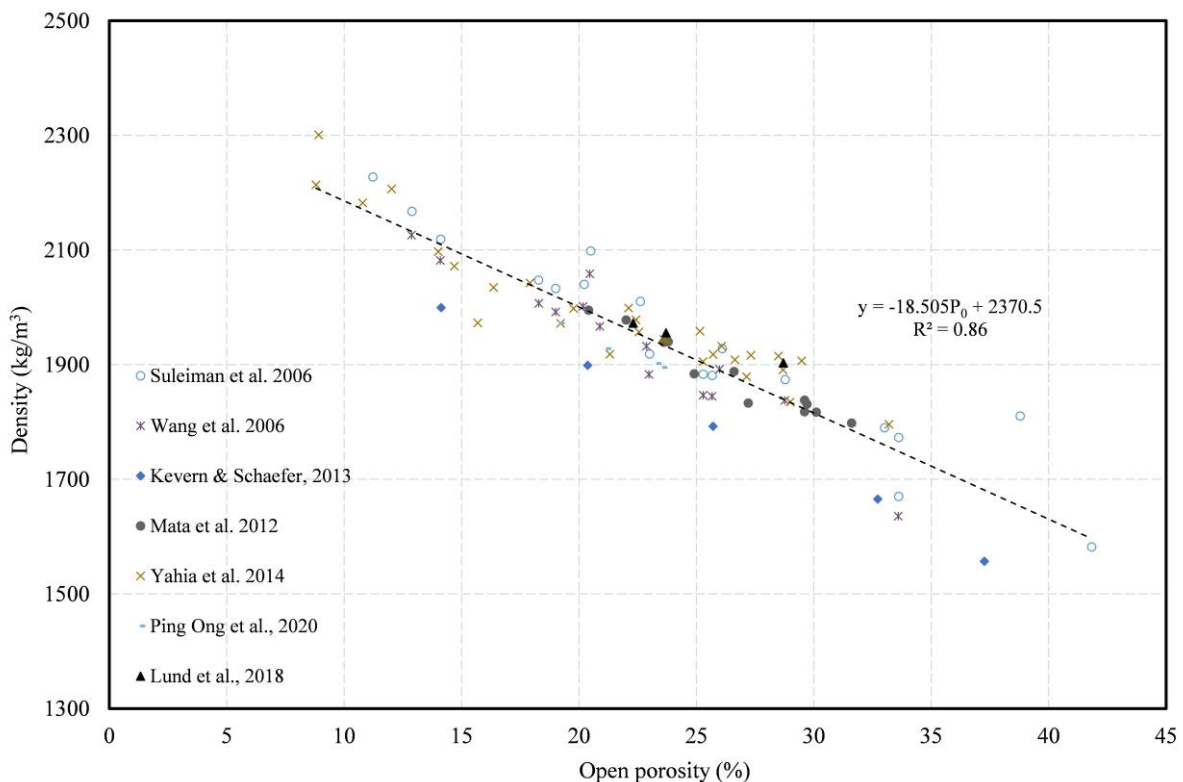


Fig. 5. Variation in density as a function of porosity, found in various studies available in the literature.

2.3. Permeability of pervious concrete

Hydraulic conductivity, or permeability, is the most relevant parameter defining any type of porous medium [23]. To avoid the risk of clogging, the minimum permeability must be equal to $1 \text{ mm}\cdot\text{s}^{-1}$ [21]. Several studies in the literature have established relationships between permeability and open porosity of pervious concrete. Different types of equations have been obtained: power [134], [104] [112], polynomial [135], [136], exponential [137], [138] and linear [81], [139]. In addition, some articles in the literature have, on the same graph, plotted the permeability K (cm/s) of 15 sets of data [140] and 17 sets of data [141] as a function of their porosity values P (%). The resulting curve of all data is presented in Figure 6. A linear relationship between porosity and permeability gives a low correlation coefficient ($R^2 = 0.236$).

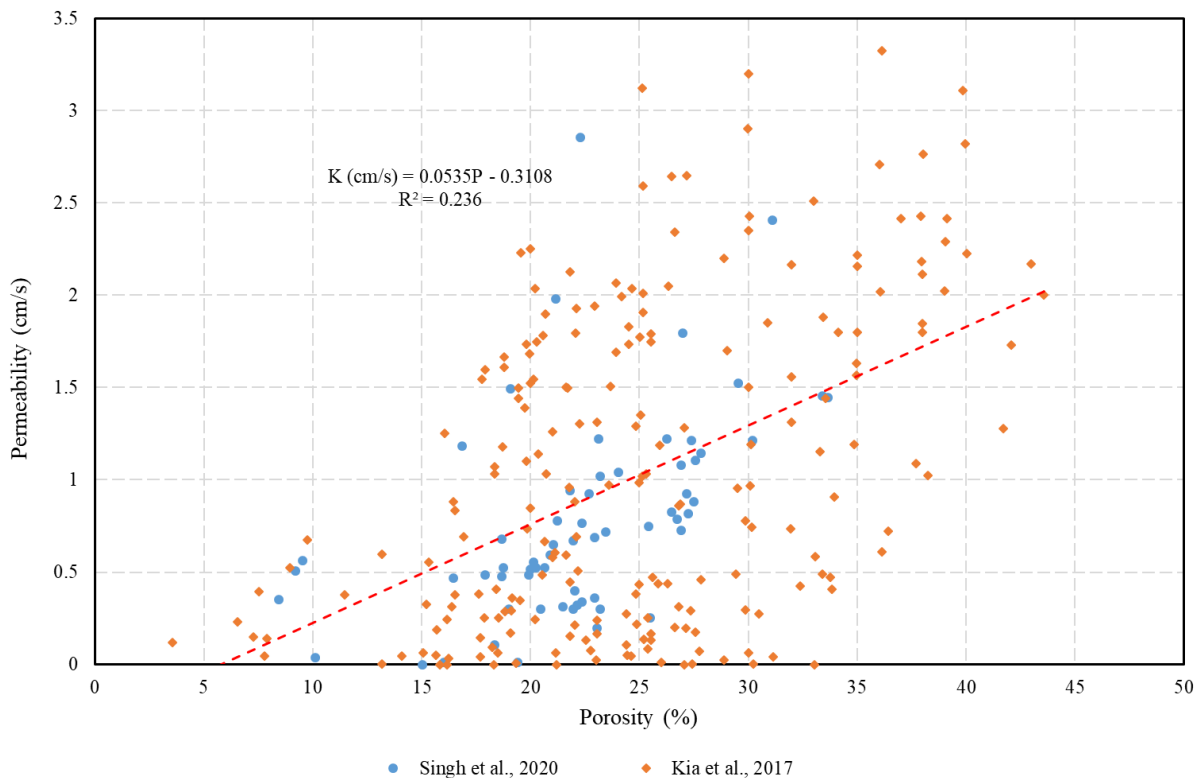


Fig. 6. Variation of permeability of pervious concrete as a function of porosity from two studies available in the literature [140], [141].

Figure 6 shows that permeability of pervious concrete increases with increasing porosity. The main reason behind the low correlation coefficients obtained is that these two graphs do not distinguish between the different types of porosity: total, interconnected and open, which have different values. In fact, the permeability of pervious concrete is more strongly related to the interconnected porosity than to the open porosity [122].

The second reason behind the low correlation coefficients is that these two graphs do not show the type of permeability measurement used in these studies. It can be seen that the permeability value of the same sample of pervious concrete can vary depending on the method used to measure it. Li et al. [122] found that the permeability obtained from a constant head permeability test (submerged water permeability) is higher than that from a falling head permeability test (un-submerged water permeability). This result is in agreement with that obtained by Sandoval et al. [142], who established a power relationship that relates the permeability coefficient obtained with these two permeability measurement methods according

to the equation: $K_{CH} = 1.518 K_{FH}^{2.95}$ ($R^2 = 0.97$) for pervious concrete mixtures made from four types of aggregates: basalt, blast furnace slag, ceramic waste, and recycled concrete aggregates.

3. Mechanical characteristics

3.1. Compressive strength of natural aggregate-based pervious concrete

One of the weak points of pervious concrete is its poor mechanical strength compared to conventional concrete. This is due to the presence of the pores within the pervious concrete, and the very thin layer of cement paste, which is insufficient to strongly bond the grains together [67]. Therefore, pervious concrete is of limited use in roads carrying heavy traffic. Generally, it is used in parking lots, where the necessary compressive strength is relatively low.

Pervious concrete mixes can offer compressive strengths ranging from 3.5 to 28 MPa [86], with a typical value of 17 MPa [31]. The compressive strength of conventional concrete, meanwhile, ranges between 20 and 40 MPa. Pervious concrete pavement is thicker than traditional concrete to compensate for its low compressive strength. For structural use as a low-traffic pavement, pervious concrete must have a compressive strength greater than 17 MPa [143]. The minimum for use in parking lots is 14 MPa. Pervious concrete with compressive strength below this value can be used for structures that do not accommodate rolling loads [144].

3.1.1. Relationship between porosity and compressive strength

Most studies show that, in general, the compressive strength of pervious concrete decreases exponentially with increasing porosity. However, there are studies that show a linear relationship between the compressive strength and porosity of pervious concrete [24], [39]. Fig. 7 shows the relationship between compressive strength (MPa) and open porosity (%) from data found in the literature [36], [37], [46], [48], [38]–[45]. The studies chosen concern only cement and natural aggregate-based pervious concrete mixtures. The **Eq. (8)** of the resulting curve gives the relationship between the 28-day compressive strength R_{28d} (MPa) and the porosity P_0 (%), calculated by means of the following formula:

$$R_{28d} = 65.341 e^{-0.067P_0} \quad (8)$$

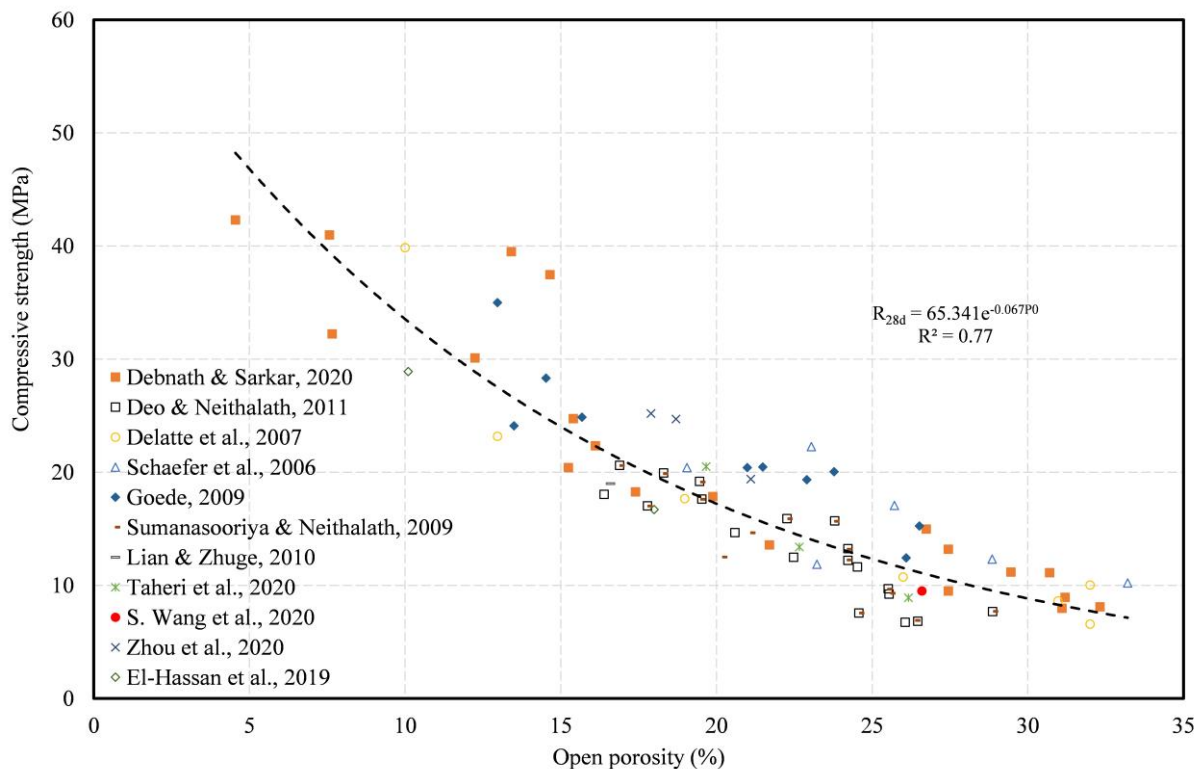


Fig. 7. Variation in compressive strength as a function of open porosity, found in several studies in the literature.

For the reported mixtures, an exponential relation (**Eq. (8)**, $R^2 = 0.7$) between 28-day compressive strength and porosity, shows a better fit for the resulting curve. The results of some studies (Fig. 7) show that the compressive strength of pervious concrete does not decrease steadily with increasing porosity. From these data and the coefficient of determination ($R^2 = 0.7$), we deduce that, while porosity is an important factor in controlling the compressive strength of pervious concrete, it cannot be used to infallibly predict that property.

3.1.2. Influence of aggregate size

Fig. 7 shows that there are other factors that influence the mechanical strength of pervious concrete. Indeed, a number of studies show that this strength decreases with increasing size of aggregate [107], [145]–[149]. In order to properly study the effect of aggregate size on the mechanical strength of pervious concrete, the only variable in the samples in each of these studies is the aggregate size; other factors, such as the degree of compaction, the W/B and aggregate/binder (A/B) ratios, and are kept constant. The properties of the mixtures from these studies are presented in Table 4.

Table 4

Design of pervious concrete mixtures based on several literature studies.

Study	Binder	Nature of the aggregates	W/B	A/B
Yang & Jiang 2003 [145]	Ordinary Portland cement	Natural gravel	0.33-0.35	-
Aagar-Ozbek et al., 2013 [146]	Alkali activated slag	Crushed basalt	0.3	5.7
Sun et al., 2018 [147]	Ordinary Portland cement	Natural gravel	-	8

Xie et al., 2020 [148]	Ordinary Portland cement	Crushing diabase stone	0.27	-
Zhong & Wille, 2016 [107]	Ordinary Portland cement	Quartz aggregates	0.55	2.5
Elango & Revathi, 2017 [149]	Ordinary Portland cement	Granite stones	0.35	3.3

All studies show that the compressive strength of pervious concrete decreases with increasing aggregate size (Fig. 8). A given particle size does not always result in identical compressive strengths. For example, the mechanical strengths of the pervious concrete from the study by Aagar-Ozbek et al. [146] were higher than those found by Sun et al. [147] (Fig. 8) with respect to the samples with particle sizes 2-4 mm and 4-8 mm. The difference in strength between the two studies is related to the condition of each experiment and to other factors such as the cement paste content, the degree of compaction, the nature of the aggregates used and their physical and mechanical characteristics. Indeed, the higher strength of the aggregates results in higher strength of the pervious concrete [150], [151].

Moreover, a different result was found by Yu et al. [93] who studied the effect of aggregate size on the compressive strength of pervious concrete. Eight pervious concrete samples were made up with the same W/C and A/C ratios, and relatively constant porosity of between 20.5% and 21.25%. The results show that when the equivalent aggregate size (average aggregate size of the narrow gradation aggregate [152]) is less than a certain value (approximately 7 mm), the compressive strength increases rapidly with increasing aggregate size. However, when larger than 7 mm, increasing the aggregate size does not significantly affect the compressive strength. This result also demonstrates that porosity alone is not sufficient to predict the compressive strength of pervious concrete, as the compressive strength of these eight samples ranges between 19.86 MPa and 32 MPa with almost equal porosity.

For pervious concrete samples with the same aggregate size, same porosity and same W/C and A/C, the compressive strengths vary depending on the type of aggregates used and their mechanical, physical and geometric properties [151].

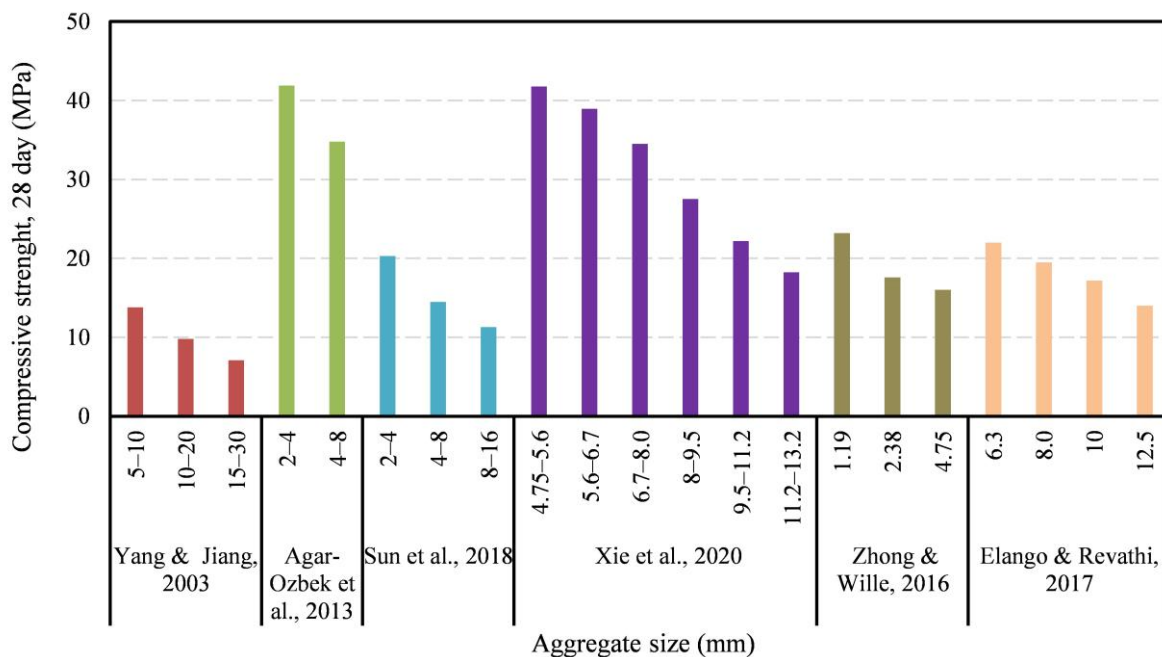


Fig. 8. Variation in compressive strength as a function of aggregate size,

found in several studies in the literature.

3.1.3. Influence of the water/cement ratio

The water/cement ratio is an essential factor which influences the compressive strength of pervious concrete. Xie et al. [148] measured the compressive strength of six pervious concrete samples with the same A/C ratio, the same aggregate size and the same cement paste thickness. Their results show that compressive strength decreases as the W/C ratio increases (Fig. 9).

In addition, some studies on pervious concrete where W/C is the only variable show that the relationship between the W/C ratio and compressive strength is not linear, and that there is an optimal W/C ratio for maximum compressive strength. Lian and Zhuge [148] shows that this optimal ratio is between 0.32 and 0.36. However, the study by Joung and Grasley [67] shows a value of between 0.3 and 0.35 for this optimal ratio. Joung and Grasley concluded that a low W/C ratio leads to poor workability and poor hydration of the cement, and therefore poor cohesion between the cement paste and the aggregates, which reduces the compressive strength. On the other hand, a high W/C ratio, produced when a large quantity of water is used, leads to an increase in capillary porosity, reducing the strength of the cement paste that binds the aggregates together. Although the workability is good, a large quantity of water and high W/C ratio decreases the compressive strength of the pervious concrete.

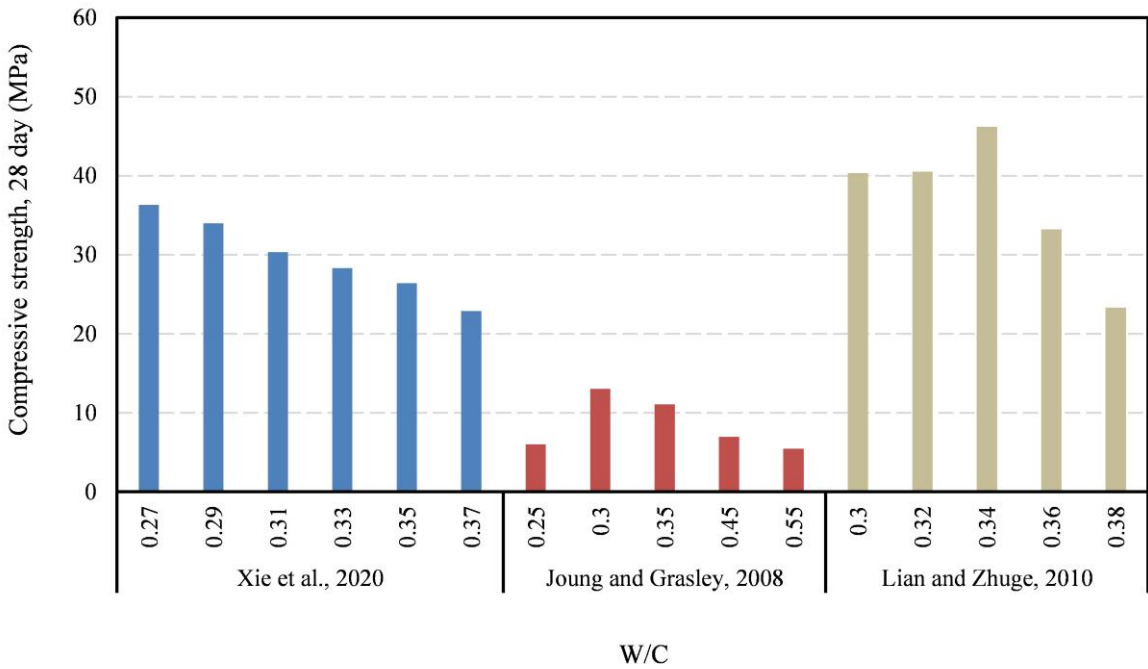


Fig. 9. Variation in compressive strength as a function of the W/C ratio, found in several studies in the literature.

3.1.4. Influence of thickness of cement paste

The amount of cement used affects the thickness of the paste coating the aggregates, which affects the pervious concrete’s porosity and other mechanical properties. Fig. 10 shows the variation in compressive strength as a function of the thickness of the cement paste for two studies in the literature [148], [153].

There is no developed standard for determining the cementitious paste thickness of a pervious concrete sample; A new procedure was established in the study by Torres et al. [153] which

defined the “cementitious paste thickness” as the average thickness of cementitious paste that surrounds each individual aggregate particle in a pervious concrete system. That is the maximum length from the edge of an individual aggregate particle to the outermost edge of the cement paste, which surrounds that individual piece of aggregate. In order to quantify the cementitious paste thickness, the samples were cut widthwise into cross-sections that were 100 mm (4 in.) wide. Once the relevant grid was overlaid on the cross-section, a digital measuring caliper was used to measure the cementitious paste thickness while measuring across each vertical and horizontal line. On the other hand, Xie et al. [148] used a different method to measure the thickness of the cement paste, based on the principle of image processing.

These two studies [148], [153] tested the compressive strength of pervious concrete samples with the same aggregate size and the same W/C ratio. The results show that this resistance increases as the thickness of the cement paste increases. In addition, the study by Xie et al. [148] shows that the compressive strength of pervious concretes F_c increases linearly with increasing compressive strength of the cement paste F_p . The relation between the two properties is described by **Eq. (9)**:

$$F_c = 0.279 F_p - 0.213 \quad (9)$$

In addition, the study by Torres et al. [153] shows that when the compaction energy increases for samples with the same dosage and the same amount of cement, the thickness of the cement paste increases and so, therefore, does the compressive strength of the samples.

The study by Joung and Grasley [67] shows that cement paste content and porosity tend to have more influence on the compressive strength than does the W/C ratio.

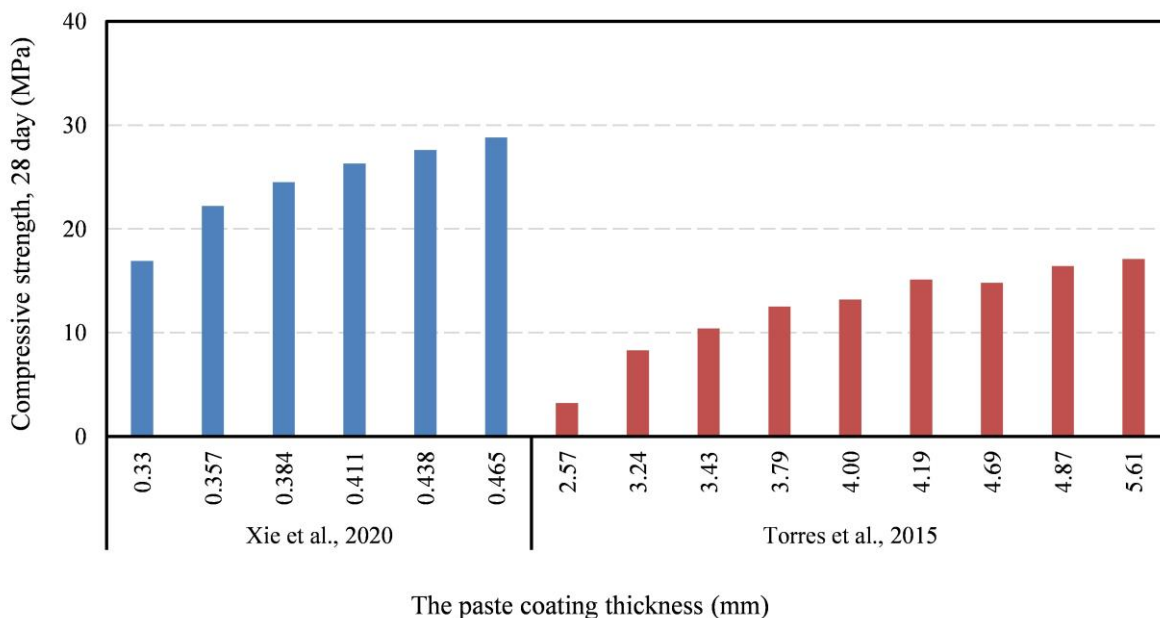


Fig. 10. Variation in compressive strength as a function of the cement paste thickness, found in several studies in the literature.

3.1.5. Influence of the aggregate/cement ratio (A/C)

To study the influence of the A/C ratio on the mechanical strength of pervious concrete, Fig. 11 presents the results of three studies [154]–[156] showing the variation of compressive

strength as a function of the A/C ratio. The results for each study concern concrete mixtures in which the A/C ratio is a variable (the W/C ratio and the size of the aggregates of the mixtures tested are identical). The studies by Zhong and Wille, 2016 [155] and by Sun et al. [156] show that compressive strength decreases as the A/C ratio increases. However, the results of the study by Wang et al. [154] show that there is an optimal A/C ratio for the maximum compressive strength of pervious concrete. According to this study, the optimum A/C ratio is 4.5, below which the compressive strength decreases because the cement dosage is not sufficient to completely coat the aggregates. In addition, if the A/C ratio is higher than 4.5, the compressive strength also decreases. This decrease is caused by the heat of hydration generated by the excess cement added to the mix. This creates a temperature difference between the inside and outside of the concrete, causing cracks and reducing the compressive strength.

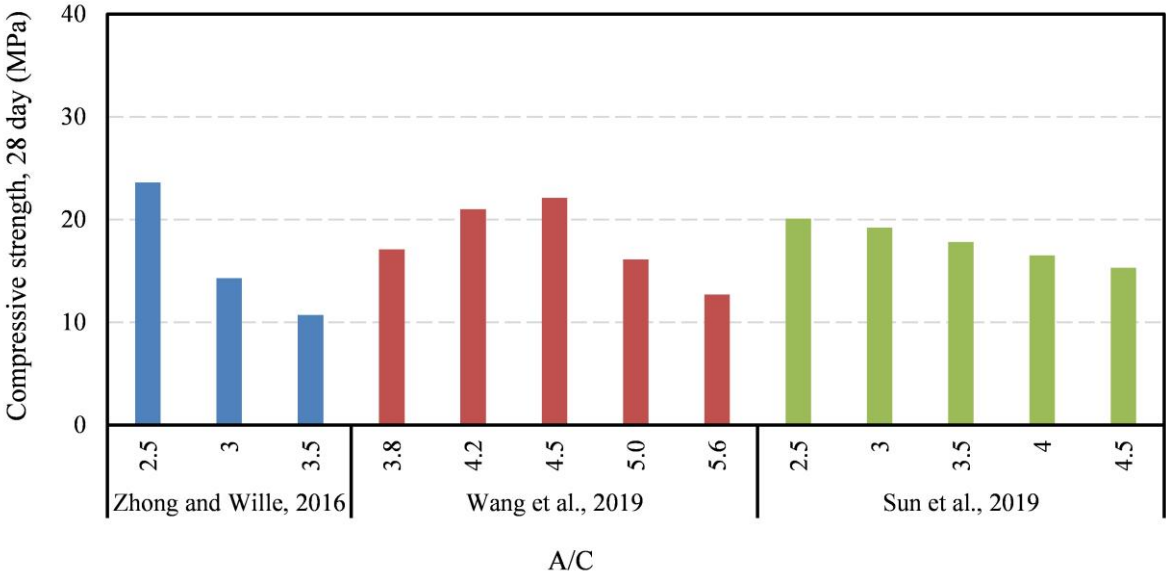


Fig. 11. Variation in compressive strength as a function of the A/C ratio, found in several studies in the literature.

Figs 8, 9 and 11 show that the compressive strength of pervious concrete is influenced by the W/C and A/C ratios and the aggregate size. Sun et al. [156] performed a sensitivity analysis (SA) to assess the influence of these variables on the prediction of compressive strength of pervious concrete using the importance score (IS), as shown in Fig. 12. This figure shows that compressive strength is more sensitive to the A/C ratio (IS = 0.0674) than to the W/C ratio (IS = 0.0487), while the size of the aggregates has less of an influence (IS = 0.0235). These results are in close accord with those obtained in earlier studies [70].

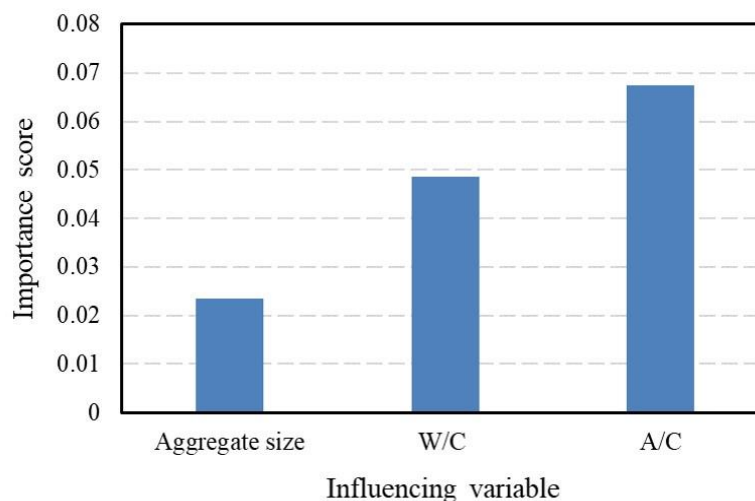


Fig. 12. Variable importance of compressive strength using SA

It should be noted that the IS was acquired based on the dataset for this study [156]. However, the study by Xie et al. [148] (Fig. 8) shows that the difference in simple compressive strength of pervious concrete between the sample with the smallest aggregate size (4.75-5.6 mm) and the sample with the largest aggregate size (11.2-13.2 mm) is 23.6 MPa, which represents a 56.5% decrease. Furthermore, in the same study, the difference in simple compressive strength of pervious concrete between the sample with the lowest W/C ratio (0.27) and the sample with the highest W/C ratio (0.37) is found to be 13.43 MPa, which is a 37% reduction (Fig. 9). Therefore, from this study, the aggregate size seems to have a greater influence on the compressive strength of the pervious concrete than does the W/C ratio, which contradicts the results of the sensitivity study presented in Fig. 12. We deduce that to obtain more representative results, a larger dataset with more influencing variables needs to be applied, so as to more accurately assess each factor's influence on the mechanical properties of the pervious concrete.

3.1.6. Empirical equations for predicting compressive strength

In most cases, compressive strength is determined by laboratory tests. Laboratory tests are more accurate, but they are expensive and laborious, since a large number of samples must be prepared and tested [156]. To alleviate this problem, some empirical equations have been put forward (Table 5).

Table 5

Reference	Matrix strength	Value Range	m	n	R ²	Equation
Zhong and Wille, 2016 [125]	UHSM ($f_0 = 174$ MPa)	AS: 1.19-4.75 mm; W/B: 0.44-0.55; A/B: 2.5-3.5; P_t : 17.02-32.75%	2.7	-0.25	0.669	$f_c = f_0(1 - mP_t)\left(\frac{d_a}{d_p}\right)^n$
	HSM ($f_0 = 61$ MPa)		2.6	-0.07	0.969	
	NSM ($f_0 = 29$ MPa)		2.5	0.2	0.997	

Chindaprasirt et al., 2009 [157]	$30 \text{ MPa} \leq f_0 \leq 135 \text{ MPa}$	AS: 2.5-20 mm; W/B: 0.225-0.30; A/B: 3-10.9; P_t : 15-35%	0.1962	0.0174	0.954-0.971	$f_c = f_0 e^{[-(m-n\varepsilon)P_t]}$
----------------------------------	--	--	--------	--------	-------------	--

Empirical equations for predicting the compressive strength of pervious concrete.

Here, UHSM, HSM and P-NSM represent the series of ultra-high strength matrix, high strength matrix and normal strength matrix respectively. AS is the size of the aggregates. m and n are empirical constants; P_t is the total porosity; f_c and f_0 are the 28-day unconfined compressive strength of the pervious concrete and of the matrix, respectively; d_a is the size of the aggregate; \bar{d}_p is the average pore size; ε is the fineness modulus of the aggregate.

According to Zhong and Wille's study [125], the matrix strength (cement paste strength) f_0 is obtained by using a 2-inch cube in accordance with ASTM C109/C109M-13. The compressive strength of pervious concrete f_c was determined based on ASTM C39. The average pore size \bar{d}_p is derived from the pore size distribution determined using linear path function, and d_a represents the sieve size that retained the aggregate. The total porosity P_t is defined as the ratio of total pore volume to the total volume of the sample (**Eq. (10)**). It takes account of the volume of accessible pores and the volume of non-accessible pores.

$$P_t = \frac{V_p}{V} = 1 - \frac{\rho}{\rho_t} \tag{10}$$

$$\rho = \frac{M}{V}$$

where V_p is the total volume of the pore system, V and ρ are the bulk volume and bulk density respectively and ρ_t is the density of the void free pervious concrete which can be calculated by **Eq. (11)**.

$$\rho_t = \frac{m_{agg} + m_m}{V_{agg} + V_m - \Delta V_m} = \frac{M}{V_{agg} + V_m - \Delta V_m} = \frac{(1 + \frac{A}{B}) \times m_m}{V_{agg} + V_m - \Delta V_m} = \frac{(1 + \frac{A}{B}) \times m_m}{V_{agg} + (1 - \frac{\Delta V_m}{V_m}) \times V_m}$$

$$V_{agg} = \frac{m_{agg}}{\rho_{agg}} \tag{11}$$

$$V_m = \frac{m_m}{\rho_{agg}}$$

where m_{agg} , m_m are the weight of aggregate and matrix respectively, V_{agg} and V_m are the dry volume of the aggregate and matrix, respectively, ΔV_m is the matrix volume reduction after hydration and ρ_{agg} is the density of aggregate. Research has shown that after hydration, the matrix volume reduction is 25% of the volume of the non-evaporable water (V_{new}) [155]. Neville [158] reported that the weight of non-evaporable water is about 23% of anhydrous

cement based on the assumption that cement is fully hydrated. This leads to **Eq. (12)** to calculate ΔV_m :

$$\Delta V_m = 25\% \times V_{\text{new}} = 25\% \times 23\% \times \frac{m_{\text{c hydrated}}}{\rho_w} \quad (12)$$

where $m_{\text{c hydrated}}$ is the mass of anhydrous cement which will be fully hydrated and ρ_w is the density of water.

From the correlation coefficients presented in Table 5, it can be seen that the equation proposed by Zhong et al. [125] works very well for the pervious concrete specimen with HSM and NSM, though less accurate for predicting the compressive strength of pervious concrete with UHSM. Interested readers may refer to the study by Zhong et al. [155] for further information on obtaining compressive strengths and the mixture proportions of the different matrices, such as normal strength matrix (NSM), high strength matrix (HSM) and ultra-high strength matrix (UHSM).

The equation proposed by Chindapasirt et al. [157] shows that the compressive strength of pervious concrete is controlled by two factors: the total porosity P_t and the fineness modulus of aggregate ϵ . Total porosity was measured using the test method for porous concrete as suggested by the Committee for Eco-concrete Research [159]. The compressive strength of paste was determined in accordance with ASTM C 39. The fineness modulus was obtained by adding the cumulative percentages of aggregates retained on each of the standard sieves ranging from 80 mm to 150 microns and dividing this sum by 100. This is an empirical factor which represents the average size of the aggregates. The equation proposed by this study is highly accurate in predicting the compressive strength of pervious concrete specimens with matrix strength ranging from 30 to 135 MPa.

As test data for the physical and mechanical properties of pervious concrete, regression models were also developed to relate the mechanical properties of pervious concrete with the proportions of the mixture components. Nassiri and AlShareedah [160] developed regression models to relate compressive strength with porosity, cement content, and water-to-cement ratio, while the model of Ibrahim et al. [161], relates the compressive strength of pervious concrete to the water and cement content, the water to cement ratio and aggregate size. The compressive strength regression models are shown in Table 6.

Table 6
Statistical models for predicting the compressive strength of pervious concrete.

Reference	Value Range	R ²	Statistical model
Nassiri & AlShareedah, 2017 [160]	f_c : 0.9-23.7 MPa; P_0 : 13-24% (ASTM C1754); W/C: 0.14-0.4; C: 150-415 kg/m ³	0.92	$f_c = 25.38 - 0.539P_0 - 13.12\left(\frac{W}{C}\right) + 0.0045$
Ibrahim et al., 2014 [161]	f_c : 1-6.95 MPa; C: 150-250 kg/m ³ ; W/C: 0.3-0.4; W: 45-100 kg/m ³ ;	0.85	$f_c = 0.8967 + 0.7289C + 8.163\left(\frac{W}{C}\right) + 1.4418W - 0.1824A1 - 0.1637A2 - 0.1693A3$

	Aggregate: 1500-1800 kg/m ³	
--	--	--

Here, A1, A2 and A3 represent 4.5 mm, 9.5 mm and 19.54 mm aggregate content (kg/m³) respectively.

The two models have relatively high correlation coefficients (0.85 and 0.92), but Ibrahim et al.'s [161] model is not as precise as Nassiri & Alshareedah's [160]. The reason may be related to the fact that this model does not consider the porosity factor, which is an essential factor that determines the mechanical properties.

3.2. Tensile strength

Existing research on the mechanical properties of pervious concrete has mainly focused on the effects of porosity and mix design on compressive strength [50]. While compressive strength is important for quality control and for assessing the mechanical behavior of pervious concrete, tensile strength is an important parameter in the design of conventional pavements [162].

Split tensile strength tests are generally performed according to the standard test method, using cylindrical concrete specimens (ASTM C496/C496 M-11) [163]. The tensile strength of pervious concrete varies from 0.85 to 4.3 MPa [164], while for conventional concrete it ranges from 2.4 to 4.1 MPa [165]. This represents 9 to 15% of the compressive strength of pervious concrete [22], [39], [86], [164]. These ratios are greater than those observed for conventional concrete whose tensile strength represents 7 to 12% of its compressive strength [166], [167].

There are many equations which correlate tensile strength and compressive strength for conventional concrete [54], [168], [169], but few which do the same for pervious concrete. Researchers have already compared the tensile and compressive strengths of pervious concrete, but very few have developed equations to precisely correlate these two properties. They have, however, produced equations which give the relationship between tensile strength F_{st} and compressive strength F_c [112], [170]–[172] or between tensile strength and porosity P [173]. These equations are summarized in Table 7.

Table 7

Equations for predicting the tensile strength of pervious concrete

References	Equation proposed	Observation
Ghafoori & Dutta, 1995 [112]	$F_{st} = c \times F_c^{0.5}$	Crushed limestone aggregates were used for the pervious concrete
Crouch et al., 2006 [170]	$F_{st} = 0.28 F_c^{0.55}$	Gravel and limestone aggregates were used for the pervious concrete
Delatte et al., 2009 [173]	$F_{st} = 5 e^{-0.0522P}$	Gravel and limestone aggregates were used for the pervious concrete
Ibrahim et al., 2014 [171]	$F_{st} = 0.0478 + 0.1706 F_c$	Crushed limestone aggregates were used for the pervious concrete
Caedicke et al., 2016 [172]	(1) $F_{st} = 0.177 F_c^{0.873}$ (2) $F_{st} = 0.203 F_c^{0.811}$ (3) $F_{st} = 0.224 F_c^{0.842}$ (4) $F_{st} = 0.181 F_c^{0.875}$	For the pervious concrete, (1) for the gravel aggregates, (2) for the limestone aggregates, (3) for the recycled aggregate mixtures and (4) for all three types of aggregates.

ACI 318, 2011 [174]	$F_{st} = 0.56F_c^{0.5}$	For conventional concrete
ACI 363, 1997 [175]	$F_{st} = 0.59 F_c^{0.5}$	For high-performance concrete

Note: "c" equals 5.67, 5.9 and 6.15 at the ages of 28, 60 and 90 days respectively; F_{st} and F_c are in psi (1 psi = 0.00689476 MPa) for the equation proposed by Ghafoori and Dutta and in MPa for the other equations; P is expressed in (%).

As with compressive strength, pervious concrete mixes containing smaller aggregates have higher tensile strength [149]. The addition of latex and fiber significantly improves the tensile and compressive strengths of pervious concrete. On the other hand, pervious concrete mixes containing sand sometimes had an even lower tensile strength than mixtures without sand [84].

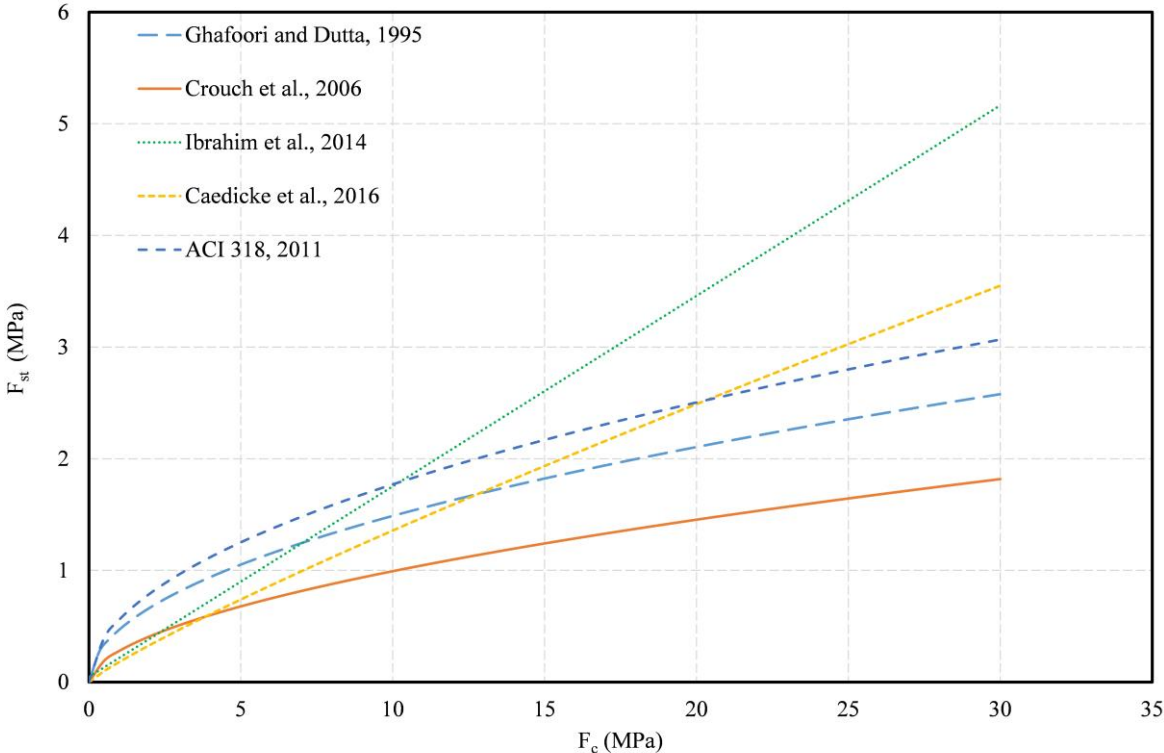


Fig. 13. Variation of tensile strength as a function of simple compressive strength from several studies on pervious concrete compared to that of conventional concrete.

All the curves presented in Fig. 13 show that tensile strength positively correlates with compressive strength. However, different values of tensile strength can be obtained for a given compressive strength. The reason may be related to the different dosages of pervious concrete used in each of these studies (types and sizes of aggregates, W/C and A/C, etc.). Furthermore, the ACI 318 equation, which establishes a correlation between the tensile and compressive strength of conventional concrete (Fig. 13), systematically overestimates the tensile strength of pervious concrete obtained with the equations proposed by Crouch et al. and by Ghafoori and Dutta, irrespective of the compressive strength value. It also overestimates the tensile strength obtained with the equation proposed by Caedicke et al. for a compressive strength of less than 20 MPa, as well as that obtained with the equation proposed by Ibrahim et al. for a compressive strength of less than 10 MPa. However, the equation proposed by Ibrahim et al. does not tally with the physical law on strength of materials – the tensile strength obtained with this equation is non-zero for a compressive strength of 0 MPa.

3.3. Simple flexural strength

The flexural strength of pervious concrete in a rigid pavement is a crucially important design factor [31]. The flexural strength of pervious concrete is between 1 and 3.8 MPa [31], [63], [86]. Many factors influence flexural strength – in particular, the degree of compaction, the aggregate/cement ratio, and the porosity [31]. An increased aggregate size leads to a decrease in the compressive and flexural strengths due to the increased porosity [176]. This strength is determined in accordance with ASTM C 7802 (ASTM, 2004), which uses a beam measuring $152.4 \times 152.4 \times 508 \text{ mm}^3$. One of the problems in determining the flexural strength is that the behavior is assumed to be elastic up to the point of failure, which is not the case. This misapprehension can lead to discrepancies between the measured and predicted values [144].

It is therefore common to measure compressive strengths and to use an empirical method to determine the flexural strength of pervious concrete. There are many equations which correlate the flexural strength and the compressive strength of conventional concrete [53]–[55]. According to ACI report 552R-10 on pervious concrete [59], Crouch et al.'s, 2006 relation [144] between the flexural strength F_{fs} and compressive strength F_c of pervious concrete most closely matches the equation established by Ahmad and Shah, 1985 [177] for conventional concrete: $F_{fs} = 2.3 F_c^{2/3}$ (F_{fs} and F_c in psi) or $F_{fs} = 0.445 F_c^{2/3}$ (F_{fs} and F_c in MPa). This relation is recommended and is promulgated by the ACI 330 committee “Guide for Design and Construction of Concrete Parking Lots” [178].

Few studies in the literature have yet compared the flexural and compressive strengths of pervious concrete, with a virtual absence of models or equations that precisely correlate these two properties. On the same graph, we presented the results of certain studies after 2006, for two reasons. The first is to propose an equation to connect these two properties – a global equation, whatever the combinations used in the formulation of the pervious concrete. The second is to assess the accuracy of Ahmad and Shah's relation for predicting the flexural strength of pervious concrete on the basis of the compressive strength. The pervious concretes used in the selected studies, which are presented in Table 8, have differing dosages and various aggregate types.

Table 8

Various studies comparing the flexural and compressive strengths of pervious concrete.

References	Observation
Ahmad & Shah, 1985 [177]	Conventional concrete based on natural aggregates
Crouch et al., 2006 [144]	Pervious concrete, gravel and limestone aggregates were used
Cheng et al., 2011 [179]	Pervious concrete based on recycled aggregates obtained from construction waste
Chindaprasirt et al., 2014 [180]	Pervious concrete based on recycled lightweight aggregates from autoclaved cellular concrete block waste
Ibrahim et al., 2014 [171]	Pervious concrete based on crushed limestone aggregates
Liu et al., 2018 [181]	Pervious concrete based on coarse natural granite aggregates
Grubeša et al., 2018 [182]	Pervious concrete based on two different types of aggregates: dolomite and steel slag

Ulloa-Mayorg et al., 2018 [183]	Pervious concrete based on two different types of recycled aggregates from construction and demolition waste: (1) ceramic brick aggregates, and (2) crushed concrete aggregates
Vieira et al., 2020, [95]	Pervious concrete formulated from two types of coarse aggregates: natural basaltic aggregate and recycled aggregate from construction and demolition waste

The relations between the flexural and compressive strengths in the studies shown in Table 8 are illustrated in Fig. 14.

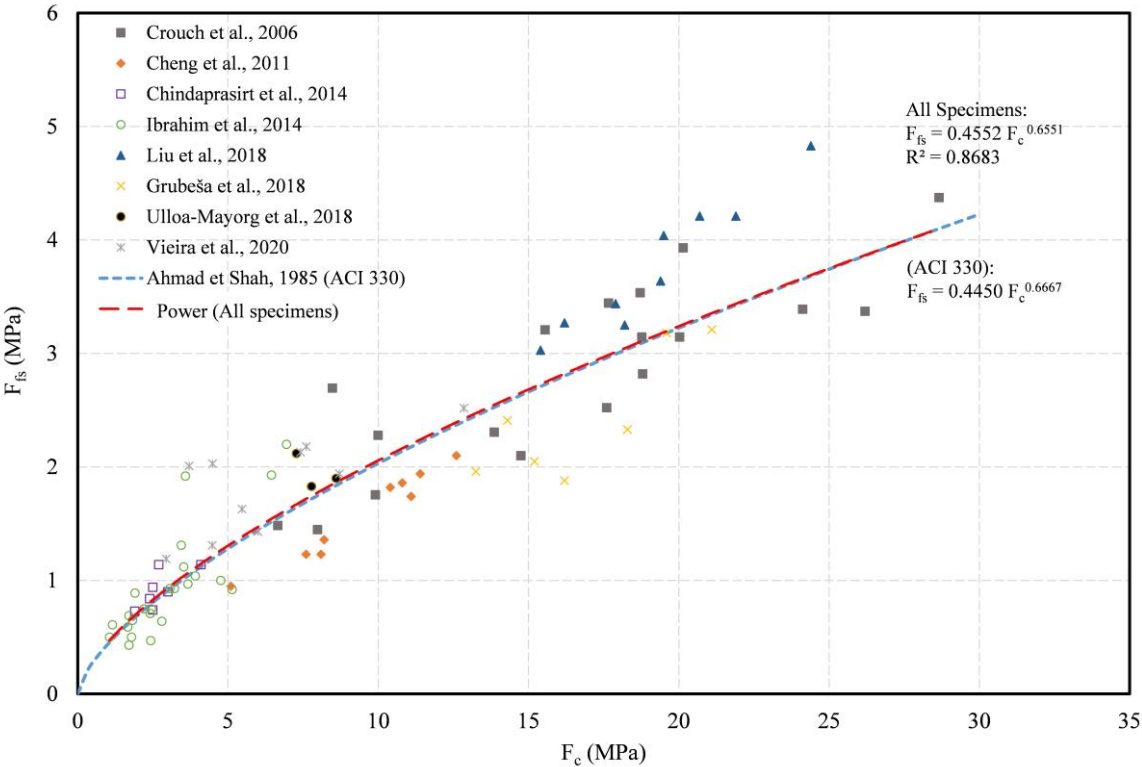


Fig. 14. Variation of flexural strength as a function of simple compressive strength, on the basis of several studies on pervious concrete, compared to the same correlation in conventional concrete.

Fig. 14 shows that the flexural and compressive strengths of ordinary concrete and all combinations of pervious concrete are positively correlated. In addition, it can be deduced that the relation recommended by ACI 330, which was established by Ahmad and Shah, is representative not only for pervious concrete mixes based on natural aggregates of gravel and limestone, but also for all other mixes based on natural and recycled aggregates. Indeed, the curve for all the pervious concrete samples and that of the ACI 330 relation are almost identical. There is a difference between them of 0–2.3% for a compressive strength varying from 1 to 30 MPa.

Conclusions and avenues for future research

Pervious concrete is a coating material with low mechanical strength because of its porous structure, which limits its applicability. There is abundant literature documenting the different mechanical properties of pervious concrete, but a lack of a systematic series of studies to summarize these properties. In this context, the objective of this paper was to methodically

examine the current state of knowledge as to the mechanical aspect of pervious concrete, with emphasis on the influencing factors. The main conclusions that can be drawn are:

- The density of pervious concrete decreases linearly with increasing porosity. This density depends on other factors such as the type of natural aggregates and their physical and geometric properties, the A/C ratio, the cement paste content and the amount of fine aggregates used.
- The permeability of pervious concrete increases with increasing porosity. The type of porosity and the method of permeability measurement need to be specified to better correlate the permeability to the porosity of the paving material.
- The compressive strength of pervious concrete decreases exponentially with increasing porosity. Porosity alone is insufficient to accurately predict this property, which depends on other factors such as W/C and A/C, cement paste content, plus the type and mechanical, physical and geometric properties of the aggregates.
- For structural use as a low-traffic pavement, pervious concrete needs to have a compressive strength greater than 17 MPa. In order to maximize the compressive strength of pavement concrete from a practical perspective, it should be proportioned with a W/C ratio of 0.3 to 3.6 and an A/C ratio of 4.2 to 5 based on results found in the literature. In addition, the use of finer aggregates always provides higher compressive strength. Compressive strength can also be improved with the addition of a certain amount of sand, up to a maximum of 10% of the aggregate mass and increasing the degree of compaction. However, many studies fail to provide sufficient detail on the method and degree of compaction, making the comparison of mechanical and other performance indicators invalid in some cases. These techniques may negatively impact the infiltration rate of pervious concrete. A permeability test is required to verify that the permeability is greater than $1 \text{ mm}\cdot\text{s}^{-1}$ so that the pavement continues to serve its principal function of stormwater management.
- A limited number of studies have developed equations which give the relationship between tensile and compressive strengths of pervious concrete. There are discrepancies between the values of the tensile strength obtained from these models. In addition, the model for predicting the tensile strength of conventional concrete cannot be applied to pervious concrete.
- The model to predict flexural strength of pervious concrete on the basis of its compressive strength, established from the data of various studies, is almost the same as that for conventional concrete. Consequently, the model for conventional concrete latter can be used to predict the flexural strengths of pervious concrete mixes from their compressive strengths.

Given the significant number of factors that influence the mechanical strength of pervious concrete, a sensitivity study on a large dataset, considering all the influencing variables, is necessary. Such a study would improve the design of pervious concrete mixtures, helping to find the most influential factors and the optimal dosage to maximize the mechanical strengths (whereas up until now, the use of pervious concrete has been limited to parking areas or roads with little traffic). This study must also consider the influence of all these factors on hydraulic conductivity, as rainwater management is the main role of such coatings.

As to modeling pervious concrete, there have been few studies devoted to establishing a quantitative relation between the properties of the pores, such as their size, shape, distribution and tortuosity. Advanced modeling and characterization could revolutionize the use of pervious concrete technology. This study has focused on the relationship between porosity and the mechanical characteristics of conventional cement-based pervious concretes, with densities

between 1300 kg/m^3 and 2300 kg/m^3 . In the future, it would be beneficial to establish the same relations for pervious concretes which have a density of between 500 and 1300 kg/m^3 – generally the case for pervious concretes based on lightweight aggregates – given that these frequently exhibit poor mechanical strength which limits their use.

Bibliography

- [1] Y. Azzout, S. Barraud, F. N. Cres, and E. Alfakih, “Techniques Alternatives en Assainissement Pluvial”, *Technique et Documentation*. p. 372, 1994.
- [2] J.-L. Bertrand-Krajewski, “Cours d’hydrologie urbaine”, Insa Lyon, 2006.
- [3] E. Z. Bean, W. F. Hunt, D. A. Bidelspach, and R. J. Burak, “Study on the infiltration rate of permeable pavements”, 2004.
- [4] N. Jayasuriya and N. Kadurupokune, “Impact of Pervious Pavements on Drainage Infrastructure”, pp. 1–10, 2008.
- [5] A. Mohajerani, J. Bakaric, and T. Jeffrey-Bailey, “The urban heat island effect, its causes, and mitigation, with reference to the thermal properties of asphalt concrete”, *J. Environ. Manage.*, vol. 197, pp. 522–538, 2017, doi: 10.1016/j.jenvman.2017.03.095.
- [6] J. Fahed, “Etude numérique du potentiel de rafraîchissement des techniques de réduction des îlots de chaleur urbain (ICU) sous climat méditerranéen”, 2019.
- [7] Y. Yamamoto, “Measures to Mitigate Urban Heat Islands”, *Environ. Energy Res. Unit. Quaterly Rev.*, vol. 18, pp. 65–83, 2005.
- [8] M. Giguère, “Mesures de lutte aux îlots de chaleur urbains”, 2009.
- [9] Y. Qin, Y. He, J. E. Hiller, and G. Mei, “A new water-retaining paver block for reducing runoff and cooling pavement”, *J. Clean. Prod.*, vol. 199, pp. 948–956, 2018, doi: 10.1016/j.jclepro.2018.07.250.
- [10] Y. Qin and J. E. Hiller, “Understanding pavement-surface energy balance and its implications on cool pavement development”, *Energy Build.*, vol. 85, pp. 389–399, 2014, doi: 10.1016/j.enbuild.2014.09.076.
- [11] S. P., G. P., and C. W.G., “Urban evaporation rates for water-permeable pavements”, *Water Science and Technology*, vol. 62, no. 5. pp. 1161–1169, 2010.
- [12] Y. Qin and J. E. Hiller, “Water availability near the surface dominates the evaporation of pervious concrete”, *Constr. Build. Mater.*, vol. 111, pp. 77–84, 2016, doi: 10.1016/j.conbuildmat.2016.02.063.
- [13] J. Faleyieux, “Elements modulaires en beton pour revêtement des ouvrages d’infiltration des eaux pluviales: référentiel technique”, Epernon, Fr. CERIB, 2015.
- [14] G. M. Majersky, “Filtration of Polluted Waters Filtration of Polluted Waters by Pervious Concrete by Pervious Concrete by Pervious Concrete”, 2010.
- [15] D. H. Nguyen, “Étude du comportement hydromécanique des bétons drainants à base de coproduits coquilliers”, thèse de doctorat pour obtenir le Doctorat de l’Université de Caen Basse -Normandie Spécialité : Génie des Matériaux, 2014.
- [16] K. Okada, S. Matsui, T. Isobe, Y. Kameshima, and A. Nakajima, “Water-retention properties of porous ceramics prepared from mixtures of allophane and vermiculite for materials to counteract heat island effects”, *Ceram. Int.*, vol. 34, no. 2, pp. 345–350, 2008, doi: 10.1016/j.ceramint.2006.10.006.
- [17] A. Dawson, “Water in road structures: movement, drainage & effects”, vol. 5. Springer Science & Business Media, 2008.
- [18] D. Thorpe and Y. Zhuge, “Advantages and disadvantages in using permeable concrete pavement as a pavement construction material”, *Assoc. Res. Constr. Manag. ARCOM 2010 - Proc. 26th Annu. Conf.*, no. September, pp. 1341–1350, 2010.
- [19] J. P. Christory and J. Abdo, “Voiries et aménagements urbains en beton-structures reservoirs et aménagements qualitatifs”, *rev. gen. des routes*, no. 775, 1999.
- [20] M. Kováč and A. Sičáková, “Pervious concrete as a sustainable solution for pavements in urban areas”, *10th Int. Conf. Environ. Eng. ICEE 2017*, vol. 2017-April, no. April, pp. 27–28, 2017, doi: 10.3846/enviro.2017.031.
- [21] K. Wang, V. R. Schaefer, J. T. Kevern, and M. T. M. M. T. Suleiman, “Development of Mix Proportion for Functional and Durable Pervious Concrete”, *NRMCA Technol. Forum Focus Pervious Concr.*, no. December, pp. 1–12, 2006.
- [22] M. Suleiman, J. Kevern, V. R. Schaefer, and K. Wang, “Effect of compaction energy on pervious concrete properties”, *Concr. Technol. Forum-Focus Pervious Concr. Natl. Ready Mix Concr. Assoc. Nashville, TN*, no. January, pp. 23–25, 2006.
- [23] B. Debnath and P. P. Sarkar, “Permeability prediction and pore structure feature of pervious concrete using brick as aggregate”, *Constr. Build. Mater.*, vol. 213, pp. 643–651, 2019, doi: 10.1016/j.conbuildmat.2019.04.099.

- [24] J. T. Kevern, V. R. Schaefer, K. Wang, and M. T. Suleiman, "Pervious concrete mixture proportions for improved freeze-thaw durability", *J. ASTM Int.*, vol. 5, no. 2, 2008, doi: 10.1520/JAI101320.
- [25] J. X. Lu, X. Yan, P. He, and C. S. Poon, "Sustainable design of pervious concrete using waste glass and recycled concrete aggregate", *J. Clean. Prod.*, vol. 234, pp. 1102–1112, 2019, doi: 10.1016/j.jclepro.2019.06.260.
- [26] Y. Zaetang, A. Wongsas, V. Sata, and P. Chindaprasirt, "Use of lightweight aggregates in pervious concrete", *Constr. Build. Mater.*, vol. 48, pp. 585–591, 2013, doi: 10.1016/j.conbuildmat.2013.07.077.
- [27] D. H. Nguyen, M. Boutouil, N. Sebaibi, L. Leleyter, and F. Baraud, "Valorization of seashell by-products in pervious concrete pavers", *Constr. Build. Mater.*, vol. 49, pp. 151–160, 2013, doi: 10.1016/j.conbuildmat.2013.08.017.
- [28] S. P. Yap, P. Z. C. Chen, Y. Goh, H. A. Ibrahim, K. H. Mo, and C. W. Yuen, "Characterization of pervious concrete with blended natural aggregate and recycled concrete aggregates", *J. Clean. Prod.*, vol. 181, pp. 155–165, 2018, doi: 10.1016/j.jclepro.2018.01.205.
- [29] R. Sriravindrarajah, N. D. H. Wang, and L. J. W. Ervin, "Mix Design for Pervious Recycled Aggregate Concrete", *Int. J. Concr. Struct. Mater.*, vol. 6, no. 4, pp. 239–246, 2012, doi: 10.1007/s40069-012-0024-x.
- [30] S. D. Infiltration, D. E. S. Eaux, and I. O. Principaux, "Les revêtements perméables", no. 2007, 2008.
- [31] P. D. Tennis, M. L. Leming, and D. J. Akers, "Pervious Concrete Pavements", 2004.
- [32] M. Scholz and P. Grabowiecki, "Review of permeable pavement systems", *Build. Environ.*, vol. 42, no. 11, pp. 3830–3836, 2007, doi: 10.1016/j.buildenv.2006.11.016.
- [33] J. Bruinsma et al., "Guidance for Usage of Permeable Pavement at Airports", no. Project 02-64, 2017.
- [34] E. T. Cackler, T. Ferragut, D. S. Harrington, R. O. Rasmussen, and P. Wiegand, "Evaluation of US and European concrete pavement noise reduction methods", 2006.
- [35] P. T. Weiss, M. Kayhanian, J. S. Gulliver, and L. Khazanovich, "Permeable pavement in northern North American urban areas: research review and knowledge gaps", *Int. J. Pavement Eng.*, vol. 20, no. 2, pp. 143–162, 2019.
- [36] B. Debnath and P. P. Sarkar, "Characterization of pervious concrete using over burnt brick as coarse aggregate", *Constr. Build. Mater.*, vol. 242, p. 118154, 2020, doi: 10.1016/j.conbuildmat.2020.118154.
- [37] O. Deo and N. Neithalath, "Compressive response of pervious concretes proportioned for desired porosities", *Constr. Build. Mater.*, vol. 25, no. 11, pp. 4181–4189, 2011, doi: 10.1016/j.conbuildmat.2011.04.055.
- [38] N. Delatte, D. Miller, and A. Mrkajic, "Portland cement pervious concrete pavement: Field performance investigation on parking lot and roadway pavements", 2007.
- [39] V. R. Schaefer and K. Wang, "Mix design development for pervious concrete in cold weather climates", Iowa. Dept. of Transportation. Highway Division, 2006.
- [40] W. G. Goede, "Pervious Concrete: investigation into structural performance and evaluation of the applicability of existing thickness design methods", 2009.
- [41] M. S. Sumanasooriya and N. Neithalath, "Pore structure features of pervious concretes proportioned for desired porosities and their performance prediction", *Cem. Concr. Compos.*, vol. 33, no. 8, pp. 778–787, 2011, doi: 10.1016/j.cemconcomp.2011.06.002.
- [42] C. Lian and Y. Zhuge, "Optimum mix design of enhanced permeable concrete - An experimental investigation", *Constr. Build. Mater.*, vol. 24, no. 12, pp. 2664–2671, 2010, doi: 10.1016/j.conbuildmat.2010.04.057.
- [43] H. El-hassan, P. Kianmehr, and S. Zouaoui, "Properties of pervious concrete incorporating recycled concrete aggregates and slag", *Constr. Build. Mater.*, vol. 212, pp. 164–175, 2019, doi: 10.1016/j.conbuildmat.2019.03.325.
- [44] S. Kant Sahdeo, G. D. Ransinchung, K. L. Rahul, and S. Debbarma, "Effect of mix proportion on the structural and functional properties of pervious concrete paving mixtures", *Constr. Build. Mater.*, vol. 255, p. 119260, 2020, doi: 10.1016/j.conbuildmat.2020.119260.
- [45] H. Zhou, H. Li, A. Abdelhady, X. Liang, H. Wang, and B. Yang, "Experimental investigation on the effect of pore characteristics on clogging risk of pervious concrete based on CT scanning", *Constr. Build. Mater.*, vol. 212, pp. 130–139, 2019, doi: 10.1016/j.conbuildmat.2019.03.310.
- [46] S. Wang, G. Zhang, B. Wang, and M. Wu, "Mechanical strengths and durability properties of pervious concretes with blended steel slag and natural aggregate", *J. Clean. Prod.*, vol. 271, p. 122590, 2020, doi: 10.1016/j.jclepro.2020.122590.
- [47] G. Wang, X. Chen, Q. Dong, J. Yuan, and Q. Hong, "Mechanical performance study of pervious concrete using steel slag aggregate through laboratory tests and numerical simulation", *J. Clean. Prod.*, vol. 262, p. 121208, 2020, doi: 10.1016/j.jclepro.2020.121208.
- [48] B. M. Taheri, A. M. Ramezani-pour, S. Sabokpa, and M. Gapele, "Experimental evaluation of freeze-thaw durability of pervious concrete", *J. Build. Eng.*, vol. 33, no. November 2019, p. 101617, 2021, doi: 10.1016/j.job.2020.101617.

- [49] O. Deo and N. Neithalath, "Compressive behavior of pervious concretes and a quantification of the influence of random pore structure features", *Mater. Sci. Eng. A*, vol. 528, no. 1, pp. 402–412, 2010, doi: 10.1016/j.msea.2010.09.024.
- [50] C. Gaedicke, A. Torres, K. C. T. Huynh, and A. Marines, "A method to correlate splitting tensile strength and compressive strength of pervious concrete cylinders and cores", *Constr. Build. Mater.*, vol. 125, pp. 271–278, 2016, doi: 10.1016/j.conbuildmat.2016.08.031.
- [51] Y. Choi and R. L. Yuan, "Experimental relationship between splitting tensile strength and compressive strength of GFRC and PFRC", *Cem. Concr. Res.*, vol. 35, no. 8, pp. 1587–1591, 2005.
- [52] X. Chen, S. Wu, and J. Zhou, "Influence of porosity on compressive and tensile strength of cement mortar", *Constr. Build. Mater.*, vol. 40, pp. 869–874, 2013.
- [53] M. Ahmed, K. M. El Hadi, M. A. Hasan, J. Mallick, and A. Ahmed, "Evaluating the co-relationship between concrete flexural tensile strength and compressive strength", *Int. J. Struct. Eng.*, vol. 5, no. 2, pp. 115–131, 2014, doi: 10.1504/IJSTRUCTE.2014.060902.
- [54] M. I. Juki et al., "Relationship between compressive, splitting tensile and flexural strength of concrete containing granulated waste Polyethylene Terephthalate (PET) bottles as fine aggregate", in *Advanced materials research*, 2013, vol. 795, pp. 356–359.
- [55] M. I. Mousa, M. G. Mahdy, A. H. Abdel-Reheem, and A. Z. Yehia, "Mechanical properties of self-curing concrete (SCUC)", *HBRC J.*, vol. 11, no. 3, pp. 311–320, 2015, doi: 10.1016/j.hbrj.2014.06.004.
- [56] D. H. Nguyen, "Etude du comportement hydromécanique des bétons drainants à base de coproduits coquilliers." Caen, 2014.
- [57] R. Zhong and K. Wille, "Material design and characterization of high performance pervious concrete", *Constr. Build. Mater.*, vol. 98, pp. 51–60, 2015, doi: 10.1016/j.conbuildmat.2015.08.027.
- [58] Y. Aoki, "Development of pervious concrete." 2009.
- [59] ACI 552R-10, "Report on pervious concrete, American concrete institute", 2010.
- [60] E. Bush, B. Cawley, S. Durham, K. MacKenzie, J. Rottman, and D. Thomaz, "Specifier's Guide for Pervious Concrete Pavement Design", p. 24, 2008.
- [61] Y. Matsuo, K. Morino, and E. Iwatsuki, "A study of porous concrete using electric arc furnace oxidizing slag aggregate", *Bull. Aichi Inst. Technol. Part B*, vol. 40, no. 40, pp. 117–167, 2005.
- [62] A. Mulligan, "Attainable Compressive Strength of Pervious Concrete Paving Systems", p. 132, 2005.
- [63] J. Farny and F. In, "Aging gracefully: Architectural concrete panels turn 40 years old", *Concr. Technol. today*, pp. 1–8, 2004.
- [64] R. C. Meininger, "No-Fines Pervious Concrete for Paving", *Concrete International*, vol. 10, no. 8, pp. 20–27, 1988.
- [65] ACI 211, "Guide for Selecting Proportions for No-Slump Concrete Reported by ACI Committee 211", *Am. Concr. Inst.*, vol. 02, no. Reapproved, pp. 1–26, 2002.
- [66] F. B. Pereira da Costa, L. M. Haselbach, and L. C. P. da Silva Filho, "Pervious concrete for desired porosity: Influence of w/c ratio and a rheology-modifying admixture", *Constr. Build. Mater.*, no. xxxx, p. 121084, 2020, doi: 10.1016/j.conbuildmat.2020.121084.
- [67] Y. Jung and Z. Grasley, "Evaluation and optimization of durable pervious concrete for use in urban areas", *Research Report SWUTC/08/167163-1*. 82 p., vol. 7, no. 2, p. 82, 2008.
- [68] D. H. Nguyen, N. Sebaibi, M. Boutouil, L. Leleyter, and F. Baraud, "A modified method for the design of pervious concrete mix", *Constr. Build. Mater.*, vol. 73, pp. 271–282, 2014, doi: 10.1016/j.conbuildmat.2014.09.088.
- [69] "Handbook for Pervious Concrete Certification in Greater Kansas City Table of Contents", pp. 1–38, 2013.
- [70] L. K. Crouch, J. Pitt, and R. Hewitt, "Aggregate effects on pervious portland cement concrete static modulus of elasticity", *J. Mater. Civ. Eng.*, vol. 19, no. 7, pp. 561–568, 2007, doi: 10.1061/(ASCE)0899-1561(2007)19:7(561).
- [71] A. K. Chandrappa and K. P. Biligiri, "Pervious concrete as a sustainable pavement material-Research findings and future prospects: A state-of-the-art review", *Constr. Build. Mater.*, vol. 111, pp. 262–274, 2016, doi: 10.1016/j.conbuildmat.2016.02.054.
- [72] N. Neithalath, J. Weiss, and J. Olek, "Characterizing enhanced porosity concrete using electrical impedance to predict acoustic and hydraulic performance", *Cem. Concr. Res.*, vol. 36, no. 11, pp. 2074–2085, 2006.
- [73] T. R. Naik, F. Canpolat, and R. N. Kraus, "Development and demonstration of high-carbon CCPs and FGD by-products in permeable roadway base construction", *Sustain. Constr. Mater. Technol.*, vol. 2013-Augus, 2013.
- [74] E. Onstenk, A. Aguado, E. Eickschen, and A. Josa, "Laboratory study of porous concrete for its use as top-layer of concrete pavements," in *Fifth International Conference on Concrete Pavement Design and*

- RehabilitationPurdue University, School of Civil Engineering; Federal Highway Administration; Portland Cement Association; Transportation Research Board; Indiana Department of Transportation, 1993, vol. 2.
- [75] N. Jin, “Fly ash applicability in pervious concrete”, The Ohio State University, 2010.
- [76] A. Bonicelli, F. Giustozzi, and M. Crispino, “Experimental study on the effects of fine sand addition on differentially compacted pervious concrete”, *Constr. Build. Mater.*, vol. 91, pp. 102–110, 2015, doi: 10.1016/j.conbuildmat.2015.05.012.
- [77] V. R. Schaefer, J. T. Kevern, and K. Wang, “An Integrated Study of Pervious Concrete Mixture Design for Wearing Course Applications An Integrated Study of Pervious Concrete Mixture Design for Wearing”, *InTrans Proj. Reports*, no. July, pp. 1–138, 2011.
- [78] A. Beeldens, D. Van Gemert, A. S. Poupeleer, and B. Cornelis, “Behavior of porous PCC under freeze-thaw cycling”, 2001.
- [79] J. Olek, W. J. Weiss, N. Neithalath, A. Marolf, E. Sell, and W. Thornton, “Development of quiet and durable porous Portland cement concrete paving materials”, Purdue University, 2003.
- [80] C. Lian, Y. Zhuge, and S. Beecham, “The relationship between porosity and strength for porous concrete”, *Constr. Build. Mater.*, vol. 25, no. 11, pp. 4294–4298, 2011, doi: 10.1016/j.conbuildmat.2011.05.005.
- [81] J. D. Luck, S. R. Workman, and S. F. Higgins, “Hydrologic properties of pervious concrete”, in 2006 ASAE Annual Meeting, 2006, p. 1.
- [82] V. R. Schaefer, J. T. Kevern, B. Izevbekhai, K. Wang, H. E. Cutler, and P. Wiegand, “Construction and performance of pervious concrete overlay at Minnesota Road Research Project”, *Transp. Res. Rec.*, no. 2164, pp. 82–88, 2010, doi: 10.3141/2164-11.
- [83] J. T. Kevern, V. R. Schaefer, K. Wang, and P. Wiegand, “Durability of a new generation pervious concrete mixtures designed for roadway applications”, 2010.
- [84] B. Huang, H. Wu, X. Shu, and E. G. Burdette, “Laboratory evaluation of permeability and strength of polymer-modified pervious concrete”, *Constr. Build. Mater.*, vol. 24, no. 5, pp. 818–823, 2010, doi: 10.1016/j.conbuildmat.2009.10.025.
- [85] A. Bonicelli, F. Giustozzi, M. Crispino, and M. Borsa, “Evaluating the effect of reinforcing fibres on pervious concrete volumetric and mechanical properties according to different compaction energies”, *Eur. J. Environ. Civ. Eng.*, vol. 19, no. 2, pp. 184–198, 2015, doi: 10.1080/19648189.2014.939308.
- [86] B. Tong and B. Tong, “AMD-Clogging effects of portland cement pervious concrete,” 2011.
- [87] N. Neithalath, M. S. Sumanasooriya, and O. Deo, “Characterizing pore volume, sizes, and connectivity in pervious concretes for permeability prediction”, *Mater. Charact.*, vol. 61, no. 8, pp. 802–813, 2010, doi: 10.1016/j.matchar.2010.05.004.
- [88] Z. Liu, S. M. Asce, X. Yu, and M. Asce, “Laboratory Evaluation of Abrasion Resistance of Portland Cement Pervious Concrete”, *J. Mater. Civ. Eng.*, vol. 27, no. September, pp. 1239–1247, 2011, doi: 10.1061/(ASCE)MT.
- [89] A. Ibrahim, E. Mahmoud, M. Yamin, and V. C. Patibandla, “Experimental study on Portland cement pervious concrete mechanical and hydrological properties”, *Constr. Build. Mater.*, vol. 50, pp. 524–529, 2014, doi: 10.1016/j.conbuildmat.2013.09.022.
- [90] M. Gesoğlu, E. Güneş, G. Khoshnaw, and S. Ipek, “Abrasion and freezing-thawing resistance of pervious concretes containing waste rubbers”, *Constr. Build. Mater.*, vol. 73, pp. 19–24, 2014, doi: 10.1016/j.conbuildmat.2014.09.047.
- [91] A. K. Chandrappa and K. P. Biligiri, “Comprehensive investigation of permeability characteristics of pervious concrete: A hydrodynamic approach”, *Constr. Build. Mater.*, vol. 123, pp. 627–637, 2016, doi: 10.1016/j.conbuildmat.2016.07.035.
- [92] D. H. Nguyen, M. Boutouil, N. Sebaibi, F. Baraud, and L. Leleyter, “Durability of pervious concrete using crushed seashells”, *Constr. Build. Mater.*, vol. 135, no. 2017, pp. 137–150, 2017, doi: 10.1016/j.conbuildmat.2016.12.219.
- [93] F. Yu, D. Sun, J. Wang, and M. Hu, “Influence of aggregate size on compressive strength of pervious concrete”, *Constr. Build. Mater.*, vol. 209, pp. 463–475, 2019, doi: 10.1016/j.conbuildmat.2019.03.140.
- [94] K. S. Elango, D. Vivek, G. K. Prakash, M. J. Paranidharan, S. Pradeep, and M. Prabhukesavaraj, “Strength and permeability studies on PPC binder pervious concrete using palm jaggery as an admixture”, *Mater. Today Proc.*, no. xxxx, pp. 6–10, 2020, doi: 10.1016/j.matpr.2020.08.006.
- [95] G. L. Vieira, J. Z. Schiavon, P. M. Borges, S. R. da Silva, and J. J. de Oliveira Andrade, “Influence of recycled aggregate replacement and fly ash content in performance of pervious concrete mixtures”, *J. Clean. Prod.*, vol. 271, 2020, doi: 10.1016/j.jclepro.2020.122665.
- [96] G. F. B. Sandoval, I. Galobardes, A. C. De Moura, and B. M. Toralles, “Hydraulic behavior variation of pervious concrete due to clogging”, *Case Stud. Constr. Mater.*, vol. 13, p. e00354, 2020, doi: 10.1016/j.cscm.2020.e00354.

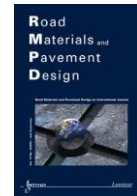
- [97] G. Leroux, “Étude d’un système innovant de rafraîchissement basse consommation pour le bâtiment To cite this version : HAL Id : tel-01705310 Etude d’un système innovant de rafraîchissement à basse consommation pour le bâtiment,” 2018.
- [98] S. Asfour, “Récupération d’énergie dans les chaussées pour leur maintien hors gel To cite this version ”, thèse de doctorat, Université Clermont-Auvergne, 2017.
- [99] A. Lencastre, “Hydraulique générale, édition Eyrolles”, Paris, 1999.
- [100] P. Sochala, “Méthodes numériques pour les écoulements souterrains et couplage avec le ruissellement”, Paris Est, 2008.
- [101] A. Trabelsi, “Études numérique et expérimentale des transferts hygrothermiques dans les matériaux poreux de construction”, La Rochelle, 2010.
- [102] M. Pigeon, “Composition et hydratation du ciment Portland”, Séminaire progrès dans le domaine du béton, Québec, (septembre 1981) p, pp. 36–72, 1981.
- [103] N. T. Duong, “Cartographie et caractérisation acoustiques des matériaux composites : application à l’évaluation du taux volumique de porosité dans un matériau composite”, 2016.
- [104] Mak Wai Kin, “An Overview of Pervious Concrete Applications in Stormwater Management and Pavement Systems”, vol. 3, no. May, p. 58, 2006.
- [105] F. Montes, S. Valavala, and L. M. Haselbach, “A new test method for porosity measurements of portland cement pervious concrete”, *J. ASTM Int.*, vol. 2, no. 1, pp. 1–13, 2005, doi: 10.1520/jai12931.
- [106] L. M. Haselbach and R. M. Freeman, “Effectively estimating in situ porosity of pervious concrete from cores”, *J. ASTM Int.*, vol. 4, no. 7, pp. 1–11, 2007.
- [107] R. Zhong and K. Wille, “Compression response of normal and high strength pervious concrete”, *Constr. Build. Mater.*, vol. 109, pp. 177–187, 2016, doi: 10.1016/j.conbuildmat.2016.01.051.
- [108] A. Kia, H. S. Wong, and C. R. Cheeseman, “Clogging in permeable concrete: A review”, *J. Environ. Manage.*, vol. 193, pp. 221–233, 2017, doi: 10.1016/j.jenvman.2017.02.018.
- [109] A. C. I. (American C. Institute), “Report on pervious concrete”, 2010.
- [110] K. Low, D. Harz, and N. Neithalath, “Statistical characterization of the pore structure of enhanced porosity concretes”, 2008.
- [111] J. Sansalone, X. Kuang, and V. Ranieri, “Permeable pavement as a hydraulic and filtration interface for urban drainage”, *J. Irrig. Drain. Eng.*, vol. 134, no. 5, pp. 666–674, 2008, doi: 10.1061/(ASCE)0733-9437(2008)134:5(666).
- [112] N. Ghafoori and S. Dutta, “Laboratory investigation of compacted no-fines concrete for paving materials”, *J. Mater. Civ. Eng.*, vol. 7, no. 3, pp. 183–191, 1995.
- [113] M. Sonebi and M. T. Bassuoni, “Investigating the effect of mixture design parameters on pervious concrete by statistical modelling”, *Constr. Build. Mater.*, vol. 38, pp. 147–154, 2013.
- [114] V. Henderson, “Evaluation of the Performance of Pervious Concrete Pavement in the Canadian Climate”, p. 276, 2012.
- [115] N. Neithalath, “Development and characterization of acoustically efficient cementitious materials”, Degree of Doctor of Philosophy, no. January 2004.
- [116] A. Yahia and K. D. Kabagire, “New approach to proportion pervious concrete”, *Constr. Build. Mater.*, vol. 62, pp. 38–46, 2014.
- [117] A. ZOUAGHI, “Permeability of no-fines concrete”, *コンクリート工学年次論文報告集*, vol. 20, no. 2, pp. 757–762, 1998.
- [118] L. M. Haselbach and R. M. Freeman, “Vertical porosity distributions in pervious concrete pavement”, *ACI Mater. J.*, vol. 103, no. 6, p. 452, 2006.
- [119] Y. Rao, Y. Ding, A. K. Sarmah, D. Liu, and B. Pan, “Vertical distribution of pore-aggregate-cement paste in statically compacted pervious concrete”, *Constr. Build. Mater.*, vol. 237, p. 117605, 2020.
- [120] D.H. Nguyen, “Étude du comportement hydromécanique des bétons drainants à base de coproduits coquilliers”, thèse de doctorat, 2014.
- [121] L. A. Mata and M. L. Leming, “Vertical distribution of sediments in pervious concrete pavement systems”, *ACI Mater. J.*, vol. 109, no. 2, pp. 149–155, 2012, doi: 10.14359/51683701.
- [122] L. G. Li, J. J. Feng, J. Zhu, S. H. Chu, and A. K. H. Kwan, “Pervious concrete: Effects of porosity on permeability and strength”, *Mag. Concr. Res.*, vol. 73, no. 2, pp. 69–79, 2021, doi: 10.1680/jmacr.19.00194.
- [123] M. S. Sumanasooriya, D. P. Bentz, and N. Neithalath, “Planar image-based reconstruction of pervious concrete pore structure and permeability prediction”, *ACI Mater. J.*, vol. 107, no. 4, pp. 413–421, 2010, doi: 10.14359/51663868.
- [124] M. S. Sumanasooriya and N. Neithalath, “Stereology- and morphology-based pore structure descriptors of enhanced porosity (Pervious) concretes”, *ACI Mater. J.*, vol. 106, no. 5, pp. 429–438, 2009, doi: 10.14359/51663143.
- [125] R. Zhong and K. Wille, “Linking pore system characteristics to the compressive behavior of pervious concrete”, *Cem. Concr. Compos.*, vol. 70, pp. 130–138, 2016, doi: 10.1016/j.cemconcomp.2016.03.016.

- [126] A. K. Chandrappa and K. P. Biligiri, "Influence of mix parameters on pore properties and modulus of pervious concrete: an application of ultrasonic pulse velocity", *Mater. Struct.*, vol. 49, no. 12, pp. 5255–5271, 2016.
- [127] M. Kayhanian, D. Anderson, J. T. Harvey, D. Jones, and B. Muhunthan, "Permeability measurement and scan imaging to assess clogging of pervious concrete pavements in parking lots", *J. Environ. Manage.*, vol. 95, no. 1, pp. 114–123, 2012, doi: 10.1016/j.jenvman.2011.09.021.
- [128] A. K. Chandrappa and K. P. Biligiri, "Pore structure characterization of pervious concrete using X-ray microcomputed tomography", *J. Mater. Civ. Eng.*, vol. 30, no. 6, p. 4018108, 2018.
- [129] L. Akand, M. Yang, and Z. Gao, "Characterization of pervious concrete through image based micromechanical modeling", *Constr. Build. Mater.*, vol. 114, pp. 547–555, 2016, doi: 10.1016/j.conbuildmat.2016.04.005.
- [130] G. P. Ong, A. Jagadeesh, and Y. M. Su, "Effect of pore network characteristics on non-Darcy permeability of pervious concrete mixture", *Constr. Build. Mater.*, vol. 259, p. 119859, 2020, doi: 10.1016/j.conbuildmat.2020.119859.
- [131] M. S. M. Lund, K. K. Hansen, R. Brincker, A. H. Jensen, and S. D. R. Amador, "Evaluation of freeze-thaw durability of pervious concrete by use of operational modal analysis", *Cem. Concr. Res.*, vol. 106, no. January, pp. 57–64, 2018, doi: 10.1016/j.cemconres.2018.01.021.
- [132] J. T. Kevern and V. R. Schaefer, "Mixture proportioning considerations for improved freeze-thaw durability of pervious concrete", *ISCORD 2013 Plan. Sustain. Cold Reg. - Proc. 10th Int. Symp. Cold Reg. Dev.*, pp. 471–481, 2013, doi: 10.1061/9780784412978.046.
- [133] K. Jones, "Density of concrete," *Phys. Factb.*, 1999.
- [134] X. Kuang, J. Sansalone, G. Ying, and V. Ranieri, "Pore-structure models of hydraulic conductivity for permeable pavement", *J. Hydrol.*, vol. 399, no. 3–4, pp. 148–157, 2011, doi: 10.1016/j.jhydrol.2010.11.024.
- [135] R. Liu et al., "Investigation of the porosity distribution, permeability, and mechanical performance of pervious concretes", *Processes*, vol. 6, no. 7, 2018, doi: 10.3390/pr6070078.
- [136] X. Cui et al., "Experimental study on the relationship between permeability and strength of pervious concrete", *J. Mater. Civ. Eng.*, vol. 29, no. 11, p. 04017217, 2017, doi: 10.1061/(asce)mt.1943-5533.0002058.
- [137] H. El-Hassan, P. Kianmehr, and S. Zouaoui, "Properties of pervious concrete incorporating recycled concrete aggregates and slag", *Constr. Build. Mater.*, vol. 212, pp. 164–175, 2019, doi: 10.1016/j.conbuildmat.2019.03.325.
- [138] O. Deo, M. Sumanasooriya, and N. Neithalath, "Permeability reduction in pervious concretes due to clogging: experiments and modeling", *J. Mater. Civ. Eng.*, vol. 22, no. 7, pp. 741–751, 2010.
- [139] Y. Zhang, H. Li, A. Abdelhady, and J. Yang, "Comparative laboratory measurement of pervious concrete permeability using constant-head and falling-head permeameter methods", *Constr. Build. Mater.*, vol. 263, p. 120614, 2020, doi: 10.1016/j.conbuildmat.2020.120614.
- [140] A. Singh, P. V. Sampath, and K. P. Biligiri, "A review of sustainable pervious concrete systems: Emphasis on clogging, material characterization, and environmental aspects", *Constr. Build. Mater.*, vol. 261, p. 120491, 2020, doi: 10.1016/j.conbuildmat.2020.120491.
- [141] A. Kia, H. S. Wong, and C. R. Cheeseman, "Clogging in permeable concrete: A review", *J. Environ. Manage.*, vol. 193, pp. 221–233, 2017, doi: 10.1016/j.jenvman.2017.02.018.
- [142] G. F. B. Sandoval, I. Galobardes, R. S. Teixeira, and B. M. Toralles, "Comparison between the falling head and the constant head permeability tests to assess the permeability coefficient of sustainable Pervious Concretes", *Case Stud. Constr. Mater.*, vol. 7, no. August, pp. 317–328, 2017, doi: 10.1016/j.cscm.2017.09.001.
- [143] NRMCA, "CIP 36 - Structural Lightweight Concrete", *Concrete*, vol. 3, pp. 3–4, 2003.
- [144] L. K. Crouch et al., "Estimating Pervious PCC Pavement Design Inputs with Compressive Strength and Effective Void Content", *Concr. Technol. Forum*, p. 15, 2006.
- [145] G. J. Jing Yang, "Experimental Study on Infiltration Properties of Pervious Concrete", *Lect. Notes Civ. Eng.*, vol. 30, pp. 367–373, 2019, doi: 10.1007/978-981-13-6717-5_36.
- [146] A. S. Agar-Ozbek, J. Weerheijm, E. Schlangen, and K. Van Breugel, "Investigating porous concrete with improved strength: Testing at different scales", *Constr. Build. Mater.*, vol. 41, pp. 480–490, 2013, doi: 10.1016/j.conbuildmat.2012.12.040.
- [147] Z. Sun, X. Lin, and A. Vollpracht, "Pervious concrete made of alkali activated slag and geopolymers", *Constr. Build. Mater.*, vol. 189, pp. 797–803, 2018, doi: 10.1016/j.conbuildmat.2018.09.067.
- [148] X. Xie et al., "Mixture proportion design of pervious concrete based on the relationships between fundamental properties and skeleton structures", *Cem. Concr. Compos.*, vol. 113, no. May, p. 103693, 2020, doi: 10.1016/j.cemconcomp.2020.103693.
- [149] K. S. Elango and V. Revathi, "Fal-G Binder Pervious Concrete", *Constr. Build. Mater.*, vol. 140, pp. 91–99, 2017, doi: 10.1016/j.conbuildmat.2017.02.086.

- [150] C. Lian and Y. Zhuge, "Investigation of the effect of aggregate on the performance of permeable concrete", in Proceedings of the 5th International Structural Engineering and Construction Conference (ISEC-5), 2009, pp. 505–510.
- [151] J. Huang, Z. Luo, and M. B. E. Khan, "Impact of aggregate type and size and mineral admixtures on the properties of pervious concrete: An experimental investigation", *Constr. Build. Mater.*, vol. 265, 2020, doi: 10.1016/j.conbuildmat.2020.120759.
- [152] F. Yu, D. Sun, M. Hu, and J. Wang, "Study on the pores characteristics and permeability simulation of pervious concrete based on 2D/3D CT images", *Constr. Build. Mater.*, vol. 200, pp. 687–702, 2019, doi: 10.1016/j.conbuildmat.2018.12.135.
- [153] A. Torres, J. Hu, and A. Ramos, "The effect of the cementitious paste thickness on the performance of pervious concrete", *Constr. Build. Mater.*, vol. 95, pp. 850–859, 2015, doi: 10.1016/j.conbuildmat.2015.07.187.
- [154] H. Wang, H. Li, X. Liang, H. Zhou, N. Xie, and Z. Dai, "Investigation on the mechanical properties and environmental impacts of pervious concrete containing fly ash based on the cement-aggregate ratio", *Constr. Build. Mater.*, vol. 202, pp. 387–395, 2019, doi: 10.1016/j.conbuildmat.2019.01.044.
- [155] R. Zhong and K. Wille, "Compression response of normal and high strength pervious concrete", *Constr. Build. Mater.*, vol. 109, pp. 177–187, 2016, doi: 10.1016/j.conbuildmat.2016.01.051.
- [156] J. Sun, J. Zhang, Y. Gu, Y. Huang, Y. Sun, and G. Ma, "Prediction of permeability and unconfined compressive strength of pervious concrete using evolved support vector regression", *Constr. Build. Mater.*, vol. 207, pp. 440–449, 2019, doi: 10.1016/j.conbuildmat.2019.02.117.
- [157] P. Chindaprasirt, S. Hatanaka, N. Mishima, Y. Yuasa, and T. Chareerat, "Effects of binder strength and aggregate size on the compressive strength and void ratio of porous concrete", *Int. J. Miner. Metall. Mater.*, vol. 16, no. 6, pp. 714–719, 2009.
- [158] A. M. Neville, "Properties of concrete", vol. 4. Longman London, 1995.
- [159] H. M. Kunieda, M. Tamai, H. Muzuguchi, S. Hatanaka and K. Y. Katahira, T. Nakazawa, "Report of the JCI Committee on Design, Construction and Recent Application of Porous Concrete", *Japan Concr. Inst.*, p. p.179, 2003.
- [160] S. Nassiri and O. AlShareedah, "Preliminary procedure for structural design of pervious concrete pavements", Washington (State). Dept. of Transportation. Research Office, 2017.
- [161] A. Ibrahim, E. Mahmoud, M. Yamin, and V. C. Patibandla, "Experimental study on Portland cement pervious concrete mechanical and hydrological properties", *Constr. Build. Mater.*, vol. 50, pp. 524–529, 2014.
- [162] N. A. Brake, H. Allahdadi, and F. Adam, "Flexural strength and fracture size effects of pervious concrete", *Constr. Build. Mater.*, vol. 113, pp. 536–543, 2016, doi: 10.1016/j.conbuildmat.2016.03.045.
- [163] R. Rizvi, S. L. Tighe, V. Henderson, and J. Norris, "Laboratory sample preparation techniques for pervious concrete", 2009.
- [164] J. T. Kevern, "Advancements in Pervious Concrete Technology", Iowa State Univ., pp. 1–108, 2008.
- [165] C.-K. Wang and C. G. Salmon, *Reinforced concrete design*. 1979.
- [166] G. Li, Y. Hu, and X. L. Zang, "Design and analysis of offset printing press plate cylinder using finite element method", *Proc. 2nd Int. Conf. Model. Simulation, ICMS2009*, vol. 7, pp. 537–540, 2009.
- [167] E. G. Nawy, *Concrete construction engineering handbook*. CRC press, 2008.
- [168] S. Ros and H. Shima, "Relationship between splitting tensile strength and compressive strength of concrete at early age with different types of cements and curing temperature histories", *Concr. Inst. Proc.*, vol. 35, pp. 427–432, 2013.
- [169] K. Yan, H. Xu, G. Shen, and P. Liu, "Prediction of splitting tensile strength from cylinder compressive strength of concrete by support vector machine", *Adv. Mater. Sci. Eng.*, vol. 2013, 2013.
- [170] L. K. Crouch et al., "Estimating pervious PCC pavement design inputs with compressive strength and effective void content", *Maryl. Silver*, p. 15, 2006.
- [171] A. Ibrahim, E. Mahmoud, M. Yamin, and V. C. Patibandla, "Experimental study on Portland cement pervious concrete mechanical and hydrological properties", *Constr. Build. Mater.*, vol. 50, pp. 524–529, 2014.
- [172] C. Gaedicke, A. Torres, K. C. T. Huynh, and A. Marines, "A method to correlate splitting tensile strength and compressive strength of pervious concrete cylinders and cores", *Constr. Build. Mater.*, vol. 125, pp. 271–278, 2016.
- [173] N. Delatte, A. Mrkajic, and D. I. Miller, "Field and laboratory evaluation of pervious concrete pavements", *Transp. Res. Rec.*, vol. 2113, no. 1, pp. 132–139, 2009.
- [174] A. C. I. C. 318, "Building code requirements for structural concrete (ACI 318-11m) and commentary", 2011.
- [175] H. G. Russell and J. Moreno, "State-of-the-Art report on high-strength concrete reported by ACI Committee 363", 1997.
- [176] A. Marolf, N. Neithalath, E. Sell, K. Wegner, J. Weiss, and J. Olek, "Influence of aggregate size and gradation on acoustic absorption of enhanced porosity concrete", *ACI Mater. J.*, vol. 101, no. 1, pp. 82–91, 2004, doi: 10.14359/12991.

- [177] S. H. Ahmad and S. P. Shah, “Structural properties of high strength concrete and its implications for precast prestressed concrete”, *PCI J.*, vol. 30, no. 6, pp. 92–119, 1985.
- [178] W. R. Hook, L. W. Cole, V. T. Cost, D. H. Diulus, and J. I. Mullarky, “Guide for design and construction of concrete parking lots reported by ACI Committee 330”, *Concrete*, vol. 92, no. Reapproved, pp. 1–32, 2001.
- [179] A. Cheng, H. M. Hsu, S. J. Chao, and K. L. Lin, “Experimental study on properties of pervious concrete made with recycled aggregate”, *Int. J. Pavement Res. Technol.*, vol. 4, no. 2, pp. 104–110, 2011, doi: 10.6135/ijprt.org.tw/2011.4(2).104.
- [180] P. Chindaprasirt, P. Nuaklong, Y. Zaetang, P. Sujumnongtokul, and V. Sata, “Mechanical and Thermal Properties of Recycling Lightweight Pervious Concrete”, *Arab. J. Sci. Eng.*, vol. 40, no. 2, pp. 443–450, 2015, doi: 10.1007/s13369-014-1563-z.
- [181] H. Liu, G. Luo, H. Wei, and H. Yu, “Strength, permeability, and freeze-thaw durability of pervious concrete with different aggregate sizes, porosities, and water-binder ratios”, *Appl. Sci.*, vol. 8, no. 8, 2018, doi: 10.3390/app8081217.
- [182] I. Netinger Grubeša, I. Barišić, T. Keser, and M. Vračević, “Wearing characteristics assessment of pervious concrete pavements”, *Road Mater. Pavement Des.*, vol. 20, no. 3, pp. 727–739, 2019, doi: 10.1080/14680629.2017.1421568.
- [183] V. A. Ulloa-Mayorga, M. A. Uribe-Garcés, D. P. Paz-Gómez, Y. A. Alvarado, B. Torres, and I. Gasch, “Performance of pervious concrete containing combined recycled aggregates”, *Ing. e Investig.*, vol. 38, no. 2, pp. 34–41, 2018, doi: 10.15446/ing.investig.v38n2.67491.

Chapter III State of the art on the hydraulic properties of pervious concrete



Résumé et objectif

Les chaussées en béton drainant ont peu ou pas de particules fines, et contiennent des vides interconnectés qui permettent la pénétration de l'eau. Cependant, il est long et coûteux de réaliser des tests de perméabilité avec de multiples variables d'influence. Cet article présente la composition et la méthode de formulation du béton drainant, en identifiant les différents facteurs qui influencent la porosité. Dans le chapitre 1, il a été montré que la porosité est insuffisante pour prédire avec précision la perméabilité du béton drainant. De plus, pour la même valeur de porosité, la perméabilité peut varier en fonction du type de porosité mesurée (porosité ouverte ou porosité totale). Dans la littérature il existe des modèles qui permettent de relier la porosité du béton drainant et sa perméabilité. Cependant, ces modèles ne prennent pas en compte le type de porosité ni la méthode de mesure de perméabilité ce qui conduit à des équations ayant des faibles coefficients de corrélations. Pour ces raisons, et pour obtenir des modèles plus fiables, l'objectif de cette étude est d'établir des relations entre la porosité et la perméabilité du béton drainant mesurée à partir d'un perméamètre à charge constante et d'un perméamètre à charge variable. La comparaison des résultats a permis de trouver une méthode de mesure de perméabilité précise. De plus, les équations des courbes obtenues ont montré que la perméabilité est influencée par d'autres paramètres qui n'ont pas été largement étudiés dans la littérature existante. Par conséquent, il est important de se concentrer sur la relation entre la perméabilité et d'autres paramètres tels que le type, la taille et la forme des granulats, la teneur en pâte de ciment, les ratios eau/ciment E/C et granulats/ciment A/C. Cette étude présente également les différentes équations et modèles afin d'examiner leur précision dans la prédiction du coefficient de perméabilité du béton drainant.

Les résultats obtenus montrent que la porosité du béton drainant est le principal facteur influençant sa densité et ses propriétés hydrauliques. La densité et la porosité du béton drainant dépendent des propriétés physiques et géométriques des granulats naturels utilisés, du rapport massique A/C, du rapport E/C, de la teneur en pâte de ciment et de la quantité de granulats fins utilisées. La perméabilité du béton drainant est souvent mesurée à l'aide d'un perméamètre à charge variable ou à charge constante, qui sont tous deux des applications directes de la loi de Darcy. La perméabilité d'un échantillon de béton varie en fonction du type de perméamètre utilisé. Les résultats des modèles obtenus montrent que la méthode de mesure de perméabilité à charge constante présente moins d'incertitude dans la mesure de la perméabilité, comparé à la méthode de mesure de perméabilité à charge variable.

La variation de la perméabilité entre deux échantillons ayant la même valeur de porosité ouverte dans une même étude signifie que le facteur de porosité ouverte est insuffisant pour prédire la perméabilité du béton drainant. En revanche, cette propriété diminue avec l'augmentation de l'épaisseur de la pâte de ciment et du rapport E/C, et augmente avec l'augmentation du rapport A/C. Elle varie également en fonction de la forme des granulats, qui influence la forme des pores interconnectés même pour des échantillons ayant la même porosité.

La comparaison entre les différents modèles de prédictions de perméabilité montre que les modèles empiriques qui ne tiennent compte que de l'influence de la porosité présentent des écarts très importants dans le calcul de la perméabilité. Les équations de Kozeny-Carman modifiées présentent de faibles écarts avec les équations des courbes résultantes (perméabilité/porosité ouverte) établies à partir de plusieurs études expérimentales de la littérature. Cela confirme qu'elles sont plus précises que les modèles empiriques pour prédire la perméabilité du béton drainant. Il a été déduit que les modèles de prédiction de la perméabilité les plus précis sont ceux qui tiennent compte des paramètres de la structure des pores tels que la porosité, la tortuosité et la taille, la distribution et la connectivité des pores. Ces paramètres sont influencés par le dosage du mélange, la granulométrie et la forme des agrégats, les techniques de compactage et les additifs.

La synthèse bibliographique présentée dans les chapitres 1 et 2 a permis de comprendre les propriétés hydrauliques et mécaniques du béton drainant et de concevoir des mélanges ayant une porosité et une perméabilité supérieure aux seuils minimaux. C'était une étape importante afin d'étudier les propriétés thermiques et l'effet rafraichissant du béton drainant sur des échantillons qui permettent d'assurer leurs fonctions principales de gestion des eaux pluviales.

Dans la première partie, les propriétés mécaniques, hydrauliques et thermiques du béton drainant ont été étudiées. Avant d'étudier le comportement thermique du béton drainant dans des conditions climatiques contrôlées en laboratoire en conditions sèches et humides, une étude préliminaire sur l'effet de rafraîchissement de 9 formulations de chaussées perméables dans des conditions réelles a été effectuée. Cette étude est présentée dans le chapitre suivant et a permis d'identifier les facteurs qui influencent le taux d'évaporation des chaussées perméables.

Khaled Seifeddine ^a, Sofiane Amziane ^a, Evelyne Toussaint ^a

^a Université Clermont Auvergne, CNRS, SIGMA Clermont, Institut Pascal, F-63000 Clermont-Ferrand, France.

Highlights:

- This paper presents the composition and formulation method of pervious concrete based on cement and natural aggregates.
- Factors affecting the porosity of pervious concrete are identified.
- Correlations between permeability and open porosity of pervious concrete, are established.
- Factors influencing the permeability of pervious concrete are studied.
- Methods of measuring permeability are presented, and the results obtained with these different methods are compared.
- Different models for predicting the permeability of pervious concrete are presented.

Keywords:

Pervious concrete; Total and open porosity; Tortuosity; Permeability; Falling head and constant head permeameter; Permeability prediction model.

1. Introduction

Stormwater management is a crucially important issue in the context of burgeoning urban sprawl, and the resulting increase in soil impermeabilization [1]. Permeable surfaces have become impermeable due to the construction of buildings, parking lots and other structures. This leads to increased frequency and severity of flooding [2], [3], falling water tables and a disrupted natural water cycle [4], degraded natural environments and increased localized pollution at points of discharge, such as wastewater treatment plants [5]. To address these problems, sustainable stormwater management is obviously of prime importance in an urban development strategy.

Permeable pavements, as a low-impact development, help minimize impervious surfaces and have the potential to improve quality of life in communities and reduce other environmental impacts [6]. For example, they help reduce stormwater runoff [7]–[10], and associated water pollution [11]–[14], reduce the need for stormwater management facilities, and improve on-site infiltration for vegetation growth and groundwater recharge. Other benefits of these pavements include reduction of heat flow from the pavement surface to the atmosphere, which helps to mitigate urban heat islands [15]–[18], promotes evapotranspiration [19]–[22] and sound absorption [23]–[28]. In addition, owing to its excellent drainage and skid resistance, permeable pavement obviously improves road safety [11].

Pervious concrete is a specific type of concrete pavement, primarily composed of coarse aggregate and cementitious materials with a rational grading, which gives the mix an internal structure with interconnected macropores [29]. The limited amount or absence of fines in pervious concrete creates interconnected pores that allow water infiltration. Pervious concrete can be used in specific applications requiring high permeability. There is also growing interest in pervious concrete in low-traffic roads, parking lots, pedestrian and cycle paths, driveways, and sidewalks to reduce the risk of flash flooding runoff [30]–[35]. The durability, hydraulic

and mechanical properties of this type of pavement have been extensively studied in the literature [32], [36]–[44].

Although pervious concrete clearly has many advantages, it is essential to design it to optimize its hydraulic performance. Existing research on the hydraulic properties of pervious concrete has mainly focused on the effect of porosity on permeability [45]–[47]. However, there are not enough studies in the literature that summarize the different factors influencing the permeability of traditional pervious concrete. In addition, there is little research that establishes predictive models which relate pore characteristics (size, shape, connectivity and tortuosity) to hydraulic conductivity [48]–[50].

In this context, the objective of this paper is to critically review the available studies on pervious concrete, the number of which has increased considerably in recent years. This review summarizes work in these different areas of expertise in order to understand the hydraulic characteristics of pervious concrete. This paper begins by presenting the composition and formulation methods. Then, it examines the hydraulic characteristics of pervious concrete by detailing the measurement methods, minimum permeability thresholds and factors that influence the hydraulic characteristics. Finally, this document presents the different equations and models used to predict the permeability of pervious concrete. Comparisons and analyses of the results obtained with these models are discussed.

2. Composition and formulation method for pervious concrete

Pervious concrete pavements are made of the same materials as conventional concrete, excluding fines. The mix is rather made of coarse aggregates with uniform grading that allow for higher porosity and low connectivity between particles [8]. The design of a pervious concrete mix should provide a void structure that allows water to drain from the surface. It must also provide a pavement of adequate durability for the intended users to minimize surface degradation.

2.1. Cementitious materials or binder

In general, Portland cement meeting the requirements of ASTM C 150 is used for the production of pervious concrete [35], [51]. The amount of cement generally depends on the mix design – i.e. the volume of aggregate used, the Water/Cement ratio (W/C) and the target open porosity. Cement content generally varies from 250 to 400 kg/m³ [35].

Additional cementitious materials can be used as a substitute for some of the cement or as a substitute for some of the fine aggregates [52]. All supplementary cementitious materials used must meet the requirements of ASTM C 1697. Incorporating small amounts of fly ash results in better mechanical performance [53], though larger replacements above 30% do not necessarily result in better mechanical performance [54]. For improved mechanical properties, silica fume can be used in the formulation of pervious concrete [55]. Adil et al. [56] reported that the addition of 5% silica fume as a partial replacement for cement increases density, reduces porosity and improves mechanical properties.

Several studies [57]–[62] have thoroughly investigated the fundamental scientific aspects of polymer-modified pervious concrete mixtures, such as the role of the polymer in modifying the mechanical properties and characteristics of the porous structure. The results of the study by Tabatabaeian et al. [58] show that the use of polymer composites, including polyester and epoxy resins, significantly improves the mechanical properties and durability of pervious concrete compared to ordinary cement-based pervious concrete.

2.2. Coarse Aggregates

Coarse aggregates must meet the requirements of ASTM C 33 [51]. As for conventional concrete, the mechanical properties of pervious concrete are influenced by aggregate size, texture, type and content [63]. In order to maintain sufficient voids in the material, pervious concrete is generally composed of aggregates with a grain size varying between 9.5 and 19 mm [64]. However, some studies have used coarse aggregates with a grain size varying between 2.36 and 9.5 mm, with the main objective of improving the strength [65]–[68]. Other global physical properties, such as type, shape, and distribution, are also important in determining the mechanical and hydraulic properties and affect the durability of pervious concrete pavements [69]–[71]

2.3. Fine Aggregates

When strong mechanical performance is required, a certain amount of sand can be added to the pervious concrete mix. However, the sand used must meet the requirements of ASTM C 33 [51]. To achieve higher strengths, a volume of sand up to 7% of the total volume of the coarse aggregate can significantly improve the mechanical strength. This improvement can achieve up to a 50% increase in compressive strength without significantly affecting hydraulic conductivity [72], [73]. In addition, up to 20% sand volume has been used to formulate a pervious concrete with a 28-day compressive strength of 50 MPa [55].

2.4. Water and additives

The amount of water is a critical factor in obtaining an acceptable quality of pervious concrete. A large amount of water would lead to a very liquid cement paste. This results in high mobility of the cement paste, which will clog the voids. On the other hand, a small amount of water will result in a material that is difficult to handle and with low mechanical strength development.

Admixtures used should meet the requirements of ASTM C 494. When low W/C ratios are used (0.27 to 0.34), it is necessary to use a water-reducing agent or a superplasticizer to have better workability and improved mechanical properties [32], [72], [74]. On the other hand, if the W/C ratio is higher than 0.34, an admixture may not be necessary [51], [75], [76].

Other admixtures are also used, including set retarders, viscosity improvers and air entraining agents [77]. Viscosity improvers are often used to facilitate the placement of pervious concrete [63]. In cases where mixtures have significant tendencies to slump and an appropriate consistency is desired to avoid separation between the aggregates and the cement paste, the use of a colloidal agent is a suitable solution.

2.5. Fibers

The use of fibers in the pervious concrete mix can improve its structural and mechanical properties. Fiber-reinforced pervious concrete can be beneficial because fibers (if used in the proper dose and size) tend to limit and control crack propagation by preventing the generation of strains and stresses during load application [78].

Wang et al. [36] showed that the addition of 0.3 kg/m³ of polypropylene fibers in the mix of natural gravel-based pervious concrete increases the permeability (168%), compressive strength (24%) and tensile strength (21%). These fibers also improve the durability of pervious concrete against freeze-thaw cycles [36], [79]. However, these fibers do not effectively increase the abrasion resistance [80], [81].

Hardened carbon-fiber composites have also been used as reinforcement to improve the mechanical properties of pervious concrete. Rangelov et al. [82] show that the use of 0.5 to 1.5% (volumetric fractions) of these materials improves workability, 28-day compressive strength (4 to 11%), 7-day split tensile strength (11 to 46%), and modulus of elasticity (4 to 46%), and makes infiltration rates higher despite low porosity values. In addition, Rodin et al. [83] show that the use of 3 to 5% (volumetric fractions) of this type of material in the pavement mix improves the impact strength, abrasion resistance and 7-day and 28-day modulus of rupture by 84% and 36-65% respectively.

Table 1 shows the different dosages used in several studies in the literature.

Table 1

Dosages of pervious concrete based on natural aggregates.

Study	Water (W) (kg/m ³)	Cement (C) (kg/m ³)	Fine aggregates (kg/m ³)	Coarse aggregates (A) (kg/m ³)	(W/C) ratio	(A/C) ratio
Cui et al., 2016 [84]	121	335	0	1622	0.36	4.8
	94	262	0	1622	0.36	6.2
	68	189	0	1622	0.36	8.6
Nguyen et al., 2017 [85]	111	301	110	1574	0.37	5.2
Chandrappa & Biligiri, 2018 [86]	99.6	331.9	0	1659.6	0.30	5.0
	117	389.9	0	1559.7	0.30	4.0
	141.8	472.5	0	1417.5	0.30	3.0
	113.8	325.2	0	1625.9	0.35	5.0
	133.2	380.7	0	1522.6	0.35	4.0
Chen et al., 2019 [87]	96.25	356	0	1682	0.27	4.7
Bright Singh et al., 2020 [81]	150	430	0	1521	0.35	3.5
AlShareedah et al., 2021 [88]	97	285	0	1400	0.34	4.9
	105	309	0	1720	0.34	5.6
	77	285	0	1630	0.27	5.7
	105	309	0	1630	0.34	5.3
Rao and Yang, 2021 [89]	113	402	0	1539	0.28	3.8
Park et al., 2022 [90]	120.5	482	0	1546.2	0.25	3.2
	132.9	443.1	0	1546.2	0.30	3.5

3. Characterization of physical properties

Porosity is the most essential design characteristic of pervious concrete. However, there is still confusion about the definition of porosity and the type of porosity to be used to characterize pervious concrete. Not all voids in pervious concrete contribute to water infiltration. Some pores are isolated and others are connected only to one side of the pavement [91]. In addition,

there are smaller pores, such as capillary pores and obstructed pores, which retain fluids due to surface tension and capillary effect and do not contribute effectively to the hydraulic function. On the other hand, these pores do influence the mechanical strength of the pervious concrete [92].

It is therefore important to distinguish between the open porosity and the total porosity of the pavement. Open porosity is defined as the ratio of the volume of interconnected and blind pores (which are only connected by one path to the pavement surfaces) to the total volume of the material. This type of porosity is essential for the hydraulic performance of pervious concrete [93]. On the other hand, total porosity is defined as the ratio of the total pore volume to the total volume of the material. It dictates the mechanical strength of the pervious concrete [94]. Total porosity takes account of the volume of the non-accessible pores and the open pores. The volume of non-accessible pores can be divided into isolated pores left in the space between the aggregates and the matrix pores. The water-accessible porosity measured in the void is considered equal to the total porosity [91].

For pervious concrete, most studies have measured open porosity, based on Archimedes' principle [36], [39], [72], [95], [96]. This measurement consists of drying the sample for 3 days at 40°C. Then, the sample is immersed in water for 30 minutes. The mass of the sample in the dry state and under water are determined. The open porosity of the sample is calculated by **Eq. (1)**. With this measuring method, it is possible to deduce the air density (40°C).

$$P_0 = \left[1 - \left(\frac{M_s - M_i}{\rho_w \times V_t} \right) \right] \times 100 \quad (1)$$

where P_0 = open porosity (%), V_t = total volume of the sample (m^3), ρ_w = density of water ($kg.m^{-3}$), M_s = oven dry weight, (kg), M_i = mass of the sample under water (kg).

The open porosity of pervious concrete generally varies between 15 to 35%, while total porosity varies between 15 to 40% [64], [66], [91], [97], [98]. Table 2 shows that there is a linear relationship between open porosity and total porosity of pervious concrete. These relationships are not identical because the results depend on the porosity measurement method used.

Table 2
Relationship between open porosity and total porosity of pervious concrete.

Reference	Eq.	Mix compositions	Equations
Lian et al., 2011 [99]	(2)	Aggregate type: quartzite, limestone and dolomite Coarse aggregate size: 4.45-13.2 mm W/C: 0.3-0.38	$P_t = 0.78P_0 + 14.25$
Zhong and Wille, 2016 [94]	(3)	Aggregate type: quartzite Coarse aggregate size: 1.19-4.75 mm W/C: 0.22-0.55	$P_t = 0.67P_0 + 12$

Ghafoori & Dutta, 1995 [100]	(4)	Aggregate type: crushed limestone Coarse aggregate size: 0.3-9.5 mm (ASTM 0448-86) W/C : 0.37-0.42	$P_t = 0.855 P_0 + 4.72$
Nguyen, 2014 [91]	(5)	Aggregate type: gravel Coarse aggregate size: 2-6.3 mm W/C : 0.3-0.37	$P_t = 0.76 P_0 + 14.5$
Liu et al., 2018 [101]	(6)	Aggregate type: granite Coarse aggregate size: 4.75–16 mm W/C : 0.25-0.35	$P_t = 1.076 P_0 + 1.96$

The volumetric porosity test is another method for measuring porosity. This method consists of saturating all the interstitial voids in a sample with water, in order to correlate the porosity with the total volume of water used. For this purpose, the samples are placed into non-deformable molds and covered with a PVC film to ensure watertightness. The mold and the sample inside are placed on a scale and water is added to fill the interstices of the pervious concrete. Considering the weight difference between the dry mass and the saturated mass, the volume of water is obtained. Then, the volumetric porosity is calculated as the volume of added water divided by the volume of the sample. The associated test method has been used in many studies [46], [50], [102].

Image analysis has also been used to determine the porosity of pervious concrete. This technique can measure total, connected and isolated porosity [71], [103]. This method also provides additional information such as pore volume, shapes, tortuosity, sizes, areas, dispersion and connectivity [97], [104]–[108]. In addition, Sansalone et al., [109] and Kuang et al. [110] used X-ray tomography (XRT) to determine the total porosity. The results of XRT analysis and gravimetric-geometric measurements to obtain total porosity were compared with each other. This comparison shows that the two methods are mutually compatible [109].

The internal structure of the pervious concrete can be investigated using ultrasonic wave testing as a non-destructive test [111]–[114]. Previous studies [115], [116] have reported a correlation between the ultrasonic wave velocity and the porosity of the pervious concrete. In a recent study, Ridengaoqier et al. [117] proposed a method to estimate the porosity of pervious concrete using ultrasonic wave testing, which can be applied during the construction of pervious concrete on site. The results of this study show that the quantitative relationship between the porosity of pervious concrete and the ultrasonic wave velocity can be approximated by a quadratic function. Furthermore, the thickness of the pervious concrete sample does not affect the ultrasonic wave velocity measured by this method.

Regardless of the test methodology for measuring porosity, there is an inverse relationship between porosity and density of pervious concrete – i.e. as porosity increases, the density and strength of pervious concrete decrease, and vice versa [36], [37], [96], [118]–[127]. Indeed, the factors that influence the porosity of the pervious concrete will indirectly influence the density and mechanical properties. Studies have suggested that incorporating some amount of fine aggregates (0-30%) can help improve mechanical strength while maintaining permeability and

porosity requirements [55], [123], [128]. Sonebi & Bassuoni [129] and Meininger & Richard [75] found that porosity decreased with increasing W/C ratio, while Henderson [130] found no correlation between them. The porosity of pervious concrete also increases with increasing aggregate sizes [72], [131], with decreasing compaction energy [72], [91], and with decreasing cement paste content [75], [91], [127], [129], [132]. In addition, several studies [105], [129], [133], [134] have shown that the porosity varies with the thickness of the pavement concrete.

Based on this information, and given that open porosity is the most widely studied factor in the literature on the hydraulic properties of pervious concrete, this porosity was used in the remainder of this study to establish predictive models for the permeability of pervious concrete.

4. Hydraulic characteristics of pervious concrete

Hydraulic conductivity or permeability is the most relevant parameter to define any type of porous medium [38]. It is one of the most significant characteristics of pervious concrete that determines its performance in relation to its main function: stormwater management [54], [135].

Permeability of pervious concrete depends on the composition and the method of placement. In the literature, a wide range of water permeability values can be found, including 0.22 to 0.54 cm/s [35], 0.2 to 1.2 cm/s [128], 0.025 to 0.61 cm/s [136], 0.076 to 3.5 cm/s [137], and 0.2 to 0.6 cm/s [72]. In addition, this permeability must be adjusted according to the local rainfall and the desired degree of protection against clogging and flooding. The permeability of pervious concrete must be higher than 0.0054 cm/s, which is a critical value above which a concrete can be qualified as pervious [138]. In addition, to avoid the risk of clogging, the minimum permeability must be 0.1 cm/s [36].

4.1. Methods of measuring permeability in the laboratory

To measure permeability of pervious concrete, a falling head permeameter or a constant head permeameter are generally used, both of which are direct applications of Darcy's law.

The hydraulic conductivity measurements are based on the assumption of laminar flow. In case of turbulent flow, the assumptions on which Darcy's law is based are no longer valid [139], [140]. The study by Montes and Haselbach [141] shows that the flow regime inside pervious concrete for many typical applications is laminar. Therefore, Darcy's law can be used to describe the hydraulic conductivity and intrinsic permeability of this material.

Darcy's law is a physical law that expresses the flow rate of an incompressible fluid filtering through a porous medium. The flow of this fluid between two points is determined by the hydraulic conductivity or the permeability coefficient K of the substrate and by the pressure gradient of the fluid. Darcy's law expresses the flow rate Q of an incompressible fluid flowing in the steady state through a porous medium of section A and length L due to a difference in charge ΔH (Eq. (7)).

$$Q = K A \frac{\Delta H}{L} \quad (7)$$

The constant head permeability test is recommended by ACI [45]; this test measures the quantity of water that passes through a sample in a specified time t (s). A schematic view of this test is presented in Fig. 1. Note the sample of pervious concrete, with a section and height of A (cm²) and L (cm), respectively; the volume of water through the sample q (cm³); and h

(cm), which corresponds to the sum of the heights of the sample and the water column. The permeability measured with a constant head permeameter K_{CH} (cm/s) is calculated by **Eq. (8)**.

$$K_{CH} \text{ (cm/s)} = \frac{q L}{A h t} \quad (8)$$

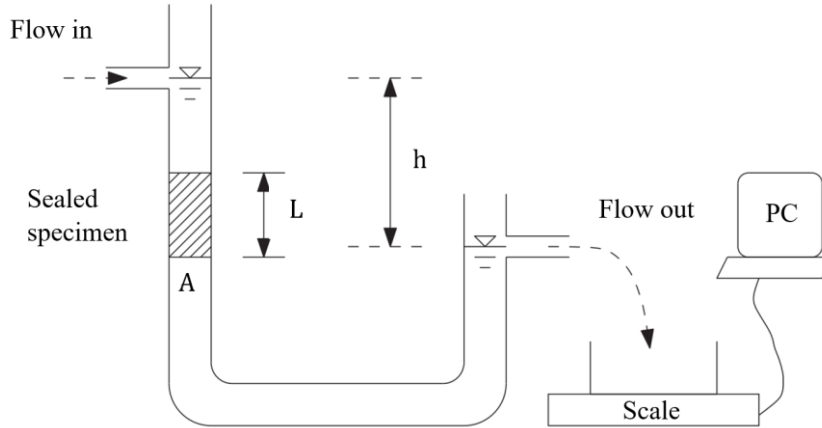


Fig. 1. Diagrammatic sketch of constant-head permeability test device [48].

The falling head permeability test is illustrated in Fig. 2. The test measures the time t (s) it takes for a column of water of height h_1 (cm) to pass through a sample of pervious concrete. The time begins when a valve at the bottom of the equipment is opened and ends when h_2 (cm) is reached. A (cm²) and a (cm²) are the cross-sectional areas of the sample and the tube respectively, and L (cm) is the length of the sample. The permeability measured with a falling head permeameter K_{FH} (cm/s) is calculated by **Eq. (9)** [100].

$$K_{FH} \text{ (cm/s)} = \frac{a L}{A t} \ln \left(\frac{h_2}{h_1} \right) \quad (9)$$

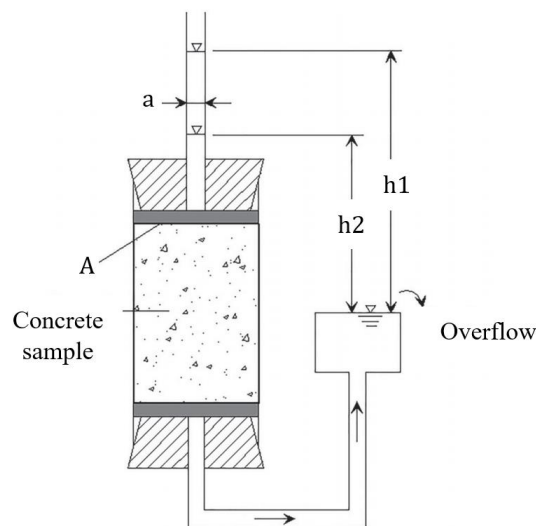


Fig. 2. Diagrammatic sketch of falling-head permeability test device [142].

The constant flow test (Fig. 3) is also a method used to measure the permeability of pervious concrete. This test is a variation of the constant head permeability test and uses horizontally flowing water and a measurement of the pressure drop across the pervious concrete sample. The advantages of such a configuration are that it allows for the study of a wide variety of

pressure gradients in a constant flow and lends itself to automated measurements through a data acquisition system with appropriate flow and pressure transducers. The study by Lederle et al. [143] shows that the permeability values of the same pervious concrete sample measured with the constant head permeability test and the constant flow test are similar for different hydraulic gradient values. However, the permeability values measured with the falling head permeameter are higher than those obtained with previous tests.

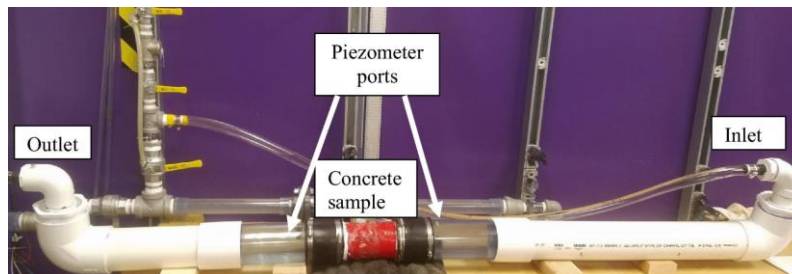


Fig. 3. Constant flow test apparatus [143].

4.2. Comparison of laboratory permeability measurement methods

The number of steps and duration of the constant head permeability test and the amount of equipment used are higher than for the falling head permeability test. In addition, the falling head permeability test can be easily performed by one person, whereas the constant head permeability test requires two people to perform the test (if the laboratory has continuous water supply facilities). However, due to the rapid drop in water level with the falling head permeability test, the time required for recording is relatively short and therefore the time error caused by the delay in manual timing negatively affects the accuracy of the test result. Therefore, the accuracy of the test is relatively low compared to constant head permeability tests [144].

Qin et al. [145] investigated the differences in permeability for crushed limestone aggregate pervious concrete mixtures measured with the falling head permeameter and the constant head permeameter. They found that the values measured with the constant head permeameter were lower than those obtained with the falling head permeameter. These results are in agreement with those found by Zhang et al. [144] for pervious concrete mixtures based on natural basalt aggregates, who have established the following linear relationship: $K_{FH} = 2.75 K_{CH} - 0.08$, and with those found by Akkaya & Çağatay [146], for pervious concrete mixtures based on crushed limestones aggregates: $K_{FH} = 1.712 K_{CH} - 0.275$. However, Li et al. [93] found that the permeability obtained with a constant head permeameter is higher than those obtained by a falling head permeameter. These results are in agreement with those found by Sandoval et al. [147] who have established a power relationship linking the permeability coefficients obtained with these two permeability measurement methods: $K_{CH} = 1.518 K_{FH}^{2.95}$ for pervious concrete mixtures based on four types of aggregates: basalt, blastfurnace slag, ceramic waste, and recycled concrete aggregates.

The constant flow permeameter and the constant head permeameter have lower levels of uncertainty compared to the falling head permeameter [143], [144].

4.3. Field permeability measurement methods

There are field permeameters that are used for permeability measurement of permeable pavements. The first is the NCAT permeameter (Fig. 4), which was developed by the National

Centre for Asphalt Technology (NCAT) in the late 1990s and uses the principle of the falling head permeameter (Eq. (9)). However, this method has not been published as a standard.

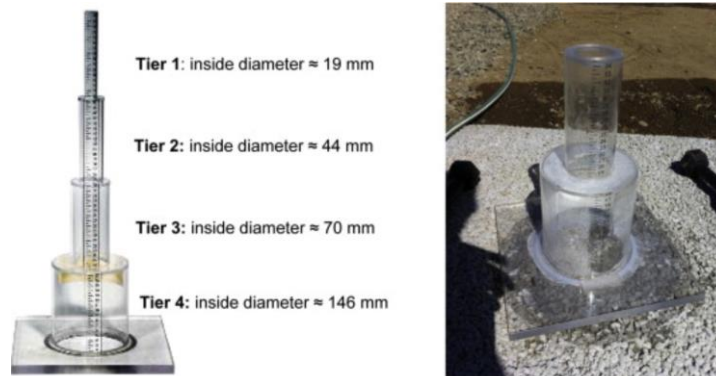


Fig. 4. NCAT field permeameter: four cylindrical levels with different inside diameters [148].

The second is the ASTM C 1701 Permeameter which was developed under the jurisdiction of ASTM Technical Committee C09 on Concrete and Concrete Aggregates and is under the direct responsibility of Subcommittee C09.49 on Pervious Concrete. This permeameter uses the constant head permeameter principle. The specification of the ASTM C1701 permeameter and the device used is shown in Fig. 5. The infiltration rate (permeability coefficient or hydraulic conductivity) is calculated by Eq. (10) [148].

$$I = \frac{K M}{D^2 t} \quad (10)$$

where I = infiltration rate, mm/h [in./h]; M = infiltrated water mass, kg [lb.]; D = inner diameter of the infiltration ring, mm [in.]; t = time required for the measured quantity of water to infiltrate the pavement (s) and K (constant number) = 4,583,666,000 or 126 870 for the unit (inch-pound).

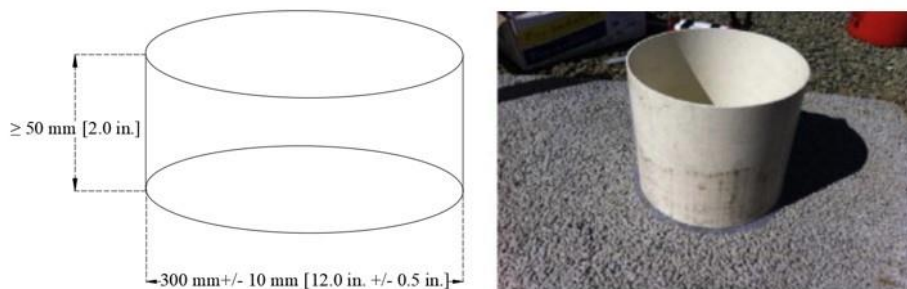


Fig. 5. ASTM C1701 field permeameter with the required dimensions specified by the ASTM C1701 standard.

Li et al. [148] compared the permeability values of six pervious concrete pavements using these two field permeameters. Their results show that the permeability measured with the ASTM C1701 method was 50 to 90% lower than the value measured with the NCAT method.

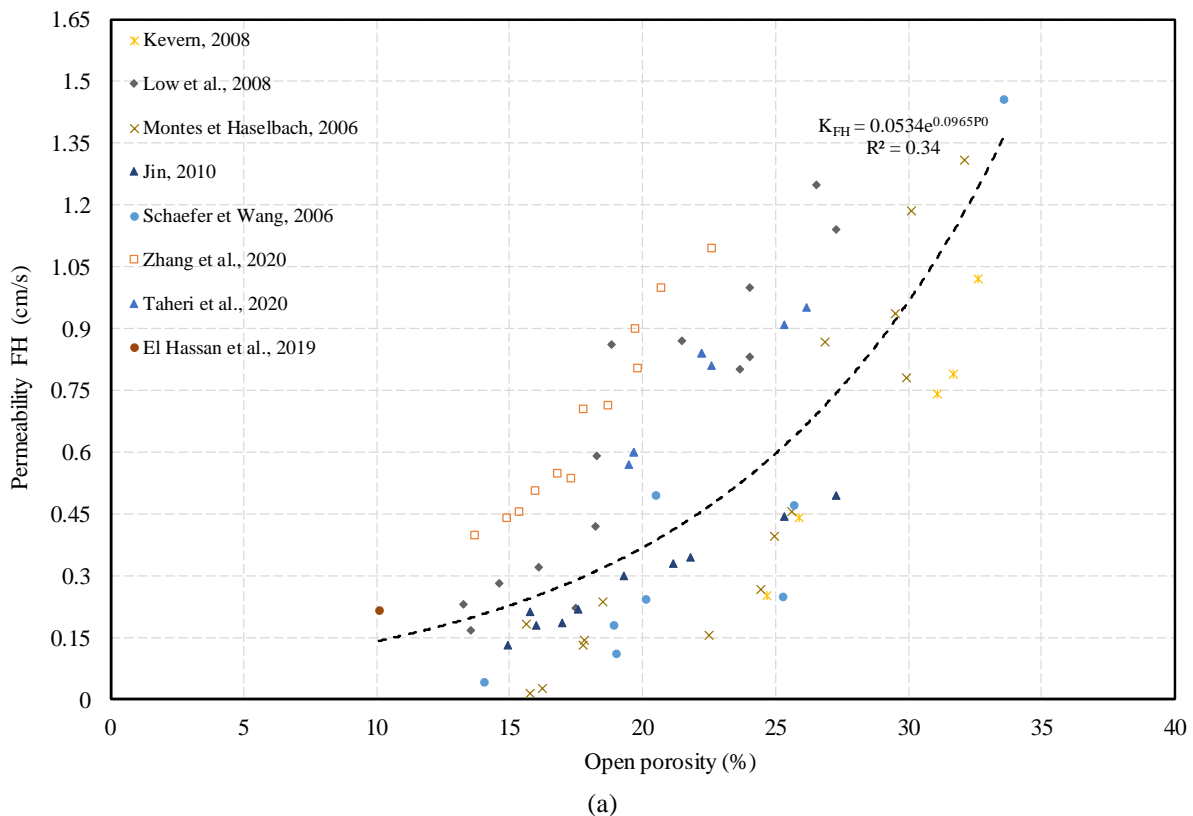
In conclusion, in order to evaluate and compare the hydraulic performance of pervious concrete from several studies, it is necessary to verify that these studies have used the same permeability measurement method. Indeed, the results found in the literature show that the permeability value of the same pavement sample can vary depending on the permeability measurement method, whether with laboratory or field permeameters.

5. Factors influencing the permeability of pervious concrete

5.1. Relationship between open porosity and permeability

Some studies in the literature have, on the same graph, plotted the permeability results of 15 datasets [149] and 17 datasets [150] as a function of their porosity values (%). These graphs show dispersed results and cannot be used to establish a predictive model of permeability. The main reason for this dispersion is that these two graphs do not distinguish between the method of permeability measurement or between the different types of porosity: total, interconnected and open, which have different values.

In order to precisely investigate the influence of open porosity on the permeability of pervious concrete, the selected studies concern only cement-based mixtures and natural aggregates (Basalt, Gravel, Limestone). Furthermore, these studies were separated into two categories according to the permeability measurement method (falling head or constant head permeameter), since as shown previously, the permeability of a pervious concrete sample varies depending on the measurement method used. Fig. 6a shows the relationship between the permeability measured with the falling head permeameter and the open porosity from data present in the literature [47], [54], [141], [144], [151]–[154]. Similarly, Fig. 6b shows the relationship between the permeability measured with the constant head permeameter and the open porosity from data present in the literature [144], [147], [155]–[160].



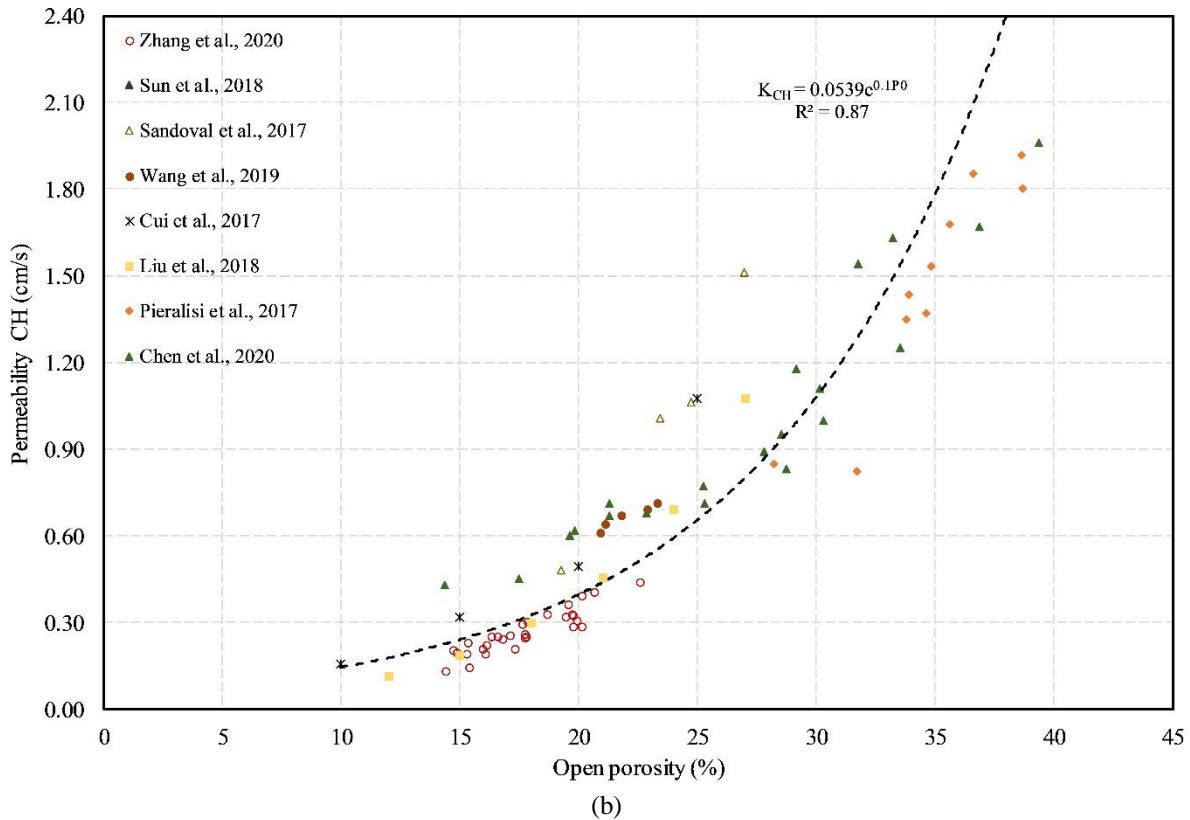


Fig. 6. Variation in permeability measured with a falling head permeameter (a) and with a constant head permeameter (b) from several studies available in the literature as a function of open porosity.

An exponential relationship for the resulting curves between open porosity and permeability gives the best correlation and the highest coefficient of determination R^2 . **Eq. (11)** gives the relationship between open porosity P_0 (%) and permeability K_{FH} (cm/s) measured with a falling head permeameter. **Eq. (12)** gives the relationship between open porosity P_0 (%) and permeability K_{CH} (cm/s) measured with a constant head permeameter.

$$K_{FH}(\text{cm/s}) = 0.0534e^{0.0965P_0} \quad (11)$$

$$K_{CH}(\text{cm/s}) = 0.0539e^{0.1P_0} \quad (12)$$

These exponential equations relating open porosity and permeability are valid only for the samples and range of values covered by this research, but can serve as a guide to stormwater system planners and designers.

Figs. 6a and 6b show that in general, permeability of pervious concrete increases as open porosity increases. However, the results of some of the studies presented in this figure show that two or more pervious concrete specimens with nearly identical porosity do not necessarily have the same permeability value. For example, the study of Montes and Haselbach [141] (Fig. 6a), shows two permeability values: 1.18 cm/s and 0.78 cm/s (difference = 51%) for two pervious concrete samples with an open porosity of 30%.

The correlation coefficient of the resulting curve in Fig. 6b ($R^2 = 0.87$) is higher than that of the resulting curve in Fig. 6a ($R^2 = 0.34$) and the permeability measured with the constant head permeability test shows less deviation between different studies compared to the falling head permeability test. This shows that the permeability measurement with the constant head

permeameter is more accurate and shows less uncertainty in permeability measurement compared to the falling head permeameter, which is in keeping with the results in the literature [143], [144].

Although the prediction of the permeability of pervious concrete using the exponential expression is not perfect in relation to these two methods of permeability measurement, it can be deduced from these correlations that, although porosity is a factor with a high influence on permeability, it is insufficient on its own to predict the permeability of the pervious concrete, which depends on other factors as well.

5.2. Influence of aggregate size and pore size on permeability

Several studies show that aggregate size affects the permeability of pervious concrete [38], [70], [72], [161]. Fig. 7 shows different permeability results of pervious concrete with aggregate size as the only variable (W/C and A/C ratios are identical for the mixtures in each study). This figure shows that the permeability of pervious concrete increases with increasing aggregate size [155], [162]–[165].

For a specific aggregate size, the permeability may change from one study to another depending on the pavement mix design of each study: the cement paste content, the W/C and A/C ratio, the type and form of aggregate used and the method of permeability measurement.

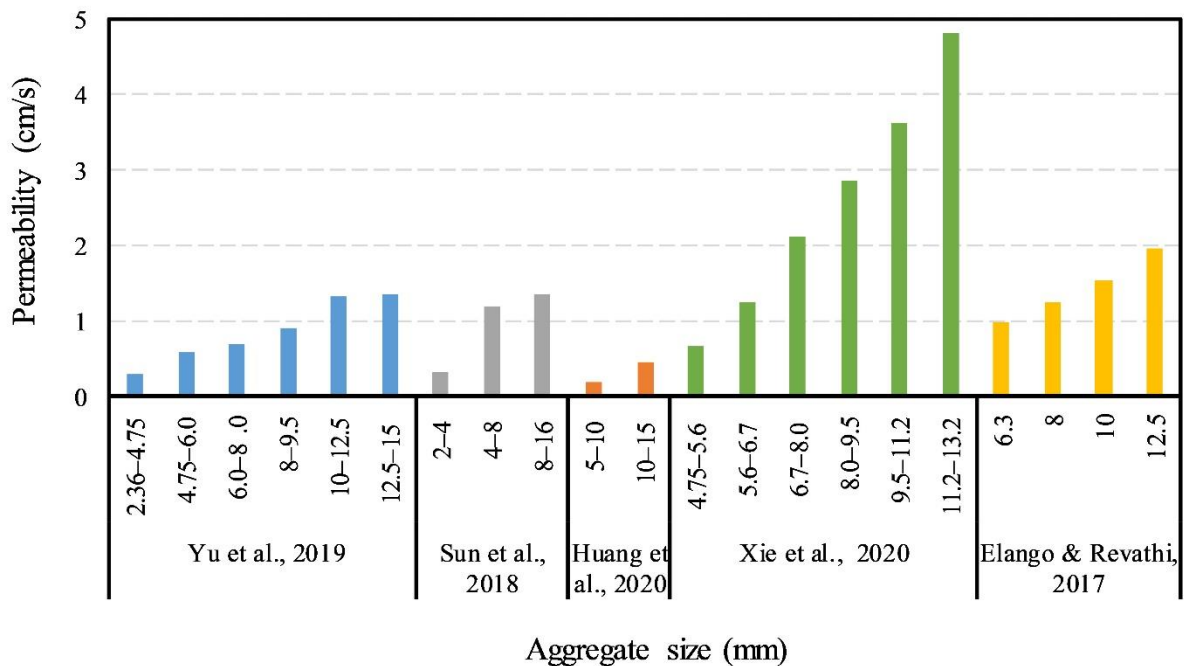


Fig. 7. Variation in permeability as a function of aggregate size, from several studies found in the literature.

The study by Yu et al. [164] shows that the permeability of pervious concrete samples increases with increasing aggregate size in these mixes (mixes having the same W/C and A/C ratios and having almost the same open porosity, ranging from 20.5% to 21.25%). Although each mixture has almost identical porosities, the permeability values vary greatly depending on the size of the aggregates. This parameter must therefore be taken into consideration.

This study also shows that the permeability of these eight pervious concrete samples, with nearly the same porosity, increases in a linear fashion as the 2D surface area A_{av} ($R^2 = 0.8289$) and the 2D surface area A_{50} ($R^2 = 0.9277$) increase (Fig. 8a), with A_{av} being the average pore

area and A50 defined as the pore size corresponding to 50% of the cumulative frequency distribution. On the other hand, a better correlation between the permeability coefficient and the 3D pore volume is given by a polynomial relation, i.e. $R^2 = 0.9319$ for $V_{av.}$ and $R^2 = 0.9414$ for V50 (Fig. 8b), with $V_{av.}$ being the average pore volume and V50 defined as the pore volume corresponding to 50% of the cumulative frequency distribution. Therefore, the aggregate size used in the pervious concrete mix is an important factor influencing the permeability of the pervious concrete, because it has a direct influence on the pore size.

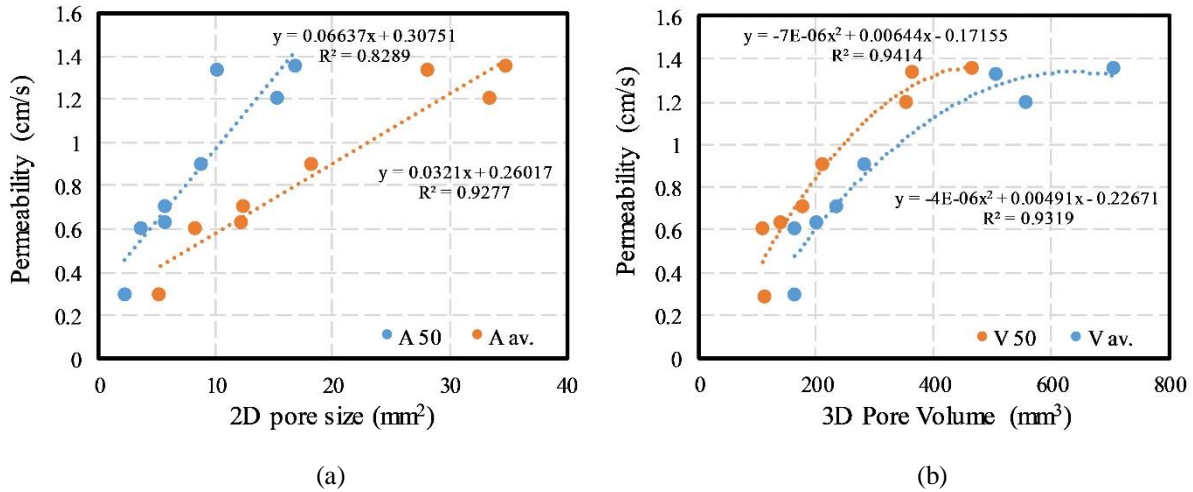


Fig. 8. (a) Relationship between 2D pore size and permeability coefficient, (b) relationship between 3D pore size and permeability coefficient [164].

Therefore, the average pore size $A_{av.}$ is more accurate than A50 in predicting permeability. Furthermore, as the pore volume increases, the permeability coefficient increases rapidly at first and then increases slowly as the pore volume exceeds 500 mm³. Indeed, as the aggregate size increased, the number and thickness of flow channels increased, contributing to higher permeability [164], [166]. Fig. 8b also shows that the permeability is most sensitive to the small pore content, followed by the large pore content, and least sensitive to the medium pore content.

5.3. Influence of aggregate shape and water/cement ratio on permeability

Pervious concrete mixtures from each selected study [91], [137], [165], [167] (Fig. 9) to investigate the influence of W/C ratio on permeability have the same aggregate size. These studies show that the permeability of pervious concrete decreases with increasing W/C ratio. This is because with a low W/C ratio, the reduced water content makes the pervious concrete mix harder, resulting in better compaction resistance and thus higher porosity and permeability. In addition, a high W/C ratio makes the cement paste very fluid, which causes segregation and deposition of the cement paste in the lower layer of the pavement concrete, making it almost impermeable [38], [137], [165], [168].

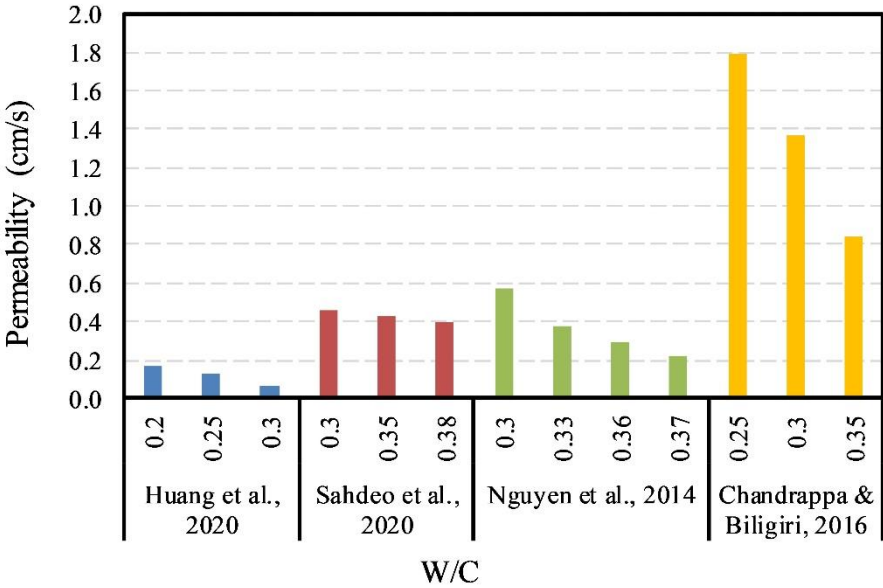


Fig. 9. Variation in permeability as function of the W/C ratio, found in several studies in the literature

The type of aggregate also influences the permeability of pervious concrete for a specific W/C ratio. Indeed, the study of Huang et al. [165] shows that the permeability of two pervious concrete samples with the same porosity (18%) and the same aggregate size (5-10 mm) varies depending on the type of aggregate used (Fig. 10).

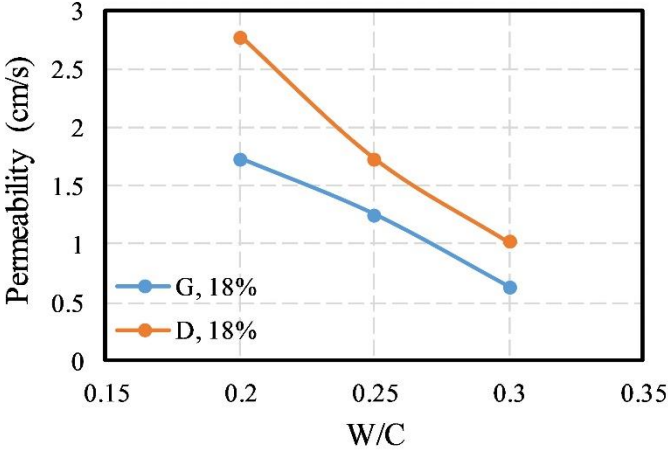


Fig. 10. Permeability variation of Dolerite (D) and Granite (G) pervious concrete with 18% porosity as a function of W/C ratio [165].

Fig. 10 shows that for a specific porosity and W/C ratio, Dolerite-based samples have a higher permeability coefficient than Granite-based samples. The main reason is the different shape of the particles. Dolerite particles are mainly round and spherical while granite particles are flaky, elongated and needle-shaped [165]. It can be deduced that permeability is also a function of the shape of the aggregates, which influence the shape of the pores. The study of Chandrappa et al. [108], characterizing the pore structure of pervious concrete using X-ray tomography, shows that rod-shaped pores are dominant (35-40%) in the pore structure of pervious concrete, followed by spheroidal (22%), blade-shaped (20%) and oblate (18%) pores. The results of this study show that increasing the proportion of spherical pores leads to an increase in permeability, which is in agreement with the results of the previous study [165]. These results are further

evidence that porosity is not a sufficient factor, on its own, to accurately predict the permeability of pervious concrete.

5.4. Influence of cement paste thickness on permeability

The amount of cement used affects the thickness of the cement paste that coats the aggregates, which affects the porosity and therefore permeability of the pervious concrete. There is no standard developed for determining the thickness of the cement paste of a paving concrete sample. Fig. 11 shows the variation of permeability as a function of cement paste thickness for two studies in the literature. The first is by Torres et al. [125] who determined thickness experimentally using a grid and a digital caliper. The second is that of by Xie et al. [162] who used a different method to measure the thickness of the cement paste, based on image processing.

For specimens with the same aggregate size, these studies show that as the cement paste thickness increases, the permeability of the pervious concrete specimens decreases. This is because the thicker cement paste fills the intergranular pores, reduces the number and size of pores, and causes disconnection of the pore network, which decreases permeability [168]. In addition, the study by Torres et al. [125] shows that when the compaction energy increases for specimens with the same dosage and amount of cement, the thickness of the cement paste increases and the permeability decreases as a result. Several studies also show that increasing compaction energy reduces void content and permeability [98], [102], [169].

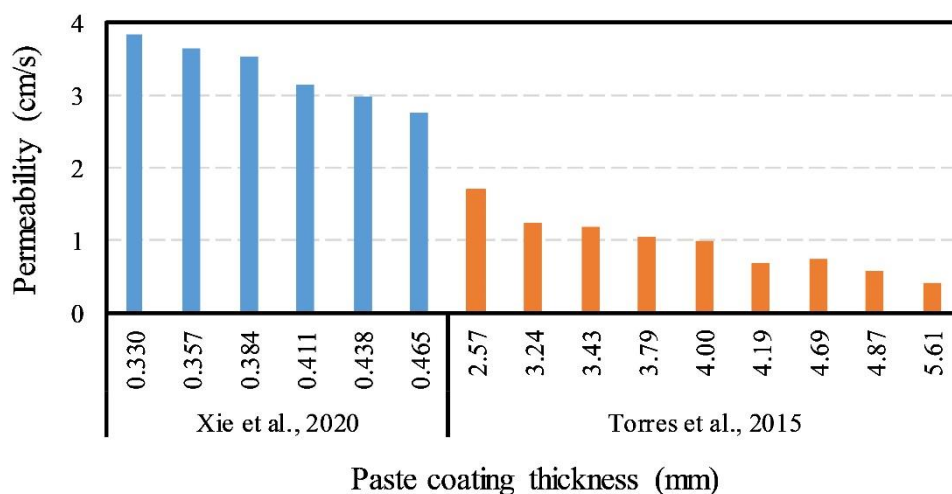


Fig. 11. Variation in permeability as a function of the cement paste thickness, found in several studies in the literature.

5.5. Influence of the aggregate/cement ratio on permeability

To investigate the influence of the A/C ratio on the permeability of pervious concrete, the results of two studies [144], [170] are presented in Fig. 12. The permeability results concern pervious concrete mixtures with the A/C ratio as the only variable (the aggregate size and W/C ratio are identical for all samples in each study). Fig. 12 shows that permeability increases with increasing A/C ratio. Indeed, when the A/C ratio decreases, the pore volume decreases due to a lower compaction resistance offered by a reduced amount of aggregates, which leads to a decrease in porosity and permeability. However, as the A/C ratio increases, the reduction in cement paste thickness and the increase in compaction strength, offered by a larger volume of aggregate, result in higher porosity and permeability of pervious concrete mixtures.

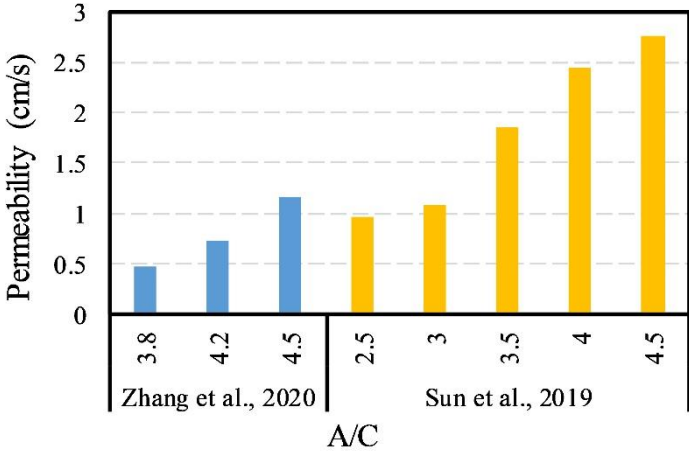


Fig. 12. Variation in permeability as a function of the A/C ratio, found in several studies in the literature.

Figs. 7, 9, and 12 show that the permeability of pervious concrete is influenced by aggregate size, W/C and A/C ratios. Sun et al. [170] performed a sensitivity analysis (SA), to assess the influence of these variables on the permeability of pervious concrete using the importance score (IS) [171], as shown in Fig. 13. This figure shows that permeability of pervious concrete is slightly more sensitive to the aggregate size (IS = 0.0297) than to the A/C ratio (IS = 0.0284), while the W/C ratio has less of an influence (IS = 0.0129).

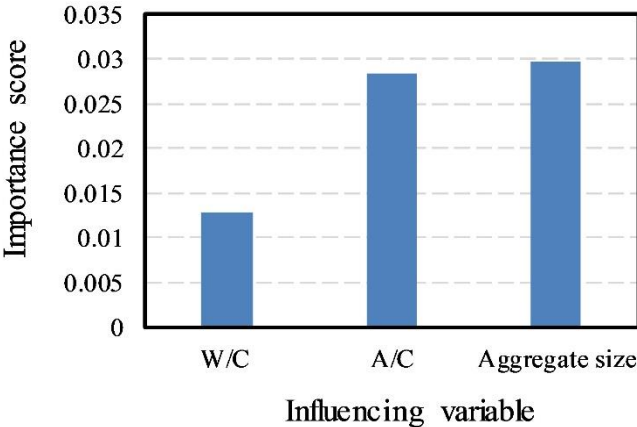


Fig. 13. Variable importance for permeability coefficient using SA.

It should be noted that these results are obtained for the dataset used in this study [170] and more representative results can be obtained with a larger dataset, and by investigating more factors that influence permeability, in order to more accurately assess the influence of each on the hydraulic properties of pervious concrete.

It can be deduced that the permeability of pervious concrete increases with increasing open porosity, aggregate size and A/C ratio. On the contrary, it decreases with increasing W/C ratio and cement paste thickness. Other parameters influence the permeability, such as the type and shape of the aggregates. To improve accuracy in the calculation of permeability, it is also necessary to study the parameters of the pore structure – not only the porosity but the pore size distribution and pore connectivity, which are influenced by the proportions of the mixtures, the gradation and shape of the aggregates, the compaction techniques and the additives.

6. Permeability prediction models

6.1. Empirical models for permeability prediction

There are three fundamental properties that affect the hydraulic conductivity of a porous medium: pore connectivity, tortuosity, and porosity [139]. Most mathematical relations expressing the relationship between hydraulic conductivity, porosity, pore connectivity, and tortuosity are semi-empirical. These models are complicated and of limited practical use [172].

Due to the complexity of determining tortuosity or pore connectivity versus porosity, the majority of studies have relied on open porosity to predict hydraulic conductivity of pervious concrete. There are a number of studies in the literature which relate open porosity and permeability with different forms of mathematical models such as linear, exponential, power and polynomial models. Table 3 shows 32 models for predicting permeability as a function of open porosity.

Table 3

Different forms of mathematical models for predicting permeability and open porosity.

Empirical model	Type of equation	Reference
$K = a P_0 + c$	Linear	[101], [173]–[186]
$K = a P_0^2 + b P_0 + c$	Polynomial	[187], [188]
$K = a e^{b P_0}$	Exponential	[189]–[198]
$K = a P_0^b$ $K = a P_0^b + c$	Power	[100], [147], [199]–[201]

6.2. Modified Kozeny-Carman model

The Kozeny-Carman (K-C) model (**Eq. (13)**) is a well-known pore structure model, taking account of porosity, specific surface area and pore tortuosity. The K-C model for porous media is based on two important assumptions: flow through the viscous, laminar permeable material and a porous flow path consisting of several identical rounded flow channels.

$$K \text{ (m/s)} = \frac{1}{C \tau S^2} \frac{P^3}{(1-P)^2} \quad (13)$$

where P = porosity (%), τ = tortuosity (dimensionless), S = specific surface based on solid volume (m^2/m^3), C = constant.

For pervious concrete samples, due to their random heterogeneous pore structure, these two assumptions are not perfectly satisfied [38]. As a result, the original K-C model is modified to cater for the specific properties of pervious concrete [48], [110], [137], [202].

Eq. (13) can be further reduced to the form where the tortuosity, specific surface area and constant term can be represented by the parameter α . Montes and Haselbach [141] used the K-C equation to model the relationship between open porosity and hydraulic conductivity in field-

placed pervious concrete. Nonlinear regression was used to fit **Eq. (14)** to the dataset obtained from all field samples used. Since the parameters C and S (**Eq. (13)**) are unknown for the field-placed pervious concrete, the factor α was used as the nonlinear fitting constant (**Eq. (14)**).

$$K \text{ (cm/s)} = \alpha \frac{P_0^3}{(1-P_0)^2} \quad (14)$$

where $\alpha = (g C_0) / (v M_s)$, g = acceleration due to gravity (cm.s^{-2}), v = kinematic viscosity of water ($\text{cm}^2.\text{s}^{-1}$), M_s = specific surface of the material (cm^{-1}), and C_0 = empirical constant.

Eq. (14) was fitted to the data using the Marquardt method of the NLIN procedure in SAS/STAT statistical software version 8.2 [203], [204]. The results show that the model proposed in this equation fitted the data well where $\tau = L_e/L > 1 = 18$. It is valid for pervious concrete with aggregates of about 1 cm and open porosity ranging from 15 to 32%.

Few research projects have been conducted to quantify the influence of pore tortuosity on the hydraulic conductivity of pervious concrete [48], [50]. Pore tortuosity is defined as the ratio of effective path length to sample length $\tau = L_e/L > 1$ [205]. The study of Sansalone et al. [109] based on three-dimensional X-ray tomography (XRT) and image analysis techniques shows that the tortuosity value of pervious concrete is between 2.89 and 5.91.

The influence of the tortuosity on the permeability is illustrated in Fig. 14 for two samples with the same length L . This figure shows that for the same value of open porosity P_0 , when the tortuosity of the porous system increases, the permeability decreases.

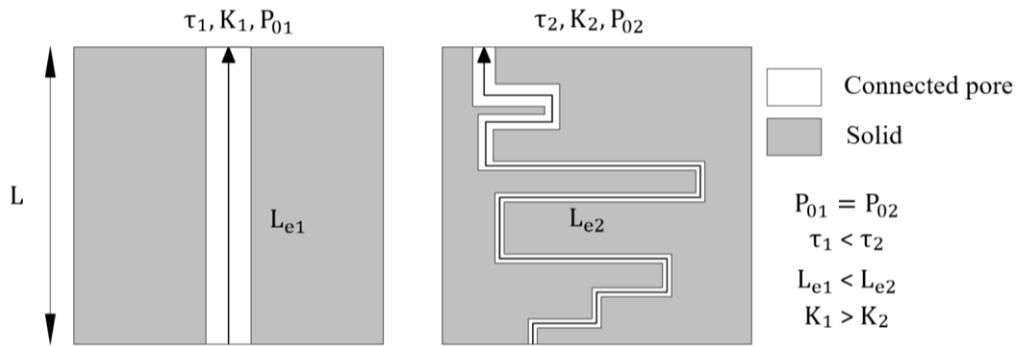


Fig. 14. Schematic illustration of the influence of pore tortuosity on hydraulic conductivity.

A modified Kozeny-Carman model (**Eq. (15)**) was established by Zhong et al. [48] that includes tortuosity, to calculate the permeability of pervious concrete. In this study, the authors related the tortuosity of pervious concrete to the relative average pore size \bar{d}_p / d_a . This ratio is equal to the average pore size \bar{d}_p divided by the average aggregate diameter d_a . The average pore size is obtained from the pore size distribution indicative of the microstructure of the pore system [141].

$$K \text{ (m/s)} = \frac{\rho g d_a^2}{72 \mu} \frac{P_0^3}{(1-P_0)^2 \tau^2} \quad (15)$$

where P_0 = open porosity (%), ρ = density (kg/m^3), μ = dynamic viscosity of the fluid ($\text{kg}\cdot\text{m}^{-1}\cdot\text{s}^{-1}$) and τ = tortuosity.

The results of this study show that the model obtained (**Eq. (15)**) presents a better prediction of the hydraulic conductivity ($R^2 = 0.98$, for the predicted permeability versus measured permeability curve) compared to an exponential model that relates the open porosity to the hydraulic conductivity ($R^2 = 0.89$). This study concerns pervious concrete samples with open porosity ranging from 15.7 to 29.6% and aggregate size ranging from 1.19 to 4.75 mm.

6.3. Modified Katz-Thompson model

The Katz-Thompson (K-T) equation is commonly used to predict the permeability of porous materials [206]. For a porous medium of characteristic length scale L_c , the intrinsic permeability K can be expressed by **Eq. (16)**.

$$K = \frac{1}{226} \frac{\sigma_{\text{eff}}}{\sigma_0} L_c^2 \quad (16)$$

The coefficient ($1/226$) in **Eq. (16)** is a constant developed by Katz and Thompson for rock samples. It is based on a number of assumptions, including cylindrical pore geometry and equivalence of the local conductivity of the rock to the conductivity of the pore solution. The factors σ_{eff} and σ_0 represent the effective electrical conductivity and the electrolyte conductivity, respectively. Experimental details for measuring these two factors can be found elsewhere [50], [97], [207].

Neithalath et al. [49] introduced a hydraulic connectivity factor based on the Katz-Thompson equation, to integrate the three essential factors that control permeability in pervious concrete: open porosity P_0 , pore connectivity β and pore size d , to improve accuracy in the calculation of permeability. $\sigma_{\text{eff}} / \sigma_0$ was replaced by the factor $P_0 \beta$, which represents the combined effect of the amount of pore space and its connectivity. The characteristic length L_c was considered to be related to the size of the characteristic pores d in the porous materials. The final equation is presented in **Eq. (17)**.

$$K = \frac{1}{226} P_0 \beta d^2 \quad (17)$$

Fig. 15b shows the contour plot of the measured permeability as a function of $P_0 \beta$ and the critical pore size $d = 2r_{\text{critical}}$; r_{critical} is the critical pore radius for pervious concrete and defined using the first peak of the derivative curve of the granulometric opening distribution (Fig. 15a).

It was found that an increase in pore size or pore structure factor $P_0 \beta$ results in an increase in permeability. For the same value of $P_0 \beta$, an increase in pore size results in an increase in permeability. At higher values of $P_0 \beta$, pore size does not appear to influence permeability significantly, as shown by the roughly parallel contour lines.

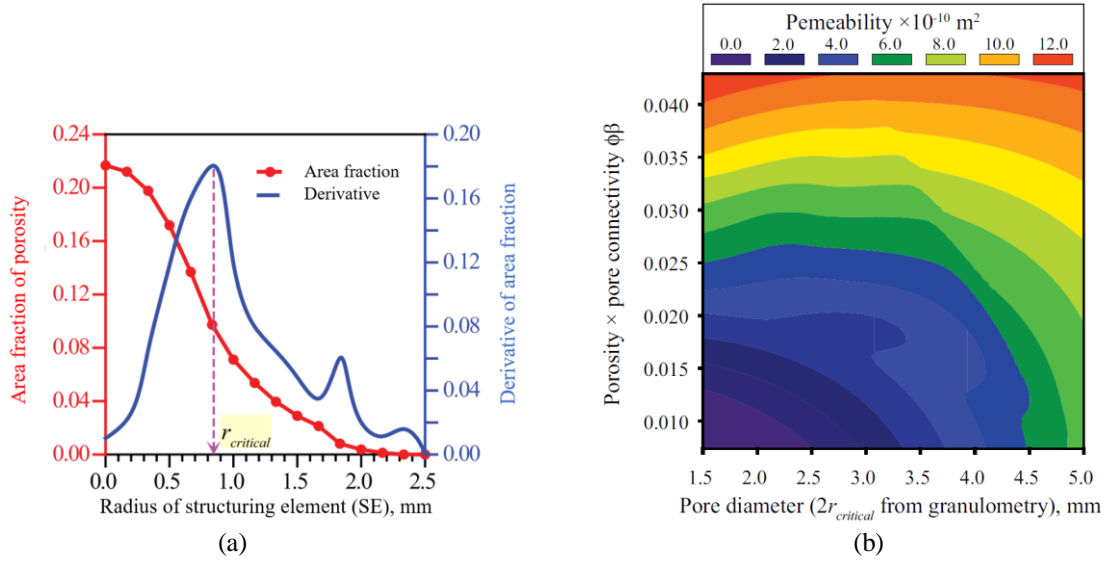


Fig. 15. Permeability as a function of critical pore size and the product of porosity and pore connectivity [49].

The study by Sumanasooriya et al. [102] shows that the application of **Eq. (17)** results in an overestimation of intrinsic permeability, especially for mixtures with larger aggregate sizes (≥ 4.75 mm) and larger pores (≥ 2.5 mm). On the other hand, when a correction factor for use with the denominator in the K-T constant, expressed as the ratio of the predicted permeability using **Eq. (17)** to the experimental permeability, is determined, it shows a very close correlation with the critical pore sizes. This required correction factor for the K-T constant was found to vary linearly with the critical pore size. This factor improves the permeability prediction of pervious concrete mixtures using a modified K-T equation.

The distributions of cement paste and aggregates determine the pore structure and permeability. Moreover, they can be quantitatively controlled in advance. Since it is difficult to directly predict the pore structure of a pervious concrete sample, Wang et al. [208] proposed a new model based on the predicted average cement paste thickness and average aggregate size. The permeability prediction model based on these two parameters is shown in **Eq. (18)**. The authors found a good fit by comparing the permeability values predicted with this model with the model developed by Neithalath et al. [49] presented previously (**Eq. (17)**).

$$K \text{ (mm/s)} = 0.0412 e^{P_t} \left(\frac{\bar{d}_a}{\bar{t}} \right)^{1.812} \quad (18)$$

where P_t = total porosity (%), \bar{t} = average thickness of the cement paste (mm), \bar{d}_a = average aggregate size (mm). P_t is obtained by calculating the volume of the aggregate and the volume of the paste.

It can be concluded that the porosity factor is necessary, but insufficient to predict the hydraulic conductivity of pervious concrete. Models based on pore characteristics such as tortuosity, connectivity, and pore sizes offer greater accuracy for calculating the permeability coefficient. In addition, it is important to validate the new prediction model proposed by Wang et al. [208] (**Eq. (18)**) on a larger number of samples with different formulations, as this model has similar reliability to the K-T model (**Eq. (17)**) which uses pore characteristics that are not easily determined.

6.4. Comparison between different permeability prediction models

Several prediction models are shown in Fig. 16 to investigate their reliability in predicting the permeability of pervious concrete. These models are divided into: models obtained from the results of research works in the literature that have carried out similar and therefore comparable works to predict the permeability of pervious concrete based on cements and natural aggregates using a falling head permeameter (**Eq. (11)**) and a constant head permeameter (**Eq. (12)**). Fig. 16 also shows the permeability results obtained with the modified Kozeny-Carman models presented previously in **Eq. (14)** [141] and **Eq. (15)** [48]. In addition, several empirical models are also shown in Fig. 16. They are presented in Table 4.

In order to increase precision in the comparison of the prediction models and since pervious concrete can be fabricated with different types of aggregates, the selected models concern only cement-based and natural aggregate-based pervious concrete mixtures to predict the permeability as a function of the open porosity.

Table 4

Empirical models to predict the permeability of pervious concrete based on natural aggregates.

Reference	Aggregate type	Eq.	Type of equation	Mathematical model
Luck et al., 2006 [45]	Gravel, Limestone	(19)	Linear	$K \text{ (cm/s)} = 0.131P_0 \text{ (%) } - 2.044$
Deo et al., 2010 [46]	Limestone	(20)	Exponential	$K \text{ (cm/s)} = 0.2e^{0.0891P_0 \text{ (%)}}$
Cui et al., 2017 [157]	Limestone	(21)	Polynomial	$K \text{ (cm/s)} = 2.8358 \times 10^{-3}P_0^2 \text{ (%) } - 0.045P_0 \text{ (%) } + 0.3281$
Xu et al., 2018 [201]	Limestone, diabase	(22)	Power	$K \text{ (cm/s)} = \left(\frac{P_0 \text{ (%)}}{20.406}\right)^{4.756} - 0.3894$

The empirical models shown in Fig. 16 deviate significantly from each other in terms of permeability prediction. For example, at an open porosity of 25%, different permeability values are obtained with these models, ranging between 0.98 and 2.78 cm/s. Moreover, they show significant deviation from the open porosity-permeability curves based on experimental work in the literature – **Eq. (11)** and **Eq. (12)** – especially for open porosity values above 20%. These significant deviations may stem from the different compositions and mix design methods of the pervious concrete used in each study, yielding different characteristics of the pore systems (size, shape, connectivity and pore distribution).

The results obtained with the modified K-C models **Eq. (14)** and **Eq. (15)** deviate less from the open porosity-permeability curves based on experimental work in the literature – **Eq. (11)**

and Eq. (12). These results show that the modified K-C models are more comprehensive and accurate in predicting the permeability of pervious concrete, because they include additional factors in the calculation.

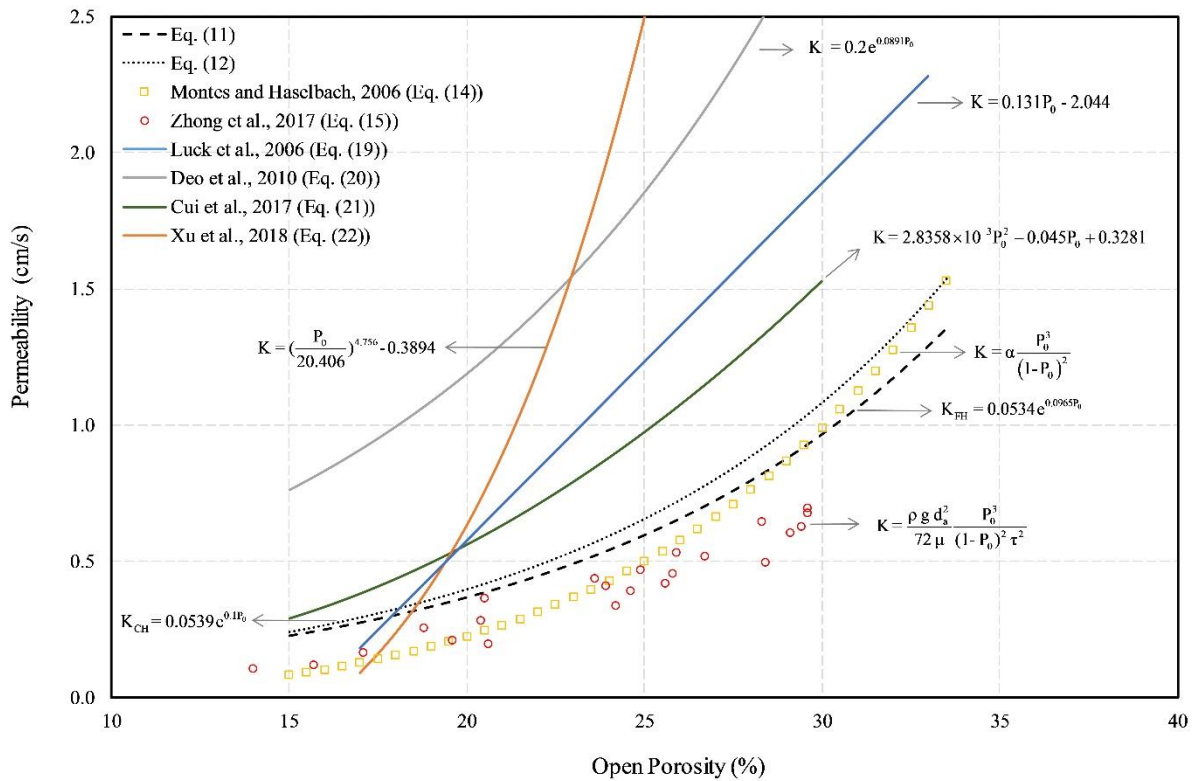


Fig. 16. Comparison of permeability prediction models for pervious concrete.

Conclusions

This paper reviews the current state of knowledge on the hydraulic properties of pervious concrete pavements. The main objective was to study the different factors that influence the permeability of pervious concrete. The main conclusions that can be drawn from this work are:

- Porosity of pervious concrete is the main factor influencing its density and hydraulic properties. Density and porosity of pervious concrete depends on the physical and geometrical properties of the natural aggregates used, the Aggregates/Cement mass ratio, the cement paste content and the quantity of fine aggregates used.
- The hydraulic conductivity of pervious concrete is often measured using a falling head permeameter or a constant head permeameter, both of which are direct applications of Darcy’s Law. The permeability of a pervious concrete sample varies with the type of permeameter used and there are different equations to correlate the permeability coefficients obtained with these two types of permeameters.
- The constant head permeameter has less uncertainty in measuring the permeability of pervious concrete, compared to the falling head permeameter.
- The variation in permeability of two samples having the same open porosity value in the same study means that the porosity factor is insufficient to predict the permeability of pervious concrete.
- Permeability of pervious concrete increases with increasing aggregate size, even for samples with the same open porosity value. Increasing the aggregate size results in

increased pore size; a better correlation is obtained when pore volume is the representative element of pore size to predict the permeability of pervious concrete.

- Permeability of pervious concrete decreases with increasing cement paste thickness and W/C ratio, and increases with increasing A/C ratio. It also varies depending on the shape of the aggregates, which influences the shape of the interconnected pores.
- Empirical models that only take account of the influence of porosity show very broad deviations in the permeability calculation. The modified Kozeny-Carman equations show small deviations with the equations of the resulting curves (permeability/open porosity) from several experimental studies in the literature. This confirms that they are more accurate than the empirical models in predicting the permeability of pervious concrete.
- The most accurate permeability prediction models are those that take account of pore structure parameters such as porosity, tortuosity and pore size, distribution and connectivity. These parameters are influenced by mix proportions, aggregate gradation and shape, compaction techniques and additives.

Bibliography

- [1] T. Younes, F. M. W. Ni, and S. Tighe, "Risk analysis in paving operations using discrete event simulation: a case study of Taiwan permeable asphalt concrete pavement pilot road project", *Int. J. Pavement Eng.*, vol. 21, no. 7, pp. 830–840, 2020, doi: 10.1080/10298436.2018.1511785.
- [2] A. Kia, H. S. Wong, and C. R. Cheeseman, "High-strength clogging resistant permeable pavement", *Int. J. Pavement Eng.*, vol. 22, no. 3, pp. 271–282, 2021, doi: 10.1080/10298436.2019.1600693.
- [3] J. W. Lee, E. Yang, J. Jang, and T. S. Yun, "Effect of clogging and cleaning on the permeability of pervious block pavements", *Int. J. Pavement Eng.*, vol. 0, no. 0, pp. 1–10, 2021, doi: 10.1080/10298436.2021.1884861.
- [4] Y. Azzout, S. Barraud, F. N. Cres, and E. Alfakih, "Techniques Alternatives en Assainissement Pluvial", *Technique et Documentation*. p. 372, 1994.
- [5] J.-L. Bertrand-Krajewski, "Cours d'hydrologie urbaine", Insa Lyon, 2006.
- [6] H. Li, J. Harvey, and Z. Ge, "Experimental investigation on evaporation rate for enhancing evaporative cooling effect of permeable pavement materials", *Constr. Build. Mater.*, vol. 65, pp. 367–375, 2014, doi: 10.1016/j.conbuildmat.2014.05.004.
- [7] X. Chen, H. Wang, C. Li, W. Zhang, and G. Xu, "Computational investigation on surface water distribution and permeability of porous asphalt pavement", *Int. J. Pavement Eng.*, vol. 0, no. 0, pp. 1–13, 2020, doi: 10.1080/10298436.2020.1797734.
- [8] E. Z. Bean, W. F. Hunt, D. A. Bidelspach, and R. J. Burak, "Study on the infiltration rate of permeable pavements", *Critical transitions in water and environmental resources management*, 2004. p. 1-10.
- [9] Jayasuriya, Niranjali, and N. Kadurupokune. "Impact of pervious pavements on drainage infrastructure", *Proceedings of 11th ICUD, Melbourne, 31st of August to the 5th of September (2008)*.
- [10] P. T. Weiss, M. Kayhanian, J. S. Gulliver, and L. Khazanovich, "Permeable pavement in northern North American urban areas: research review and knowledge gaps", *Int. J. Pavement Eng.*, vol. 20, no. 2, pp. 143–162, 2019, doi: 10.1080/10298436.2017.1279482.
- [11] J. Hu, Z. Qian, P. Liu, D. Wang, and M. Oeser, "Investigation on the permeability of porous asphalt concrete based on microstructure analysis", *Int. J. Pavement Eng.*, vol. 21, no. 13, pp. 1683–1693, 2020, doi: 10.1080/10298436.2018.1563785.
- [12] E. O. Nnadi, S. J. Coupe, L. A. Sañudo-Fontaneda, and J. Rodriguez-Hernandez, "An evaluation of enhanced geotextile layer in permeable pavement to improve stormwater infiltration and attenuation", *Int. J. Pavement Eng.*, vol. 15, no. 10, pp. 925–932, 2014, doi: 10.1080/10298436.2014.893325.
- [13] J. Faleyeux, "Elements modulaires en beton pour revêtement des ouvrages d'infiltration des eaux pluviales: référentiel technique", Epernon, Fr. CERIB, 2015.
- [14] G. M. Majersky, "Filtration of Polluted Waters Filtration of Polluted Waters by Pervious Concrete by Pervious Concrete by Pervious Concrete", 2010.
- [15] A. Mohajerani, J. Bakaric, and T. Jeffrey-Bailey, "The urban heat island effect, its causes, and mitigation, with reference to the thermal properties of asphalt concrete", *J. Environ. Manage.*, vol. 197, pp. 522–538, 2017, doi: 10.1016/j.jenvman.2017.03.095.
- [16] FAHED, Jeff, "Etude numérique du potentiel de rafraîchissement des techniques de réduction des îlots de chaleur urbain (ICU) sous climat méditerranéen", 2018. Doctoral thesis. Toulouse, INSA.

- [17] Y. Yamamoto, “Measures to Mitigate Urban Heat Islands”, *Environ. Energy Res. Unit. Quaterly Rev.*, vol. 18, pp. 65–83, 2005.
- [18] Giguère, Mélissa, “Mesures de lutte aux îlots de chaleur urbains”, *revue de littérature*, Institut national de santé publique du Québec, 2009.
- [19] Y. Qin, Y. He, J. E. Hiller, and G. Mei, “A new water-retaining paver block for reducing runoff and cooling pavement”, *J. Clean. Prod.*, vol. 199, pp. 948–956, 2018, doi: 10.1016/j.jclepro.2018.07.250.
- [20] Y. Qin and J. E. Hiller, “Understanding pavement-surface energy balance and its implications on cool pavement development”, *Energy Build.*, vol. 85, pp. 389–399, 2014, doi: 10.1016/j.enbuild.2014.09.076.
- [21] Starke, P., P. Göbel, and W. G. Coldewey, “Urban evaporation rates for water-permeable pavements”, *Water Science and Technology* 62.5 (2010): 1161-1169.
- [22] Y. Qin and J. E. Hiller, “Water availability near the surface dominates the evaporation of pervious concrete”, *Constr. Build. Mater.*, vol. 111, pp. 77–84, 2016, doi: 10.1016/j.conbuildmat.2016.02.063.
- [23] M. J. Chen and Y. D. Wong, “Gradation design of porous asphalt mixture (PAM) for low-strength application in wet environment”, *Int. J. Pavement Eng.*, vol. 19, no. 7, pp. 611–622, 2018, doi: 10.1080/10298436.2016.1199873.
- [24] K. Okada, S. Matsui, T. Isobe, Y. Kameshima, and A. Nakajima, “Water-retention properties of porous ceramics prepared from mixtures of allophane and vermiculite for materials to counteract heat island effects”, *Ceram. Int.*, vol. 34, no. 2, pp. 345–350, 2008, doi: 10.1016/j.ceramint.2006.10.006.
- [25] A. Dawson, “Water in road structures: movement, drainage & effects”, vol. 5. Springer Science & Business Media, 2008.
- [26] D. Thorpe and Y. Zhuge, “Advantages and disadvantages in using permeable concrete pavement as a pavement construction material”, *Assoc. Res. Constr. Manag. ARCOM 2010 - Proc. 26th Annu. Conf.*, no. September, pp. 1341–1350, 2010.
- [27] J. P. Christory and J. Abdo, “Voiries et aménagements urbains en béton – structures réservoirs et aménagements qualitatifs”, *rev. gen. des routes*, no. 775, 1999.
- [28] M. Kováč and A. Sičáková, “Pervious concrete as a sustainable solution for pavements in urban areas”, *10th Int. Conf. Environ. Eng. ICEE 2017*, vol. 2017-April, no. April, pp. 27–28, 2017, doi: 10.3846/enviro.2017.031.
- [29] A. K. Chandrappa and K. P. Biligiri, “Pervious concrete as a sustainable pavement material-Research findings and future prospects: A state-of-the-art review”, *Constr. Build. Mater.*, vol. 111, pp. 262–274, 2016, doi: 10.1016/j.conbuildmat.2016.02.054.
- [30] B. Nantasai and S. Nassiri, “Winter temperature prediction for near-surface depth of pervious concrete pavement”, *Int. J. Pavement Eng.*, vol. 20, no. 7, pp. 820–829, 2019, doi: 10.1080/10298436.2017.1353389.
- [31] A. Yahia and K. D. Kabagire, “New approach to proportion pervious concrete”, *Constr. Build. Mater.*, vol. 62, pp. 38–46, 2014, doi: 10.1016/j.conbuildmat.2014.03.025.
- [32] K. Seifeddine, S. Amziane, and E. Toussaint, “State of the art on the mechanical properties of pervious concrete”, *Eur. J. Environ. Civ. Eng.*, pp. 1–29, 2021.
- [33] E. T. Cackler, T. Ferragut, D. S. Harrington, R. O. Rasmussen, and P. Wiegand, “Evaluation of US and European concrete pavement noise reduction methods”, *National Concrete Pavement Technology Center*, 2006.
- [34] P. T. Weiss, M. Kayhanian, J. S. Gulliver, and L. Khazanovich, “Permeable pavement in northern North American urban areas: research review and knowledge gaps”, *Int. J. Pavement Eng.*, vol. 20, no. 2, pp. 143–162, 2019.
- [35] Tennis, Paul D., Michael L. Leming, and David J. Akers, “Pervious concrete pavements”, No. PCA Serial No. 2828. Skokie, IL: Portland Cement Association, 2004
- [36] K. Wang, V. R. Schaefer, J. T. Kevern, and M. T. Suleiman, “Development of mix proportion for functional and durable pervious concrete”, *NRMCA concrete technology forum: focus on pervious concrete*. Nashville, 2006.
- [37] M. Suleiman, J. Kevern, V. R. Schaefer, and K. Wang, “Effect of compaction energy on pervious concrete properties”, *Concr. Technol. Forum-Focus Pervious Concr. Natl. Ready Mix Concr. Assoc. Nashville, TN*, no. January, pp. 23–25, 2006.
- [38] B. Debnath and P. P. Sarkar, “Permeability prediction and pore structure feature of pervious concrete using brick as aggregate”, *Constr. Build. Mater.*, vol. 213, pp. 643–651, 2019, doi: 10.1016/j.conbuildmat.2019.04.099.
- [39] J. T. Kevern, V. R. Schaefer, K. Wang, and M. T. Suleiman, “Pervious concrete mixture proportions for improved freeze-thaw durability”, *J. ASTM Int.*, vol. 5, no. 2, 2008, doi: 10.1520/JAI101320.
- [40] J. X. Lu, X. Yan, P. He, and C. S. Poon, “Sustainable design of pervious concrete using waste glass and recycled concrete aggregate”, *J. Clean. Prod.*, vol. 234, pp. 1102–1112, 2019, doi: 10.1016/j.jclepro.2019.06.260.
- [41] Y. Zaetang, A. Wongsas, V. Sata, and P. Chindaprasirt, “Use of lightweight aggregates in pervious concrete”, *Constr. Build. Mater.*, vol. 48, pp. 585–591, 2013, doi: 10.1016/j.conbuildmat.2013.07.077.

- [42] D. H. Nguyen, M. Boutouil, N. Sebaibi, L. Leleyter, and F. Baraud, “Valorization of seashell by-products in pervious concrete pavers”, *Constr. Build. Mater.*, vol. 49, pp. 151–160, 2013, doi: 10.1016/j.conbuildmat.2013.08.017.
- [43] S. P. Yap, P. Z. C. Chen, Y. Goh, H. A. Ibrahim, K. H. Mo, and C. W. Yuen, “Characterization of pervious concrete with blended natural aggregate and recycled concrete aggregates”, *J. Clean. Prod.*, vol. 181, pp. 155–165, 2018, doi: 10.1016/j.jclepro.2018.01.205.
- [44] R. Sriravindrarajah, N. D. H. Wang, and L. J. W. Ervin, “Mix Design for Pervious Recycled Aggregate Concrete”, *Int. J. Concr. Struct. Mater.*, vol. 6, no. 4, pp. 239–246, 2012, doi: 10.1007/s40069-012-0024-x.
- [45] J. D. Luck, S. R. Workman, and S. F. Higgins, “Hydrologic properties of pervious concrete”, in 2006 ASAE Annual Meeting, 2006, p. 1.
- [46] O. Deo, M. Sumanasooriya, and N. Neithalath, “Permeability reduction in pervious concretes due to clogging: experiments and modeling”, *J. Mater. Civ. Eng.*, vol. 22, no. 7, pp. 741–751, 2010.
- [47] J. T. Keavern, “Advancements in Pervious Concrete Technology”, retrospective theses and dissertations, Iowa State Univ., pp. 1–108, 2008.
- [48] R. Zhong, M. Xu, R. V. Netto, and K. Wille, “Influence of pore tortuosity on hydraulic conductivity of pervious concrete: Characterization and modeling”, *Constr. Build. Mater.*, vol. 125, pp. 1158–1168, 2016.
- [49] N. Neithalath, D. Bentz, and M. Sumanasooriya, “Predicting the Permeability of Pervious Concrete: Advances in Characterization of Pore Structure and Transport Properties”, *Concr. Int.*, vol. 32, no. 5, pp. 35–40, 2010.
- [50] N. Neithalath, J. Weiss, and J. Olek, “Characterizing enhanced porosity concrete using electrical impedance to predict acoustic and hydraulic performance”, *Cem. Concr. Res.*, vol. 36, no. 11, pp. 2074–2085, 2006.
- [51] ACI 211, “Guide for Selecting Proportions for No-Slump Concrete Reported by ACI Committee 211”, *Am. Concr. Inst.*, vol. 02, no. Reapproved, pp. 1–26, 2002.
- [52] S. H. Kosmatka, B. Kerkhoff, W. C. Panarese, N. F. MacLeod, and R. J. McGrath, “Dosage et contrôle des mélanges de béton”, *Bull. d’ingenierie EB101*, Cem. Assoc. Canada, 2004.
- [53] N. Aravind and T. I. Abdulrehman, “A review and sequel experimental analysis on physical and mechanical properties of permeable concrete for pavement construction”, *Int. J. Pavement Eng.*, vol. 0, no. 0, pp. 1–14, 2021, doi: 10.1080/10298436.2021.1936519.
- [54] N. Jin, “Fly ash applicability in pervious concrete.” The Ohio State University, 2010.
- [55] J. Yang and G. Jiang, “Experimental study on properties of pervious concrete pavement materials”, *Cem. Concr. Res.*, vol. 33, no. 3, pp. 381–386, 2003.
- [56] G. Adil, J. T. Keavern, and D. Mann, “Influence of silica fume on mechanical and durability of pervious concrete”, *Constr. Build. Mater.*, vol. 247, p. 118453, 2020.
- [57] X. Yang, J. Liu, H. Li, and Q. Ren, “Performance and ITZ of pervious concrete modified by vinyl acetate and ethylene copolymer dispersible powder”, *Constr. Build. Mater.*, vol. 235, p. 117532, 2020, doi: 10.1016/j.conbuildmat.2019.117532.
- [58] M. Tabatabaiean, A. Khaloo, and H. Khaloo, “An innovative high performance pervious concrete with polyester and epoxy resins”, *Constr. Build. Mater.*, vol. 228, p. 116820, 2019.
- [59] B. Huang, H. Wu, X. Shu, and E. G. Burdette, “Laboratory evaluation of permeability and strength of polymer-modified pervious concrete”, *Constr. Build. Mater.*, vol. 24, no. 5, pp. 818–823, 2010.
- [60] F. Giustozzi, “Polymer-modified pervious concrete for durable and sustainable transportation infrastructures”, *Constr. Build. Mater.*, vol. 111, pp. 502–512, 2016, doi: 10.1016/j.conbuildmat.2016.02.136.
- [61] N. F. Ariffin, M. F. M. Jaafar, N. H. A. Shukor Lim, M. A. R. Bhutta, and M. W. Hussin, “Mechanical properties of polymer-modified porous concrete”, *IOP Conf. Ser. Mater. Sci. Eng.*, vol. 342, no. 1, 2018, doi: 10.1088/1757-899X/342/1/012081.
- [62] W. Shen, L. Shan, T. Zhang, H. Ma, Z. Cai, and H. Shi, “Investigation on polymer-rubber aggregate modified porous concrete”, *Constr. Build. Mater.*, vol. 38, pp. 667–674, 2013, doi: 10.1016/j.conbuildmat.2012.09.006.
- [63] D. K. Kibenga, O. Bonneau, R. Gagné, and S. Mohammed, “Nouvelle approche de formulation des bétons drainants aux propriétés mécaniques et drainantes améliorées”, Doctoral thesis, Université de Sherbrooke, 2013.
- [64] A. C. I. (American C. Institute), “Report on pervious concrete,” 2010.
- [65] D. H. Nguyen, N. Sebaibi, M. Boutouil, L. Leleyter, and F. Baraud, “A modified method for the design of pervious concrete mix”, *Constr. Build. Mater.*, vol. 73, pp. 271–282, 2014, doi: 10.1016/j.conbuildmat.2014.09.088.
- [66] L. K. Crouch, J. Pitt, and R. Hewitt, “Aggregate effects on pervious portland cement concrete static modulus of elasticity”, *J. Mater. Civ. Eng.*, vol. 19, no. 7, pp. 561–568, 2007, doi: 10.1061/(ASCE)0899-1561(2007)19:7(561).
- [67] J. T. Keavern, V. R. Schaefer, and K. Wang, “Evaluation of pervious concrete workability using gyratory compaction”, *J. Mater. Civ. Eng.*, vol. 21, no. 12, pp. 764–770, 2009.

- [68] O. Deo and N. Neithalath, "Compressive response of pervious concretes proportioned for desired porosities", *Constr. Build. Mater.*, vol. 25, no. 11, pp. 4181–4189, 2011, doi: 10.1016/j.conbuildmat.2011.04.055.
- [69] J. T. KeVERN, K. Wang, and V. R. Schaefer, "Effect of coarse aggregate on the freeze-thaw durability of pervious concrete", *J. Mater. Civ. Eng.*, vol. 22, no. 5, pp. 469–475, 2010.
- [70] A. K. Jain and J. S. Chouhan, "Effect of Shape of Aggregate on Compressive Strength and Permeability Properties of Pervious Concrete", *Int. J. Adv. Eng. Res. Stud.*, vol. 1, no. 1, pp. 120–126, 2011.
- [71] K. Ćosić, L. Korat, V. Ducman, and I. Netinger, "Influence of aggregate type and size on properties of pervious concrete", *Constr. Build. Mater.*, vol. 78, pp. 69–76, 2015.
- [72] V. R. Schaefer and K. Wang, "Mix design development for pervious concrete in cold weather climates", Iowa. Dept. of Transportation. Highway Division, 2006.
- [73] J. T. KeVERN, K. Wang, and V. R. Schaefer, "A novel approach to characterize entrained air content in pervious concrete", *J. ASTM Int.*, vol. 5, no. 2, pp. 1–10, 2008.
- [74] J. Farny and F. In, "Aging gracefully: Architectural concrete panels turn 40 years old", *Concr. Technol. today*, pp. 1–8, 2004.
- [75] R. C. Meininger, "No-Fines Pervious Concrete for Paving", *Concrete International*, vol. 10, no. 8. pp. 20–27, 1988.
- [76] A. Mulligan, "Attainable Compressive Strength of Pervious Concrete Paving Systems", p. 132, 2005.
- [77] M. A. Bury, C. A. Mawby, and D. Fisher, "Making pervious concrete placement easy using a novel admixture system", *Concr. Focus*, vol. 5, no. 3, pp. 55–59, 2006.
- [78] P. N. Balaguru and S. P. Shah, *Fiber-reinforced cement composites*. 1992.
- [79] Z. Yang, "Freezing-and-thawing durability of pervious concrete under simulated field conditions", *Mater. J.*, vol. 108, no. 2, pp. 187–195, 2011.
- [80] H. Wu, B. Huang, X. Shu, and Q. Dong, "Laboratory Evaluation of Abrasion Resistance of Portland Cement Pervious Concrete", *J. Mater. Civ. Eng.*, vol. 23, no. 5, pp. 697–702, 2011, doi: 10.1061/(asce)mt.1943-5533.0000210.
- [81] S. Bright Singh and M. Murugan, "Effect of aggregate size on properties of polypropylene and glass fibre-reinforced pervious concrete", *Int. J. Pavement Eng.*, vol. 0, no. 0, pp. 1–15, 2020, doi: 10.1080/10298436.2020.1836562.
- [82] M. Rangelov, S. Nassiri, L. Haselbach, and K. Englund, "Using carbon fiber composites for reinforcing pervious concrete", *Constr. Build. Mater.*, vol. 126, pp. 875–885, 2016, doi: 10.1016/j.conbuildmat.2016.06.035.
- [83] H. Rodin III, M. Rangelov, S. Nassiri, and K. Englund, "Enhancing mechanical properties of pervious concrete using carbon fiber composite reinforcement", *J. Mater. Civ. Eng.*, vol. 30, no. 3, p. 4018012, 2018.
- [84] X. Cui, J. Zhang, D. Huang, W. Tang, L. Wang, and F. Hou, "Experimental simulation of rapid clogging process of pervious concrete pavement caused by storm water runoff", *Int. J. Pavement Eng.*, vol. 20, no. 1, pp. 24–32, 2019, doi: 10.1080/10298436.2016.1246889.
- [85] D. H. Nguyen, M. Boutouil, N. Sebaibi, F. Baraud, and L. Leleyter, "Durability of pervious concrete using crushed seashells", *Constr. Build. Mater.*, vol. 135, no. 2017, pp. 137–150, 2017, doi: 10.1016/j.conbuildmat.2016.12.219.
- [86] A. K. Chandrappa and K. P. Biligiri, "Effect of pore structure on fatigue of pervious concrete", *Road Mater. Pavement Des.*, vol. 20, no. 7, pp. 1525–1547, 2019, doi: 10.1080/14680629.2018.1464500.
- [87] J. Chen, R. Chu, H. Wang, L. Zhang, X. Chen, and Y. Du, "Alleviating urban heat island effect using high-conductivity permeable concrete pavement", *J. Clean. Prod.*, vol. 237, p. 117722, 2019.
- [88] O. AlShareedah and S. Nassiri, "Spherical discrete element model for estimating the hydraulic conductivity and pore clogging of pervious concrete", *Constr. Build. Mater.*, vol. 305, no. April, p. 124749, 2021, doi: 10.1016/j.conbuildmat.2021.124749.
- [89] Y. Rao and T. Yang, "Three volumetric methods for measuring the vertical porosity distribution of pervious concrete pavement", *Int. J. Pavement Eng.*, vol. 0, no. 0, pp. 1–12, 2021, doi: 10.1080/10298436.2021.1939343.
- [90] S. Park, S. Ju, H.-K. Kim, Y.-S. Seo, and S. Pyo, "Effect of the rheological properties of fresh binder on the compressive strength of pervious concrete", *J. Mater. Res. Technol.*, vol. 17, pp. 636–648, 2022, doi: 10.1016/j.jmrt.2022.01.045.
- [91] D. H. Nguyen, "Thèse de doctorat pour obtenir le Doctorat de l' Université de Caen Basse -Normandie Spécialité: Génie des Matériaux Étude du comportement hydromécanique des bétons drainants à base de coproduits coquilliers", *Doctoral thesis, Université de Caen Basse-Normandie*, 2014.
- [92] R. Zhong, Z. Leng, and C. sun Poon, "Research and application of pervious concrete as a sustainable pavement material: A state-of-the-art and state-of-the-practice review", *Constr. Build. Mater.*, vol. 183, pp. 544–553, 2018, doi: 10.1016/j.conbuildmat.2018.06.131.
- [93] L. G. Li, J. J. Feng, J. Zhu, S. H. Chu, and A. K. H. Kwan, "Pervious concrete: Effects of porosity on permeability and strength", *Mag. Concr. Res.*, vol. 73, no. 2, pp. 69–79, 2021, doi: 10.1680/jmacr.19.00194.

- [94] R. Zhong and K. Wille, “Compression response of normal and high strength pervious concrete”, *Constr. Build. Mater.*, vol. 109, pp. 177–187, 2016, doi: 10.1016/j.conbuildmat.2016.01.051.
- [95] F. Montes, S. Valavala, and L. M. Haselbach, “A new test method for porosity measurements of portland cement pervious concrete”, *J. ASTM Int.*, vol. 2, no. 1, pp. 1–13, 2005, doi: 10.1520/jai12931.
- [96] L. A. Mata and M. L. Leming, “Vertical distribution of sediments in pervious concrete pavement systems”, *ACI Mater. J.*, vol. 109, no. 2, pp. 149–155, 2012, doi: 10.14359/51683701.
- [97] N. Neithalath, M. S. Sumanasooriya, and O. Deo, “Characterizing pore volume, sizes, and connectivity in pervious concretes for permeability prediction”, *Mater. Charact.*, vol. 61, no. 8, pp. 802–813, 2010, doi: 10.1016/j.matchar.2010.05.004.
- [98] A. Kia, H. S. Wong, and C. R. Cheeseman, “Clogging in permeable concrete: A review,” *J. Environ. Manage.*, vol. 193, pp. 221–233, 2017, doi: 10.1016/j.jenvman.2017.02.018.
- [99] C. Lian, Y. Zhuge, and S. Beecham, “The relationship between porosity and strength for porous concrete”, *Constr. Build. Mater.*, vol. 25, no. 11, pp. 4294–4298, 2011, doi: 10.1016/j.conbuildmat.2011.05.005.
- [100] N. Ghafoori and S. Dutta, “Laboratory investigation of compacted no-fines concrete for paving materials,” *J. Mater. Civ. Eng.*, vol. 7, no. 3, pp. 183–191, 1995.
- [101] H. Liu, G. Luo, H. Wei, and H. Yu, “Strength, permeability, and freeze-thaw durability of pervious concrete with different aggregate sizes, porosities, and water-binder ratios”, *Appl. Sci.*, vol. 8, no. 8, p. 1217, 2018.
- [102] M. S. Sumanasooriya and N. Neithalath, “Pore structure features of pervious concretes proportioned for desired porosities and their performance prediction”, *Cem. Concr. Compos.*, vol. 33, no. 8, pp. 778–787, 2011.
- [103] I. N. Grubeša, I. Barišić, V. Ducman, and L. Korat, “Draining capability of single-sized pervious concrete”, *Constr. Build. Mater.*, vol. 169, pp. 252–260, 2018.
- [104] R. Zhong and K. Wille, “Linking pore system characteristics to the compressive behavior of pervious concrete”, *Cem. Concr. Compos.*, vol. 70, pp. 130–138, 2016, doi: 10.1016/j.cemconcomp.2016.03.016.
- [105] Y. Rao, Y. Ding, A. K. Sarmah, D. Liu, and B. Pan, “Vertical distribution of pore-aggregate-cement paste in statically compacted pervious concrete”, *Constr. Build. Mater.*, vol. 237, p. 117605, 2020.
- [106] A. K. Chandrappa and K. P. Biligiri, “Influence of mix parameters on pore properties and modulus of pervious concrete: an application of ultrasonic pulse velocity”, *Mater. Struct.*, vol. 49, no. 12, pp. 5255–5271, 2016.
- [107] M. Kayhanian, D. Anderson, J. T. Harvey, D. Jones, and B. Muhunthan, “Permeability measurement and scan imaging to assess clogging of pervious concrete pavements in parking lots”, *J. Environ. Manage.*, vol. 95, no. 1, pp. 114–123, 2012, doi: 10.1016/j.jenvman.2011.09.021.
- [108] A. K. Chandrappa and K. P. Biligiri, “Pore structure characterization of pervious concrete using X-ray microcomputed tomography”, *J. Mater. Civ. Eng.*, vol. 30, no. 6, p. 4018108, 2018.
- [109] J. Sansalone, X. Kuang, and V. Ranieri, “Permeable pavement as a hydraulic and filtration interface for urban drainage”, *J. Irrig. Drain. Eng.*, vol. 134, no. 5, pp. 666–674, 2008, doi: 10.1061/(ASCE)0733-9437(2008)134:5(666).
- [110] X. Kuang, J. Sansalone, G. Ying, and V. Ranieri, “Pore-structure models of hydraulic conductivity for permeable pavement”, *J. Hydrol.*, vol. 399, no. 3–4, pp. 148–157, 2011, doi: 10.1016/j.jhydrol.2010.11.024.
- [111] N. Delatte, A. Mrkajic, and D. I. Miller, “Field and laboratory evaluation of pervious concrete pavements”, *Transp. Res. Rec.*, vol. 2113, no. 1, pp. 132–139, 2009.
- [112] K. Amini, A. Lesak, A. Sohal, J. Adato, and N. Delatte, “Using ultrasonic pulse velocity to predict properties and performance of pervious concrete”, *Transportation Research Board 93rd Annual Meeting*, 2014.
- [113] A. K. Chandrappa and K. P. Biligiri, “Investigations on pervious concrete properties using ultrasonic wave applications”, *J. Test. Eval.*, vol. 45, no. 5, pp. 1736–1749, 2017.
- [114] K. Amini, X. Wang, and N. Delatte, “Statistical modeling of hydraulic and mechanical properties of pervious concrete using nondestructive tests”, *J. Mater. Civ. Eng.*, vol. 30, no. 6, p. 4018077, 2018.
- [115] T. Kamada, M. Kunieda, I. Shimazaki, and K. Rokugo, “Evaluation of Void Structure of Porous Concrete Using Ultrasonic Pulse Velocity”, *Proc. Japan Concr. Inst.*, vol. 20, no. 2, pp. 733–738, 1998.
- [116] S. Ishiguro, K. Ito, and M. Kudo, “Ultrasonic wave velocity of porous concrete specimen,” in *The 6th symposium on Non-Destructive inspection of concrete structures (Improvement of examination and inspection technologies for Non-Destructive inspection of concrete structures)*, 2015, pp. 111–114.
- [117] R. E, S. Hatanaka, P. Palamy, and S. Kurita, “Experimental study on the porosity evaluation of pervious concrete by using ultrasonic wave testing on surfaces”, *Constr. Build. Mater.*, vol. 300, p. 123959, 2021, doi: 10.1016/j.conbuildmat.2021.123959.
- [118] O. Deo and N. Neithalath, “Compressive behavior of pervious concretes and a quantification of the influence of random pore structure features”, *Mater. Sci. Eng. A*, vol. 528, no. 1, pp. 402–412, 2010, doi: 10.1016/j.msea.2010.09.024.
- [119] A. Singh, G. S. Jagadeesh, P. V. Sampath, and K. P. Biligiri, “Rational approach for characterizing in situ infiltration parameters of two-layered pervious concrete pavement systems”, *J. Mater. Civ. Eng.*, vol. 31, no. 11, p. 4019258, 2019.

- [120] M. U. Magesvari and V. L. Narasimha, “Studies on characterization of pervious concrete for pavement applications”, *Procedia-Social Behav. Sci.*, vol. 104, pp. 198–207, 2013.
- [121] N. S. HALIFAX, “Optimizing the strength and permeability of pervious concrete,” 2010.
- [122] A. Torres, J. Hu, and A. Ramos, “The effect of the cementitious paste thickness on the performance of pervious concrete”, *Constr. Build. Mater.*, vol. 95, pp. 850–859, 2015, doi: 10.1016/j.conbuildmat.2015.07.187.
- [123] A. Ibrahim, E. Mahmoud, M. Yamin, and V. C. Patibandla, “Experimental study on Portland cement pervious concrete mechanical and hydrological properties”, *Constr. Build. Mater.*, vol. 50, pp. 524–529, 2014.
- [124] A. Yahia and K. D. Kabagire, “New approach to proportion pervious concrete”, *Constr. Build. Mater.*, vol. 62, pp. 38–46, 2014.
- [125] G. P. Ong, A. Jagadeesh, and Y. M. Su, “Effect of pore network characteristics on non-Darcy permeability of pervious concrete mixture”, *Constr. Build. Mater.*, vol. 259, p. 119859, 2020, doi: 10.1016/j.conbuildmat.2020.119859.
- [126] M. S. M. Lund, K. K. Hansen, R. Brincker, A. H. Jensen, and S. D. R. Amador, “Evaluation of freeze-thaw durability of pervious concrete by use of operational modal analysis”, *Cem. Concr. Res.*, vol. 106, no. January, pp. 57–64, 2018, doi: 10.1016/j.cemconres.2018.01.021.
- [127] J. T. Kevern and V. R. Schaefer, “Mixture proportioning considerations for improved freeze-thaw durability of pervious concrete”, *ISCORD 2013 Plan. Sustain. Cold Reg. - Proc. 10th Int. Symp. Cold Reg. Dev.*, pp. 471–481, 2013, doi: 10.1061/9780784412978.046.
- [128] ACI 552R-10, Report on pervious concrete, American concrete institute. 2010.
- [129] M. Sonebi and M. T. Bassuoni, “Investigating the effect of mixture design parameters on pervious concrete by statistical modelling”, *Constr. Build. Mater.*, vol. 38, pp. 147–154, 2013.
- [130] V. Henderson, “Evaluation of the Performance of Pervious Concrete Pavement in the Canadian Climate”, Doctoral thesis, p. 276, University of Waterloo, Canada, 2012
- [131] N. Neithalath, “Development and characterization of acoustically efficient cementitious materials”, Doctoral thesis, Purdue University, 2014..
- [132] A. ZOUAGHI, “Permeability of no-fines concrete”, *コンクリート工学年次論文報告集*, vol. 20, no. 2, pp. 757–762, 1998.
- [133] N. Delatte, D. Miller, and A. Mrkajic, “Portland cement pervious concrete pavement: Field performance investigation on parking lot and roadway pavements”, *Engineering*, 2007.
- [134] L. M. Haselbach and R. M. Freeman, “Vertical porosity distributions in pervious concrete pavement”, *ACI Mater. J.*, vol. 103, no. 6, p. 452, 2006.
- [135] B. Debnath and P. P. Sarkar, “Pervious concrete as an alternative pavement strategy: a state-of-the-art review”, *Int. J. Pavement Eng.*, vol. 21, no. 12, pp. 1516–1531, 2020, doi: 10.1080/10298436.2018.1554217.
- [136] “Freeze thaw resistance of pervious concrete”, National Ready Mixed Concrete Association, May 2004.” [Online]. Available: <https://www.nrmca.org/>.
- [137] A. K. Chandrappa and K. P. Biligiri, “Comprehensive investigation of permeability characteristics of pervious concrete: A hydrodynamic approach”, *Constr. Build. Mater.*, vol. 123, pp. 627–637, 2016, doi: 10.1016/j.conbuildmat.2016.07.035.
- [138] Probeton, PTV 122 - “Prescriptions techniques pour les pavés et dalles en béton perméables à l’eau”, 3ème édition, 12 p., 2009.
- [139] J. Bear, “Dynamics of fluids in porous media Dover Publications,” INC, New York, 1988.
- [140] J. K. Lindly and A. Elsayed, “Open-graded highway bases make permeameter setup important”, *J. Transp. Eng.*, vol. 124, no. 2, pp. 144–148, 1998.
- [141] F. Montes and L. Haselbach, “Measuring hydraulic conductivity in pervious concrete”, *Environ. Eng. Sci.*, vol. 23, no. 6, pp. 960–969, 2006.
- [142] H. El-Hassan and P. Kianmehr, “Pervious concrete pavement incorporating GGBS to alleviate pavement runoff and improve urban sustainability”, *Road Mater. Pavement Des.*, vol. 19, no. 1, pp. 167–181, 2018.
- [143] R. Lederle, T. Shepard, and V. De La Vega Meza, “Comparison of methods for measuring infiltration rate of pervious concrete”, *Constr. Build. Mater.*, vol. 244, p. 118339, 2020, doi: 10.1016/j.conbuildmat.2020.118339.
- [144] Y. Zhang, H. Li, A. Abdelhady, and J. Yang, “Comparative laboratory measurement of pervious concrete permeability using constant-head and falling-head permeameter methods”, *Constr. Build. Mater.*, vol. 263, p. 120614, 2020, doi: 10.1016/j.conbuildmat.2020.120614.
- [145] Y. Qin, H. Yang, Z. Deng, and J. He, “Water permeability of pervious concrete is dependent on the applied pressure and testing methods”, *Adv. Mater. Sci. Eng.*, vol. 2015, pp. 1–7, 2015, doi: 10.1155/2015/404136.
- [146] A. Akkaya and İ. H. Çağatay, “Investigation of the density, porosity, and permeability properties of pervious concrete with different methods”, *Constr. Build. Mater.*, vol. 294, 2021, doi: 10.1016/j.conbuildmat.2021.123539.

- [147] G. F. B. Sandoval, I. Galobardes, R. S. Teixeira, and B. M. Toralles, “Comparison between the falling head and the constant head permeability tests to assess the permeability coefficient of sustainable Pervious Concretes”, *Case Stud. Constr. Mater.*, vol. 7, no. August, pp. 317–328, 2017, doi: 10.1016/j.cscm.2017.09.001.
- [148] H. Li, M. Kayhanian, and J. T. Harvey, “Comparative field permeability measurement of permeable pavements using ASTM C1701 and NCAT permeameter methods”, *J. Environ. Manage.*, vol. 118, pp. 144–152, 2013, doi: 10.1016/j.jenvman.2013.01.016.
- [149] A. Singh, P. V. Sampath, and K. P. Biligiri, “A review of sustainable pervious concrete systems: Emphasis on clogging, material characterization, and environmental aspects”, *Constr. Build. Mater.*, vol. 261, p. 120491, 2020, doi: 10.1016/j.conbuildmat.2020.120491.
- [150] A. Kia, H. S. Wong, and C. R. Cheeseman, “Clogging in permeable concrete: A review”, *J. Environ. Manage.*, vol. 193, pp. 221–233, 2017, doi: 10.1016/j.jenvman.2017.02.018.
- [151] H. El-Hassan, P. Kianmehr, and S. Zouaoui, “Properties of pervious concrete incorporating recycled concrete aggregates and slag”, *Constr. Build. Mater.*, vol. 212, pp. 164–175, 2019, doi: 10.1016/j.conbuildmat.2019.03.325.
- [152] K. Low, D. Harz, and N. Neithalath, “Statistical characterization of the pore structure of enhanced porosity concretes”, *Concrete Technology Forum. Focus on Sustainable Development*, National Ready Mixed Concrete Association, 2008.
- [153] B. M. Taheri, A. M. Ramezani-pour, S. Sabokpa, and M. Gapele, “Experimental evaluation of freeze-thaw durability of pervious concrete”, *J. Build. Eng.*, vol. 33, no. November 2019, p. 101617, 2021, doi: 10.1016/j.jobe.2020.101617.
- [154] Mak Wai Kin, “An Overview of Pervious Concrete Applications in Stormwater Management and Pavement Systems”, vol. 3, no. May, p. 58, 2006.
- [155] Z. Sun, X. Lin, and A. Vollpracht, “Pervious concrete made of alkali activated slag and geopolymers”, *Constr. Build. Mater.*, vol. 189, pp. 797–803, 2018, doi: 10.1016/j.conbuildmat.2018.09.067.
- [156] H. Wang, H. Li, X. Liang, H. Zhou, N. Xie, and Z. Dai, “Investigation on the mechanical properties and environmental impacts of pervious concrete containing fly ash based on the cement-aggregate ratio”, *Constr. Build. Mater.*, vol. 202, pp. 387–395, 2019, doi: 10.1016/j.conbuildmat.2019.01.044.
- [157] X. Cui et al., “Experimental Study on the Relationship between Permeability and Strength of Pervious Concrete”, *J. Mater. Civ. Eng.*, vol. 29, no. 11, p. 04017217, 2017, doi: 10.1061/(asce)jmt.1943-5533.0002058.
- [158] R. Liu et al., “Investigation of the porosity distribution, permeability, and mechanical performance of pervious concretes”, *Processes*, vol. 6, no. 7, 2018, doi: 10.3390/pr6070078.
- [159] R. Pieralisi, S. H. P. Cavalaro, and A. Aguado, “Advanced numerical assessment of the permeability of pervious concrete”, *Cem. Concr. Res.*, vol. 102, no. August, pp. 149–160, 2017, doi: 10.1016/j.cemconres.2017.09.009.
- [160] X. Chen et al., “Design of a chitosan modifying alkali-activated slag pervious concrete with the function of water purification”, *Constr. Build. Mater.*, vol. 251, p. 118979, 2020, doi: 10.1016/j.conbuildmat.2020.118979.
- [161] M. S. Sumanasooriya, D. P. Bentz, and N. Neithalath, “Predicting the permeability of pervious concretes from planar images”, in *NRMCA Concrete Technology Forum*, 2009, vol. 11.
- [162] X. Xie et al., “Mixture proportion design of pervious concrete based on the relationships between fundamental properties and skeleton structures”, *Cem. Concr. Compos.*, vol. 113, no. May, p. 103693, 2020, doi: 10.1016/j.cemconcomp.2020.103693.
- [163] K. S. Elango and V. Revathi, “Fal-G Binder Pervious Concrete”, *Constr. Build. Mater.*, vol. 140, pp. 91–99, 2017, doi: 10.1016/j.conbuildmat.2017.02.086.
- [164] F. Yu, D. Sun, M. Hu, and J. Wang, “Study on the pores characteristics and permeability simulation of pervious concrete based on 2D/3D CT images”, *Constr. Build. Mater.*, vol. 200, pp. 687–702, 2019, doi: 10.1016/j.conbuildmat.2018.12.135.
- [165] J. Huang, Z. Luo, and M. B. E. Khan, “Impact of aggregate type and size and mineral admixtures on the properties of pervious concrete: An experimental investigation”, *Constr. Build. Mater.*, vol. 265, 2020, doi: 10.1016/j.conbuildmat.2020.120759.
- [166] A. Singh, P. V. Sampath, and K. P. Biligiri, “A review of sustainable pervious concrete systems: Emphasis on clogging, material characterization, and environmental aspects”, *Constr. Build. Mater.*, vol. 261, p. 120491, 2020, doi: 10.1016/j.conbuildmat.2020.120491.
- [167] S. Kant Sahdeo, G. D. Ransinchung, K. L. Rahul, and S. Debbarma, “Effect of mix proportion on the structural and functional properties of pervious concrete paving mixtures”, *Constr. Build. Mater.*, vol. 255, p. 119260, 2020, doi: 10.1016/j.conbuildmat.2020.119260.
- [168] [168] L. K. Crouch, P. E. Smith, E. I. Walker, C. Adam, T. R. Dunn, and A. Sparkman, “Determining Pervious Portland Cement Concrete Permeability with Simple Triaxial Flexible-Wall Constant Head Permeameter”, *Transportation Research Board 85th Annual Meeting*, 2006.

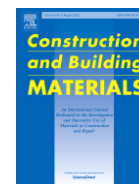
- [169] M. Ahmed, K. M. El Hadi, M. A. Hasan, J. Mallick, and A. Ahmed, “Evaluating the co-relationship between concrete flexural tensile strength and compressive strength”, *Int. J. Struct. Eng.*, vol. 5, no. 2, pp. 115–131, 2014, doi: 10.1504/IJSTRUCTE.2014.060902.
- [170] J. Sun, J. Zhang, Y. Gu, Y. Huang, Y. Sun, and G. Ma, “Prediction of permeability and unconfined compressive strength of pervious concrete using evolved support vector regression”, *Constr. Build. Mater.*, vol. 207, pp. 440–449, 2019, doi: 10.1016/j.conbuildmat.2019.02.117.
- [171] P. Cortez and M. J. Embrechts, “Using sensitivity analysis and visualization techniques to open black box data mining models”, *Inf. Sci. (Ny)*, vol. 225, pp. 1–17, 2013, doi: 10.1016/j.ins.2012.10.039.
- [172] R. W. Vervoort and S. R. Cattle, “Linking hydraulic conductivity and tortuosity parameters to pore space geometry and pore-size distribution”, *J. Hydrol.*, vol. 272, no. 1–4, pp. 36–49, 2003, doi: 10.1016/S0022-1694(02)00253-6.
- [173] W.-T. Kuo, Y.-S. Gao, and C.-U. Juang, “Influence of BOF and GGBFS based alkali activated materials on the properties of porous concrete”, *Materials (Basel)*, vol. 12, no. 14, p. 2214, 2019.
- [174] G. F. B. Sandoval, I. Galobardes, C. Dias, A. Campos, and B. M. Toralles, “Pervious concrete made with electric furnace slag (FEA): mechanical and hydraulic properties”, *Rev. IBRACON Estruturas e Mater.*, vol. 12, pp. 590–607, 2019.
- [175] Y. Zhang, H. Li, A. Abdelhady, and J. Yang, “Comparative laboratory measurement of pervious concrete permeability using constant-head and falling-head permeameter methods”, *Constr. Build. Mater.*, vol. 263, p. 120614, 2020.
- [176] C.-Y. Sung and T.-H. Kim, “Engineering properties of permeable polymer concrete for pavement using powdered waste glass and recycled coarse aggregate”, *J. Korean Soc. Agric. Eng.*, vol. 53, no. 6, pp. 59–65, 2011.
- [177] H. TOKUSHIGE, M. KAWAKAMI, and N. SAEKI, “Mix Design and Properties of Water Permeable Concrete Compacted by Vibration”, *Int. J. Soc. Mater. Eng. Resour.*, vol. 8, no. 2, pp. 38–42, 2000.
- [178] S. B. Park, B. J. Lee, J. Lee, and Y. Il Jang, “A study on the seawater purification characteristics of water-permeable concrete using recycled aggregate”, *Resour. Conserv. Recycl.*, vol. 54, no. 10, pp. 658–665, 2010.
- [179] A. Cheng, H.-M. Hsu, S.-J. Chao, and K.-L. Lin, “Experimental study on properties of pervious concrete made with recycled aggregate”, *Int. J. pavement Res. Technol.*, vol. 4, no. 2, p. 104, 2011.
- [180] M. A. R. Bhutta, K. Tsuruta, and J. Mirza, “Evaluation of high-performance porous concrete properties”, *Constr. Build. Mater.*, vol. 31, pp. 67–73, 2012.
- [181] W.-T. Kuo, C.-C. Liu, and D.-S. Su, “Use of washed municipal solid waste incinerator bottom ash in pervious concrete”, *Cem. Concr. Compos.*, vol. 37, pp. 328–335, 2013.
- [182] R. Zhong and K. Wille, “Material design and characterization of high performance pervious concrete”, *Constr. Build. Mater.*, vol. 98, pp. 51–60, 2015.
- [183] S.-H. Lim, “An Experimental Study on the Properties of Porous Concrete according to the Mix Factors and Compaction Load”, *J. Korea Inst. Struct. Maint. Insp.*, vol. 19, no. 3, pp. 83–91, 2015.
- [184] R. Mahalingam and S. Vaithiyalingam Mahalingam, “Analysis of pervious concrete properties”, *Gradevinar*, vol. 68, no. 06., pp. 493–501, 2016.
- [185] S. Hatanaka, Z. Kamalova, and M. Harada, “Construction of a nonlinear permeability model of pervious concrete and drainage simulation of heavy rain in a residential area”, *Results Mater.*, vol. 3, p. 100033, 2019.
- [186] H. B. Liu, W. J. Li, H. Yu, G. B. Luo, and H. B. Wei, “Mechanical properties and freeze-thaw durability of recycled aggregate pervious concrete”, in *IOP Conference Series: Materials Science and Engineering*, 2019, vol. 634, no. 1, p. 12011.
- [187] R. Liu et al., “Investigation of the porosity distribution, permeability, and mechanical performance of pervious concretes”, *Processes*, vol. 6, no. 7, p. 78, 2018.
- [188] X. Cui et al., “Experimental study on the relationship between permeability and strength of pervious concrete”, *J. Mater. Civ. Eng.*, vol. 29, no. 11, p. 4017217, 2017.
- [189] N. Yoobanpot, P. Jamsawang, K. Krairan, P. Jongpradist, and S. Likitlersuang, “Laboratory investigation of the properties of cement fly ash gravel for use as a column-supported embankment”, *Constr. Build. Mater.*, vol. 257, p. 119493, 2020.
- [190] P. Chindaprasirt, P. Nuaklong, Y. Zaetang, P. Sujumngtokul, and V. Sata, “Mechanical and thermal properties of recycling lightweight pervious concrete”, *Arab. J. Sci. Eng.*, vol. 40, no. 2, pp. 443–450, 2015.
- [191] V. Sata, A. Wongsas, and P. Chindaprasirt, “Properties of pervious geopolymer concrete using recycled aggregates”, *Constr. Build. Mater.*, vol. 42, pp. 33–39, 2013.
- [192] Y. Zaetang, A. Wongsas, V. Sata, and P. Chindaprasirt, “Use of lightweight aggregates in pervious concrete”, *Constr. Build. Mater.*, vol. 48, pp. 585–591, 2013.
- [193] S. Hatanaka, N. Mishima, T. Nakagawa, H. Morihana, and P. Chindaprasirt, “Finishing methods and compressive strength-void ratio relationships of in-situ porous concrete pavement”, *Comput. Concr.*, vol. 10, no. 3, pp. 231–240, 2012.
- [194] S.-B. Park, J. Lee, D.-S. Seo, and E.-S. Yoon, “sc,” *Int. J. Highw. Eng.*, vol. 7, no. 3, pp. 31–42, 2005.

- [195] Y. Yao, “Blending ratio of recycled aggregate on the performance of pervious concrete”, *Frat. ed Integrità Strutt.*, vol. 12, no. 46, 2018.
- [196] H. Peng, J. Yin, and W. Song, “Mechanical and hydraulic behaviors of eco-friendly pervious concrete incorporating fly ash and blast furnace slag”, *Appl. Sci.*, vol. 8, no. 6, p. 859, 2018.
- [197] P. Shen, H. Zheng, S. Liu, J.-X. Lu, and C. S. Poon, “Development of high-strength pervious concrete incorporated with high percentages of waste glass”, *Cem. Concr. Compos.*, vol. 114, p. 103790, 2020.
- [198] X. Chen et al., “Design of a chitosan modifying alkali-activated slag pervious concrete with the function of water purification”, *Constr. Build. Mater.*, vol. 251, p. 118979, 2020.
- [199] E. Lim, K. H. Tan, and T. F. Fwa, “High-strength high-porosity pervious concrete pavement”, in *Advanced Materials Research*, 2013, vol. 723, pp. 361–367.
- [200] L. Yang, S. Kou, X. Song, M. Lu, and Q. Wang, “Analysis of properties of pervious concrete prepared with difference paste-coated recycled aggregate”, *Constr. Build. Mater.*, vol. 269, p. 121244, 2021.
- [201] G. Xu et al., “Investigation on the properties of porous concrete as road base material”, *Constr. Build. Mater.*, vol. 158, pp. 141–148, 2018.
- [202] C. M. Regalado and R. Muñoz-Carpena, “Estimating the saturated hydraulic conductivity in a spatially variable soil with different permeameters: A stochastic Kozeny-Carman relation”, *Soil Tillage Res.*, vol. 77, no. 2, pp. 189–202, 2004, doi: 10.1016/j.still.2003.12.008.
- [203] N. R. Draper and H. Smith, *Applied regression analysis*, vol. 326. John Wiley & Sons, 1998.
- [204] S. A. S. SAS and S. U. Guide, “Version 8. Cary, NC: SAS Institute.” Inc, 1999.
- [205] B. Lu and S. Torquato, “Lineal-path function for random heterogeneous materials”, *Phys. Rev. A*, vol. 45, no. 2, p. 922, 1992.
- [206] A. J. Katz and A. H. Thompson, “Quantitative prediction of permeability in porous rock”, *Phys. Rev. B*, vol. 34, no. 11, p. 8179, 1986.
- [207] N. Neithalath, “Extracting the performance predictors of Enhanced Porosity Concretes from electrical conductivity spectra”, *Cem. Concr. Res.*, vol. 37, no. 5, pp. 796–804, 2007.
- [208] Z. Wang, D. Zou, T. Liu, A. Zhou, and M. Shen, “A novel method to predict the mesostructure and performance of pervious concrete”, *Constr. Build. Mater.*, vol. 263, p. 120117, 2020, doi: 10.1016/j.conbuildmat.2020.120117

Chapter IV Experimental investigation of physical characteristics to improve the cooling effect of permeable pavements

Article publié dans le journal : Construction and Building Materials

Seifeddine, K., Amziane, S., & Toussaint, E. (2022). Experimental investigation of physical characteristics to improve the cooling effect of permeable pavements. *Construction and Building Materials*.



Résumé et objectif

Les chaussées imperméables traditionnelles ont des surfaces sombres et une forte inertie thermique. Pendant les périodes chaudes, elles absorbent et stockent le rayonnement solaire, ce qui contribue à la formation d'îlots de chaleur urbains (ICUs). Parallèlement, l'utilisation de revêtements perméables se développe en raison de leurs avantages environnementaux, tels que la réduction du bruit, la gestion des eaux pluviales et le contrôle des polluants. Ces revêtements sont également efficaces pour atténuer l'effet des ICUs grâce au refroidissement par évaporation. Cependant, les facteurs qui influencent l'effet de refroidissement par évaporation de différents matériaux de chaussée perméables n'ont pas été largement étudiés dans la littérature. Dans cette étude, l'effet de refroidissement par évaporation de neuf formulations de revêtements perméables a été étudié pendant trois jours chauds. L'objectif principal est de trouver les facteurs de premier ordre influençant le taux d'évaporation des chaussées évaporatives perméables. Cette étude permet d'optimiser la conception des mélanges de chaussées perméables afin de maximiser l'effet de refroidissement par évaporation. Deux formulations de chaussées perméables ont été étudiées : les revêtements perméables à base de granulats de pneus recyclés et de pouzzolane locale, et les pavés de granulats poreux.

Il a été déduit à partir des résultats obtenus que l'augmentation du taux d'évaporation dans les revêtements perméables entraîne une augmentation de l'effet de refroidissement par évaporation. Ce taux augmente de façon exponentielle (jusqu'à 0,5652 mm/h) avec l'augmentation de la porosité ouverte (de 23 à 60%) dans les revêtements perméables, à l'exception des revêtements poreux à base de sable. De plus, le phénomène d'évaporation dans les revêtements perméables est contrôlé par la présence d'eau près de la surface. Cette condition a mis en évidence l'importance des remontées capillaires pour assurer la présence d'eau à la surface sur une plus longue période, ce qui a augmenté la durée de l'effet de refroidissement. L'augmentation du coefficient d'absorption d'eau WA assure un effet de refroidissement plus important sur une plus longue période (jusqu'à 3 jours).

Dans les conditions climatiques de cette expérience, l'effet de refroidissement par évaporation dans les revêtements perméables à base de pouzzolane locale et de granulats de pneus recyclés peut durer jusqu'à deux jours par rapport aux chaussées en asphalte traditionnel. Cette baisse de température varie de façon importante le premier jour, et est faible dès le second jour pendant les heures les plus chaudes de la journée. De plus, les résultats montrent que la température de surface de tous les revêtements perméables pendant la nuit est inférieure à celle de l'asphalte,

même après la fin de l'effet de refroidissement par évaporation, en raison de leur nature poreuse et de leur faible conductivité thermique.

Selon les résultats obtenus, bien que la porosité ait une influence significative sur le taux d'évaporation, elle est insuffisante à elle seule pour prédire le taux d'évaporation, qui dépend d'autres facteurs, tels que le niveau d'eau dans le revêtement, le coefficient d'absorption d'eau, la perméabilité et la présence ou l'absence de remontées capillaires. Des résultats plus représentatifs et plus précis pourraient être obtenus si les essais étaient réalisés sur des échantillons de plus grandes dimensions, ce qui réduirait la contribution des effets de bord.

Cette étude présente des limites potentielles. L'expérience a été réalisée dans des conditions de vent faible. Une étude future sur l'influence des mêmes facteurs dans des conditions de vents plus forts est nécessaire, afin d'étudier l'effet combiné des facteurs contrôlables et non contrôlables sur le comportement thermique des chaussées perméables. En outre, des recherches expérimentales et théoriques supplémentaires sont nécessaires pour trouver la porosité optimale, en tenant compte de l'effet de la taille, de la forme, de la distribution et de la tortuosité des pores, dans le but d'obtenir de bonnes performances hydrauliques, mécaniques et thermiques.

Après avoir identifié les différents facteurs qui influencent le taux d'évaporation des chaussées perméables. Les deux chapitres suivants concernent l'étude du comportement thermique du béton drainant. Ces études ont été réalisées en laboratoire dans des conditions climatiques contrôlées, dans la mesure où il est impossible de garantir plusieurs jours de canicule pour réaliser les expériences. Pour cette raison, un banc expérimental innovant a été conçu spécifiquement pour réaliser cette étude en laboratoire. Dans le chapitre suivant, le comportement du béton drainant en conditions sèches a été étudié, puisqu'il existe des pays où les précipitations sont faibles pendant l'été et où les techniques d'arrosage sont compliquées. L'objectif principal est d'optimiser la conception du mélange du béton drainant afin de réduire sa température de surface en conditions sèches.

Khaled Seifeddine^a, Sofiane Amziane^a, Evelyne Toussaint^a

^a Université Clermont Auvergne, CNRS, SIGMA Clermont, Institut Pascal, F-63000 Clermont-Ferrand, France.

Highlights

- A new type of permeable pavement based on pozzolan and recycled tire aggregate was developed.
- The evaporation rate of nine different types of permeable pavement was measured.
- Factors that influence the evaporation rate were identified.
- Increasing open porosity, permeability and absorption rate improves cooling by evaporation.
- The phenomenon of capillary rise provides a long-lasting evaporative cooling effect.

Keywords

Urban heat island; Evaporation rate; Capillary rise; Evaporative cooling; Permeable pavement;

1. Introduction

Urban heat islands (UHIs) are defined as urban areas with significantly higher temperatures than suburban and surrounding rural areas [1], [2]. UHIs are the result of many controllable factors, such as population density, building composition and structure, anthropogenic heat, and green space. There are other factors that cannot be controlled, caused by natural conditions, such as season, wind speed, and cloudiness [3].

UHIs negatively impact public health because they create heat stress in humans [4]. They can impact the environment by degrading outdoor air quality through the diffusion of pollution [5] and can also have impacts on water and energy consumption [6].

The leading cause of UHIs is the fact that urban development increases the surface area covered by impervious substances that absorb heat, and reduces natural vegetation. Several studies show that ordinary asphalt can be up to 20°C warmer than grass [7]. The amount of vegetation in cities is decreasing, and impervious pavements now cover an increasing proportion of surface area, contributing to heat islands [6], [8]. Impervious pavements prevent cooling by evaporation. Since there is no water in the pavement structure, solar energy absorption is converted into sensible heat rather than latent heat [9].

There are several ways to combat UHI formation, such as promoting vegetation by reducing the use of concrete and asphalt [6], reducing anthropogenic heat emission and promoting evapotranspiration by reducing the impermeability of cities [4]. As pavements cover about 20 to 40% of a city's total surface area [10], using cool pavements to reduce UHIs is an innovative solution.

The term 'cool pavements' refers to a variety of both established and emerging materials and technologies. Such pavement materials and technologies have the potential to lower the surface temperature of pavements and emit less heat to the atmosphere than traditional pavements [11]. There are different types of cool pavements: reflective pavements [12]–[17], evaporative pavements [4], [18]–[20], pavements that modify the amount of heat they store, such as

pavements containing phase-change materials [21]–[25], highly conductive pavements [26] and pavements with energy-recuperation systems [27].

Some of the techniques used to make cool pavement have several drawbacks. For example, reflective pavement can cause glare, esthetic problems and other adverse effects on the thermal comfort and health of residents [7]. In addition, the aging of reflective pavements greatly decreases its solar reflectance index due to wear and tear produced by external conditions, which affects its durability [7], [28]. Furthermore, pavements containing phase-change materials and highly conductive pavements are effective in reducing surface temperature during the day compared to conventional pavements; however, the effect is reversed during the night due to their thermal properties, aggravating the urban heat island effect at night [26], [29]. On the other hand, evaporative pavements have a high cooling capacity during both day and night [30], [31]. In addition, they address other issues, such as stormwater management [32], water quality improvement, pollution reduction, sound absorption and reduction of vehicle rolling noise [33].

Through the latent heat absorbed during the phase change of water, evaporation substantially reduces pavement temperature [19]. The evaporation rate is one of the most significant factors influencing the evaporative cooling efficiency of permeable pavements [34].

The main objective of this study is to quantify and compare the evaporation rate of nine permeable pavement formulations in outdoor conditions. These formulations fall into two categories: permeable pavements based on recycled tire aggregates and local pozzolan, and aggregate porous pavement. The aim is to find the first-order factors that influence the evaporation rate, highlighting the influence of open porosity on the evaporative cooling effect. It is therefore crucial to study the evaporation rate of several types of permeable pavements with different physical properties.

For this study, the samples were placed outside during a natural 3-day heatwave from 6/23/2020 to 6/26/2020, while meteorological data were recorded. During the three days of the experiment, the surface temperature and amount of water evaporated from each sample were measured, which provides a picture of the evolution of the evaporation rate and the latent heat flux absorbed (evaporation flux) for each sample as a function of time.

This study helps to better understand the effect of different factors (open porosity, permeability, thermal conductivity, water absorption coefficient of aggregates, water level in the pavement and capillary rise) on the evaporation rate and thermal behavior of several types of permeable pavements. Some of these factors have not been studied, or at least have not been sufficiently studied, in the existing body of literature. In addition, the thermal behavior of a new type of permeable pavement based on pozzolan and recycled tire aggregates was compared to that of conventional pavements.

2. Experimental study

2.1. Materials

Nine samples were prepared to perform this experiment. The samples fall into two categories. The first is composed of 6 permeable pavement formulations (G1, G2, S1, S2, P1, and P2) containing one of three types of natural aggregates (gravel, sand, and pozzolan) with different particle sizes (Table 2). This category refers to stabilizing slabs upon which a granular pavement can be built on the exterior (Fig. 1). This type of pavement makes the ground more stable, water permeable and resistant. Such materials are used as a stabilizing base for

driveways, access roads, pathways, landscaped parks, and parking lots. The selection of these 6 permeable pavement formulations allows the researchers to study the effect of aggregate size and type on evaporation rates.

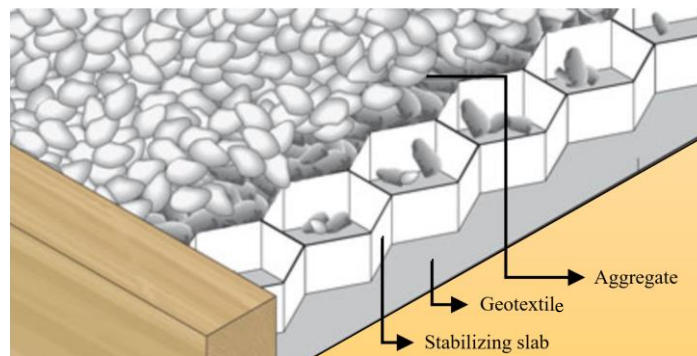


Fig. 1. Draining aggregate stabilizer.

The second category is composed of three permeable pavement formulations (D1, D2 and D3), each comprising a permeable surface layer on top, and a natural gravel fill layer (base layer) on the bottom (Table 2). This structure simulates the permeable pavement's entire structure (surface layer + reservoir layer). These three types of permeable surface layer (Table 1) are made from local pozzolan, recycled tire aggregate and polyurethane resin as a binder. They are made from the same type of aggregates, allowing for a comparison of granular skeletons with a view to obtaining maximum cooling effect. A tenth sample was filled with water as a control.

The pozzolan used is locally sourced from the *Parc naturel regional des Volcans d'Auvergne* volcanic natural park, France, located in the Chaîne des Puys mountain range. Three different sizes of pozzolan are used: coarse (5-18 mm), medium (2-8 mm) and fine (0-0.1 mm).

Recycled tire aggregates are made from used tires that cannot be reused, from a variety of vehicle types (light vehicles, trucks, motorcycles, etc.). The tires are mechanically shredded to transform them into aggregate. During the transformation process, there are no gaseous, liquid, solid or additives required or released. Two sizes of tire aggregates are used: coarse (1.6-10 mm), shown in Fig. 2a, and medium (1-4 mm), shown in Fig. 2b.



Fig. 2. Two sizes of recycled tire aggregate: (a) coarse (1.6-10 mm), (b) medium (1-4 mm).

The binder used is a polyurethane resin that hardens with air humidity. It is Stobieplast® S131.87 resin, which has a setting time of about 30 minutes.

The gravel and sand used are natural aggregates. Two sizes of gravel are used: coarse (5-25 mm) and medium (1.6-12.5 mm). Two sizes of sand are used: coarse (1-8 mm) and fine (0.08-8 mm).

The test to determine the geometric characteristics (particle-size distribution) of the aggregates is carried out in accordance with the standard NF EN 993-1. The particle-size distribution of the fine pozzolan was obtained using a Mastersizer Micro device from Malvern Instruments. The measurement range of this device is from 0.3 to 300µm, which corresponds to the measurement range of conventional cements. The Blaine fineness of the fine pozzolan = 3365 cm².g⁻¹. It was measured by means of the air permeability method (Blaine Method, NF EN 196-6). Fig. 3 shows the particle-size distribution of the aggregates used ((C) for Coarse aggregate, (M) for Medium size aggregate and (F) for Fine aggregate).

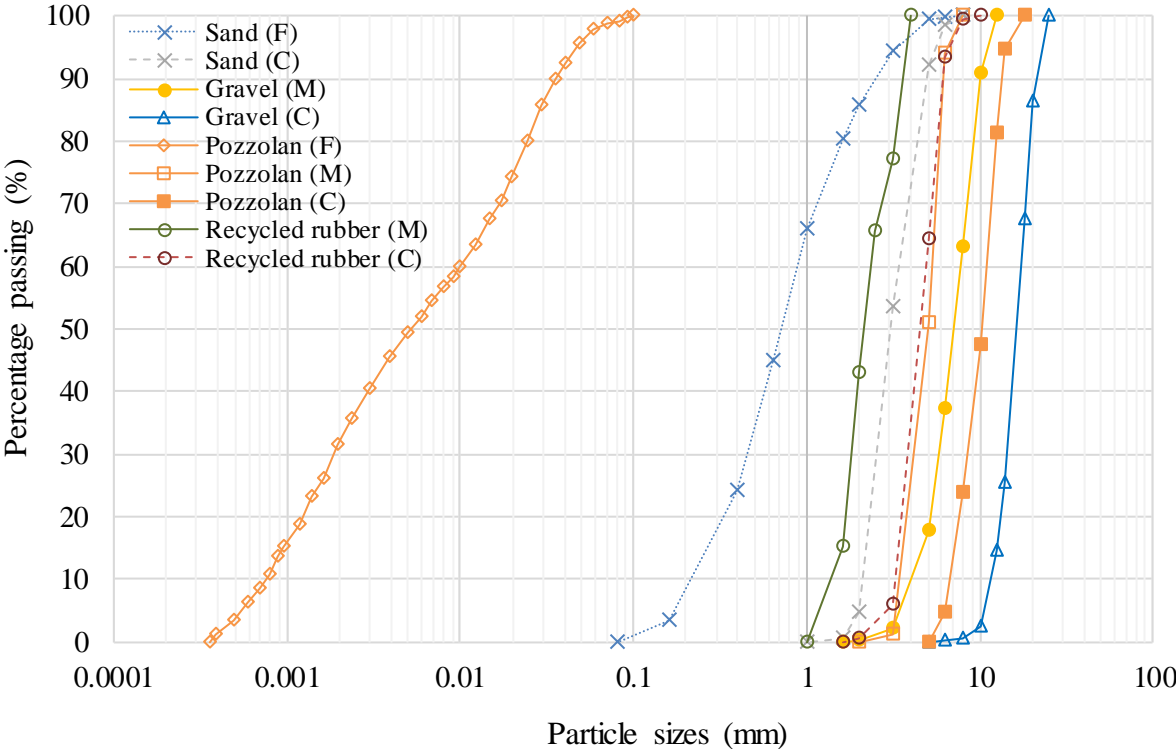


Fig. 3. Particle-size distribution of aggregates.

The cylindrical samples are produced in sealed tubes of 11 cm diameter and 22 cm height. The composition and physical properties of each sample are presented in Table 2.

Table 2
Physical characteristics of the permeable pavements used in this study.

Samples	Composition	Thickness (mm)	Density (kg/m ³)	Open porosity (%)	Absorption coefficient (%)	Permeability (cm/s)	Albedo (%)	Thermal conductivity (W.m ⁻¹ .K ⁻¹)
G1	Gravel (5-25 mm)	21 cm	1700	45	2.37	3.52	11.60	0.201
G2	Gravel (1.6-12.5 mm)	21 cm	1757	40	2.65	1.92	13.5	0.179
S1	Sand (1-8 mm)	21 cm	1795	38	2.76	1.13	14	0.165
S2	Sand (0.08-8 mm)	21 cm	1940	31	4.29	0.05	15.2	0.162
P1	Pozzolan (5-18 mm)	21 cm	1110	60	13.2	2.48	17.7	0.141
P2	Pozzolan (2-8 mm)	21 cm	1202	57	15.08	1.51	20.5	0.10
D1	MC-C	5 cm	1178	31	-	1.54	6.3	0.163
	+ Gravel (5-25 mm)	+ 16 cm	1700	45		0.98	6.6	0.176
D2	MC-M	5 cm	1222	24	-	0.48	7.4	0.317
	+ Gravel (5-25 mm)	+ 16 cm	1700	45		-	-	-
D3	FMC-M	5 cm	1348	23	-	-	-	-
	+ Gravel (5-25 mm)	+ 16 cm	1700	45		-	-	-
A	Impermeable asphalt	-	2400	-	-	-	8	2.2
W	Water	21 cm	1000	-	-	-	-	-

Table 2 shows that the density and thermal conductivity of gravel and sand samples (G1, G2, S1 and S2) are higher than those of pozzolan samples (P1 and P2). This stems primarily from the porous structure and the high intergranular porosity of pozzolanic aggregates, which increase its water retention capacity and make it more insulating. The high water-absorption capacity of the pozzolanic aggregates ensures there is a larger amount of water near the surface, providing a greater evaporative cooling effect. On the other hand, the permeability of these

samples is more closely related to the size of the aggregates, which has a direct influence on pore size, than to the types of aggregates.

The albedo of the pozzolan samples is higher than that of the samples containing sand and gravel because they are lighter in color than the G1, G2, S2 and S2 samples, which are made up mostly of dark aggregates. Moreover, Table 2 shows that for the same type of aggregates, the samples composed of smaller aggregates have a higher albedo. The roughness of the surface increases as the size of the aggregates increases, which reduces the reflectivity of the pavement.

The albedo of samples D1, D2 and D3 is slightly lower than that of the impermeable asphalt due to the presence of pores on the surface of these samples. On the other hand, the thermal conductivity and density of these samples are much lower than those of the impermeable asphalt due to the presence of a porous network in their structures which limits heat transfer within the pavement and may increase surface temperature in dry conditions.

2.2. Dosages and sample preparation

The three types of permeable surface pavements based on pozzolan and recycled tire aggregates have the same proportion of aggregates: 70% pozzolan and 30% tire (percentage by mass in relation to the total mass of aggregates), and the same resin content: 13% of the aggregates' total mass. The pavements differ from each other in terms of the grain size used in each mix. The nomenclature of each permeable pavement obeys the following formula: XYZ-W; where X, Y and Z represent the size of pozzolan aggregate used in the mix, and W the size of recycled tire aggregate used. In addition, YZ-W means that only two sizes of pozzolan were used in the permeable pavement mix. Table 1 presents the three types of permeable surface pavements tested and the mass dosages used.

Table 1
Dosage of permeable pavements.

Permeable surface pavement	Pozzolan (kg/m ³)			Recycled tire aggregates (kg/m ³)		Polyurethane resin (kg/m ³)
	Coarse (C) (5-18 mm)	Medium (M) (2-8 mm)	Fine (F) (0-2 mm)	Coarse (1.6-10 mm)	Medium (1-4 mm)	
MC-C	365	365	0	313	0	135
MC-M	380	380	0	0	325	141
FMC-M	278	278	278	0	358	155

2.3. Methodologies and measuring devices

2.3.1. Open porosity measurement

The open porosity of samples was determined by a method from previous studies [35], [36]. The open porosity of a sample is correlated with the total volume of water used with this method, which involves saturating it with water. For this purpose, the samples were placed into non-deformable molds and covered with a PVC film to ensure watertightness. Then, the mold and the sample inside were placed on a balance and water was added to fill the interstices of these permeable samples. The volume of water is calculated using the weight difference between the dry and the saturated mass. Then, knowing the volume of water V_w (m³) and the

volume of the sample V_s (m^3), the open porosity P_0 (%) is calculated by means of **Eq. (1)**. The results of open porosity of each sample can be found in Table 2.

$$P_0 = \frac{V_w}{V_s} \times 100 \quad (1)$$

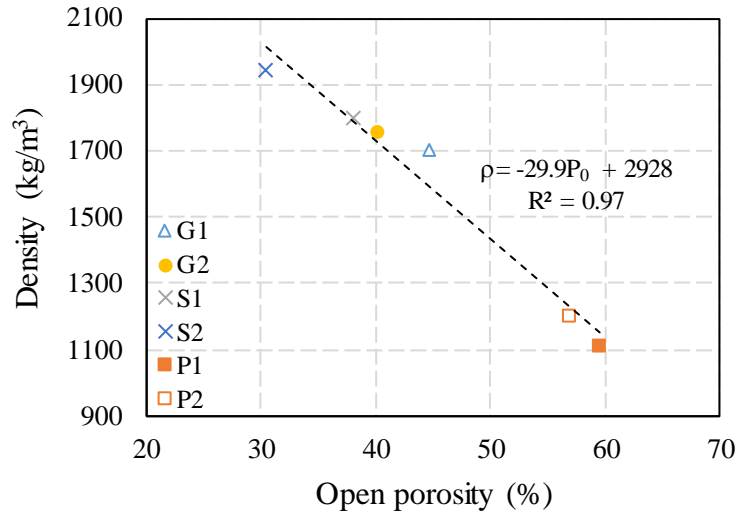


Fig. 4. Variation in density of natural aggregates (pozzolan, gravel and sand) as a function of open porosity.

Several studies in the literature have shown that there is a linear relationship between the porosity P_0 (%) and density ρ (kg/m^3) of different permeable pavements [37]–[39]. For the samples containing the natural aggregates (sand, gravel and pozzolan), a linear relationship was also found (Fig. 4). It is presented in **Eq. (2)**.

$$\rho = -29.9P_0 + 2928 \quad (2)$$

2.3.2. Albedo measurement

The albedo is a dimensionless property, representing the fraction of solar energy reflected by a surface. It is expressed as a percentage or as a number between 0 (all light is absorbed) and 1 (all light is reflected). This property has been measured in accordance with ASTM E1918 using a CMP3 pyranometer, which gives the radiation over the entire range of the solar spectrum from 300 to 2800 nm with a sensitivity of 5 to 20 $V/W/m^2$ and a maximum irradiance of 2000 W/m^2 .

The device used calculates the albedo based on alternating readings of incoming solar radiation and reflected solar radiation on a surface using a single pyranometer. This test method is suitable for measurements on all types of flat surfaces, including textured or irregular surfaces such as gravel pavements. However, only one pyranometer is used to measure both incoming solar radiation and reflected solar radiation on a surface. After measuring the incoming solar radiation, the pyranometer must be turned over to measure the reflected solar radiation [40].

In this study, the albedo was measured outdoors using samples of $50 \times 50 \times 5$ cm^3 (Fig. A1, Appendix A). To validate the results obtained, the albedo of the samples was also measured in the laboratory under controlled climatic conditions using an experimental bench (Fig. A2, Appendix A). This bench is equipped with several devices: infrared lamps located on top of the bin, power regulation of the infrared lamps, pyranometers and a central data acquisition system. The samples were placed in the bin measuring $40 \times 30 \times 15$ cm^3 . The bin was covered in a black

cloth with high solar absorption to measure the albedo in the laboratory without the effect of the intensity of solar radiation, the angle of incidence and the surrounding conditions, in accordance with the experimental protocol used by Chen et al. [13].

2.3.3. Permeability measurement

The permeability of permeable pavements was measured using an ASTM C 1701 permeameter. This method uses the principle of the constant-head permeameter. The infiltration rate (permeability or hydraulic conductivity) is calculated by **Eq. (3)** [41].

$$I = \frac{\gamma M}{D^2 t} \quad (3)$$

where I = infiltration rate (mm/h); M = infiltrated water mass (kg); D = inner diameter of the infiltration ring (mm); t = time required for the measured amount of water to infiltrate the pavement (s); γ (constant value) = 4,583,666,000 in SI units.

2.3.4. Thermal conductivity measurement

Thermal conductivity was measured using a CTMF conductivity meter. The method entails producing a temperature gradient across the thickness of the sample to be characterized and measuring the heat flow through it. The temperature difference between the two faces of the sample is applied by specially designed thermoelements. The thermopiles measure the heat flow in accordance with standards (ASTM C518; ISO 8301; EN 12667). The setup is designed to accommodate specimens of $150 \times 150 \text{ mm}^2$ with thicknesses ranging from 5 to 20 mm.

2.3.5. Capillary rise height measurement

The height of the capillary rise was measured with a transparent Plexiglass tube $100 \times 250 \times 500 \text{ mm}^3$, a high-resolution camera pco.2000 capable of fast image recording at 160 MB/s, and two halogen light sources KL 2500 LCD.

2.3.6. Bulk density measurement

The apparent densities ρ_d (kg/m^3) of the aggregates used were determined in accordance with NF EN 1097-3 using **Eq. (4)**.

$$\rho_d = \frac{M_1 - M_2}{V} \quad (4)$$

where M_1 (kg) is the mass of the container filled with dry aggregate, M_2 (kg) is the mass of the clean, empty container and V (m^3) is the volume of the container.

2.3.7. Water-absorption coefficient measurement

The water-absorption coefficient WA (%) was determined by the procedure described in NF EN 1097-6: the aggregates are immersed in water at 22°C for 24 hours. The measurement of water absorption involves the determination of the saturated surface dry (SSD) state. This state is defined as one where the intra-granular porosity is saturated with a thin film of water on the surface and no inter-granular water remains. Once this state is determined, the mass in the

saturated surface dry state is recorded M_{SSD} (g), and then the sample is dried to constant mass in an oven at 105°C M_{DRY} (g). WA is given by Eq. (5).

$$WA = \frac{M_{SSD} - M_{DRY}}{M_{DRY}} \times 100 \quad (5)$$

2.3.8. Evaporation rate measurement

The procedure adopted for measuring evaporation rate in this study was that developed at the University of California Pavement Research Center [19].

Samples were prepared in molds in the dry state. The aggregates were dried in an oven for 48 hours. The mass of the set, written as m_1 (kg) (dry sample + mold), was measured using an electric balance. Then, the samples were watered until the water reached the surface of the samples. For 24 hours, the samples remained saturated, as the water level can drop immediately as result of the water absorption of the porous aggregates. After 24 hours, the samples were topped up with water again to ensure complete saturation. This saturation is important to simulate permeable pavements with a reservoir structure after heavy rainfall. In addition, it allows researchers to study the effect of the level of water on the evaporation rate.

After saturation, the total mass (saturated sample + mold) is recorded as m_{20} . The total weight of each sample, including the remaining water and the container is measured over time t and recorded as m_{2t} . The remaining weight of water in the sample m_{wt} is calculated by Eq. (6).

$$m_{wt} = m_{2t} - m_1 \quad (6)$$



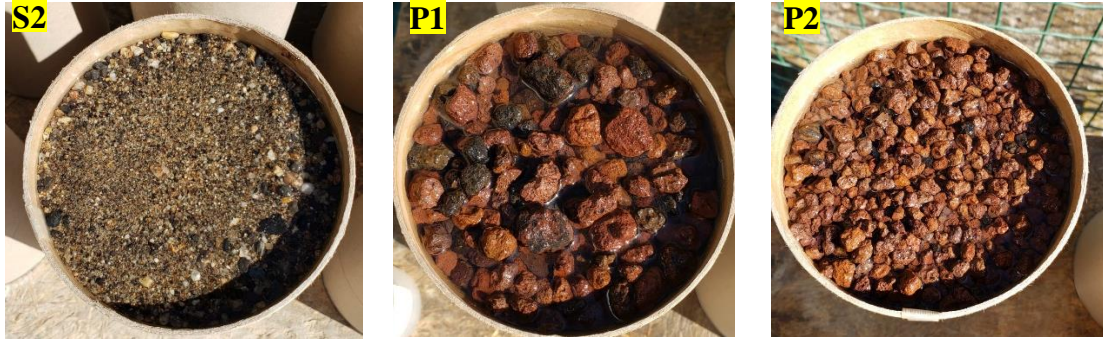


Fig. 5. Samples used to measure evaporation rate in outdoor conditions.

The samples shown in Fig. 5 are in the saturated state at the beginning of the experiment on 06/23/2020.

The mass of water that has evaporated over time Δm_{wt} is calculated by **Eq. (7)**. Δm_{wt} is the difference between the initial total mass at saturation m_{20} (kg) and the total mass at time m_{2t} (kg).

$$\Delta m_{wt} = m_{20} - m_{2t} \quad (7)$$

The evaporation rate ER (kg/m²/h or mm/h) between two times t_1 (s) and t_2 (s), is calculated by **Eq. (8)**. It corresponds to the difference between the sample's total mass at time t_1 (s) and the sample's total mass at time t_2 (s), divided by the surface of the sample exposed to the outside A (m²) and by the time $(t_2 - t_1)$.

$$ER = \frac{m_{2t1} - m_{2t2}}{A (t_2 - t_1)} \quad (8)$$

Finally, the maximum theoretical latent heat flux lost by evaporation is written Q_E (W/m²). The higher this value, the greater the cooling effect. **Eq. (9)** shows that the latent heat loss by evaporation Q_E (W/m²) of the coatings is proportional to the evaporation rate ER .

$$Q_E = \frac{L \times ER}{3.6} \quad (9)$$

where $L = 2260$ kJ/kg is the specific latent heat of vaporization of water.



Fig. 6. Samples placed outside near the weather station.

The mass at ± 0.01 g and the surface temperature at $\pm 0.1^\circ\text{C}$ of the samples was measured manually every hour between 09:00 and 22:00. To avoid overflow of water from the samples with manual weighing, the molds were filled up to 21 cm = (mold height - 1 cm). The surface temperature was measured with a "FLUKE-62 MAX+" infrared thermometer. In order to prevent the shadow formed at the edge of the surface visible during the afternoons, the average temperature of three measurements in the center of all samples was recorded. Additional tests were performed on similar samples exposed entirely outdoors (molds filled to 22 cm), showing that the shadow created at the edge of the surface has no influence ($< 1\%$ deviation) on the surface temperature nor on the amount of water evaporated (evaporation rate).

A "Davis Vantage Pro2" weather station was used to measure meteorological data (ambient temperature, relative humidity, wind speed, and radiative flux) every half hour (Fig. 6). The weather was cloudless, clear and sunny for the duration of the heatwave.

3. Results and discussion

3.1. Meteorological data evolution over time

Between June 23, 2020 at 09:00 and June 26, 2020 at 09:00, meteorological data were measured every half hour of this experiment. The maximum diurnal ambient temperature recorded was 30°C for the first day and 34.3°C for the second and third days. Relative humidity ranged from 25% to 80%. There was relatively low wind speed during this experiment, with an average of 1.4 km/h during the three days. The average maximum radiative flux was fairly constant during the diurnal period of each day, with a maximum average value of 1010 W/m^2 . The results are presented in Fig. 7.

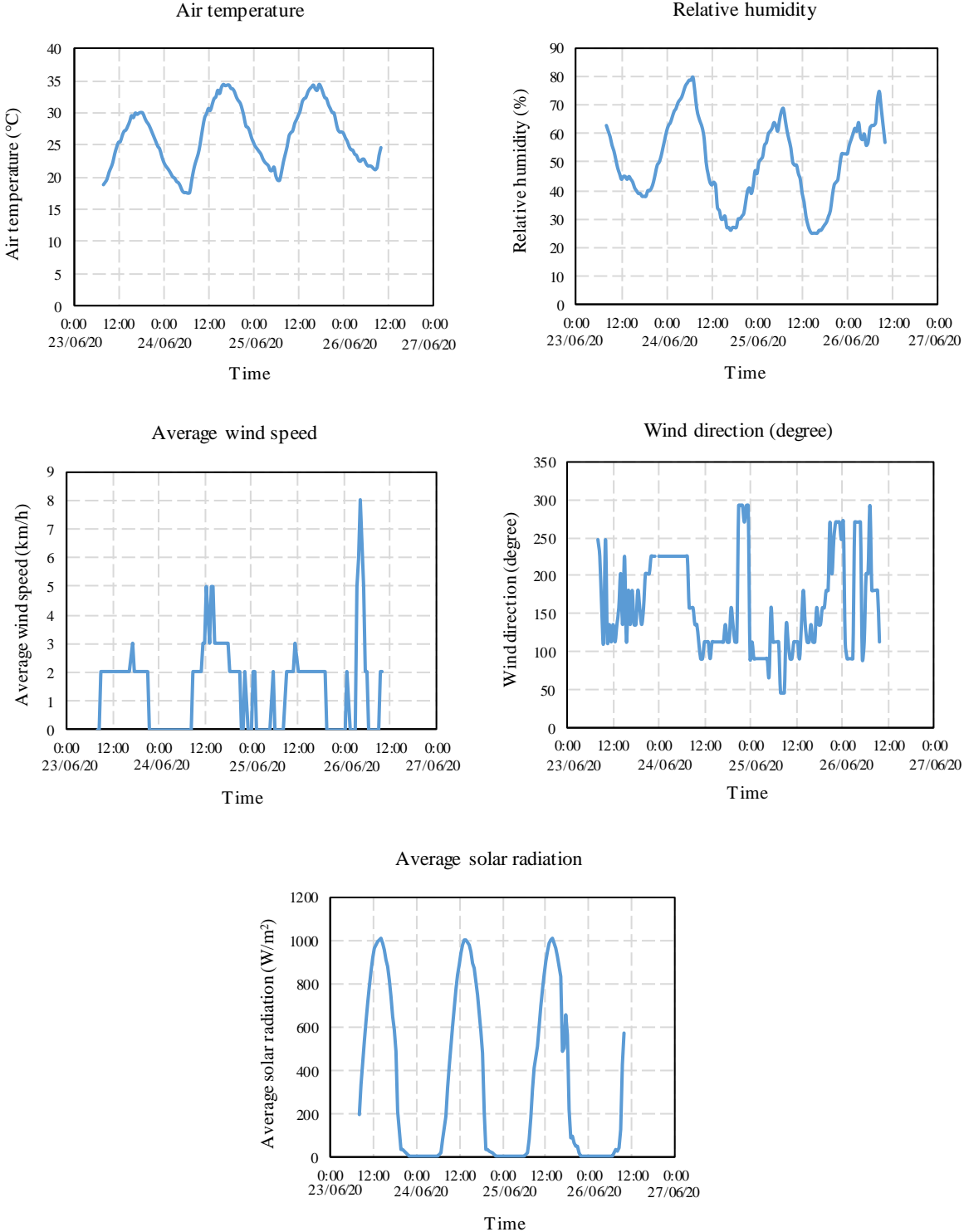


Fig. 7. Meteorological data (ambient temperature, relative humidity, wind speed, wind direction and average radiative flux) during the three days of this experiment.

This study was performed under low wind conditions. This is one of the uncontrollable factors that affect the thermal behavior of pavements. As the wind speed increases, the heat convection coefficient increases, which reduces the surface temperature of the pavement [42]. In this study, controllable factors are investigated, which should help to design permeable pavements with a high evaporative cooling effect under all weather conditions.

3.2. Evolution of the amount of water evaporated during the experiment

Table 3 shows the amount of water initially present in the samples, the mass of water remaining and the mass of water evaporated at the end of the experiment after three days.

Table 3

Total mass of water evaporated at the end of the experiment (day 3).

Samples	m_{20} (g)	Initial mass of water (g)	Remaining water mass after 3 days (g)	Mass of water evaporated after 3 days (g)
G1	4403.85	916.15	740.37	175.78
G2	4429.41	824.78	683.82	140.96
S1	4465.62	783	630.88	152.12
S2	4606.8	626.68	338.44	288.24
P1	3498.8	1221.27	901.37	319.9
P2	3635.48	1169.29	845.59	323.7
D1	3815.4	883.81	811.14	72.67
D2	3924.75	857.39	782.42	74.97
D3	3965.05	860.58	761.21	99.37
W	2311.41	2311.41	1958.09	353.32

At the end of the experiment on 6/27/2020 at 09:00, all samples still had more than 50% of the mass of water initially present. Control sample W had the highest amount of water evaporated after three days (353.32 g). Sample D1 had the lowest amount of water evaporated (72.67 g).

To present the evolution of the remaining water mass over time in a clear and understandable way, curves normalized to the initial water mass are presented in Fig. 8.

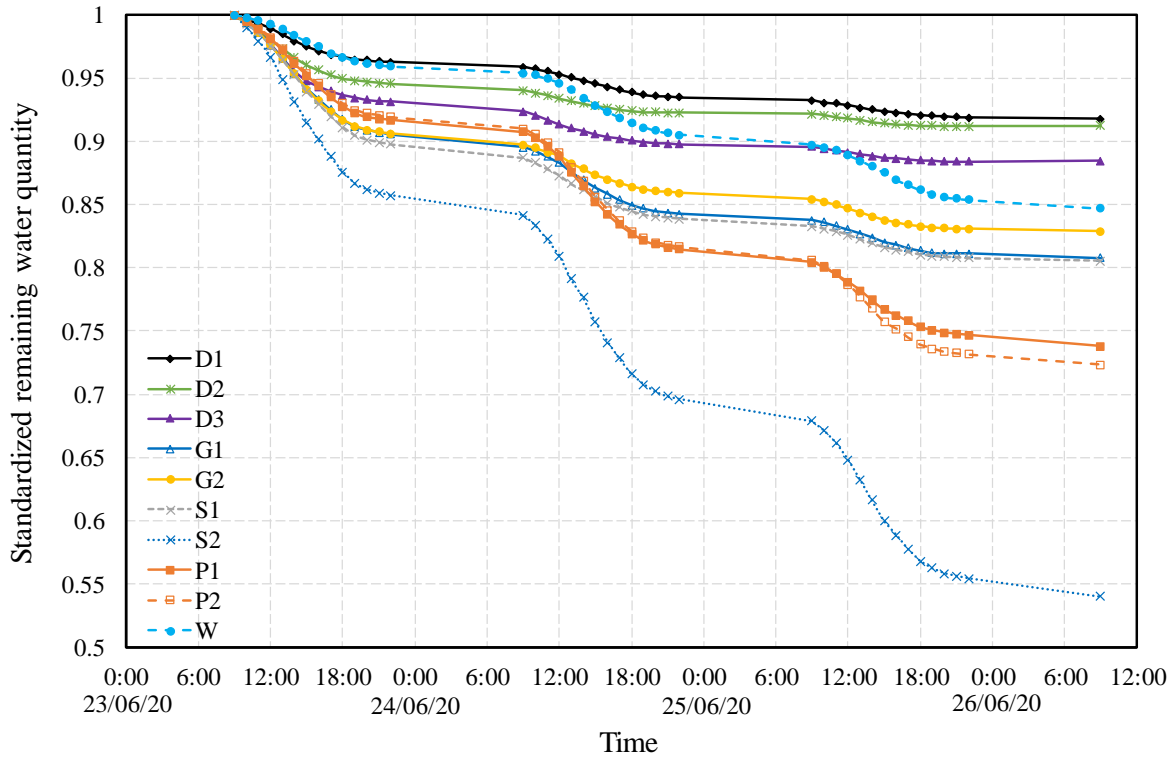


Fig. 8. Variation of water mass in the samples as a function of time (normalized curves).

The normalized curves, which present the variation of water mass Δm_{wt} in the samples during the three days of the experiment, show that the sample containing the fine sand (S2) lost the greatest amount of water (46%) compared to the amount of water initially present. On the other hand, the samples containing the permeable pavements (D1, D2 and D3), which had a higher initial amount of water at the beginning of the experiment than the S2 sample, lost the least amount of water compared to the mass of water initially present (8.2%, 8.7% and 11.5%, respectively).

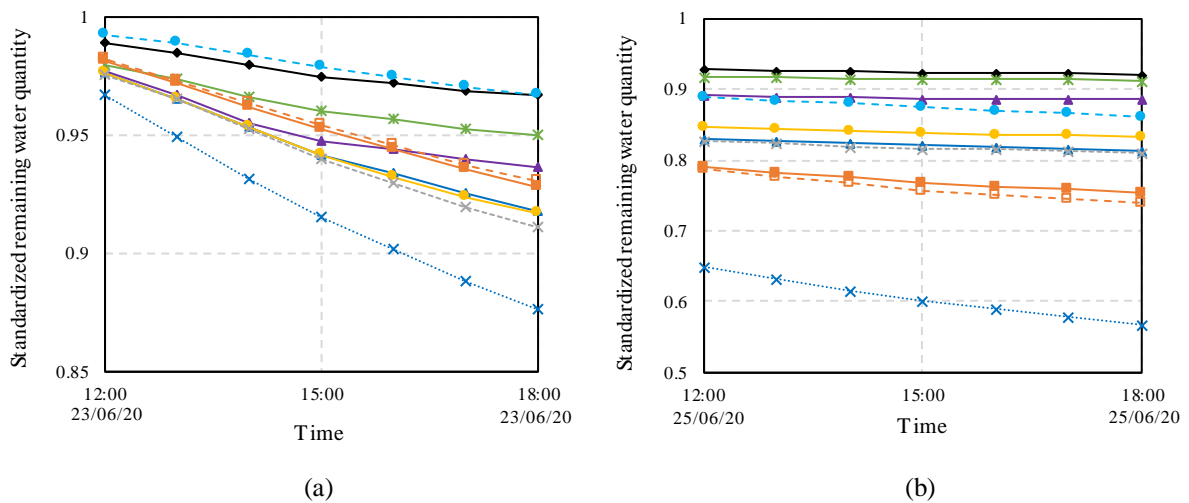


Fig. 9. Variation in the mass of water in the samples during the diurnal period of the first day (a) and the third day (b) of the experiment (normalized curves with the same legends as Fig. 8).

Figs 9a and 9b show the variation in the amount of water in the samples during the diurnal period from 12:00 to 18:00, on the first and third days. The variation of the slope of normalized curves (downward slope) presented in Fig. 9b shows that evaporation was still continuing in some samples during the third day (E, S2, P1 and P2). Other samples, such as those containing the permeable coatings (D1, D2 and D3), lost a significant proportion of their evaporative performance over time. The slope of their curves progressively decreases until an almost horizontal curve is obtained, especially from the third day onwards (Fig. 9b), which shows that evaporation in these samples has become negligible.

3.3. Study of the cooling effect of permeable pavements based on recycled tire aggregates and pozzolan

3.3.1. Evolution of surface temperature

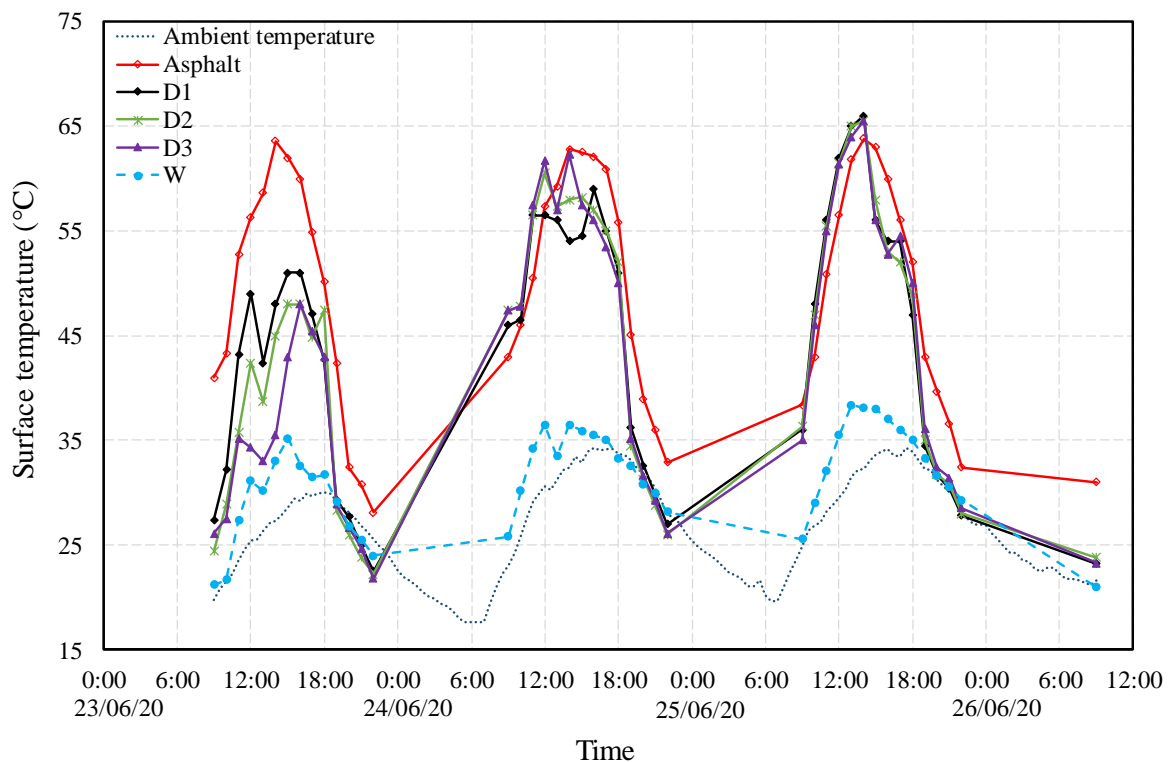


Fig. 10. Variation in surface temperature of permeable pavements (D1, D2, and D3), water, air, and impermeable asphalt with time.

Fig. 10 shows the variation in surface temperature of the permeable pavements (D1, D2, and D3) and a traditional impermeable asphalt pavement located near the samples in this experiment. The aim is to quantify the cooling effect of these new permeable pavements that have been developed in this experiment compared to a conventional impermeable asphalt pavement.

All the samples' surface temperature varied similarly to the ambient air temperature. The maximum surface temperatures for the asphalt pavement were recorded at 14:00: 63.6°C, 62.8°C, and 63.8°C on the first, second, and third days, respectively. For the first day at 14:00, the permeable pavements' surface temperature was invariably lower than that of the asphalt impermeable pavement, with the following differences: - 28.1°C, - 18.6°C, and - 15.6°C, for D3, D2 and D1, respectively.

The surface temperatures of the permeable pavements were higher than those of the asphalt pavement on the second day, between 09:00 and 12:00, with a difference varying from 0.5°C to 4.4°C. From 12:00 onwards, these permeable pavements had surface temperatures 0.5°C to 8.8°C lower than those of the asphalt pavement. The variation shows that the increase in ambient temperature, particularly in the afternoon, increased the evaporative cooling effect in these permeable pavements, although not as significantly as on the first day.

On the third day at 14:00, the surface temperature of the permeable pavements was 1.7°C to 2.2°C higher than that of the asphalt. This result showed that the evaporative cooling effect for these three pavements is insignificant after three days. In contrast, during the nocturnal period of the three days of this experiment, the surface temperatures of D1, D2 and D3 were significantly lower than that of the impermeable asphalt, even after the significant reduction of the evaporative cooling effect in permeable pavements.

3.3.2. Evolution of evaporation rate and latent heat flux

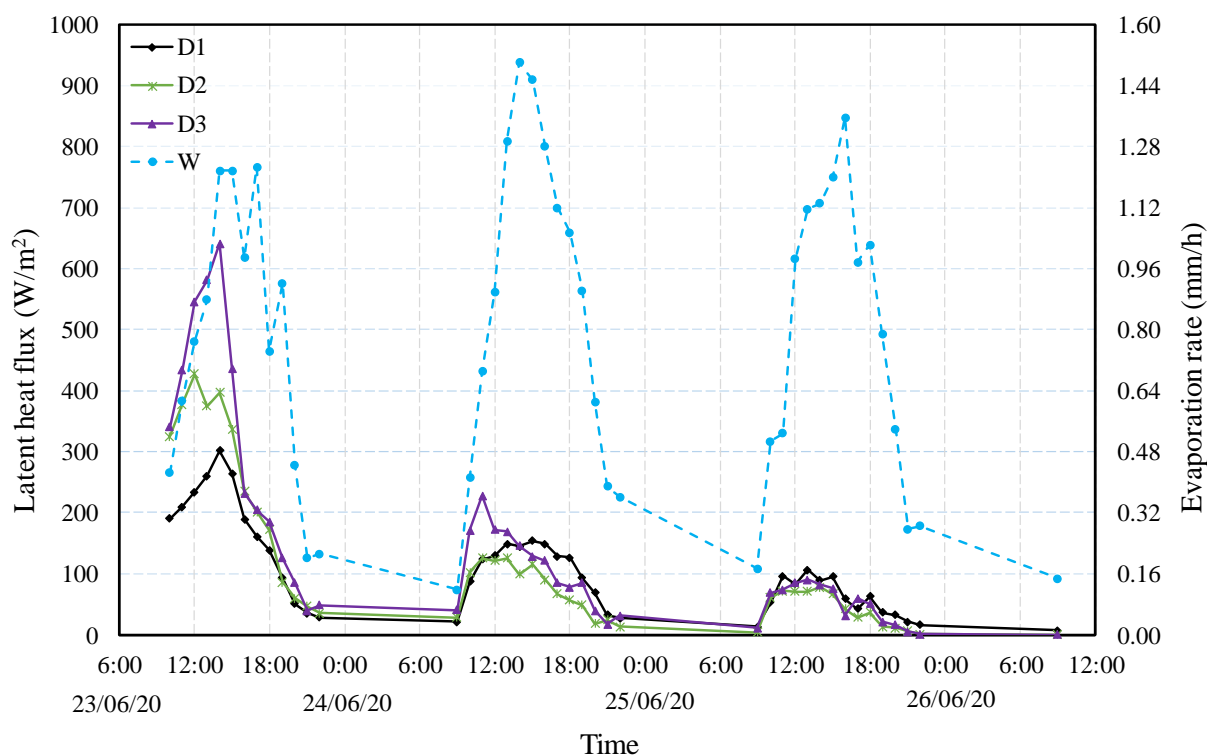


Fig. 11. Variation in evaporation rate and latent heat flux in permeable pavements (D1, D2 and D3) as a function of time.

Fig. 11 shows the variation in evaporation rate ER and latent heat flux during the three days of the experiment.

The evaporation rate on the first day was relatively high for the three types of permeable pavements during the daytime period. The maximum evaporation rates recorded at 14:00 for the three samples was: 0.48 mm/h, 0.63 mm/h and 1.02 mm/h for D1, D2 and D3 respectively. As a result of the absorption of latent heat, their surface temperatures (cooling effect) were lower than on conventional asphalt pavement. In addition, the surface temperature was found to be strongly related to the evaporation rates. Compared to D1 (0.48 mm/h) and D2 (0.63 mm/h), sample D3 had the highest evaporation rate (1.02 mm/h) on the first day, leading to a lower surface temperature than the other permeable pavements (Fig. 10).

On the second day, the evaporation rates in these permeable pavements observed at 14:00 decreased compared to the first day by 52%, 75%, and 77%. For the third day, the decrease was 70%, 81% and 87% compared to the first day. From the second day, these pavements became increasingly dry and had a surface temperature that exceeded the surface temperature of the asphalt during the hottest hours of the day. There are several reasons for this temperature increase. Firstly, the relatively low thermal conductivity of these permeable pavements compared to asphalt (Table 2) limits conductive heat transfer to the interior of the material. Their low albedo (see Table 2) leads to a significant absorption of incident short-wave radiation which causes a rapid increase in surface temperature. As a result, the heat is trapped in the surface layer. This is because permeable pavements' rough, porous surface absorbs more solar radiation than impermeable pavement surfaces. In addition, permeable pavements have less resistance to temperature drop at night due to lower thermal inertia, and hence become colder than traditional asphalt pavement. It was noted that in countries that have dry summers and where watering techniques are complicated to implement, in hot weather and dry conditions, permeable pavements should be avoided because they aggravate the problem of urban heat islands. This problem can be mitigated by increasing the thermal conductivity and albedo of permeable pavements.

It was found that after the second day of the experiment, the permeable pavements (D1, D2 and D3) lose their evaporative cooling performance even if not completely dry. The cooling effect is only notable during the first day of wetting. This is because the low evaporation rate of the permeable pavements after the second day is insufficient to dissipate heat, which leads to an increase in their surface temperature during the daytime.

The evaporation process (the transfer of heat and moisture from permeable pavements) can be divided into two stages. The first is the heavy evaporation stage. The intensity and duration of this stage is dominated by the atmospheric environment and the availability of water near the surface. The second stage occurs when the free water being retained by capillary force evaporates and the water level in the permeable pavements drops, which increases the evaporation resistance. The first stage corresponds to the first day of the experiment when the evaporation rate of the saturated permeable pavements (D1, D2 and D3) was at its maximum (Fig. 11). During this phase, water is continuously pushed from the saturated zone to the surface to evaporate. The evaporation rate is relatively high because gravity can be effectively overcome by the capillary force. This explains why sample D3 has an evaporation rate up to twice as high as sample D1. It should be noted that the surface layer of sample D3 (FMC-M) contains smaller recycled tire aggregates and fine pozzolan powder, which makes the pores smaller and improves the capillary rise effect and therefore the availability of water near the surface.

It has been deduced that a higher evaporative cooling effect can be achieved simply by optimizing the granulometry of the aggregates used, which has a direct influence on the pore size. This optimization should take account of the hydraulic function of the permeable pavements. It is always necessary to ensure that the permeability is higher than 1mm/s – the minimum permeability to avoid the risk of clogging [32].

The net radiant flux at the surface Q_{net} (Eq. (10)) represents the actual radiant energy available at the surface of the pavements. Under wet conditions, the net radiant energy captured by the surface Q_{net} is subsequently released by heat exchanges between the surface and the atmosphere by convection Q_H (Eq. (11)) which represents sensible heat flux, by evaporation Q_E (Eq. (9)) which represents latent heat flux, and by conductive exchanges Q_G (Eq. (12)). As the permeable pavements dry out, the latent heat flux is unable to release the absorbed energy

and suppress the increase of the surface temperature, which leads to the increase of the sensible heat flux.

$$Q_{\text{net}} = Q_{\text{H}} + Q_{\text{E}} + Q_{\text{G}} \quad (10)$$

$$Q_{\text{H}} = h_{\text{c}}(T_{\text{s}} - T_{\text{a}})$$

$$h_{\text{c}} = \begin{cases} 5.6 + 4.0 \times v, & |v < 5 \text{ m/s} \\ 7.2 \times v_9^{0.78}, & |v \geq 5 \text{ m/s} \end{cases} \quad (11)$$

$$Q_{\text{G}} = -\lambda_{\text{pavement}} \left(\frac{\partial T}{\partial z} \right)_{z=0} \quad (12)$$

where h_{c} = thermal convection coefficient ($\text{W} \cdot \text{m}^{-1} \cdot ^\circ\text{C}^{-1}$) [43]; v_9 (m/s) = estimated wind speed at a height of 9 m. To convert the wind speed measured in this experiment at a height of 2 m v_2 to v_9 , this equation can be used: $v_9 = v_2 \times (9/2)^{1/7}$ [42]; T_{s} = surface temperature ($^\circ\text{C}$); T_{a} = air temperature near the surface ($^\circ\text{C}$); $\lambda_{\text{pavement}}$ = thermal conductivity of the pavement ($\text{W} \cdot \text{m}^{-1} \cdot \text{K}^{-1}$).

Fig. 12 shows the variation of latent Q_{E} and sensible heat flux Q_{H} released by the permeable pavements D1, D1 and D3 during the three days of the experiment. The heat losses at the lateral walls of the samples are not taken into account. The results show that the sensible heat flux increases with decreasing evaporation flux. It was deduced that in order to achieve a better cooling effect, and to effectively combat the formation of UHIs, it is necessary to guarantee a higher evaporative flux over a longer period of time. Periodic watering of the permeable pavement is therefore essential.

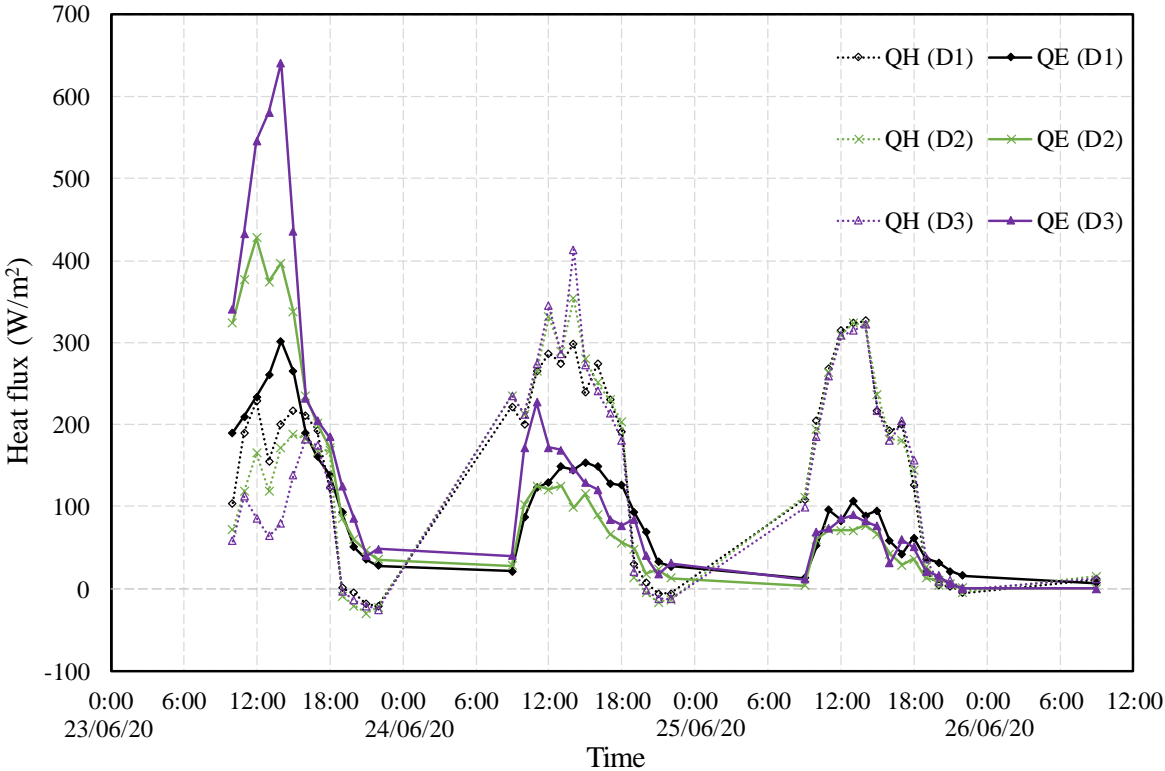


Fig. 12. Variation in latent and sensible heat fluxes as a function of time.

The results obtained with these new permeable pavements are in line with the results obtained in other studies on conventional pervious pavements: pervious concrete and pervious asphalt concrete. Indeed, Qin and Hiller [44] showed that the cooling effect of evaporation of pervious concrete at saturation lasts for about 12 to 24 hours. After this period, the pervious concrete surface temperature increases compared to traditional impermeable concrete. Nevertheless, pervious concrete has lower surface temperatures throughout the night than traditional impermeable concrete because of its low thermal conductivity. The experimental study of Li et al. [45], conducted on impermeable and permeable asphalt concrete pavements, also shows similar results and pavement behavior to those found in the present study and in the study of Qin and Hiller [44].

3.4. Study of the cooling effect of aggregate porous pavements: sand and natural gravel

3.4.1. Evolution of surface temperature

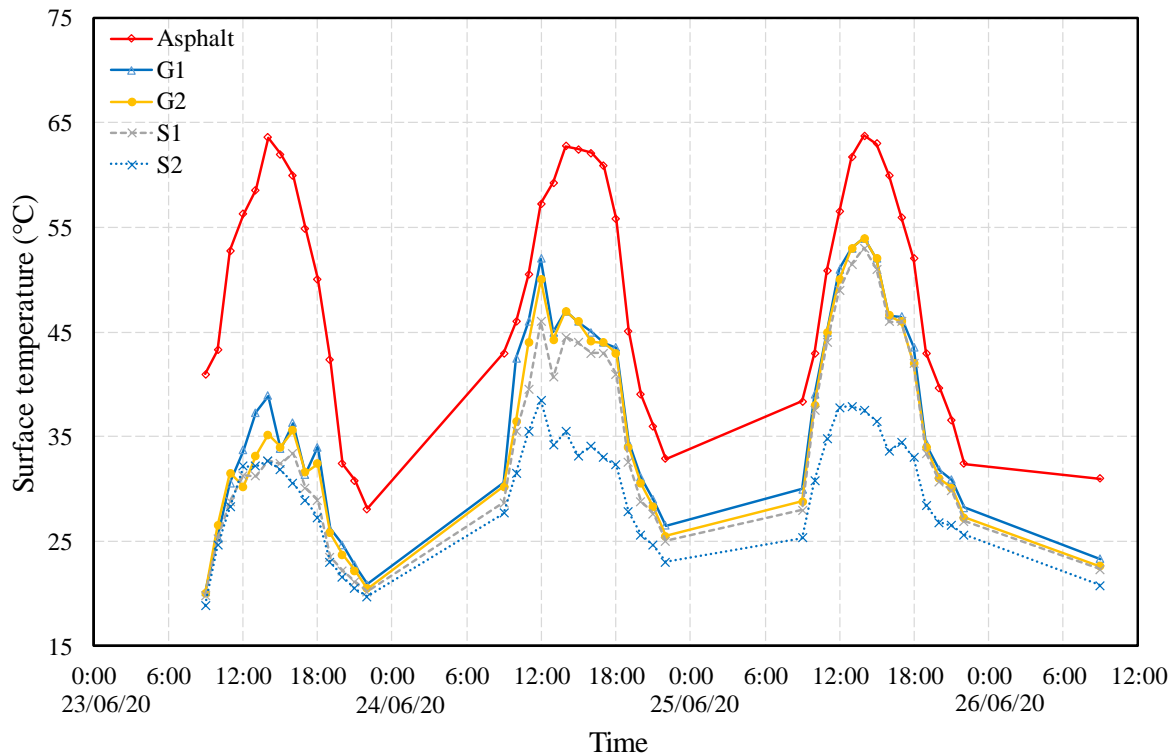


Fig. 13. Variation in surface temperature of natural aggregate-based samples (G1, G2, S1, and S2) and impermeable asphalt as a function of time.

Fig. 13 shows the variation in surface temperature of the impervious asphalt and natural aggregate-based samples (G1, G2, S1 and S2) over the course of this experiment. The choice of materials with different aggregate sizes enabled the researchers to study their effect on the surface temperature and evaporation rate under wet conditions.

On the first day at 14:00, the surface temperature of the aggregates was: 38.9°C for G1, 35.2°C for G2 and 32.7°C for S1. After 24 hours, this surface temperature increased to 47°C for G1 and G2 and to 44.5°C for S1. Moreover, on the second day, these samples reached a maximum surface temperature at 12:00. Thereafter, their surface temperature decreased in the afternoon during the hottest hours of the day. This decrease shows the continuity of the cooling effect by evaporation. During the third day, this decrease is no longer observed during this period, and the maximum surface temperatures were almost identical for these three samples, indicating that the cooling effect had practically vanished in these samples.

As to the fine sand sample (S2), its surface temperature increased slightly during the three days. The recorded surface temperatures were: 32.7°C, 35.5°C and 37.5°C for the first, second and third days at 14:00 respectively. The high evaporation rate and low surface temperature of S2 during the three days of the experiment show that this sample is able to retain water on its surface throughout that period, and consequently, its surface temperature decreased by evaporative cooling.

3.4.2. Evolution of evaporation rate and latent heat flux

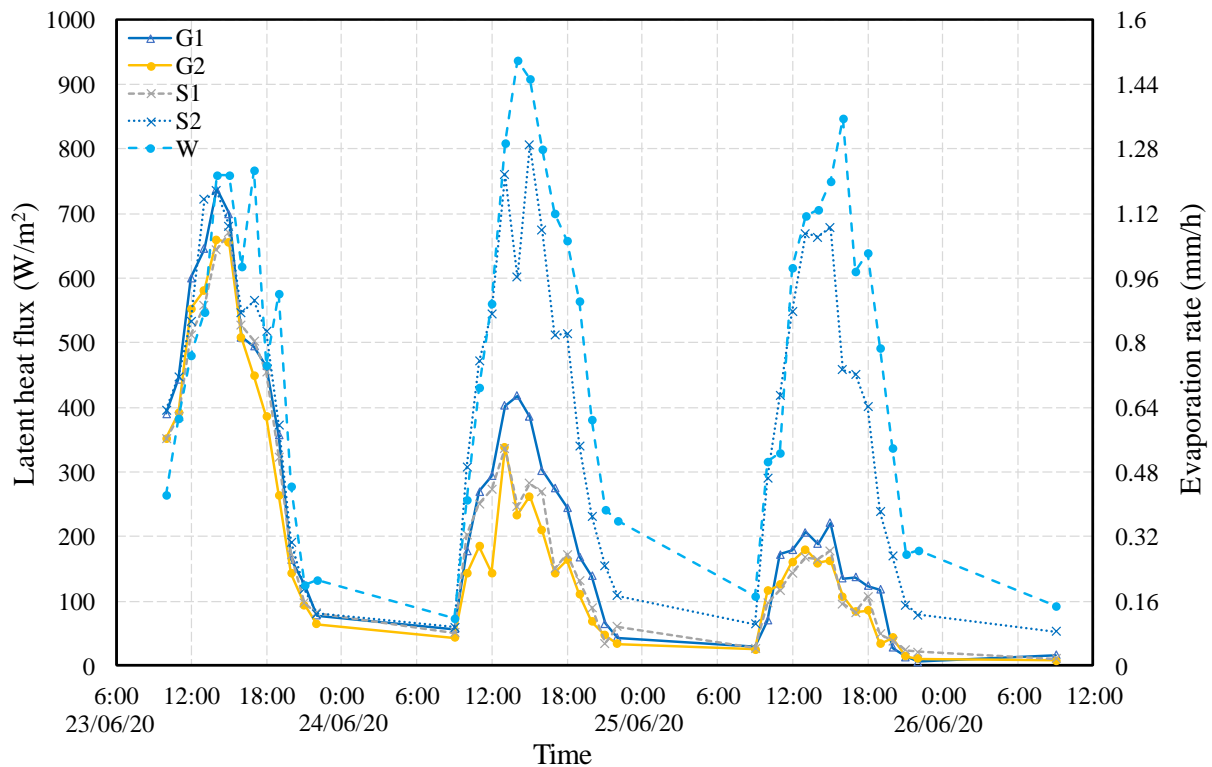


Fig. 14. Variation in evaporation rate and latent heat flux in natural aggregate samples (G1 G2, S1 and S2) as a function of time.

Fig. 14 shows the variation in evaporation rate and latent heat flux in the natural aggregate samples (G1, G2, S1, and S2) over time.

On the first day of the experiment, the evaporation rates in the natural aggregate samples recorded at 14:00 were: 1.18 mm/h for G1, 1.05 mm/h for G2 and 1.03 mm/h for S1. These rates decreased by 43%, 64.7% and 61.6% on the second day and 74.4%, 76% and 74.4% on the third day (compared to the first day) for samples G1, G2 and S1 respectively.

The evaporation rate in sample G1 ($P_0 = 45\%$) was found to be higher than that in sample G2 ($P_0 = 40\%$) and S1 ($P_0 = 38\%$) during the three days. This variation shows that when the porosity is greater and pore sizes are larger, the water present between the aggregates of these three samples will be more exposed to atmospheric heat, which increases the evaporation rate. On the other hand, the surface temperature of sample G1 (Fig. 13) was slightly higher than those of G2 and S1, indicating that there are other factors that influence the surface temperature. Furthermore, this result shows that if one sample has a higher evaporation rate than other samples of the same type with different grain size, this does not necessarily lead to the lowest surface temperature. Indeed, for these three samples, when the porosity increases, the pore sizes and surface roughness increase and thus the albedo decreases (Table 2). Thus, less of the incident solar radiation is reflected from the surface, which leads to an increase in the surface temperature.

Samples D1, D2 and D3, which are composed of a permeable surface layer and a coarse gravel layer (type G1), exhibited a lower evaporation rate and latent heat flux than those measured in

the pure sample G1. It was found that the evaporation phenomenon is strongly related to the characteristics of the surface layer.

3.4.3. The influence of capillary rise

The evaporation rate in sample S2' was significant during the three days of the experiment with an average value of 1.063 mm/h. On the third day, this evaporation rate decreased 10% compared to the first day of the experiment (Fig. 14) and the temperature increased slightly. This observation indicates that evaporation was still continuing in this sample.

An additional sample S2', identical in composition to sample S2, but in a dry state, was set up on the third day, given the high evaporation rate and cooling effect maintained on the second day in sample S2.

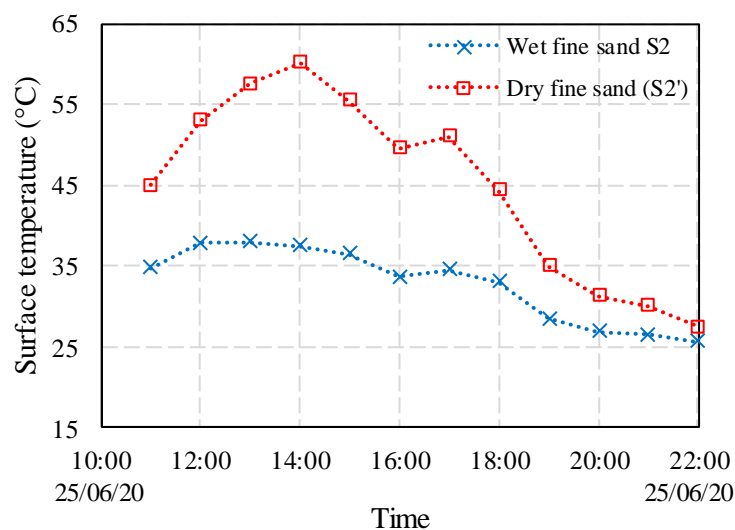


Fig. 15. Variation of the surface temperature of samples S2 and S2'.

Fig. 15 shows the variation in surface temperature of samples containing the same type of sand: S2 in the wet state and S2' in the dry state.

The surface temperature recorded at 14:00, at the hottest hour of the third day, was: 60.2°C for S2' and 37.5°C for S2. This temperature variation indicates that even after three days of drying, the evaporation still occurring in sample S2 was able to cool its surface and decrease its temperature by 22.7°C in the meteorological conditions of this experiment.

A test was performed to measure the height of capillary rise in sample S2. The sand S2 was inserted into a transparent plexiglass tube with a volume of 100×250×500 mm³. A high resolution pco.2000 camera that allows fast image recording was installed in front of the 100×500 mm² side of the tube, automatically recording one picture every 6 seconds over 20 hours. Two halogen light sources were used to improve the quality of the images. This process allowed for the selection of 20 representative images over a period of 20 hours, which were then clarified using image processing software ImageJ. The processed images show two zones: dry and wet sand, and testify as to the capillary rise over time.

The average capillary rise for each image was determined using 'GetData Graph Digitizer' software – a graph and plot digitizing program. This software creates the same grid across all

images and calculates the capillary rise as the average height of the points on the curve formed at the interface between the wet bottom and dry top of the sand in the tube (Fig. 16).

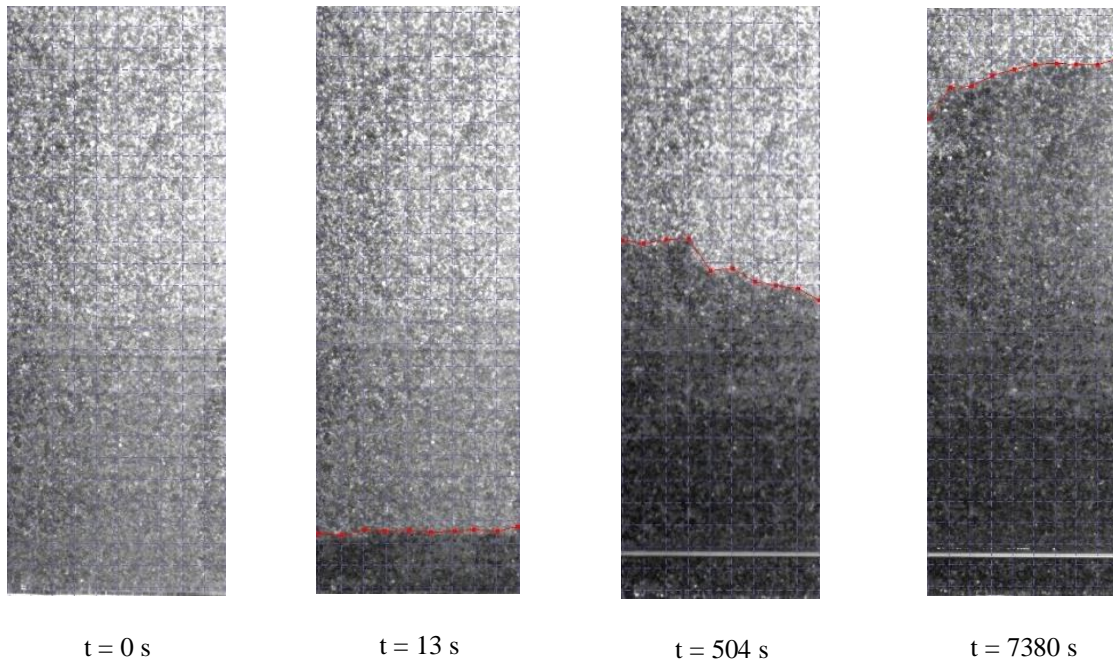


Fig. 16. Evolution of the capillary rise in sample S2 as a function of time.

Fig. 16 shows the evolution of the water level in sample S2 at different times in the experiment. The water level in each photo is not a straight line. There could be several reasons behind this observation, such as the non-homogeneity of the sample, the distribution of the sand grain sizes in the tube and the variation of the degree of compaction of the sand in the tube.

Fig. 17 shows the variation of the average height of capillary rise H (mm) as a function of time t (hours). It shows a rapid increase in the average water level in the sample during the first hour (156 mm), which accounts for 70% of the final capillary rise measured after 20 hours (222 mm). A logarithmic relation presents the best coefficient of correlation ($R^2 = 0.99$) between the average water level and time.

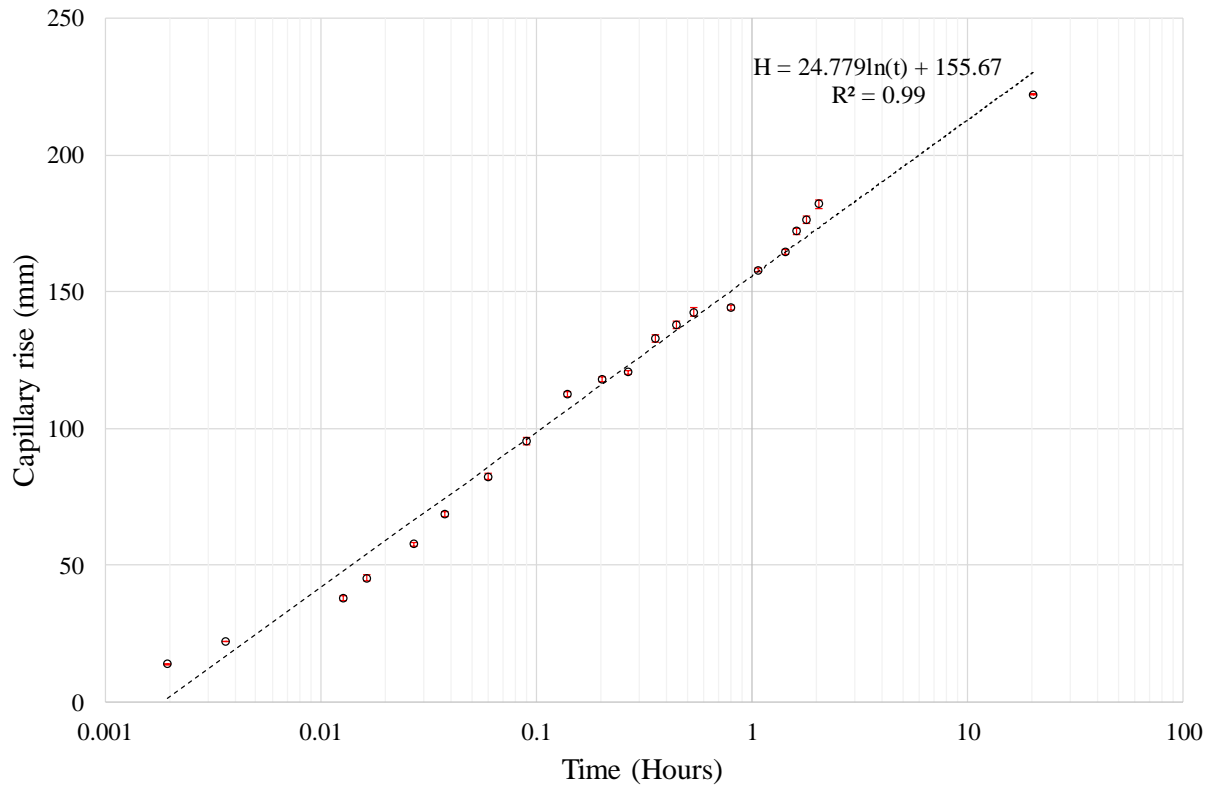


Fig. 17. Variation in capillary rise in sample S2 as a function of time.

3.5. Study of the cooling effect of pozzolan porous pavements

3.5.1. Evolution of surface temperature

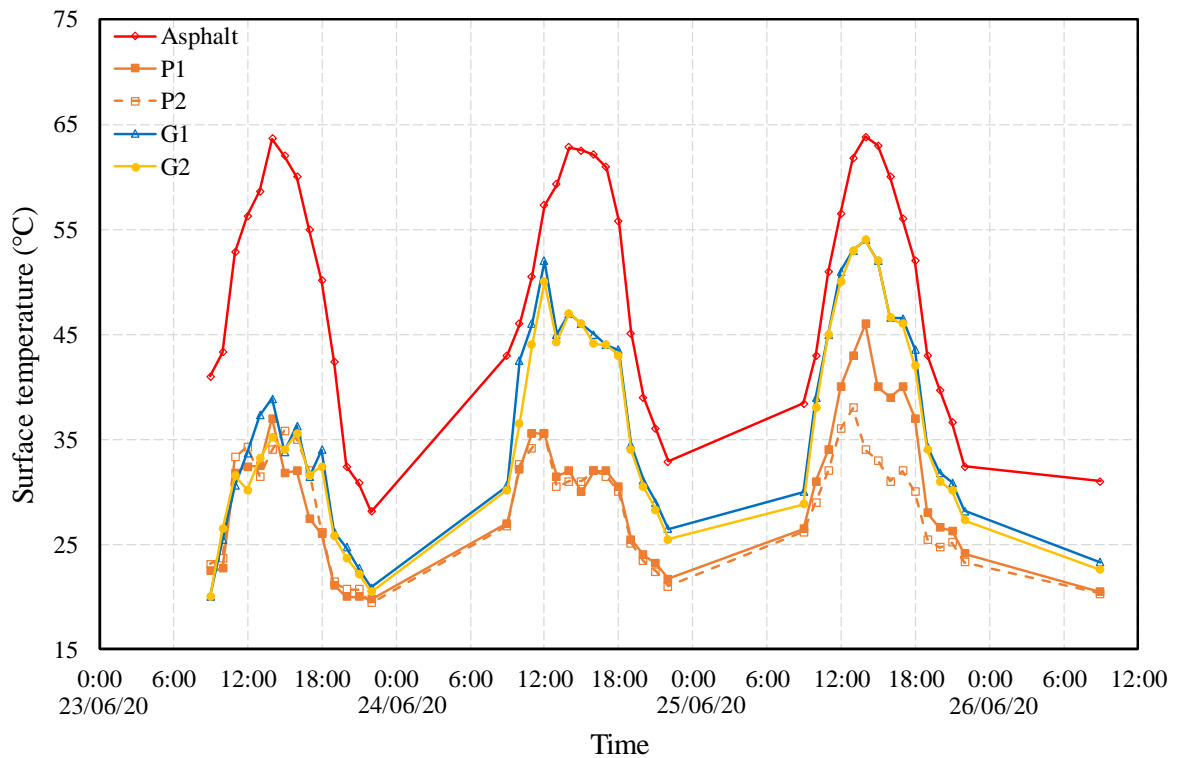


Fig. 18. Variation in surface temperature of natural aggregate-based samples (P1, P2, G1 and G2) as a function of time.

Several studies in the literature show that materials with higher water-absorption rates have a greater evaporative cooling effect [46], [47]. Fig. 18 shows the variation in surface temperature of coarse and medium natural pozzolan and gravel aggregates (P1, P2, G1 and G2) as a function of time, to investigate the influence of aggregate type on the cooling effect.

The surface temperature of P2 recorded at 14:00 was 34°C, 31°C and 34°C, for the first, second and third day of the experiment respectively. The surface temperature of P1 was 35°C on the first day and 32°C on the second day, and increased to 46°C on the third day. The difference between the surface temperature of the samples containing pozzolan (P1, P2) and gravel (G1, G2) recorded at 14:00 was slight on the first day. This difference increased significantly on the second day to an average of 16°C. On the third day, the difference was 8°C for P1 compared to G1 and 20°C for P2 compared to G2.

3.5.2. Evolution of evaporation rate and latent heat flux

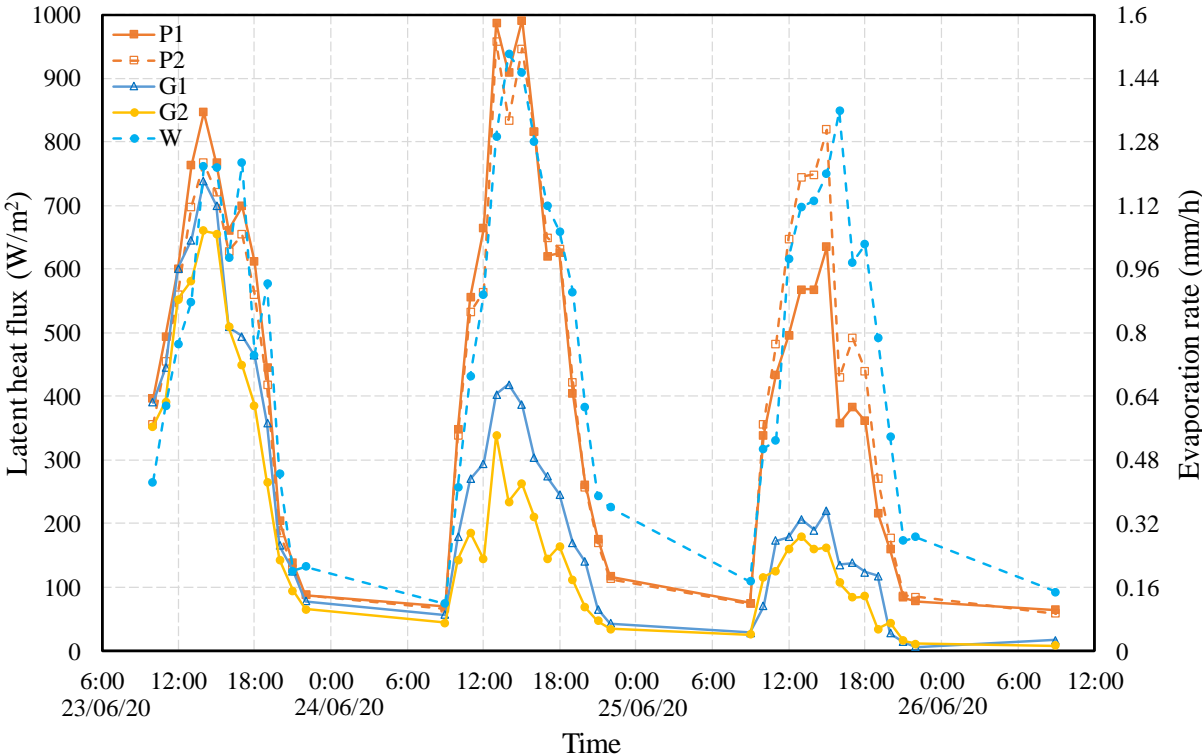


Fig. 19. Variation in evaporation rate and latent heat flux in natural aggregate samples (P1, P2, G1 and G2) as a function of time.

Fig. 19 shows the variation in evaporation rate and latent heat flux in the natural aggregate samples (P1, P2, G1 and G2). On the first day of the experiment, all five samples had a high evaporation rate at 14:00, ranging between 1.03 and 1.35 mm/h, decreasing the surface temperature of these five samples.

On the second day, the surface temperatures of G1 and G2 increased significantly compared to the surface temperatures of P1 and P2 (Fig. 18). The main reason is the decreased evaporation rate in samples G1 and G2. However, the evaporation rate in samples P1 and P2 was still significant and similar to that of water, thus keeping the surface temperature low at 32°C for P1 and 31°C for P2, measured at 14:00.

On the third day at 14:00, the surface temperature of P1 was 46°C (higher than that of P2, which was 34°C – see Fig. 18). The reason for this increase is that the P1 sample lost 37% of its evaporative cooling power compared to the second day. During the same period, sample P2 maintained the same evaporative performance, and its cooling performance was still similar to that of water (Fig. 19).

It was found that the cooling time varies in these materials: one to two days for G1 and G2, and over three days for P1 and P2 under the weather conditions encountered in this experiment. Moreover, the high porosity of the P1 (60%) and P2 (57%) samples, their high absorption coefficient and albedo, and the porous structure of pozzolan aggregates are the essential factors that increased the duration of the cooling effect compared to the G1 and G2 samples.

3.6. Effect of open porosity and permeability on evaporation rate

To investigate the effect of open porosity on the evaporation rate, the medians of the evaporation rate over the three days of the experiment (6/23/2020 to 6/26/2020) are calculated.

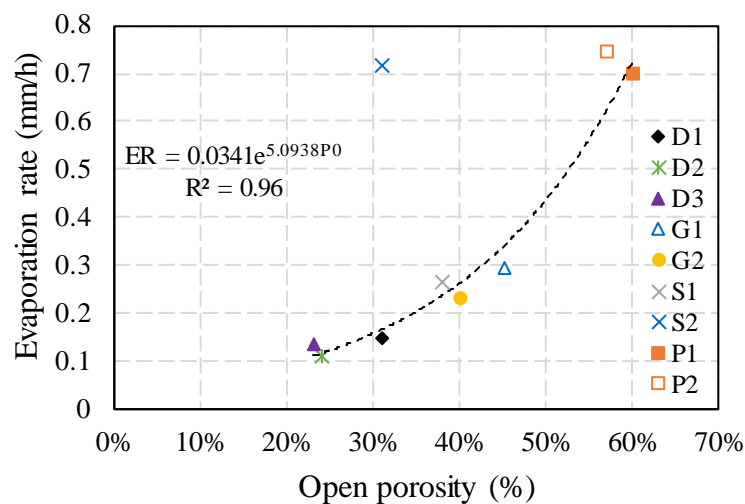


Fig. 20. Relationship between the open porosity and the average evaporation rate of the three days of the experiment.

Without considering the evaporation rate of sample S2, an exponential relationship between the open porosity and the evaporation rate of the tested samples presents a best fit for the resulting curve ($R^2 = 0.96$). The equation of the resulting curve (**Eq. (13)**) is only valid in the context of this study (type of tested samples, meteorological data). As the open porosity of a permeable pavement increases, the median evaporation rate increases (Fig. 20). These results are in agreement with the experimental results found by Li et al. [19].

$$ER = 0.0341e^{5.0938P_0} \quad (13)$$

Sample D1 has a median evaporation rate of 0.167 mm/h for an open porosity of 31%. However, for the same porosity value, sample S2 has an evaporation rate of 0.655 mm/h, which is 6 times the median evaporation rate of sample D1 over the three days. Indeed, fine sand (S2) has a high evaporation rate due to its ability to move moisture to the surface by capillary action, which improves the availability of water near the surface and thus enhances evaporation. In addition, fine sand has a small pore size, a large surface/volume ratio and therefore a significant capillary effect compared to materials with large pores.

This phenomenon is also observed for sample S1. Its median evaporation rate is slightly higher than that of sample G2. This could be related to the weak effect of capillary rise in this sample, as S1 has smaller pores than G2. It should be noted that when the aggregates are finer, the capillary rise phenomenon becomes increasingly significant.

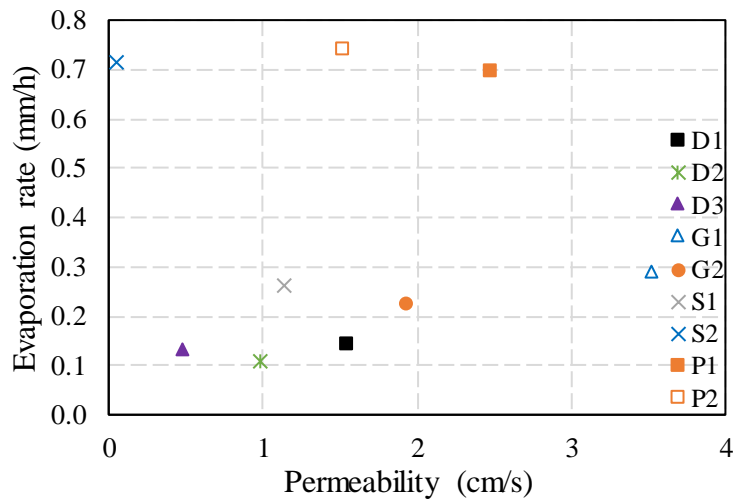


Fig. 21. Relationship between permeability and average evaporation rate for the three days of the experiment.

Fig. 21 shows that permeability is not always positively correlated with evaporation rate. Indeed, the permeability depends heavily on aggregate sizes, granular arrangement and the open porosity of the samples. However, the evaporation rate is strongly dependent on the availability of water near the surface and the absorption coefficient of the samples. For example, sample P1 has a lower permeability than sample G1, but it has a higher absorption coefficient due to its high capacity to absorb water into the pozzolan aggregates. For this reason, P1 offers more water exposed to the external environment. As to the permeable coatings (D1, D2 and D3) which contain 70% pozzolan (mass percentage), the resin which coats the aggregates decreases the intergranular and intragranular porosity.

There are several factors that affect the evaporation rate in the porous materials studied. Some are uncontrollable factors, such as high ambient temperature, high wind speed and low air humidity. In addition, as can be seen from the results of this experiment, there are controllable factors such as porosity, permeability, water absorption coefficient and capillary rise. Each factor influences the evaporation rate of permeable pavements in different ways. A sensitivity study on a larger number of samples would be useful, studying the sensitivity of the evaporation rate to the variation of each factor, with a view to optimizing permeable pavement design

3.7. Effect of water depth in samples on evaporation rate

As the water evaporates, the amount of water in the samples decreases. To investigate the effect of this decrease on the evaporation, the relationships between evaporation rate and water depth in the samples are plotted in Fig. 22. The calculated depths were estimated from the water mass remaining in each sample over time. The water levels (h) shown in Fig. 22 are values calculated from the surface of each sample.

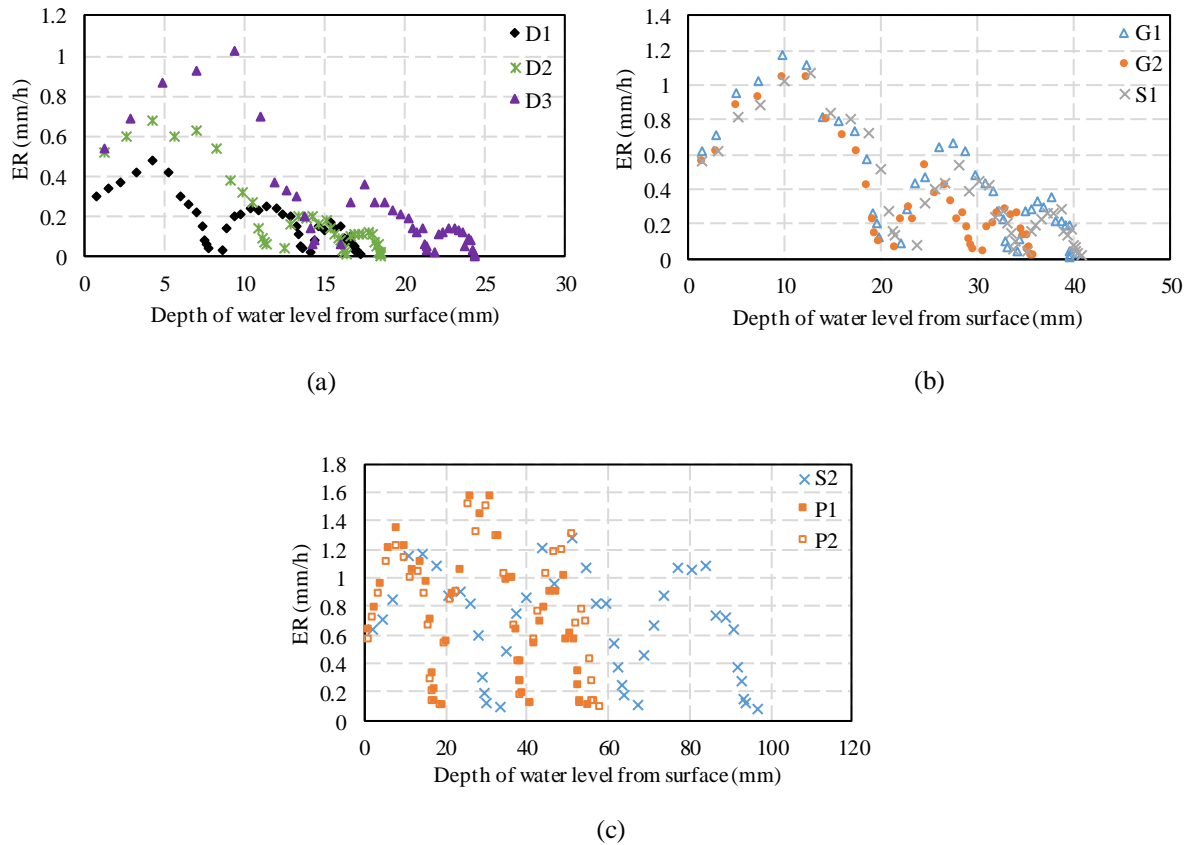


Fig. 22. Variation in evaporation rate as a function of water level in the samples: (a) for D1, D2 and D3, (b) for G1, G2 and S1, (c) for S2, P1 and P2.

Fig. 22 shows that for all samples, the evaporation rate during the daytime decreases from one day to the next as the water depth increases.

Regarding the permeable pavements D1, D2 and D3 (Fig. 22a), the different dosages presented in Table 1 meant the experiment included three permeable pavements possessing different pore sizes. The smallest pore sizes are present in coating D3, then in coating D2, and D1 has the largest pore sizes. At the end of the experiment on day three, D3 had the lowest depth ($h = 24.33$ mm), followed by D2 ($h = 18.47$ mm) and D1 ($h = 17.27$ mm). These values indicate that for these permeable materials, as the pore sizes decrease, the sample is able to evaporate water at deeper levels.

Regarding the natural gravel and sand samples (Fig. 22b and 22c), sample S2 ($h = 96.58$ mm) had a greater water depth than G1 ($h = 40.26$ mm), G2 ($h = 35.89$ mm) and S1 ($h = 40.79$ mm). The reason is, again, capillary rise, which displaces water from the interior of the materials to the surface of the samples. On the other hand, the height of 96.58 mm calculated for sample S2 does not represent a stable water level, because capillary rise separates the sample into two zones: saturated and semi-saturated.

The capillary rise test carried out for the fine sand showed that after 20 hours, this material was able to raise the water up to 22.2 cm = height of the mold S2 (Fig. 17). Moreover, after the three days of experimentation, the mass of water remaining in sample S2 was 338.44 g – this mass corresponds to a water level of 96.58 mm, which indicates that sample S2 is able to cool its surface for more than 3 days.

The water depth of pozzolan samples P1 ($h = 55.01$ mm) and P2 ($h = 58.14$ mm) is higher than those of G1 and G2, due to the porous structure of the pozzolan aggregate, which allows this type of aggregate to behave like a sponge to draw water from the lower levels of the sample and store it within its structure, thanks to its high absorption capacity.

Several researchers in the literature have indicated the importance of the presence of water near the surface of permeable pavements to enhance evaporation [18], [19], [47], [48]. It was found that permeable pavements D1, D2 and D3 are able to effectively decrease their surface temperature if the depth of water in these pavements is within the following ranges: (0 mm-13.6 mm) for D1, (0 mm-16.3 mm) for D2 and (0 mm-21.4 mm) for D3. The maximum value of each interval corresponds to the water level calculated at the end of the second day of the experiment. These results are in agreement with those found by Nemirovsky et al. [49] that when the water is pooled at or close to the surface of pervious concrete (0 or 25 mm), the evaporative cooling effect is dramatic and is expected to decrease with the pavement temperature. If the pooling water levels deeper (76 mm, 152 mm), the evaporative fluxes are compromised and contribute much less to the cooling effect. This means that the influence of the water level on the evaporation rate for different types of permeable pavements is similar."

It was deduced from these results that there are several techniques to improve the evaporative cooling effect of permeable pavements in wet conditions. These include the use of coarser aggregates which increase the open porosity and permeability and thus improve the moisture exposure to the atmosphere and increase the evaporation rate. The results show that the capillary effect provides greater cooling over a longer period. From a practical point of view, to improve the capillary effect, it is necessary to use very fine aggregates, but the usefulness of this technique is limited by the hydraulic properties of permeable pavements. Further experimental and theoretical research is required to determine the optimal size of aggregates to be used to improve the capillary rise while ensuring adequate permeability.

In addition, the use of aggregates having a high water-absorption coefficient such as lightweight aggregates improves the water-retention capacity of the pavement and thus improves the evaporation rate. This technique may also be limited by mechanical properties, as lightweight aggregates generally have low density and strength which may reduce the mechanical strength of permeable pavements. This is especially undesirable for permeable pavements intended to support traffic on low-traffic roads, which require a compressive strength greater than 17 MPa [32]

When the permeable pavement surface is regularly watered, it is largely possible to guarantee a lower surface temperature than with impermeable asphalt pavement at all times. The effect of the watering time (day or night) to guarantee a longer cooling time has not been investigated and can certainly be optimized.

4. Conclusion and prospects

This experiment investigated the evaporative cooling effect of several types of permeable pavements and the factors that influence this cooling effect in outdoor weather conditions. The thermal behavior of these pavements was compared to that of traditional asphalt pavement. Since the factors studied are controllable, this study will be useful in optimizing the design of permeable pavement mixtures to maximize the evaporative cooling effect. For this experimental study, several conclusions can be cited:

- (a) Increasing the evaporation rate in permeable coating materials brings about an increase in the evaporative cooling effect.
- (b) The evaporation rate increases exponentially (up to 0.5652 mm/h) with increasing open porosity (from 23 to 60%) in permeable pavements, except for sand-based porous pavements.
- (c) Evaporation in permeable coatings is controlled by the presence of water near the surface. This condition highlighted the importance of capillary rise to ensure the presence of water at the surface over a longer period of time, which increased the duration of the cooling effect (as was the case with sample S2).
- (d) The increase in water-absorption coefficient (case of sample P1 (WA = 15.08%) compared to G1 (WA = 2.37%)) ensures a greater cooling effect over a longer period (up to 3 days).
- (e) Under the weather conditions of this experiment, the evaporative cooling effect in the permeable pavements based on local pozzolan and recycled tire aggregate (D1, D2, and D3) can last up to two days compared to the traditional asphalt pavement. This temperature decrease varies from 15.6°C to 28.1°C on the first day, and from 0.5°C to 8.8°C on the second day during the hottest hours of the day.
- (f) The surface temperature of all permeable pavements during the night is lower than that of traditional asphalt pavement, even after the cooling effect by evaporation has ended, due to their porous natures and low thermal conductivities.
- (g) According to the results obtained, although porosity has a significant influence on the rate of evaporation, it is insufficient on its own to predict the rate of evaporation, which depends on other factors, such as the level of water in the pavement, the coefficient of water absorption, the permeability and the presence or absence of capillary rise.

More representative and precise results could be obtained, if the tests were carried out on samples of larger dimensions, which would reduce the contribution of the edge effects.

This study has potential limitations. The experiment was performed under low wind conditions. A future study on the influence of the same factors under higher wind conditions is important, to investigate the combined effect of controllable and non-controllable factors on the thermal behavior of permeable pavements. Moreover, further experimental and theoretical research is needed to find the optimal porosity, taking account of the effect of pore size, shape, distribution and tortuosity, defined as the ratio of actual flow path length to the straight distance between the ends of the flow path, with the objective of achieving good hydraulic, mechanical, and thermal performance. This work is beyond the scope of this paper and will be the next step in the study.

Acknowledgements

The authors would like to thank the Auvergne Region Council (France) and the European FEDER funding program for their financial support of this work through CPER ECOMAT program.

Appendix A. Albedo measurement method

Fig. A1 shows the experimental setup used to measure the albedo of samples outdoors.

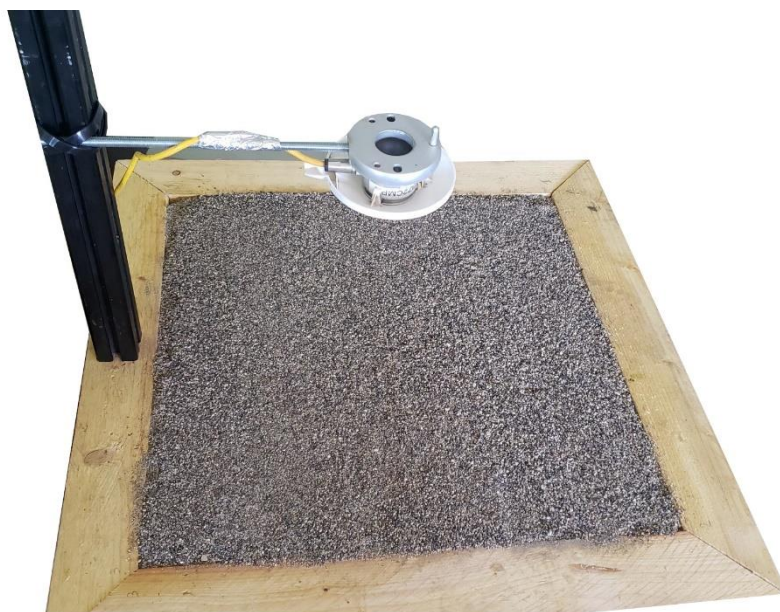


Fig. A1. Experimental setup for outdoor albedo measurement.

Fig. A2 shows the experimental bench used to measure the albedo of samples in the laboratory under controlled climatic conditions.

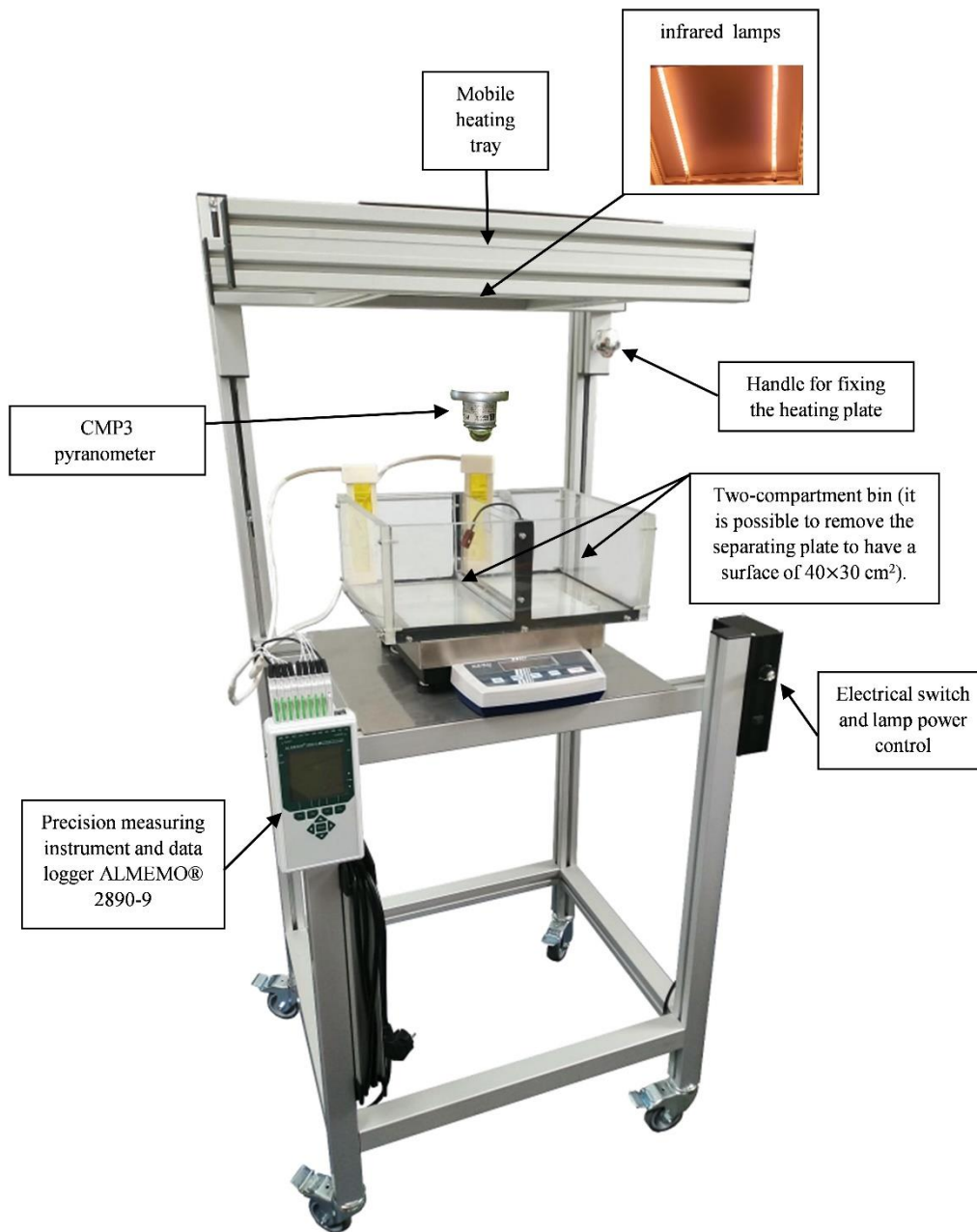


Fig. A2. Experimental bench used to measure the albedo in the laboratory.

Bibliography

- [1] M. Taleghani, “Outdoor thermal comfort by different heat mitigation strategies - A review”, *Renew. Sustain. Energy Rev.*, vol. 81, no. October 2016, pp. 2011–2018, 2018, doi: 10.1016/j.rser.2017.06.010.
- [2] M. Carpio, Á. González, M. González, and K. Verichev, “Influence of pavements on the urban heat island phenomenon: A scientific evolution analysis”, *Energy Build.*, vol. 226, p. 110379, 2020, doi: 10.1016/j.enbuild.2020.110379.
- [3] T. Plocoste, “Étude de la dispersion nocturne de polluants atmosphériques issus d’une décharge d’ordures ménagères : Mise en évidence d’un îlot de chaleur urbain”, no. April 2013, Doctoral dissertation, Antilles-Guyane, doi: 10.13140/2.1.4639.7765.
- [4] B. R. Anupam, U. C. Sahoo, A. K. Chandrappa, and P. Rath, “Emerging technologies in cool pavements: A review”, *Constr. Build. Mater.*, vol. 299, p. 123892, 2021, doi: 10.1016/j.conbuildmat.2021.123892.
- [5] H. Akbari, M. Pomerantz, and H. Taha, “Cool surfaces and shade trees to reduce energy use and improve air quality in urban areas”, *Sol. Energy*, vol. 70, no. 3, pp. 295–310, 2001, doi: 10.1016/S0038-092X(00)00089-X.

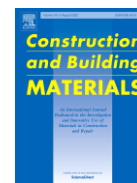
- [6] M. Giguère, “Mesures de lutte aux îlots de chaleur urbains: revue de littérature”, Institut national de santé publique du Québec, 2009.
- [7] A. Mohajerani, J. Bakaric, and T. Jeffrey-Bailey, “The urban heat island effect, its causes, and mitigation, with reference to the thermal properties of asphalt concrete”, *J. Environ. Manage.*, vol. 197, pp. 522–538, 2017, doi: 10.1016/j.jenvman.2017.03.095.
- [8] M. Santamouris, “Using cool pavements as a mitigation strategy to fight urban heat island—A review of the actual developments”, *Renew. Sustain. Energy Rev.*, vol. 26, pp. 224–240, 2013, doi: 10.1016/j.rser.2013.05.047.
- [9] Y. Qin and J. E. Hiller, “Understanding pavement-surface energy balance and its implications on cool pavement development”, *Energy Build.*, vol. 85, pp. 389–399, 2014, doi: 10.1016/j.enbuild.2014.09.076.
- [10] H. Akbari and L. S. Rose, “Characterizing the fabric of the urban environment: A case study of Metropolitan Chicago, Illinois and Executive Summary”, *Lawrence Berkeley National Laboratory Report LBNL-49275*, Berkeley, CA, 2001.
- [11] R. U. H. Islands, “Compendium of Strategies-Cool Pavements”, *US Environ. Prot. Agency*, 2008.
- [12] Y. Qin, “Urban canyon albedo and its implication on the use of reflective cool pavements”, *Energy Build.*, vol. 96, pp. 86–94, 2015.
- [13] J. Chen, Z. Zhou, J. Wu, S. Hou, and M. Liu, “Field and laboratory measurement of albedo and heat transfer for pavement materials”, *Constr. Build. Mater.*, vol. 202, pp. 46–57, 2019, doi: 10.1016/j.conbuildmat.2019.01.028.
- [14] A. Synnefa, T. Karlessi, N. Gaitani, M. Santamouris, D. N. Assimakopoulos, and C. Papakatsikas, “Experimental testing of cool colored thin layer asphalt and estimation of its potential to improve the urban microclimate”, *Build. Environ.*, vol. 46, no. 1, pp. 38–44, 2011, doi: 10.1016/j.buildenv.2010.06.014.
- [15] L. A. Balan, B. R. Anupam, and S. Sharma, “Thermal and mechanical performance of cool concrete pavements containing waste glass”, *Constr. Build. Mater.*, vol. 290, p. 123238, 2021, doi: 10.1016/j.conbuildmat.2021.123238.
- [16] S. Alghamdy, J. E. Alleman, and T. Alowaibdi, “Cool white marble pavement thermophysical assessment at Al Masjid Al-Haram, Makkah City, Saudi Arabia”, *Constr. Build. Mater.*, vol. 285, p. 122831, 2021, doi: 10.1016/j.conbuildmat.2021.122831.
- [17] Q. Li, T. Hu, S. Luo, L. Gao, C. Wang, and Y. Guan, “Evaluation of cooling effect and pavement performance for thermochromic material modified asphalt mixtures under solar radiation”, *Constr. Build. Mater.*, vol. 261, p. 120589, 2020, doi: 10.1016/j.conbuildmat.2020.120589.
- [18] N. Tziampou, S. J. Coupe, L. A. Sañudo-fontaneda, A. P. Newman, and D. Castro-fresno, “Fluid transport within permeable pavement systems : A review of evaporation processes , moisture loss measurement and the current state of knowledge”, *Constr. Build. Mater.*, vol. 243, p. 118179, 2020, doi: 10.1016/j.conbuildmat.2020.118179.
- [19] H. Li, J. Harvey, and Z. Ge, “Experimental investigation on evaporation rate for enhancing evaporative cooling effect of permeable pavement materials”, *Constr. Build. Mater.*, vol. 65, pp. 367–375, 2014, doi : 10.1016/j.conbuildmat.2014.05.004.
- [20] T. Saadon, B. Gómez-Mejide, and A. Garcia, “Prediction of water evaporation and stability of cold asphalt mixtures containing different types of cement”, *Constr. Build. Mater.*, vol. 186, pp. 751–761, 2018, doi: 10.1016/j.conbuildmat.2018.07.218.
- [21] N. P. Sharifi and K. C. Mahboub, “Application of a PCM-rich concrete overlay to control thermal induced curling stresses in concrete pavements”, *Constr. Build. Mater.*, vol. 183, pp. 502–512, 2018.
- [22] D. Yinfei, L. Pusheng, W. Jiacheng, D. Hancheng, W. Hao, and L. Yingtao, “Effect of lightweight aggregate gradation on latent heat storage capacity of asphalt mixture for cooling asphalt pavement”, *Constr. Build. Mater.*, vol. 250, p. 118849, 2020, doi: 10.1016/j.conbuildmat.2020.118849.
- [23] B. R. Anupam, U. C. Sahoo, and P. Rath, “Phase change materials for pavement applications: A review”, *Constr. Build. Mater.*, vol. 247, p. 118553, 2020, doi: 10.1016/j.conbuildmat.2020.118553.
- [24] A. Marani and M. L. Nehdi, “Integrating phase change materials in construction materials: Critical review”, *Constr. Build. Mater.*, vol. 217, pp. 36–49, 2019, doi : 10.1016/j.conbuildmat.2019.05.064.
- [25] D. Zhang, M. Chen, S. Wu, M. Riar, J. Wan, and Y. Li, “Thermal and rheological performance of asphalt binders modified with expanded graphite/polyethylene glycol composite phase change material (EP-CPCM)”, *Constr. Build. Mater.*, vol. 194, pp. 83–91, 2019, doi: 10.1016/j.conbuildmat.2018.11.011.
- [26] J. Chen, R. Chu, H. Wang, L. Zhang, X. Chen, and Y. Du, “Alleviating urban heat island effect using high-conductivity permeable concrete pavement”, *J. Clean. Prod.*, vol. 237, p. 117722, 2019, doi: 10.1016/j.jclepro.2019.117722.
- [27] S. Asfour, F. Bernardin, and E. Toussaint, “Experimental validation of 2D hydrothermal modelling of porous pavement for heating and solar energy retrieving applications”, *Road Mater. Pavement Des.*, vol. 21, no. 3, pp. 666–682, 2020.
- [28] Y. Qin, “A review on the development of cool pavements to mitigate urban heat island effect”, *Renew.*

- Sustain. Energy Rev.*, vol. 52, pp. 445–459, 2015, doi: 10.1016/j.rser.2015.07.177.
- [29] T. Asaeda, V. T. Ca, and A. Wake, “Heat storage of pavement and its effect on the lower atmosphere”, *Atmos. Environ.*, vol. 30, no. 3, pp. 413–427, 1996, doi: 10.1016/1352-2310(94)00140-5.
- [30] J. Wei and J. He, “Numerical simulation for analyzing the thermal improving effect of evaporative cooling urban surfaces on the urban built environment”, *Appl. Therm. Eng.*, vol. 51, no. 1–2, pp. 144–154, 2013, doi: 10.1016/j.applthermaleng.2012.08.064.
- [31] H. Takebayashi and M. Moriyama, “Study on surface heat budget of various pavements for urban heat island mitigation”, *Adv. Mater. Sci. Eng.*, vol. 2012, 2012, doi: 10.1155/2012/523051.
- [32] K. Seifeddine, S. Amziane, and E. Toussaint, “State of the art on the mechanical properties of pervious concrete”, *Eur. J. Environ. Civ. Eng.*, pp. 1–29, 2021, doi: 10.1080/19648189.2021.2008511.
- [33] D. H. Nguyen, “Étude du comportement hydromécanique des bétons drainants à base de coproduits coquilliers”, Doctoral dissertation, Caen, 2014.
- [34] J. Wang, Q. Meng, K. Tan, L. Zhang, and Y. Zhang, “Experimental investigation on the influence of evaporative cooling of permeable pavements on outdoor thermal environment”, *Build. Environ.*, vol. 140, pp. 184–193, 2018, doi: 10.1016/j.buildenv.2018.05.033.
- [35] N. Neithalath, M. S. Sumanasooriya, and O. Deo, “Characterizing pore volume, sizes, and connectivity in pervious concretes for permeability prediction”, *Mater. Charact.*, vol. 61, no. 8, pp. 802–813, 2010, doi: 10.1016/j.matchar.2010.05.004.
- [36] N. Neithalath, J. Weiss, and J. Olek, “Characterizing enhanced porosity concrete using electrical impedance to predict acoustic and hydraulic performance”, *Cem. Concr. Res.*, vol. 36, no. 11, pp. 2074–2085, 2006, doi: 10.1016/j.cemconres.2006.09.001.
- [37] A. Yahia and K. D. Kabagire, “New approach to proportion pervious concrete”, *Constr. Build. Mater.*, vol. 62, pp. 38–46, 2014, doi: 10.1016/j.conbuildmat.2014.03.025.
- [38] L. A. Mata and M. L. Leming, “Vertical distribution of sediments in pervious concrete pavement systems”, *ACI Mater. J.*, vol. 109, no. 2, pp. 149–155, 2012, doi: 10.14359/51683701.
- [39] B. J. Putman and A. I. Neptune, “Comparison of test specimen preparation techniques for pervious concrete pavements”, *Constr. Build. Mater.*, vol. 25, no. 8, pp. 3480–3485, 2011, doi: 10.1016/j.conbuildmat.2011.03.039.
- [40] A. Astm, “06: Standard test method for measuring solar reflectance of horizontal and low-sloped surfaces in the field”, 2006.
- [41] H. Li, M. Kayhanian, and J. T. Harvey, “Comparative field permeability measurement of permeable pavements using ASTM C1701 and NCAT permeameter methods”, *J. Environ. Manage.*, vol. 118, pp. 144–152, 2013, doi: 10.1016/j.jenvman.2013.01.016.
- [42] T. Bao, Z. L. Liu, X. Zhang, and Y. He, “A drainable water-retaining paver block for runoff reduction and evaporation cooling”, *J. Clean. Prod.*, vol. 228, pp. 418–424, 2019, doi: 10.1016/j.jclepro.2019.04.142.
- [43] Y. Qin and J. E. Hiller, “Ways of formulating wind speed in heat convection significantly influencing pavement temperature prediction”, *Heat Mass Transf.*, vol. 49, no. 5, pp. 745–752, 2013, doi: 10.1007/s00231-013-1116-0.
- [44] Y. Qin and J. E. Hiller, “Water availability near the surface dominates the evaporation of pervious concrete”, *Constr. Build. Mater.*, vol. 111, pp. 77–84, 2016, doi: 10.1016/j.conbuildmat.2016.02.063.
- [45] H. Li, J. T. Harvey, T. J. Holland, and M. Kayhanian, “The use of reflective and permeable pavements as a potential practice for heat island mitigation and stormwater management”, *Environ. Res. Lett.*, vol. 8, no. 4, 2013, doi: 10.1088/1748-9326/8/4/049501.
- [46] J. Wang *et al.*, “Impacts of the water absorption capability on the evaporative cooling effect of pervious paving materials”, *Build. Environ.*, vol. 151, no. January, pp. 187–197, 2019, doi: 10.1016/j.buildenv.2019.01.033.
- [47] J. Wang, Q. Meng, K. Tan, L. Zhang, and Y. Zhang, “Experimental investigation on the influence of evaporative cooling of permeable pavements on outdoor thermal environment”, *Build. Environ.*, vol. 140, no. January, pp. 184–193, 2018, doi: 10.1016/j.buildenv.2018.05.033.
- [48] H. Li, “Chapter 7 - Evaporation Rate and Evaporative Cooling Effect of Pavement Materials”, *Pavement Materials for Heat Island Mitigation*, H. Li, Ed. Boston: Butterworth-Heinemann, 2016, pp. 135–153.
- [49] E. M. Nemirovsky, A. L. Welker, and R. Lee, “Quantifying evaporation from pervious concrete systems: Methodology and hydrologic perspective”, *J. Irrig. Drain. Eng.*, vol. 139, no. 4, pp. 271–277, 2013, doi: 10.1061/(ASCE)IR.1943-4774.0000541.

Chapter V Thermal behavior of pervious concrete in dry conditions

Article publié dans le journal : Construction and Building Materials

Seifeddine, K., Amziane, S., & Toussaint, E. (2022). Thermal behavior of pervious concrete in dry conditions. *Construction and Building Materials*. <https://doi.org/10.1016/j.conbuildmat.2022.128300>



Résumé et objectif

Après avoir présenté les propriétés mécaniques (chapitre 1) et les propriétés hydrauliques (chapitre 2) du béton drainant, ce chapitre présente une étude sur le comportement thermique du béton drainant en condition sèche. Le travail de synthèse présenté dans le chapitre 3 met en évidence que la température de surface du béton drainant est supérieure à celle du béton conventionnel imperméable durant les périodes des canicules. Cependant, il n'existe pas de travaux de recherche qui ont étudié en détail les facteurs qui influent sur la température de surface du béton drainant en condition sèche. L'étude du comportement thermique du béton drainant sec est essentielle vu qu'il existe des pays qui ont des étés secs et où les techniques d'arrosage sont compliquées à mettre en œuvre. Pour ces raisons, l'objectif principal de cet article est d'étudier l'influence des paramètres thermophysiques sur la température de surface du béton drainant, en vue de concevoir un mélange qui minimise sa température de surface en conditions sèches. Le comportement thermique du béton drainant et du béton imperméable ordinaire a été étudié à la fois analytiquement et expérimentalement. L'étude expérimentale a été effectuée grâce à un banc expérimental innovant qui a été conçu pour étudier le comportement thermique des revêtements perméables en conditions sèches et humides dans des conditions climatiques contrôlées en laboratoire. Tous les flux de chaleur impliqués dans le bilan énergétique à la surface des deux chaussées ont été analysés.

Les résultats montrent que le béton drainant est jusqu'à 6°C plus chaud que le béton ordinaire pendant la période diurne, et jusqu'à 4°C plus froid la nuit. En outre, l'augmentation de la conductivité thermique du béton drainant n'est bénéfique que pendant la période diurne, puisque l'augmentation de la conductivité thermique a rendu sa température de surface maximale légèrement inférieure pendant le jour, mais plus chaude pendant la nuit. D'autre part, l'augmentation de l'albédo du béton drainant réduit l'effet des îlots de chaleur urbains pendant les périodes diurnes et nocturnes : l'augmentation de l'albédo permet de réduire sa température de surface pendant le jour et pendant la nuit. L'étude de sensibilité a montré que la température de surface du béton drainant est plus sensible à l'albédo qu'à la conductivité thermique. Par conséquent, l'albédo est à privilégier dans la conception de chaussées en béton drainant rafraichissant.

Cette étude a cependant certaines limites. Le modèle n'a pas pris en compte l'effet de la variation de la conductivité thermique et de l'albédo sur la valeur d'émissivité du béton drainant, ce qui peut influencer la précision des résultats obtenus. De plus, une étude expérimentale sur le terrain

avec des échantillons de plus grandes dimensions dans des conditions météorologiques réelles est nécessaire pour s'assurer des résultats obtenus.

D'un point de vue pratique, il est possible d'optimiser la conception du béton drainant afin de réduire sa température de surface maximale en conditions sèches sans avoir recours à d'autres techniques telles que la peinture du revêtement ou l'ajout de produits destinés à augmenter la conductivité thermique (par exemple, des fibres d'acier) ou l'albédo (par exemple, des pigments réfléchissant les infrarouges). Cette optimisation peut être obtenue en utilisant un liant et des granulats de couleur claire (augmentant l'albédo), des granulats plus fins (surface moins rugueuse) et ayant une conductivité thermique plus élevée (par exemple, le quartzite).

Étant donné que l'influence des caractéristiques des pores (taille, distribution, connectivité et tortuosité) sur les propriétés hydrauliques et mécaniques du béton drainant a été largement étudiée, leur influence sur le comportement thermique du béton drainant devrait également être étudiée. L'objectif est de concevoir un revêtement en béton drainant rafraichissant qui présente une résistance mécanique élevée tout en remplissant sa fonction première de gestion des eaux pluviales.

Après avoir étudié le comportement thermique du béton drainant en condition sèche, le chapitre suivant présente des essais complémentaires avec ce banc expérimental pour évaluer l'effet de différents facteurs (albédo, porosité, conductivité thermique et coefficient d'absorption capillaire, teneur en eau) sur le comportement thermique du béton drainant en conditions humides. Le comportement thermique d'une nouvelle formulation de béton drainant à base de pouzzolane a été étudié permettant de maximiser l'effet rafraichissant de ce type de matériaux.

Khaled Seifeddine^a, Sofiane Amziane^a, Evelyne Toussaint^a

^a Université Clermont Auvergne, CNRS, SIGMA Clermont, Institut Pascal, F-63000 Clermont-Ferrand, France.

Highlights

- Thermal behavior of pervious concrete (PC) was assessed.
- An original experimental bench was designed to study the thermal behavior in the laboratory.
- The maximum surface temperature of PC is more sensitive to the albedo than to the thermal conductivity.
- To decrease the maximum temperature of PC, it is recommended to avoid the use of lightweight aggregates
- It's recommended the use of finer and lighter colored aggregates (to increase the albedo).

Keywords

Pervious concrete; Urban heat island; Surface heat budget; Surface temperature reduction; Heat mitigation.

1. Introduction

Currently, more than 50% of the world's population lives in cities. By 2050, this will increase to two-thirds, or about 6.5 billion people [1]. One effect produced by the growth of cities is the urban heat island (UHI), defined as an urban area that has a significantly higher temperature than the surrounding rural and suburban areas [2].

The foremost reason for UHIs is that urbanization leads to an increase in impervious surfaces that absorb heat, and a decrease in natural vegetation [3]. Numerous studies have shown that the temperature of ordinary asphalt can be 15 to 20°C higher than that of grass [4]–[7]. In our cities, the amount of vegetation is decreasing, and growing amounts of impervious pavements now cover the cities, causing heat islands [8]. Impervious pavements eliminate cooling by evaporation, and the solar energy absorbed is released as sensible heat more than latent heat [9].

There are several solutions to reduce heat-island formation, such as reducing the use of asphalt and concrete by promoting vegetation, reducing the impermeability of cities by promoting evapotranspiration and reducing anthropogenic heat emission [3]. As pavements represent 30 to 45% of the total surface of cities [1], the idea of using cool pavements to combat UHIs is an interesting solution in today's world.

Evaporative pavements are among the most common types of cool pavements. These pavements are generally permeable and reduce the effects of UHIs through cooling by evaporation [10]. In this category, we can distinguish several types of pavements that decrease their surface temperature in wet conditions thanks to the latent heat absorbed during water evaporation such as: porous vegetated pavers [11], impermeable pavers with permeable joints

[12], permeable pavements such as pervious concrete [13] and permeable asphalt pavements [14], and water-retaining pavement [15].

Pervious concrete pavements are among the most widely used permeable pavements. Pervious concrete is a composite material. It is made up of the same components as traditional concrete: water, cement and aggregates. The only difference is that there are almost no fine particles to fill the voids between the coarse aggregates, creating interconnected voids that allow water to pass through the PC [16]. This permeable pavement has a total porosity ranging from 15 to 40%, and an open porosity ranging from 15 to 35% [17]. Several studies in the literature have highlighted the mechanical and hydraulic properties of pervious concrete [18]–[30]. However, to date, there have been relatively few studies on the thermal behavior of this type of material [13], [31] compared to that of other types of materials [32]–[37].

There are studies in the literature that have highlighted the cooling capacity of pervious concrete pavements [13], [38]–[40]. The numerical study of Qin and Hiller [13] shows that pervious concrete has a higher surface temperature than ordinary concrete in dry conditions. On the other hand, after watering, evaporative flow can keep its temperature cooler than that of ordinary concrete for 12 to 24 hours. Due to the low water absorption and retention capacity of PC, in order to prolong its evaporative cooling effect, Tan et al. [40] added biochar particles to PC as hygroscopic filler. The addition of these particles improves the evaporative cooling effect compared to conventional pervious concrete.

Pervious concrete can only be a solution to reduce UHIs if it is in a wet condition and is periodically watered. This strategy therefore requires the presence of water in the pavement structure or in the underlying soil. The use of this type of pavement could be advantageous in countries with high summer rainfall. However, in countries with very low summer precipitation, and countries where pavements cannot be watered, the evaporative pavement described above cannot be used effectively. On the other hand, there have been very few studies published on the thermal behavior of pervious concrete in dry conditions.

To address this issue, the objective of this study is to investigate the thermal behavior of cement-based pervious concrete pavements with natural aggregates with a view to reducing their surface temperature in dry conditions. This study focuses on the influence of thermophysical properties on the surface temperature, to design PC that can permanently reduce its surface temperature under dry conditions without the use of water. For this purpose, the surface temperature of PC and ordinary were calculated analytically, based on physical laws and the energy balance at the pavement surface. The analytical results were validated experimentally using an innovative experimental bench that was designed to perform the study under controlled climatic conditions in the laboratory. Finally, the influence of thermophysical factors on the surface temperature of PC was studied. The sensitivity of the surface temperature to various influencing factors was calculated by means of a sensitivity study. The influence of thermophysical properties on the thermal behavior of the PC in wet conditions has not been studied; this will be the subject of a future study.

2. Energy balance at the pavement surface – Analytical method and physical concepts

In order to characterize the energy exchanges at the surface–atmosphere interface, it is essential to define a number of parameters. This section presents these parameters and the formulas by which they are calculated.

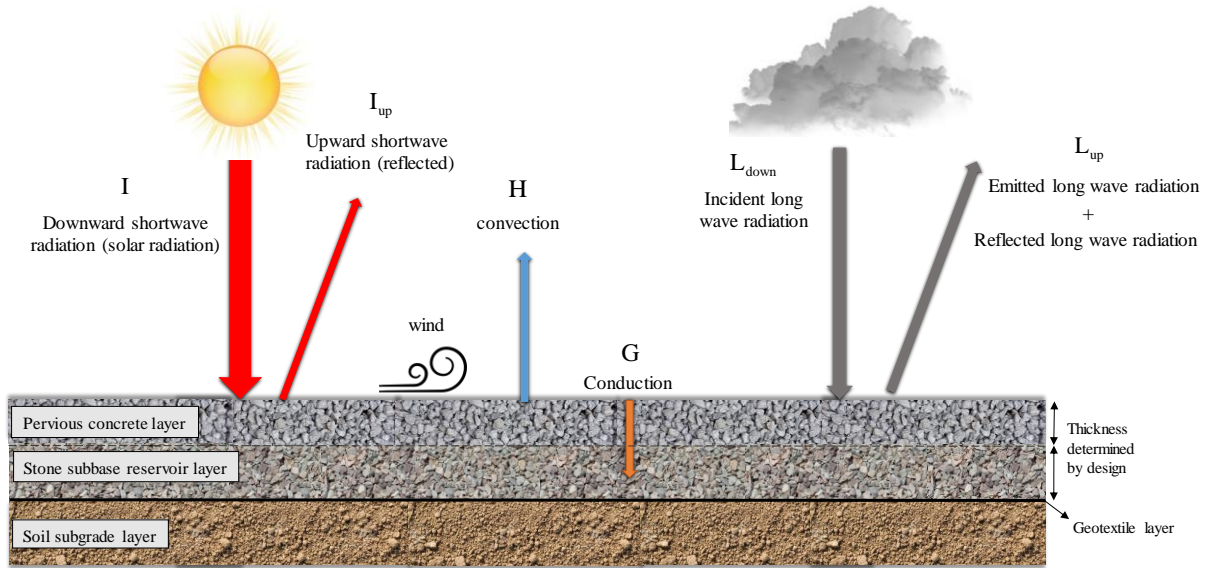


Fig. 1. Diagram of the energy balance at the surface of a pervious concrete pavement in dry conditions.

The energy balance at the surface of the dry pavement is given by **Eq. (1)**. This equation includes heat exchange due to solar radiation, infrared radiation, convection at the surface and conduction under the pavement [41], [42]. Fig. 1 shows all of these energy fluxes on a typical cross-section of pervious concrete pavement. Pervious concrete is placed on top of a stone layer which acts as a reservoir layer and also filters stormwater. The bottom layer is a subbase layer. In general, the thickness of the first two layers is determined at the design stage, depending on the intended use of the pervious concrete pavement.

$$I + L_{\text{down}} = I_{\text{up}} + G + H + L_{\text{up}} \quad (1)$$

where

- I : incident solar radiation (W/m^2);
- $I_{\text{up}} = RI$: reflected solar radiation (W/m^2), and R is the albedo of the surface (dimensionless);
- L_{down} : emitted radiation from the atmosphere (W/m^2);
- L_{up} : emitted and reflected longwave radiation by the surface (W/m^2);
- H : thermal convection on the surface of the pavement (W/m^2);
- G : conduction into the ground (W/m^2).

The terms on the left of **Eq. 1** ($I + L_{\text{down}}$) represent the inflow, while the terms on the right represent the outflow. From the perspective of pavement design, the left-hand terms are fixed by site selection and the presence or absence of radiative masks (in our case, the radiative flux is controlled). The right-hand terms depend on the thermal properties of the pavement.

The longwave radiation emitted by the atmosphere L_{down} and the longwave radiation emitted and reflected by the surface L_{up} are calculated using the Stefan–Boltzmann law, in accordance with **Eqs. (2) and (3)** [43].

$$L_{\text{down}} = \sigma \varepsilon_a (T_a + 273.15)^4 \quad (2)$$

$$L_{up} = \sigma \varepsilon_s (T_s + 273.15)^4 + (1 - \varepsilon_s) L_{down} \quad (3)$$

where ε_a = atmospheric emissivity (dimensionless); T_a = air temperature near the surface ($^{\circ}\text{C}$); σ = Stefan–Boltzmann constant equal to $5.67 \times 10^{-8} \text{ W.m}^{-2}.\text{K}^{-4}$; ε_s : emissivity of the pavement surface (dimensionless); T_s = surface temperature ($^{\circ}\text{C}$); $(1 - \varepsilon_s) L_{down}$ = reflected longwave radiation (W/m^2).

Cool pavements aim to limit their contribution to urban warming compared to standard pavement. In other terms, the objective is to modify the surface energy balance in such a way as to reduce the term H in the equation. The thermal convection H (W/m^2) at the pavement surface is governed by the Jürges formula [44] (**Eq. (4)**).

$$H = h_c (T_s - T_a) \quad (4)$$

where h_c is the thermal convection coefficient ($\text{W.m}^{-1}.\text{}^{\circ}\text{C}^{-1}$). The value of h_c is a function of the Reynolds number of the local wind R_e , the thermal conductivity of the air K_{air} ($\text{W.K}^{-1}.\text{m}^{-1}$), the Prandtl number P_r (dimensionless) of the air and the characteristic length (which is used to calculate the number R_e) [45]. According to the traditional theory of heat transfer [45], [46], h_c consists of two parts: natural convection and forced convection. The thermal convection coefficient of natural convection of air on a flat plane is about $5.6 \text{ W.m}^{-1}.\text{}^{\circ}\text{C}^{-1}$ [45], [47].

According to the Blasius solution [45], the forced convection coefficient of a flat plane is $0.332 R_e^{0.5} P_r^{1/3} K_{air} / L$ if the airflow is at low velocity (for example, $< 6 \text{ m/s}$). Therefore, the thermal convection coefficient, i.e. the modified Blasius solution, is expressed by **Eq. (5)**.

$$h_c = 5.6 + 0.332 R_e^{0.5} P_r^{1/3} K_{air} / L \quad (5)$$

where for air, $K_{air} = 0.027$, $P_r = 0.7$. For the flow of air on an infinite flat plate, $L = 0.15 \text{ m}$ [45]. The Reynold's number is given by **Eq. (6)**.

$$R_e = vL / \mu \quad (6)$$

where v is the local wind speed, and μ is the kinematic viscosity of the air, which is generally equal to $16.01 \times 10^{-6} \text{ m}^2.\text{s}^{-1}$ [45].

Eq. (7) gives another correlation proposed by Bentz [48] to calculate the thermal convection coefficient of concrete.

$$h_c = \begin{cases} 5.6 + 4.0 \times v, & |v \leq 5 \text{ m/s} \\ 7.2 \times v^{0.78}, & |v \geq 5 \text{ m/s} \end{cases} \quad (7)$$

In Equation 7, the natural convection at the pavement surface is $5.6 \text{ W.m}^{-1}.\text{}^{\circ}\text{C}^{-1}$ and is therefore within the range of the free convection coefficient of the ground surface according to traditional heat transfer theory [45]. For this study, a value of $5.6 \text{ W.m}^{-1}.\text{}^{\circ}\text{C}^{-1}$ was adopted as the thermal

convection coefficient, with the wind speed being zero in the climate chamber where the experimental bench is located.

According to Fourier's law, the heat flux density is proportional to the temperature gradient. The proportionality coefficient is called thermal conductivity λ . Therefore, the conductive flux is expressed by **Eq. (8)** [49].

$$\overline{G} = -\lambda \cdot \overline{\text{grad } T} \quad (8)$$

In this study, assuming a horizontally uniform soil temperature, there is no lateral heat conduction (thermal insulation of rock wool on the side walls of the bin). Only vertical conduction remains. It is unidirectional conduction. In the following, the conditions are the same. The heat flow by conduction G is then formulated by **Eq. (9)**. Furthermore, the heat transfer between the ground and the underlying layer can be treated as a one-dimensional transient heat transfer, as **Eq. (10)** expressed.

$$G = -\lambda_{\text{pavement}} \left(\frac{\partial T}{\partial z} \right)_{z=0} \quad (9)$$

$$c_p \rho \frac{\partial T}{\partial t} = \lambda \frac{\partial^2 T}{\partial z^2} \quad (10)$$

where c_p (J/K) and ρ (kg/m³) are the heat capacity and density of the pavement, respectively.

These equations can be used to evaluate the temperature field at any point of the solid, and the flux density. The solution for each case requires the addition of boundary conditions and an initial condition.

Eq. (1) can be simplified to **Eq. (11)**. The upward emission and the downward emission can be simplified to one term because the sky can be deemed as a black body. The parameter I_{up} can be replaced by $I \times R$, and the upward and downward long wave radiations can be replaced by L which represents the net longwave radiation ($L = L_{\text{up}} - L_{\text{down}}$) [50].

$$(1-R)I = L + H + G \quad (11)$$

By writing each of the (algebraic) energy flows in terms of temperature, an equation involving surface temperature, air temperature, and temperature at a given depth can be obtained. The air temperature should be available by measurement. The temperature at a given depth or the temperature difference between the surface and a particular depth should be measured. The resulting energy balance (**Eq. (12)**) is a fourth-degree equation, which can be solved to give the surface temperature of dry pavements.

$$(1-R)I = \varepsilon_s (\sigma (T_s + 273.15)^4 - L_{\text{down}}) + h_c (T_s - T_a) - \lambda_{\text{pavement}} \left(\frac{\partial T_z}{\partial z} \right)_{z=0} \quad (12)$$

The terms on the right depend on the properties of the pavement – more specifically, its albedo R , emissivity ε_s and thermal conductivity $\lambda_{\text{pavement}}$. When these properties are modified, cool pavements can offer better thermal performance in the city.

3. Materials and methods

Two types of pavements, pervious concrete and ordinary concrete, were studied in the laboratory under heatwave-like conditions, and their behavior was compared. The thermal behavior of the pavements was studied using the analytical model presented previously. This model is based on the energy balance of the pavement. It has been used in a range of studies to predict the surface temperature of pavements or to analyze the different heat fluxes [5], [10], [41], [42], [50], [51].

First, the thermophysical properties were determined. Next, the air temperature and the temperature at a selected depth were measured using an innovative experimental bench. These parameters were used in the analytical model to predict the surface temperature of the pavements. These results were compared to the results found experimentally in order to validate the analytical model under the conditions of this experiment. A sensitivity analysis was then performed using this model to study the influence of thermophysical parameters (albedo and thermal conductivity) on the surface temperature of the pervious concrete.

The novelty of this study is the establishment of a complete energy balance of a pervious concrete pavement under controlled meteorological conditions in the laboratory using an innovative experimental bench. All energy fluxes (conduction, convection, radiation) are analyzed and discussed. This is the first study that quantifies the influence of the variation of thermophysical parameters on the maximum surface temperature of PC in dry condition. This study therefore helps to optimize the design of the PC mix in dry conditions in order to achieve suitable mechanical, hydraulic and thermal behavior.

3.1. Dosage and sample preparation

Table 1 shows the dosages used in the pervious concrete and ordinary concrete samples. An ordinary Portland cement CEM II/B-LL 32.5 R CE NF was used. The coarse crushed gravel aggregates used in both mixes have a particle size distribution of 3.15 to 12.5 mm. Sand was used only in the ordinary concrete mix, and has a particle size distribution of 0.08 mm to 5 mm. The properties of the aggregates are presented in Table 2.

Table 1

Dosage of pervious concrete and ordinary concrete.

Specimen	Sand (kg/m³)	Gravel (kg/m³)	Cement (kg/m³)	Water (W) (kg/m³)	W/C
Ordinary concrete (OC)	996	833	400	200	0.5
Pervious concrete (PC)	0	1600	350	112	0.32

Table 2

Properties of aggregates.

Properties	Sand	Gravel
Specific gravity (dimensionless) ASTM C127-15 [52]	2.67	2.62
Bulk density (kg.m ⁻³)	1940	1757

ASTM C29 [53]		
Water absorption (%) ASTM C127-15 [52]	1.4	0.55
Void ratio (%)	31	40

The particle size distributions of the gravel and sand used are shown in Fig. 2, it was carried out by sieving (NF EN ISO17892-4 [54]).

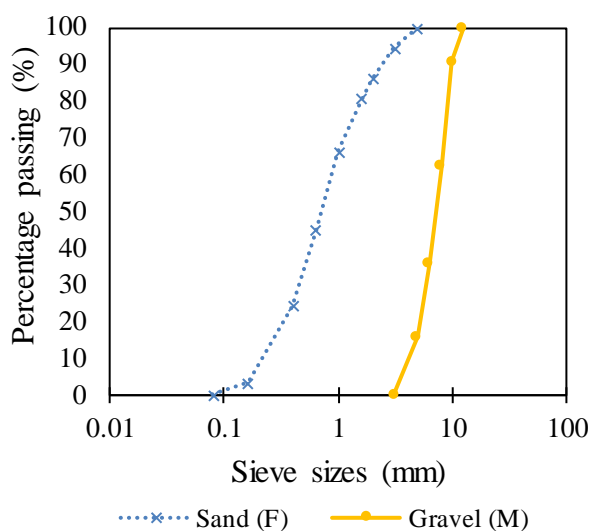


Fig. 2. Particle size distribution of the aggregates used to prepare the samples.

The PC and OC mixtures were prepared in a standard concrete mixer with a capacity of 300 liters. The aggregates (gravel for the PC and gravel + sand for the OC), the required amount of cement and a small amount of water were first mixed, and then, after a quick mixing of these materials, the remaining amount of water was added slowly. After that, the mixtures were mixed for about 3 minutes. At the end of mixing, the mixtures were poured in layers into the pre-prepared forms. They were gently tapped using a rubber mallet to ensure minimal compaction. The specimens were demoulded after 24 h and stored in water until testing age.

For each mixture, six samples were made up: 3 cylindrical samples to measure the compressive strength, the open porosity and the density, 2 parallelepiped samples to measure the thermal properties (conductivity, effusivity and thermal diffusivity), and 1 parallelepiped sample to measure the permeability and the cooling performance. The samples and their dimensions are presented in Fig. 3.

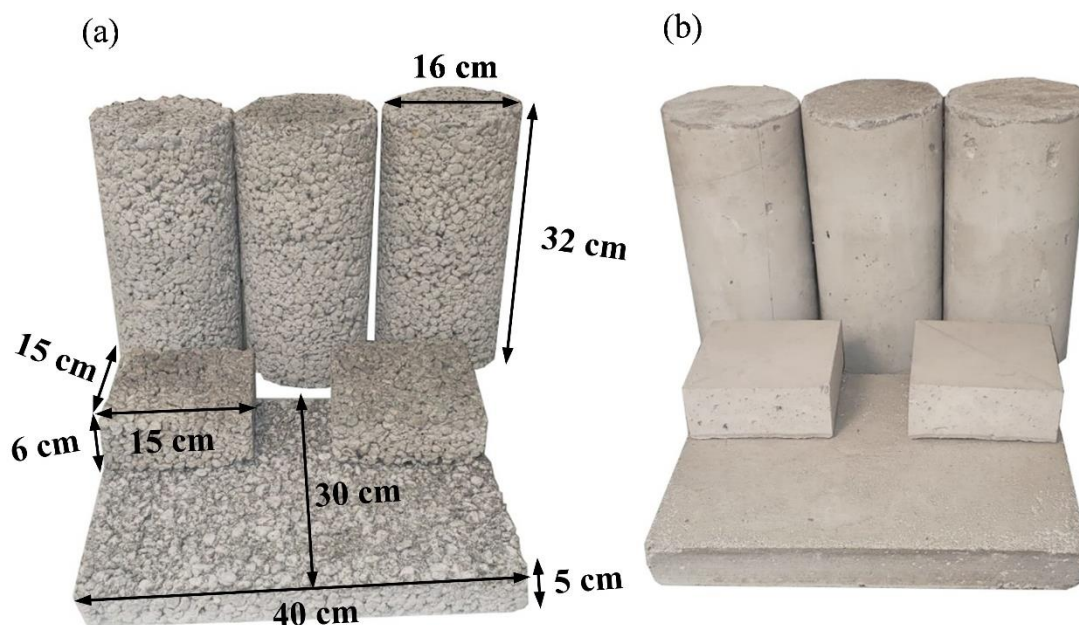


Fig. 3. Prepared samples: (a) OC, (b) PC.

3.2. Porosity of pervious concrete

The interconnected open porosity of pervious concrete samples was determined using the same methodology as employed in previous studies [55], [56]. This method consists of saturating all the interstitial voids in a sample with water, in order to correlate the open porosity with the total volume of water used. For this purpose, the samples were placed into non-deformable molds and covered with a PVC film to ensure water tightness. The mold and the sample inside were placed on a scale and water was added to fill the interstices of these porous materials. Considering the weight difference between the dry mass and the saturated mass, the volume of water V_w (m^3) is obtained. Then, the open porosity P_0 (%) is calculated using **Eq. (13)**.

$$P_0 = \frac{V_w}{V_s} \quad (13)$$

where V_s (m^3) is the volume of the sample.

Table 3 shows the average value (3 samples) of the density of the two mixes (NF EN 12390-7 [57]) and the average open porosity of the pervious concrete.

Table 3
Open porosity and density.

Specimen	Average open porosity (%)	Average density (kg/m^3)
Ordinary concrete	-	2349 ± 18.87
Pervious concrete	21.97 ± 1.67	1951 ± 42.33

3.3. Mechanical and hydraulic properties

3.3.1. Compressive strength

The compressive strength of the samples at 28 days was measured with reference to the standard NF EN 12390-3 [58]. The average measured compressive strength (3 samples) is 41.19 ± 1.140 MPa for OC and 11.6 ± 0.460 MPa for PC.

The average compressive strength of PC represents 28% of that of OC. This difference is related to the presence of pores within the structure of the PC and the weak bond between the coarse aggregates of the PC, which is formed by only a thin layer of cement paste.

3.3.2. Permeability

The permeability of the pervious concrete was measured using an ASTM C 1701 permeameter [59]. This method uses the same principles as the constant-head permeability test. The infiltration rate (coefficient of permeability or hydraulic conductivity) is calculated by Eq. (14) [60].

$$K = \frac{\gamma M}{D^2 t} \quad (14)$$

where K = infiltration rate, mm/h [in/h]; M = infiltrated water mass, kg [lb]; D = inner diameter of the infiltration ring, mm [in]; t = time required for the measured amount of water to infiltrate the pavement [s]; γ (constant value) = 4,583,666,000 in SI units or 126,870 per unit [in-lb].

The results show that the average value of the permeability of the PC (3 measurements) is equal to 1.296 ± 0.051 cm/s, which is much higher than the minimum recommended permeability for PC, which is 0.1 mm/s [17].

3.4. Thermophysical properties

3.4.1. Albedo measurement

The albedo is a dimensionless quantity, representing the fraction of global solar energy reflected by a surface. It is expressed as a percentage or as a number between 0 (all light is absorbed) and 1 (all light is reflected). This property was measured with a pyranometer in accordance with ASTM E1918 [61].

The tested pavers were dried in a ventilated oven at 105°C until a constant mass was achieved, and then cooled to ambient room temperature. Then, the pyranometer was placed over the pavers in dry conditions to measure the shortwave radiative flux reflected from the surface. Several values of reflected radiative flux were recorded by varying the incident shortwave radiative flux each time. The incident shortwave radiative flux can be modified, as the experimental bench is equipped with an infrared lamp whose power control is graduated from 0 to 100% (Appendix A). 0% means that the infrared lamps are completely off and 100% means that they have reached their maximum power. Each graduation corresponds to a specific power value of the infrared lamps and a value of the incident shortwave radiative flux that corresponds to the position of the surface of the pavements (max. 2000 W/m² relative to the position of the

pavement in the bin). These values have been established by the thermal engineering office that designed the experimental bench and verified in the laboratory using a pyranometer.

The results show that the average albedo (3 measurements) of the PC (0.203 ± 0.0073) is lower than that of the OC (0.28 ± 0.0076). In dry conditions, the pervious concrete and ordinary concrete samples had the same gray color (the color of cement). This decrease is related to the roughness of the surface and the presence of pores in the structure of the pervious concrete, which limit the reflection of incident short wave radiation [13], [62], [63]. Moreover, Zhang et al. [64] shows that the albedo of PC decreases linearly from 0.39 to 0.26 when the porosity increases from 7 to 32.4%.

3.4.2. Emissivity measurement

The emissivity of a material, written as ε_s , gives information about that material's ability to emit radiation. This property is measured using a pyrgeometer. The pyrgeometer was placed above the pavers in dry conditions to measure the longwave radiative flux given off by the surface L_e over a period of 12 hours. Measurements of surface temperature were taken in parallel. Subsequently, the emissivity of each paver was calculated using **Eq. (15)**.

$$\varepsilon_s = \frac{L_e}{T_s^4 \times \sigma} \quad (15)$$

Increasing the emissivity reduces the surface temperature of the materials [50], [65], [66]. The variations in emissivity of PC and OC pavers over time are shown in Fig. 4. The average value of emissivity chosen for this study is: $\varepsilon_s = 0.9$ for OC and $\varepsilon_s = 0.877$ for PC. The emissivity of the PC is slightly lower than that of the OC, which is a factor that will increase its surface temperature compared to the OC.

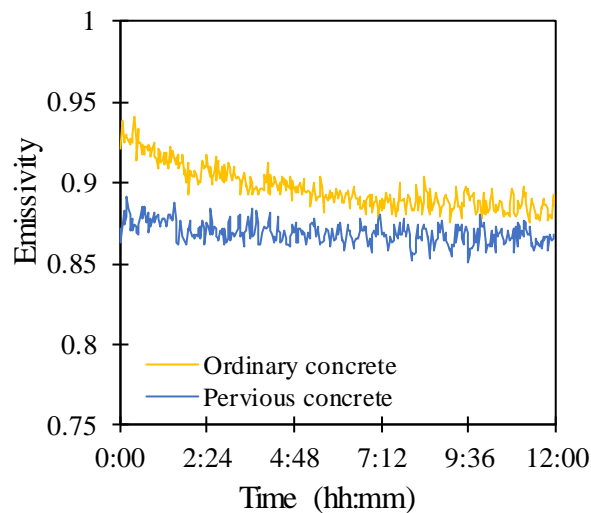


Fig. 4. Variation in emissivity of the pavers as a function of time.

3.4.3. Thermal conductivity measurement

The thermal conductivity was measured using a hot wire conductivimeter according to ASTM D5930-97 [67]. The thermal conductivity test was performed on $15 \times 15 \times 6 \text{ cm}^3$ parallelepiped samples.

The results show that the average thermal conductivity (3 measurements/sample) of PC ($0.613 \pm 0.0176 \text{ W.m}^{-1}.\text{K}^{-1}$) is lower than that of OC ($1.231 \pm 0.0802 \text{ W.m}^{-1}.\text{K}^{-1}$).

The study by Chen et al. [68] shows that the thermal conductivity of cement-based pervious concrete with natural aggregates decreases as porosity increases. In addition, the variation in thermal conductivity is affected by the tortuosity and orientation of the contacts between the air voids and the aggregates. The thermal conductivity values of the pervious concrete samples based on natural aggregates from this study and from 6 other studies [68]–[72] are presented in Fig. 5. The resulting curve shows a linear relationship between the thermal conductivity of pervious concrete based on cement and natural aggregates and its open porosity.

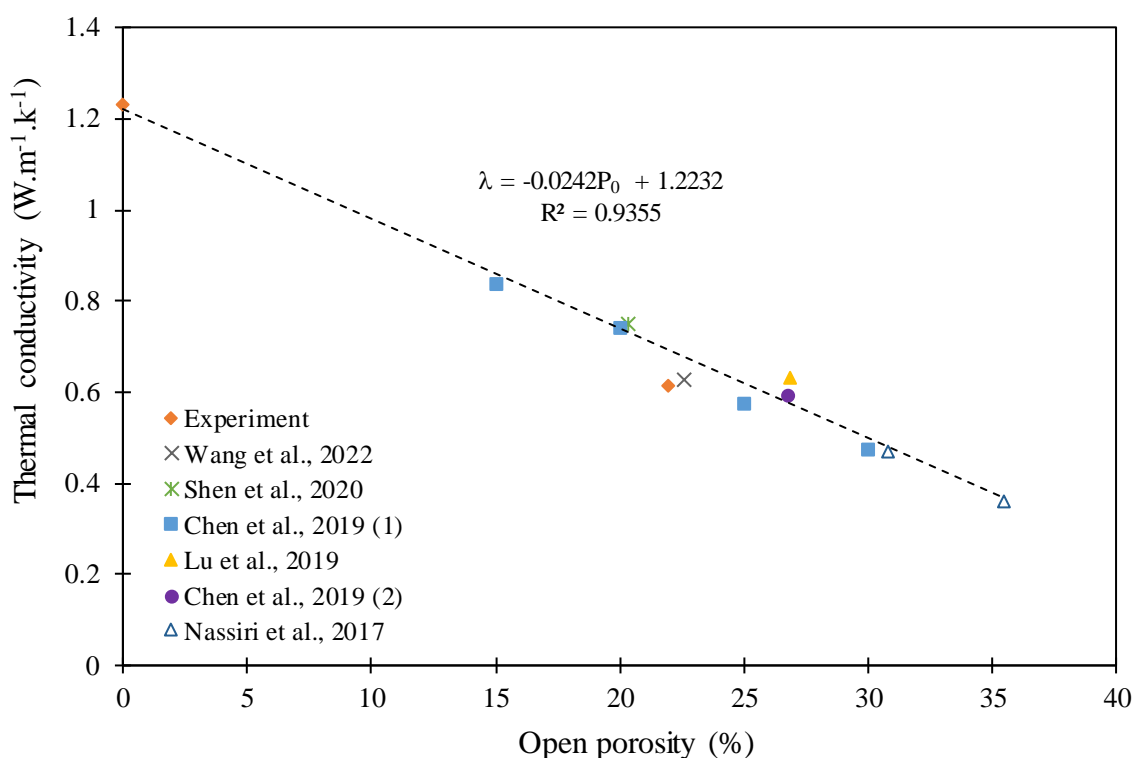


Fig. 5. Variation in thermal conductivity of pervious concrete as a function of open porosity.

4. General presentation of the experimental bench

To study the thermal behavior of pavements in wet and dry conditions, an experimental bench was designed equipped with multiple devices to establish a complete energy balance of a pavement (see Appendix A).

4.1. Two-compartment bin

The experimental bench is equipped with a two-compartment bin. The bin consists of acrylic glass plates, rubber seals, screws and threaded inserts. The bin is divided into two compartments

with a transparent polystyrene glass plate. Each compartment measures $20 \times 30 \times 15 \text{ cm}^3$. These two compartments are used to study the thermal behavior of a coating in dry and wet conditions simultaneously.

It is possible to remove this plate to use samples with a larger surface of $40 \times 30 \text{ cm}^2$. This is the choice made for this study.

4.2. Infrared lamps/heating

To simulate solar radiation, the bench is equipped with two infrared lamps of 1000 W, emitting radiation with a wavelength of 1180 nm. They are placed above the tank, so that each lamp is in the center of one half of the tank. The lamps are fixed on a mobile tray, which can move vertically. The range of movement is 14 cm (from 30 cm to 44 cm above the tank).

The bench is equipped with a lamp power regulator. This regulator has a graduation from 0 to 100%, corresponding to a power from 0 to 1000W.

4.3. Temperature sensors

4.3.1. Thermocouples in bins

The bench is equipped with two combs with 4 thermocouples positioned at several depths: 0.00 cm, 2.35 cm, 6.90 cm and 10.00 cm (Appendix A).

In the case of rigid pavements (rigid pavement + base layer), two other temperature sensors were installed inside the bench: the first was fixed at the boundary of the rigid pavement/base layer and the second was installed at the bottom of the bench.

4.3.2. Surface temperature measurement

The surface temperature was measured with two infrared temperature sensors installed on the heating plate. The measuring beam diameter of the two infrared temperature sensors depends on the distance between the sensor and the measuring surface (Appendix A).

4.4. Pyranometer and pyrgeometer

The shortwave radiative flux is measured with a CMP3 pyranometer which gives the radiation over the entire range of the solar spectrum from 300 to 2800 nm (the wavelength of radiation emitted by infrared lamps of 1180 nm falls within this range), with a sensitivity of 5 to $20 \mu\text{V}/\text{W}/\text{m}^2$ and a maximum irradiance of $2000 \text{ W}/\text{m}^2$.

The longwave radiation was measured with a CGR3 pyrgeometer which gives the longwave radiative flux in a spectral range of 4500 to 42000 nm, with a sensitivity of 5 to $15 \mu\text{V}/\text{W}/\text{m}^2$ and a net luminous flux that varies from -250 to $+250 \text{ W}/\text{m}^2$.

4.5. Data acquisition system

The bench has two data acquisition units to visualize and record the data measured by the temperature sensors, the pyranometer and the pyrgeometer.

These data acquisition units allow the testers to adjust several parameters such as the duration of the measurement cycles (speed of measurement in measures/second), the output modules,

the time, etc. The data recorded on the acquisition unit will then be transferred to a computer via ALMEMO control software. This software recovers the measurement data and offers several output formats for the recorded data.

4.6. Experimental setup

To investigate the thermal behavior of pervious concrete and ordinary concrete, the bin was filled with a 10 cm thick sand layer (0.08-5 mm) on which a 5 cm thick pavement of OC or PC was laid. This arrangement (see Appendix B) was used to simulate the complete permeable pavement structure (wearing course + reservoir layer).

To measure the temperature in the depth of this structure, two temperature sensors were introduced at two different depths: $z = 5$ cm (bottom side of the pavement) and $z = 15$ cm (bottom of the bin). An infrared temperature sensor was installed on the bench to measure the surface temperature in the center of the pavement. Then, rockwool thermal insulation ($\lambda = 0.03 \text{ W}\cdot\text{m}^{-1}\cdot\text{K}^{-1}$) was added on the side walls of the tank.

At the beginning of each experiment, the power of the infrared lamps was adjusted to the required value of incident shortwave radiation. The data from all sensors were recorded by two data acquisition systems. The recording frequency was set at one recording every two minutes. The first recording corresponds to the moment when the lamps were turned off, which represents the samples in the initial state. Immediately thereafter, the lamps were turned on using the electrical switch. After 48 hours, the lamps were turned off, the recording was stopped and the measurement data were recovered by the method presented previously.

The incident shortwave radiative flux in the case of this laboratory study is the radiative flux I emitted by the infrared lamps placed above the tank. The incident longwave radiative flux L_{down} corresponds to the radiation emitted by all the materials surrounding the bin such as laboratory equipment, infrared lamps, walls, ceiling, etc. (Appendix B).

5. Results and analysis

5.1. Prediction of surface temperature of pervious concrete and ordinary concrete

The analytical solution of Eq. (12) to predict the surface temperature of pavements requires the values of incident radiative fluxes, air temperature, temperature at a certain depth, and thermophysical characteristics of the tested pavements (thermal conductivity, emissivity, and albedo). The experimental setup was in a laboratory with controlled climatic conditions: $20^\circ\text{C} \geq \text{Ambient temperature} \leq 23^\circ\text{C}$; $35\% \geq \text{Relative humidity} \leq 40\%$.

Table 4 shows the duration of the daytime phase (lamps on) and the nighttime phase (lamps off), as well as the values of shortwave and longwave incident radiation during both phases.

Table 4

Characteristics of the day and night phases during the experiment.

	Daytime phase	Nighttime phase
Duration	24 h	24 h
Incident radiation I (W/m^2)	520	0

Incident radiation L_{down} (W/m^2)	531	430
--	-----	-----

Fig. 6 shows the variation in air temperature and temperature in the depth of the tested samples at $z = 5$ cm and $z = 15$ cm as a function of time. The data recording rate was set to one recording every 2 minutes, so as to have a continuous variation of measured temperatures during each experiment. The results shown in Figure 6 are the average values of two experiments. The maximum root mean square error (RMSE) was 0.289°C for all temperatures presented in Fig. 6a and 6b.

Fig. 6 shows that at the end of the diurnal period at $t = 24$ h, the temperatures at $z = 5$ cm decreased faster than those at $z = 15$ cm, since the temperature sensor at this position was further away from the top surface which had started to cool down. The heat stored at the base of the sample took more time to dissipate. This figure also shows that the air temperature above the PC was on average 1.1°C higher than that above the OC.

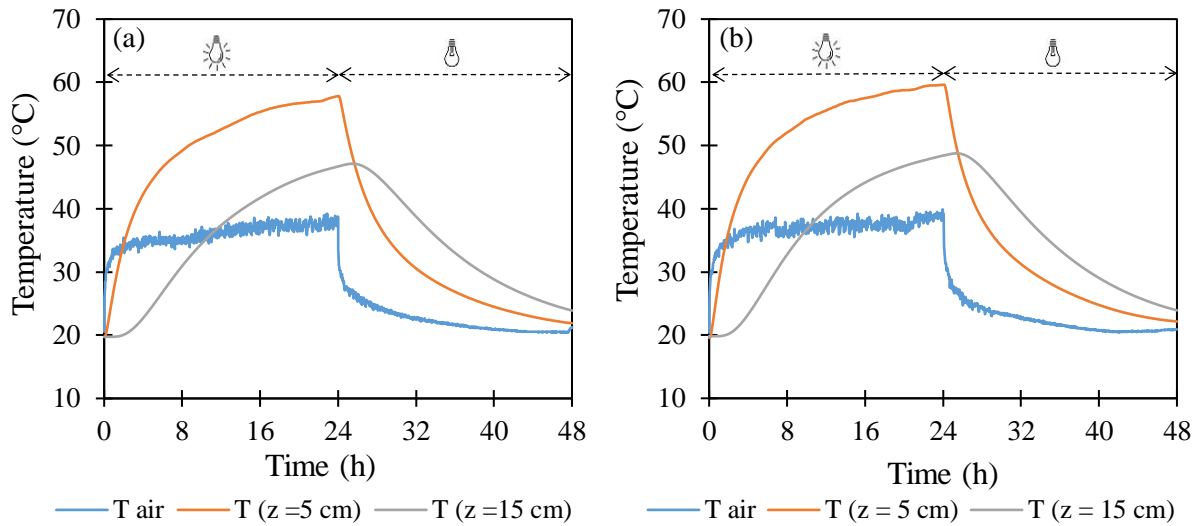


Fig. 6. Variation of air temperature and temperature at depth $z = 5$ and 15 cm as a function of time:
(a) OC, (b) PC.

Once the thermophysical parameters of the pavements were identified and the input data was measured, the surface temperature was calculated numerically by **Eq. (12)**. **Eqs. (16)** and **(17)** show an example of the surface temperature calculation of ordinary concrete at the beginning of the experiment (lamps off, $t = 0$ s) and 8 h later (lamps on, $t = 8$ h), respectively.

$$(1-R) \times 0 = \varepsilon_s (\sigma (T_s + 273.15)^4 - 430) + 5.6 (T_s - 20.4) - \lambda_{\text{pavement}} \left(\frac{T_s - 19.56}{0 - 0.05} \right) \quad (16)$$

$$(1-R) \times 520 = \varepsilon_s (\sigma (T_s + 273.15)^4 - 531) + 5.6 (T_s - 34.7) - \lambda_{\text{pavement}} \left(\frac{T_s - 49.18}{0 - 0.05} \right) \quad (17)$$

The values 19.56°C (**Eq. (16)**) and 49.18°C (**Eq. (17)**), represent the temperature at $z = 5$ cm at $t = 0$ s and at $t = 8$ h respectively.

This equation of degree 4 has real and imaginary solutions. These solutions are presented in Table 5.

Table 5

Solutions of analytical equations to predict the surface temperature of pavements.

Equation	Solution 1	Solution 2	Solution 3	Solution 4
15	-1.197	42.11+ 754.32i	42.11 – 754.32i	20.04
16	-1206.49	29.31 + 762.21i	29.31- 762.21i	55.27

The recording rate of one recording every two minutes for 48h produced 1440 equations for each experiment to calculate the surface temperature of the pavements. To solve these equations, MATLAB software was used and the surface temperature corresponds to solution 4 of each equation, whose value is always positive and real. Indeed, solution 1 always has a negative value and solutions 2 and 3 present imaginary solutions. Solution 4 of each equation was therefore chosen as the surface temperature of the pavements.

The results of these equations are shown in Fig. 7, which presents the variation of the analytical surface temperature of PC and OC pavers as a function of time.

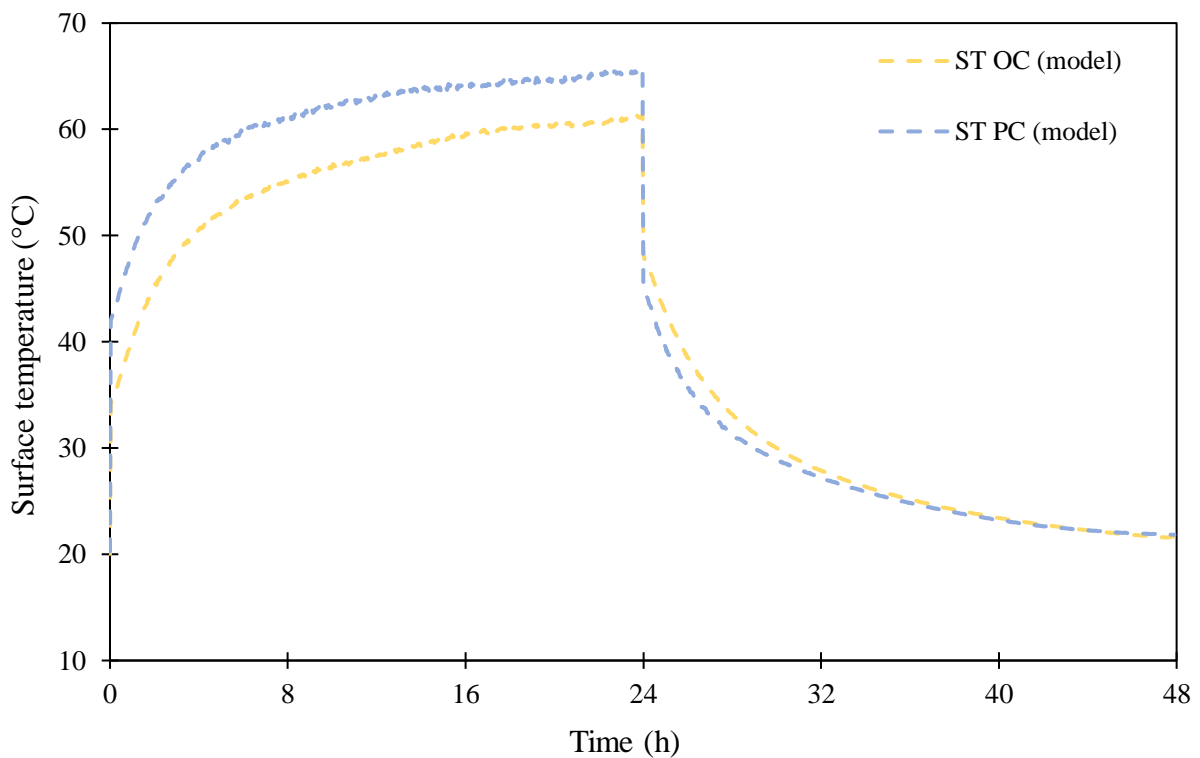


Fig. 7. Variation in surface temperature of OC and PC.

The results show that during the daytime period ($0 \leq t \leq 24$ h), the surface temperature of PC is 0 to 6°C higher than that of OC. The relatively low thermal conductivity of PC limits conductive heat transfer to the interior of the material, while its low albedo leads to a high absorption of incident short-wave radiation, causing a rapid increase in its surface temperature. The rough surface and cavities of PC tend to absorb more solar radiation than the relatively flat, plate-like surface of conventional concrete pavement.

During the nocturnal period ($24 \text{ h} < t \leq 48 \text{ h}$), due to lower thermal inertia, PC has less resistance to temperature drop and thus becomes colder than conventional concrete. These results are in keeping with the experimental results of Li et al. [73] and the numerical results of Qin and Hiller [13].

Fig. 7 also shows two transient periods that correspond to the moments when the lamps are switched on ($t = 0 \text{ s}$) and off ($t = 24 \text{ h}$). Indeed, for the resolution that corresponds to $t > 0 \text{ s}$ (e.g. for $t = 2 \text{ min}$), the shortwave radiative flux goes from 0 W/m^2 to 520 W/m^2 and the shortwave radiative flux goes from 430 W/m^2 to 531 W/m^2 and vice versa for $t > 24 \text{ h}$ at the moment when the lamps are switched off. This abrupt variation of radiative fluxes, during a relatively short time step, caused a significant temperature rise or fall, which is reflected when solving the analytical equations to calculate the temperature. However, in reality, the radiative fluxes vary in a continuous and gradual fashion.

5.2. Experimental validation

Fig. 8 shows the variation of analytical and experimental surface temperature of OC and PC pavements as a function of time. To make certain of the experimental results, each experiment was performed twice. The results show that the difference between the results of the experimental curves (ST1 and ST2) of each pavement type is small (Fig. 8). The root mean square error of the experimental results is as follows: $\text{RMSE} = 0.4028^\circ\text{C}$ for OC and $\text{RMSE} = 0.3036^\circ\text{C}$ for PC.

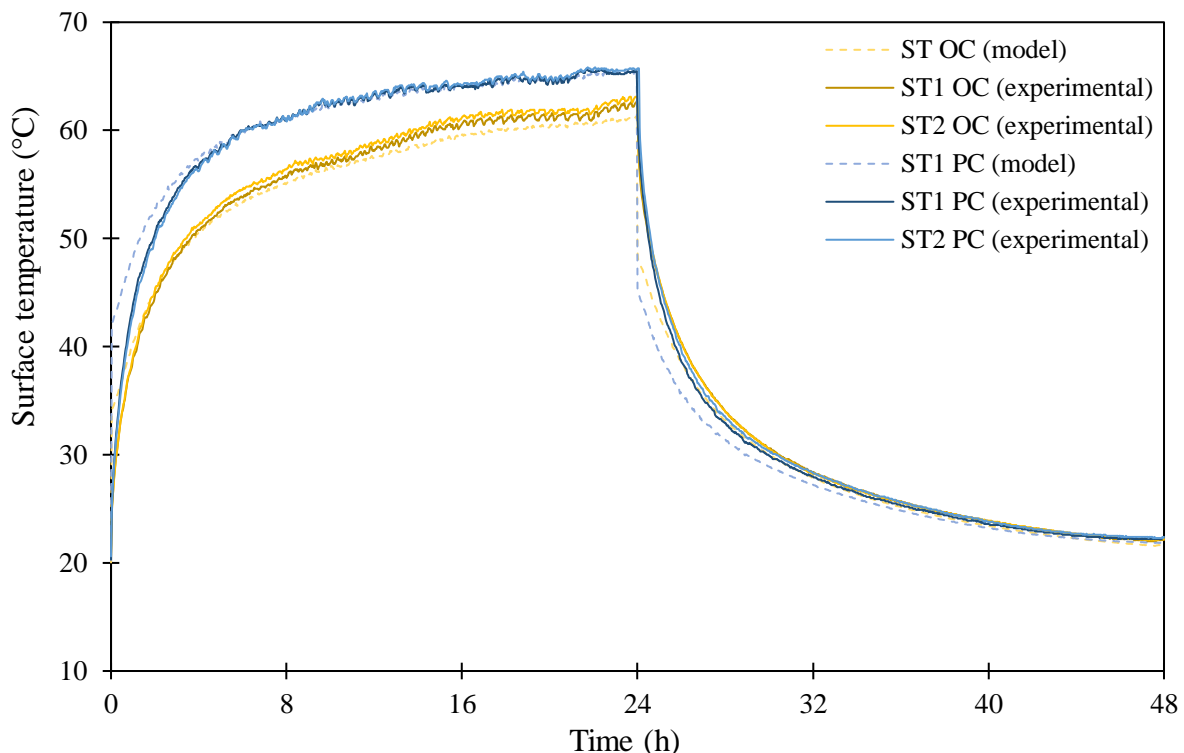


Fig. 8. Variation in the analytical and experimental surface temperature of the OC and PC.

During the daytime, the surface temperature of OC varies on average from 20.55°C to 62.80°C . The surface temperature of the PC varies on average from 20.45°C to 65.52°C . During the night period, the surface temperature of both pavements decreases to 22.2°C at the end of the experiment. The surface temperature of the pavements at the beginning and end of each

experiment corresponds to the ambient temperature in the laboratory where the experimental setup is located.

Model and experimental results of each experiment show significant discrepancies during the transient regimes (up to 2 hours after the lamps are turned on or off). During the steady state, the difference between the analytical and experimental results becomes relatively minor and varies between 0°C and $\pm 1.5^{\circ}\text{C}$.

Fig. 9 shows the relationship between the experimental and modeled surface temperature of PC and OC during the day and night period. The correlation coefficients are relatively high ($0.9691 \leq R^2 \leq 0.9919$) for both pavement types during both periods. It is noteworthy that under the conditions of this laboratory experiment, **Eq. (12)** predicts pavement surface temperature with high accuracy during the steady state, while the accuracy is less during the transient period. Better prediction during the transient period can be obtained with a short-wave radiative flux that varies gradually during this period.

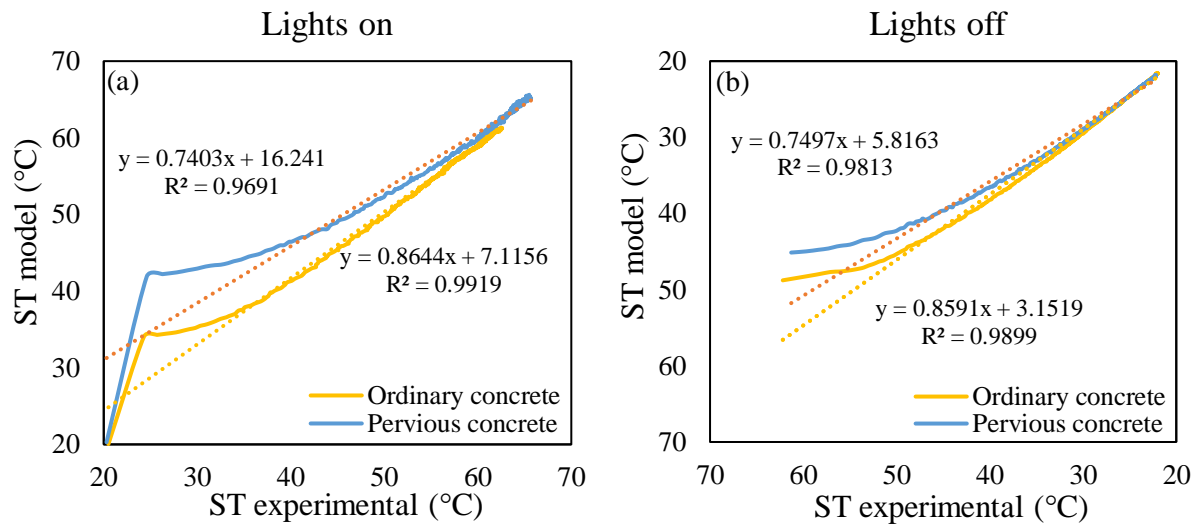


Fig. 9. Relationship between analytical and experimental surface temperature of OC and PC:

(a) daytime period, (b) nighttime period.

6. Discussion

6.1. Distribution of energy fluxes

The surface temperature of a pavement gradually increases as it is exposed to solar radiation. Once its temperature is higher than that of the air, it emits a significant amount of longwave radiation and sensible heat flux, resulting in an increase in air temperature. Fig. 10 shows the variation of energy fluxes of OC and PC pavements as a function of time.

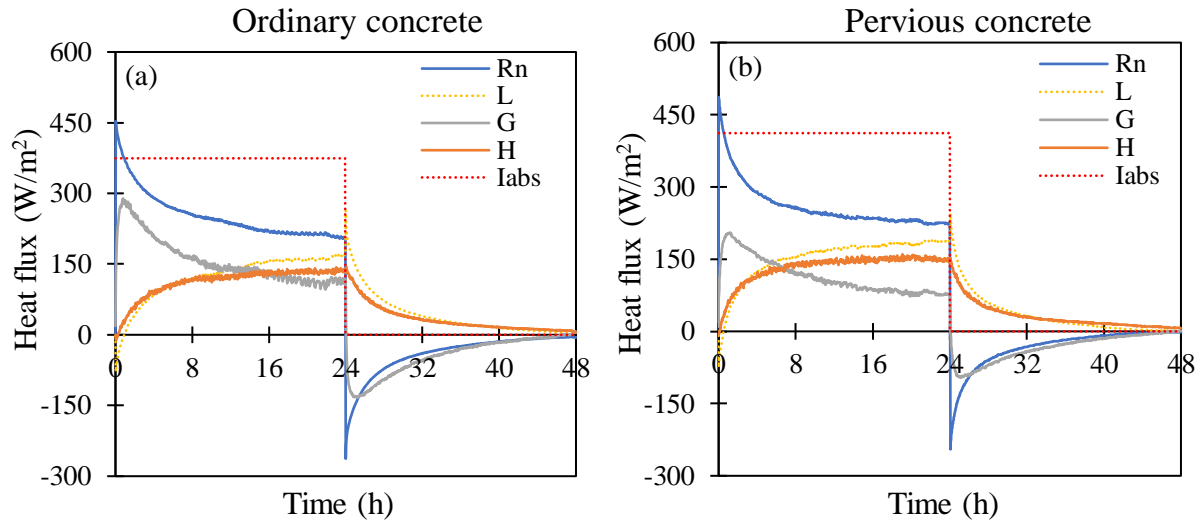


Fig. 10. Variation in OC and PC heat fluxes as a function of time.

R_n is the net radiant flux at the surface representing the actual radiant energy available at the surface. It is calculated as the difference between all incoming and outgoing radiation fluxes [43]. The net radiant flux is calculated by **Eq. (18)**.

$$R_n = I_{\text{abs}} - L \quad (18)$$

where I_{abs} is the absorbed shortwave radiative flux (**Eq. (19)**) and L represents the net longwave radiation (**Eq. (19)**).

$$I_{\text{abs}} = I - I_{\text{up}} = (1 - R)I \quad (19)$$

In dry conditions, the net radiant energy R_n captured by the surface is subsequently depleted by the thermal exchanges between the surface and the atmosphere by convection H , on the one hand, and by the mainly conductive exchanges G between the surface and the ground, on the other hand [74].

During the transient periods (when the lamps are switched on and off), the net radiative flux for both pavements is greater than the sum of the conductive and convective fluxes. However, after these two periods, the difference between R_n (**Eq. (18)**) and $H + G$ becomes smaller, with a maximum deviation of $\pm 20 \text{ W/m}^2$. These differences can be attributed to several reasons, such as the accuracy of the devices and measurement errors.

Fig. 10a and 10b show that, during the daytime, the conductive flux of PC and OC increases rapidly during the transient period. Indeed, the surface of the pavements is more sensitive to the temperature increase than the interior of the pavement. Fig. 11 shows the variation in the difference of the average surface temperature and the average temperature at $z = 5 \text{ cm}$ as a function of time, for PC and OC. The conductive flux (**Fig. 10**) and the temperature difference ΔT (**Fig. 11**) of each pavement appear similar, since the thermal conductivity of the pavements is relatively constant in dry conditions. This figure also shows that the temperature difference for the PC is always greater than that of the OC throughout the experiment; this is due to its porous structure, which limits heat transfer from the surface to the interior of the pavement or vice versa.

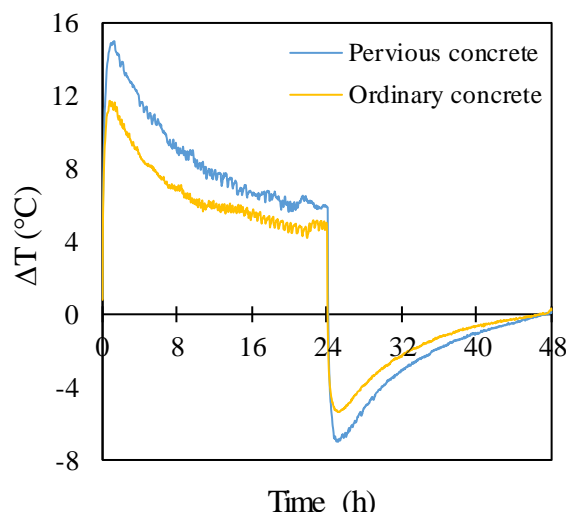


Fig. 11. Variation in the difference of the average surface temperature and the average temperature at $z = 5$ cm as a function of time.

At the beginning of the night period ($t > 24$ h), the surface of the pavements cools faster than their interior, resulting in the negative values of the conductive heat fluxes.

At the end of each experiment, the sensible heat flux H and the conductive heat flux G fall to zero. Indeed, the surface temperature, the temperature inside the pavements and the air temperature have almost the same value, which is equal to the ambient temperature of the laboratory.

During the daytime period and under the same climatic conditions, the net longwave radiative flux L and sensible heat flux H of the PC are greater than those of the OC. "On the other hand, the conductive heat flux of PC was always lower than that of OC. Indeed, the $\Delta T_{PC}/\Delta T_{OC}$ ratio (Fig. 11) varied from 0.92 to 1.83, while the $\lambda_{PC}/\lambda_{OC}$ ratio = $0.498 \text{ W}\cdot\text{m}^{-1}\cdot\text{K}^{-1}$. Thus, according to **Eq. (9)** the conductive heat flux of PC (G_{PC}) is always lower than that of OC ($G_{PC}/G_{OC} < 1$). It has been found that under dry conditions, PC aggravates the problem of urban heat islands on hot days, compared to OC.

6.2. Sensitivity analysis

With respect to urban heat islands, the maximum pavement surface temperature is the most influential factor. Since the analytical model exhibits a small deviation from the experimental results in predicting the maximum pavement surface temperature, it was used to perform a sensitivity study. The objective was to identify the factor that has the greatest influence on the surface temperature of pervious concrete pavements made of cement and natural gravel. This study will therefore be used to optimize the design of these types of pavements in dry conditions during heatwaves. The two factors studied are thermal conductivity λ ($\text{W}\cdot\text{m}^{-1}\cdot\text{K}^{-1}$) and albedo R .

Table 6 presents different pervious concrete samples and their characteristics which are needed for the sensitivity study: thermal conductivity and albedo.

Table 6

Properties of the studied pervious concrete samples.

Factor studied	Pervious pavement		Thermal conductivity (W.m ⁻¹ .K ⁻¹)	Albedo	Open porosity (%)
Thermal conductivity (λ)	Chen et al., 2019 [68]	λ_1	0.835	0.203	15%
		λ_2	0.738	0.203	20%
	Experiment	λ_3	0.613	0.203	22%
	Chen et al., 2019 [68]	λ_4	0.575	0.203	25%
		λ_5	0.473	0.203	30%
Albedo (R)	Hypothesis	R ₁	0.613	0.15	22%
	Experiment	R ₂	0.613	0.203	22%
	Hypothesis	R ₃	0.613	0.25	22%
		R ₄	0.613	0.3	22%
		R ₅	0.613	0.35	22%

To investigate the influence of thermal conductivity on the surface temperature of PC, the natural gravel and cement-based PC samples from the study by Chen et al. [68] ($\lambda_1, \lambda_2, \lambda_4, \lambda_5$) were considered. These samples are obtained by varying the open porosity from 15% to 30% which represents the typical porosity range of PC [75]. Sample λ_3 corresponds to the PC pavement used in this study. These samples can be obtained by using the same dosage (coarse aggregate and cement) and either increasing the degree of compaction or adding a certain amount of sand (0 to 10% of the overall aggregate mass). Varying the porosity by these methods has no significant effect on the roughness and color of the samples (same albedo).

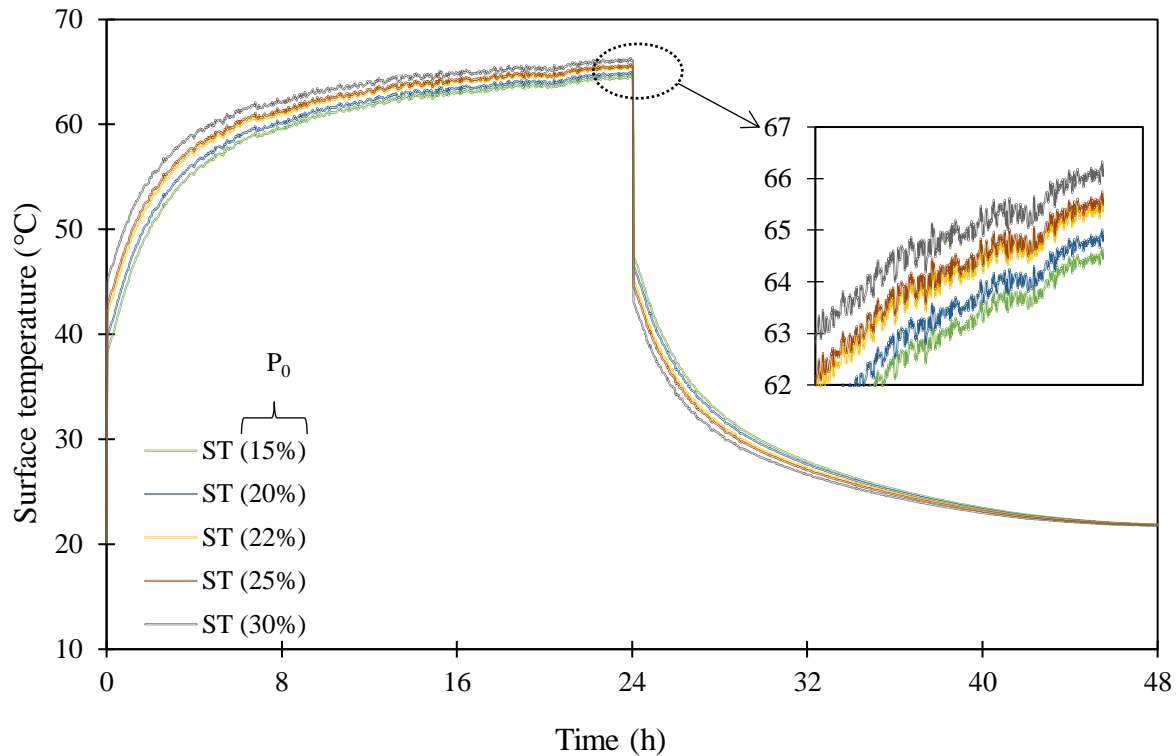


Fig. 12. Variation in surface temperature of several PC samples with different thermal conductivities as a function of time.

Fig. 12 shows the variation in surface temperature of PC samples ($\lambda_1, \lambda_2, \lambda_3, \lambda_4, \lambda_5$) as a function of time under the same conditions as this study. The open porosity values of the samples are shown in the legend.

The analytical results show that surface temperature of pervious concrete decreases with increasing thermal conductivity during the daytime period. On the contrary, the surface temperature increases during the night period. This is because the increase in thermal conductivity increases heat transfer within the pavement. The absorbed heat flux stored in the concrete is discharged at night, so that a pervious concrete pavement with a higher thermal conductivity causes a higher nighttime surface temperature than a pavement with low thermal conductivity. These results are in agreement with the results found analytically by Chen et al. [76] in evaluating the temperature field of a thermally modified asphalt pavement. This study shows that during the day, as the thermal conductivity of the asphalt pavement increases, the pavement surface temperature decreases. On the other hand, at night, the temperature of the pavement surface increases. This is mainly due to the fact that the downward heat transfer mechanism was accelerated by the increased thermal conductivity of the pavement. This heat that has been stored in the pavement comes back up to the surface during the night.

Increasing reflectivity is one of the most common techniques used to decrease the surface temperature of pavements. Concrete pavements can be highly reflective if the concrete is mixed with whitish cementitious materials and light-colored aggregates. In addition, the reflectivity of cement is the dominant factor in the albedo of PC or OC pavements while all other constituent materials have a secondary role [77]. There are other techniques such as light-colored paint that increase the reflectivity of pavements. Using these techniques, pervious concrete pavements with different albedos can be designed, while keeping the same porosity and thermal

conductivity. Therefore, the influence of albedo is studied and the results are presented in Table 6. Sample R₂ represents the PC pavement of this study.

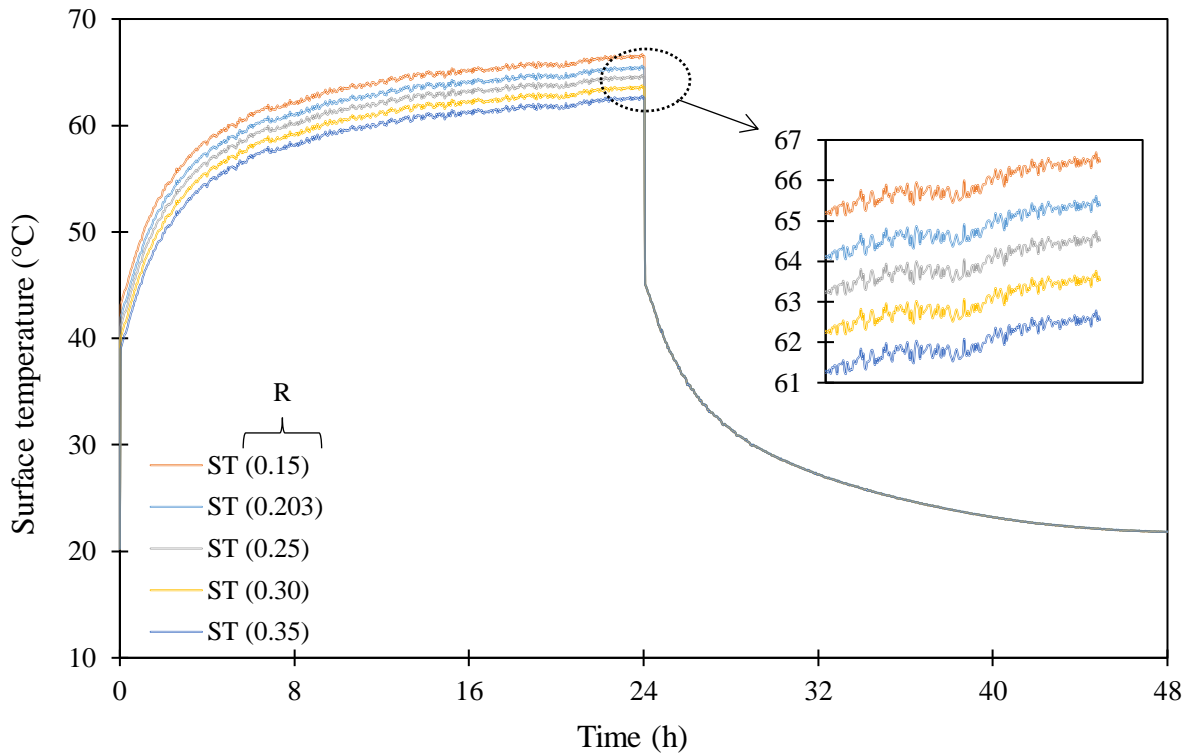


Fig. 13. Variation in surface temperature of several PC samples with different albedos as a function of time.

Fig. 13 shows the variation in surface temperature of PC samples with different albedos as a function of time. The analytical results show that the surface temperature of PC pavements decreases with increasing albedo during the daytime period. Indeed, when the albedo increases, the absorbed heat flux decreases (**Eq. (19)**) and consequently the surface temperature decreases.

It should also be noted that the temperature difference between samples λ_1 to λ_5 decreases progressively from the beginning to the end of the diurnal period (Fig. 12). On the contrary, the temperature difference between samples R1 to R5 increases progressively from the beginning to the end of the diurnal period (Fig. 13). This highlights the importance of albedo in lowering the maximum surface temperature of pervious concrete during heatwaves.

At night, the PC pavements show the same behavior and all have the same surface temperature. Indeed, during the analytical resolution of the surface temperature and to be consistent with the conditions of this experiment, the incident shortwave radiative flux I decreases from 520 W/m^2 to 0 W/m^2 at $t = 24 \text{ h}$ (when the infrared lamps are turned off). This variation causes the term R (albedo) in **Eq. (12)** to disappear, and the resolution of this equation during the night becomes independent of the albedo. In reality, the radiative solar flux decreases progressively, which can create slight variations in the daily results.

To investigate the influence of albedo during the night period, the incident shortwave radiation flux I is assumed to decrease linearly from 500 W/m^2 ($t = 24 \text{ h}$) to 0 W/m^2 ($t = 48 \text{ h}$, lamps off). Similarly, the incident longwave radiation flux L_{down} decreases from 531 W/m^2 ($t = 24 \text{ h}$) to 420 W/m^2 ($t = 48 \text{ h}$, lamps off). The variation of the incident radiation fluxes is shown in Fig. 14a.

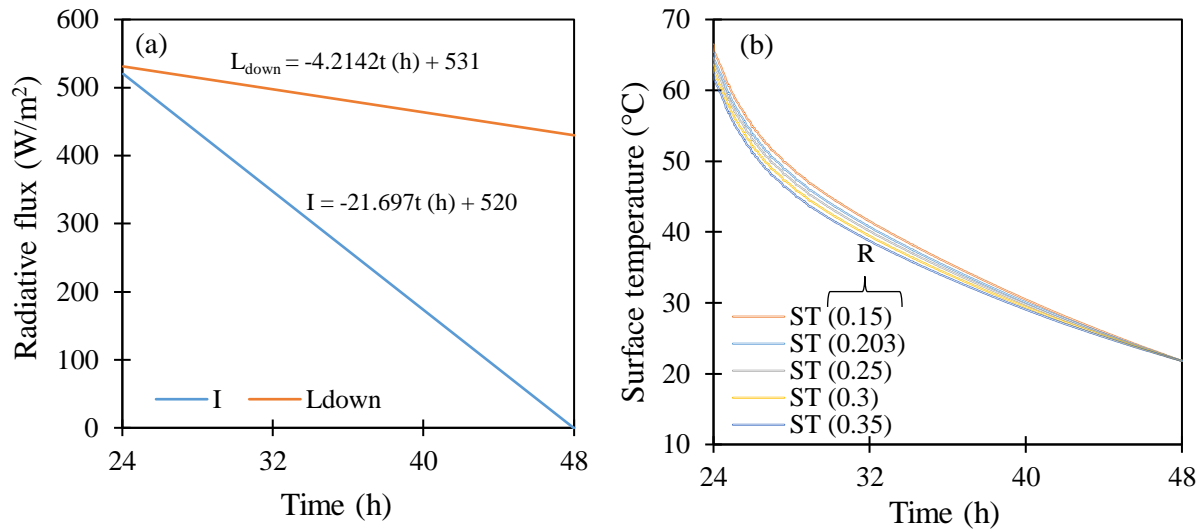


Fig. 14. Variation in incident shortwave and longwave radiation fluxes (a), and in surface temperature of PC during the night period.

Fig. 14b shows the variation in surface temperature of PC samples with different albedos during the night period considering the variation in shortwave and longwave radiation fluxes shown in Fig. 14a.

Analytical results show that the surface temperature of the pervious concrete decreases with increasing albedo. In addition, the difference between the surface temperatures of these samples decreases as the short- and longwave radiation fluxes decrease. At $t = 48$ h, these samples have the same surface temperature at the time when the shortwave radiative flux I is equal to zero. These results are in agreement with the numerical results found by Qin and Hiller [9], which show that increasing albedo significantly decreases the surface temperature during both diurnal and nocturnal periods. These results are obtained using real-time meteorological data. This is because a pavement with a high albedo reflects more solar radiation back into the atmosphere without increasing the surface temperature. As a result, pavements with high albedo release less instantaneous sensible heat (**Eq. (4)**) and longwave emissions (**Eq. (3)**), which reduces the diurnal and nocturnal UHIs.

In this study, the importance of the variables was analyzed using sensitivity analysis (SA) [78], [79]. SA was used to investigate the effects of changing two input variables (albedo and thermal conductivity) on the surface temperature of pervious concrete pavements. By measuring how the results are affected by changing an input variable, the sensitivity of the surface temperature to the input variable can be evaluated. To measure the changes produced in the output, a gradient g_a measure was adopted, based on previous research, formulated by **Eq. (20)** [80].

$$g_a = \frac{\sum_{j=2}^n |y_{a,j} - y_{a,j-1}|}{n-1} \quad (20)$$

where “a” represents the analyzed input variable (albedo or thermal conductivity) and $y_{a,j}$ is the sensitivity response for $X_{a,j}$. For example, $y_{R,1}$ is the maximum surface temperature at $t = 24$ h of sample R₁ ($X_{R,1} = 0.15$) and $y_{\lambda,1}$ is the maximum surface temperature at $t = 24$ h of

sample λ_1 ($X_{\lambda_1} = 0.834 \text{ W.K}^{-1}.\text{m}^{-1}$). n is the number of samples for each input variable ($n = 5$). After calculating the gradients of all input variables, the relative importance RI is calculated as the gradient of an input variable g_a divided by the sum of the gradients.

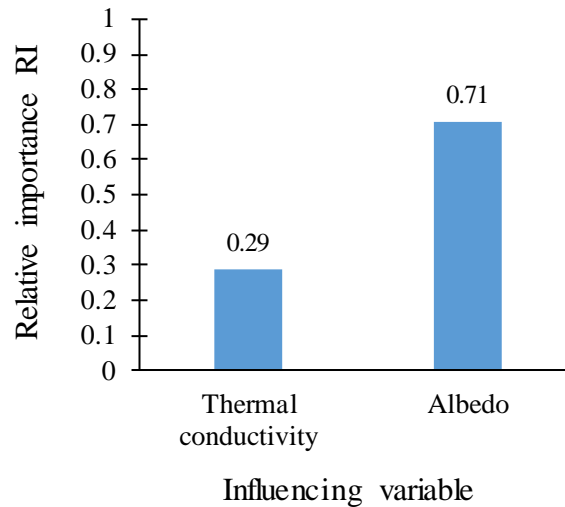


Fig. 15. Relative importance of input variables: thermal conductivity and albedo.

Fig. 15 shows that the relative importance of thermal conductivity is less than that of albedo. The albedo has a greater influence on the surface temperature of the pervious concrete during the day than thermal conductivity. These results are similar to those obtained by Gui et al. [66], who studied the impact of thermophysical properties (albedo, emissivity, diffusivity, volumetric heat capacity and thermal conductivity) on the surface temperature of asphalt pavements using a one-dimensional mathematical model based on the fundamental energy balance. The calculation of the relative importance based on the results of the temperature gradient with regard to albedo and thermal conductivity shows that the RI of albedo = 0.7 while the RI of thermal conductivity = 0.3. It was deduced that the maximum surface temperature of pervious concrete pavements and conventional asphalt pavements have the same sensitivity to the variation of albedo and thermal conductivity during daytime heat waves.

7. Conclusion

The main goal of the current study was to investigate the thermal behavior of pervious concrete and to quantify the influence of thermophysical parameters on the surface temperature under dry conditions in the laboratory. The results of the model were validated experimentally using an innovative experimental bench that allows the complete energy balance of a pavement to be established.

The results show that PC is up to 6°C warmer than OC during the diurnal period, and up to 4°C cooler at night. In addition, increasing the thermal conductivity of PC is only beneficial during the diurnal period since increasing the thermal conductivity from 0.473 to 0.835 $\text{W.m}^{-1}.\text{K}^{-1}$ made its maximum surface temperature 1.6°C lower during the day but warmer at night. On the other hand, increasing the albedo of the PC limits the UHI effect during both the diurnal and nocturnal periods: increasing the albedo from 0.15 to 0.35 made its surface temperature 4°C lower during the day and cooler during the night as well. The sensitivity study showed that the surface temperature of the PC is more sensitive to the albedo than to the thermal conductivity. Therefore, the albedo is to be prioritized in the design of cool pervious-concrete pavements.

This study has potential limitations. The model did not take account of the effect of the variation of thermal conductivity and albedo on the PC emissivity value which may influence the accuracy of the results obtained. In addition, an experimental field study using samples with larger dimensions under real metrological conditions is necessary to make certain of the results obtained.

From a practical point of view, it is possible to optimize the design of pervious concrete to reduce its maximum surface temperature in dry conditions without resorting to other techniques such as painting the pavement or adding products to increase thermal conductivity (e.g. steel fibers) or albedo (e.g. infrared reflective pigments). This optimization can be achieved by using light-colored binder and aggregates (increasing the albedo), finer aggregates (less rough surface) and having a higher thermal conductivity (e.g. quartzite).

Following this preliminary work, future complementary tests with this experimental bench will focus on assessing the effect of different factors (albedo, porosity, thermal conductivity and capillary absorption coefficient, water content) on the thermal behavior of pervious concrete under wet conditions. In addition, since the influence of pore characteristics (size, distribution, connectivity and tortuosity) on the hydraulic and mechanical properties of pervious concrete has been extensively studied, their influence on the thermal behavior of pervious concrete under dry and wet conditions should also be investigated. The objective is to design a cool pervious concrete pavement that has high mechanical strength whilst still serving its primary function of stormwater management. Finally, it would be interesting to develop a pervious concrete that has several properties of cool pavements such as a reflective and evaporative pervious concrete pavement with high thermal conductivity.

Appendix A. Experimental bench

Fig. A1 shows the experimental bench that has been designed for this experiment occupied by several devices.

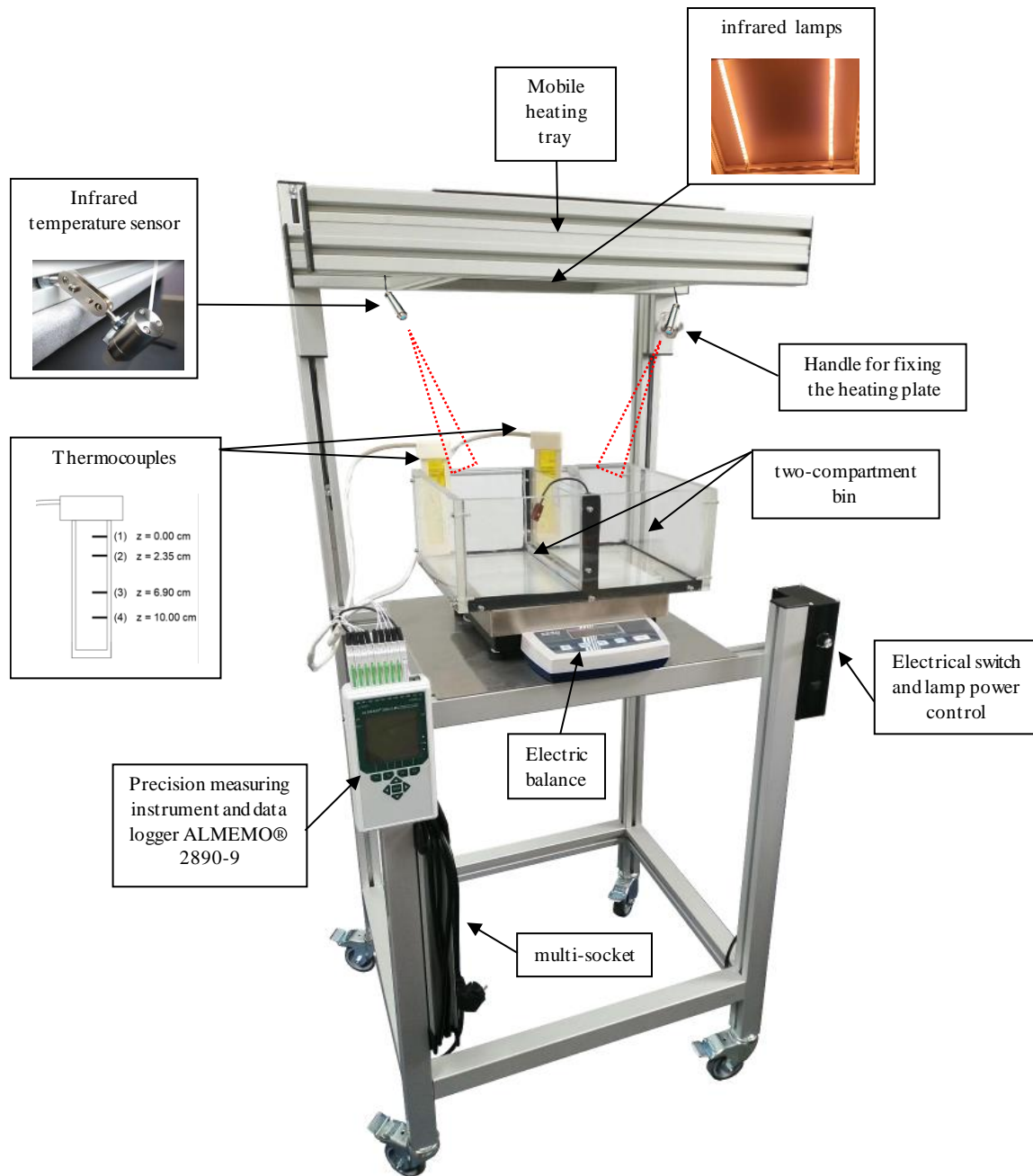


Fig. A1. Presentation of the experimental bench.

Fig. A2 shows an excerpt from the data sheet concerning the measuring beam.

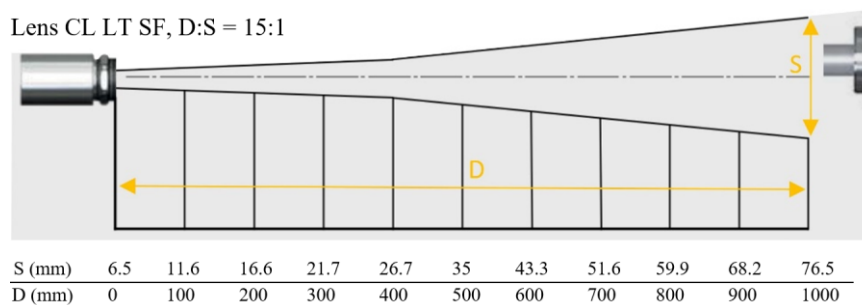


Fig. A2. Measuring beam of infrared temperature sensors. D is the distance between the sensor and the measuring surface and S is the diameter of the measuring beam.

Appendix B. Experimental setup

Fig. B1 shows the different energy fluxes in the case of this laboratory study.

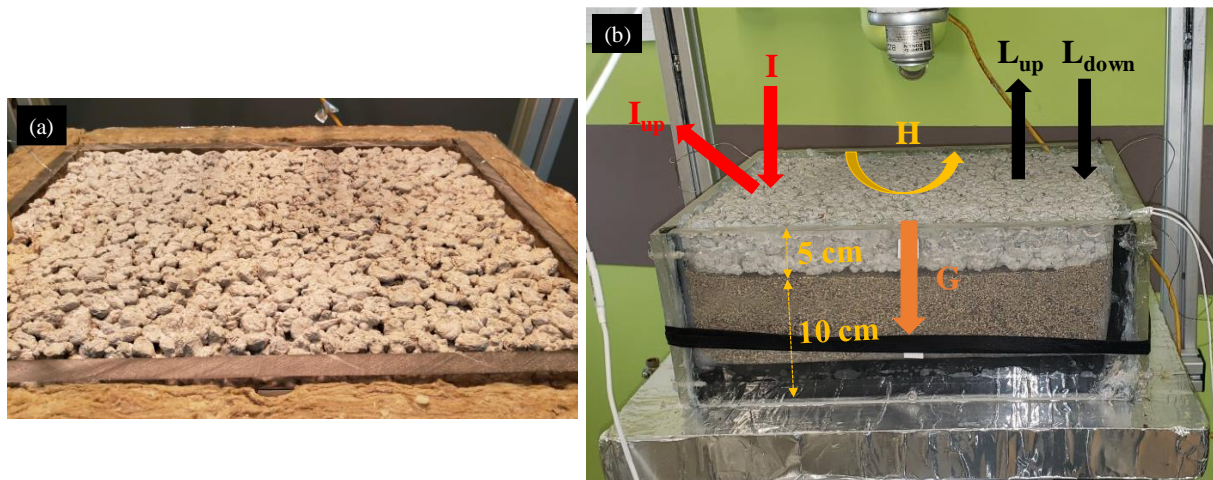


Fig. B1. The setup of the pervious concrete in the insulated bin during the daytime period (a) and the energy flows in the case of our study (description in section 2) and the dimensions of the pavement layers (b).

Bibliography

- [1] M. Carpio, Á. González, M. González, and K. Verichev, “Influence of pavements on the urban heat island phenomenon: A scientific evolution analysis”, *Energy Build.*, vol. 226, p. 110379, 2020.
- [2] M. Taleghani, “Outdoor thermal comfort by different heat mitigation strategies-A review”, *Renew. Sustain. Energy Rev.*, vol. 81, pp. 2011–2018, 2018.
- [3] Y. Shi and Y. Zhang, “Urban morphological indicators of urban heat and moisture islands under various sky conditions in a humid subtropical region”, *Build. Environ.*, vol. 214, p. 108906, 2022.
- [4] A. Mohajerani, J. Bakaric, and T. Jeffrey-Bailey, “The urban heat island effect, its causes, and mitigation, with reference to the thermal properties of asphalt concrete”, *J. Environ. Manage.*, vol. 197, pp. 522–538, 2017.
- [5] M. Hendel, S. Parison, A. Grados, and L. Royon, “Which pavement structures are best suited to limiting the UHI effect? A laboratory-scale study of Parisian pavement structures”, *Build. Environ.*, vol. 144, pp. 216–229, 2018.
- [6] A. A. Shamsipour, G. Azizi, M. K. Ahmadabad, and M. Moghbel, “Surface temperature pattern of asphalt, soil and grass in different weather condition”, *J. Biodivers. Environ. Sci.*, vol. 3, pp. 80–89, 2013.
- [7] R. Bouzoudja et al., “Experimental Comparative Study between Conventional and Green Parking Lots: Analysis of Subsurface Thermal Behavior under Warm and Dry Summer Conditions”, *Atmosphere (Basel)*, vol. 12, no. 8, p. 994, 2021.
- [8] M. Santamouris, “Using cool pavements as a mitigation strategy to fight urban heat island—A review of the actual developments”, *Renew. Sustain. Energy Rev.*, vol. 26, pp. 224–240, 2013.
- [9] Y. Qin and J. E. Hiller, “Understanding pavement-surface energy balance and its implications on cool pavement development”, *Energy Build.*, vol. 85, pp. 389–399, 2014.
- [10] C. Wang, Z.-H. Wang, K. E. Kaloush, and J. Shacat, “Cool pavements for urban heat island mitigation: A synthetic review”, *Renew. Sustain. Energy Rev.*, vol. 146, p. 111171, 2021.
- [11] H. Takebayashi and M. Moriyama, “Study on the urban heat island mitigation effect achieved by converting to grass-covered parking”, *Sol. Energy*, vol. 83, no. 8, pp. 1211–1223, 2009.
- [12] Y. Liu, T. Li, and L. Yu, “Urban heat island mitigation and hydrology performance of innovative permeable pavement: A pilot-scale study”, *J. Clean. Prod.*, vol. 244, p. 118938, 2020.
- [13] Y. Qin and J. E. Hiller, “Water availability near the surface dominates the evaporation of pervious concrete”, *Constr. Build. Mater.*, vol. 111, pp. 77–84, 2016.
- [14] L. Gao, Z. Wang, J. Xie, Y. Liu, and S. Jia, “Simulation of the cooling effect of porous asphalt pavement with different air voids”, *Appl. Sci.*, vol. 9, no. 18, p. 3659, 2019.
- [15] Y. Shimazaki, M. Aoki, K. Karaki, and A. Yoshida, “Improving outdoor human-thermal environment by optimizing the reflectance of water-retaining pavement through subjective field-based measurements”, *Build. Environ.*, vol. 210, p. 108695, 2022.

- [16] O. AlShareedah and S. Nassiri, "Pervious concrete mixture optimization, physical, and mechanical properties and pavement design: A review", *J. Clean. Prod.*, vol. 288, p. 125095, 2021.
- [17] K. Seifeddine, S. Amziane, and E. Toussaint, "State of the art on the mechanical properties of pervious concrete", *Eur. J. Environ. Civ. Eng.*, pp. 1–29, 2021.
- [18] S. Park, S. Ju, H.-K. Kim, Y.-S. Seo, and S. Pyo, "Effect of the rheological properties of fresh binder on the compressive strength of pervious concrete", *J. Mater. Res. Technol.*, 2022.
- [19] H.-Q. Nguyen, B.-V. Tran, and T.-S. Vu, "Numerical approach to predict the flexural damage behavior of pervious concrete", *Case Stud. Constr. Mater.*, vol. 16, p. e00946, 2022.
- [20] D. Li et al., "Application of polymer, silica-fume and crushed rubber in the production of Pervious concrete", *Smart Struct. Syst.*, vol. 23, no. 2, pp. 207–214, 2019.
- [21] A. Singh, K. P. Biligiri, and P. V. Sampath, "Development of framework for ranking pervious concrete pavement mixtures: application of multi-criteria decision-making methods", *Int. J. Pavement Eng.*, pp. 1–14, 2022.
- [22] A. Singh, K. P. Biligiri, and P. V. Sampath, "Engineering properties and lifecycle impacts of Pervious All-Road All-weather Multilayered pavement", *Resour. Conserv. Recycl.*, vol. 180, p. 106186, 2022.
- [23] V.-H. Vu, B.-V. Tran, B.-A. Le, and H.-Q. Nguyen, "Prediction of the relationship between strength and porosity of pervious concrete: A micromechanical investigation", *Mech. Res. Commun.*, vol. 118, p. 103791, 2021.
- [24] S. K. Pradhan and N. Behera, "Performance assessment of pervious concrete road on strength and permeability by using silica fume", *Mater. Today Proc.*, 2022.
- [25] O. AlShareedah and S. Nassiri, "Spherical discrete element model for estimating the hydraulic conductivity and pore clogging of pervious concrete", *Constr. Build. Mater.*, vol. 305, p. 124749, 2021.
- [26] L. G. Li et al., "Effects of aggregate bulking and film thicknesses on water permeability and strength of pervious concrete", *Powder Technol.*, vol. 396, pp. 743–753, 2022.
- [27] J. Shan, Y. Zhang, S. Wu, Z. Lin, L. Li, and Q. Wu, "Pore characteristics of pervious concrete and their influence on permeability attributes", *Constr. Build. Mater.*, vol. 327, p. 126874, 2022.
- [28] P. Mehrabi et al., "Effect of pumice powder and nano-clay on the strength and permeability of fiber-reinforced pervious concrete incorporating recycled concrete aggregate", *Constr. Build. Mater.*, vol. 287, p. 122652, 2021.
- [29] A. Joshaghani, A. Moazenian, and R. A. Shuaibu, "Experimental study on the use of trass as a supplementary cementitious material in pervious concrete", *J. Environ. Sci. Eng. A*, vol. 1, pp. 39–52, 2017.
- [30] A. Togholi, M. Shariati, M. R. Karim, and Z. Ibrahim, "Investigation on composite polymer and silica fume-rubber aggregate pervious concrete", *Proceedings of the 5th International Conference on Advances in Civil, Structural and Mechanical Engineering-CSM*, 2017.
- [31] J. Wang, Q. Meng, K. Tan, L. Zhang, and Y. Zhang, "Experimental investigation on the influence of evaporative cooling of permeable pavements on outdoor thermal environment", *Build. Environ.*, vol. 140, no. January, pp. 184–193, 2018.
- [32] A. K. Chandrappa and K. P. Biligiri, "Development of pavement-surface temperature predictive models: Parametric approach", *J. Mater. Civ. Eng.*, vol. 28, no. 3, p. 4015143, 2016.
- [33] M. Shariati, S. M. Davoodnabi, A. Togholi, Z. Kong, and A. Shariati, "Hybridization of metaheuristic algorithms with adaptive neuro-fuzzy inference system to predict load-slip behavior of angle shear connectors at elevated temperatures", *Compos. Struct.*, vol. 278, p. 114524, 2021.
- [34] K. Nouri, N. R. Sulong, Z. Ibrahim, and M. Shariati, "Behaviour of novel stiffened angle shear connectors at ambient and elevated temperatures", *Adv. Steel Constr.*, vol. 17, no. 1, pp. 28–38, 2021.
- [35] M. Shariati et al., "Application of Extreme Learning Machine (ELM) and Genetic Programming (GP) to design steel-concrete composite floor systems at elevated temperatures", *Steel Compos. Struct.*, vol. 33, no. 3, pp. 319–332, 2019.
- [36] S. Shahabi, N. Sulong, M. Shariati, and S. Shah, "Performance of shear connectors at elevated temperatures-A review", *Steel Compos. Struct.*, vol. 20, no. 1, pp. 185–203, 2016.
- [37] S. M. Davoodnabi, S. M. Mirhosseini, and M. Shariati, "Analyzing shear strength of steel-concrete composite beam with angle connectors at elevated temperature using finite element method", *Steel Compos. Struct.*, vol. 40, no. 6, pp. 853–868, 2021.
- [38] K. K. Meena, A. K. Chandrappa, and K. P. Biligiri, "Comprehensive laboratory testing and evaluation of the evaporative cooling effect of pavement materials", *J. Test. Eval.*, vol. 45, no. 5, pp. 1650–1661, 2017.
- [39] Y. Qin, "A review on the development of cool pavements to mitigate urban heat island effect", *Renew. Sustain. energy Rev.*, vol. 52, pp. 445–459, 2015.
- [40] K. Tan, Y. Qin, T. Du, L. Li, L. Zhang, and J. Wang, "Biochar from waste biomass as hygroscopic filler for pervious concrete to improve evaporative cooling performance," *Constr. Build. Mater.*, vol. 287, p. 123078, 2021.
- [41] S. Parison, M. Hendel, A. Grados, and L. Royon, "Analysis of the heat budget of standard, cool and watered pavements under lab heat-wave conditions", *Energy Build.*, vol. 228, p. 110455, 2020.

- [42] S. Parison, M. Hendel, A. Grados, K. Jurski, and L. Royon, “A lab experiment for optimizing the cooling efficiency and the watering rate of pavement-watering”, *Urban Clim.*, vol. 31, p. 100543, 2020.
- [43] J. R. et al. . J. Ramachandran et al., “Spatial Estimation of Net Radiation by Surface Energy Balance Algorithm for Land in Lalgudi Block”, *Int. J. Agric. Sci. Res.*, vol. 9, no. 3, pp. 277–282, 2019.
- [44] W. Jürges, *Der Wärmeübergang an einer ebenen Wand*. Druck und Verlag von R. Oldenbourg, 1924.
- [45] L. M. Jiji, “Correlation equations: forced and free convection”, *Heat Convection*, Springer, 2009, pp. 387–435.
- [46] W. M. Rohsenow, J. P. Hartnett, and Y. I. Cho, *Handbook of heat transfer*, vol. 3. McGraw-Hill New York, 1998.
- [47] Y. Qin and J. E. Hiller, “Ways of formulating wind speed in heat convection significantly influencing pavement temperature prediction”, *Heat Mass Transf. und Stoffuebertragung*, vol. 49, no. 5, pp. 745–752, 2013.
- [48] D. P. Bentz, “A computer model to predict the surface temperature and time-of-wetness of concrete pavements and bridge decks”, 2000.
- [49] G. Guyot, *Climatologie de l’environnement. De la plante aux écosystèmes*. Elsevier Mason SAS, 1997
- [50] Y. Qin, J. E. Hiller, and D. Meng, “Linearity between pavement thermophysical properties and surface temperatures”, *J. Mater. Civ. Eng.*, vol. 31, no. 11, p. 4019262, 2019.
- [51] J. Chen, H. Wang, and P. Xie, “Pavement temperature prediction: Theoretical models and critical affecting factors”, *Appl. Therm. Eng.*, vol. 158, p. 113755, 2019.
- [52] A. ASTM, “Standard test method for relative density (specific gravity) and absorption of coarse aggregate”, ASTM West Conshohocken, PA, 2015.
- [53] A. ASTM, “C29 standard test method for bulk density (‘Unit Weight’) and voids in aggregate”, *Am. Soc. Test. Mater. Annu. Book*, Pennsylvania, USA, 2009.
- [54] NF EN ISO, “17892-4 reconnaissance et essais géotechniques - Essais de laboratoire sur les sols - Partie 4 : Détermination de la distribution granulométrie des particules”, AFNOR, 2018.
- [55] N. Neithalath, M. S. Sumanasooriya, and O. Deo, “Characterizing pore volume, sizes, and connectivity in pervious concretes for permeability prediction”, *Mater. Charact.*, vol. 61, no. 8, pp. 802–813, 2010.
- [56] N. Neithalath, J. Weiss, and J. Olek, “Characterizing enhanced porosity concrete using electrical impedance to predict acoustic and hydraulic performance”, *Cem. Concr. Res.*, vol. 36, no. 11, pp. 2074–2085, 2006.
- [57] EN NF, “12390-7 essais pour béton durci-Partie 7 : masse volumique du béton durci”, AFNOR, 2012.
- [58] NF EN, “12390-3 essais pour béton durci-Partie 3 : résistance à la compression des éprouvettes” AFNOR, vol. 3.
- [59] ASTM, “C1701 standard test method for infiltration rate of in place pervious concrete”, annual book of ASTM standards, ASTM International, West Conshohocken, PA.
- [60] H. Li, M. Kayhanian, and J. T. Harvey, “Comparative field permeability measurement of permeable pavements using ASTM C1701 and NCAT permeameter methods”, *J. Environ. Manage.*, vol. 118, pp. 144–152, 2013.
- [61] ASTM “E1918-06 standard test method for measuring solar reflectance of horizontal and low-sloped surfaces in the field”, ASTM International, West Conshohocken, PA, pp. 1–3. 2015.
- [62] R. Lu et al., “Temperature characteristics of permeable asphalt pavement: Field research”, *Constr. Build. Mater.*, vol. 332, p. 127379, 2022.
- [63] P. Berdahl, H. Akbari, J. Jacobs, and F. Klink, “Surface roughness effects on the solar reflectance of cool asphalt shingles”, *Sol. energy Mater. Sol. cells*, vol. 92, no. 4, pp. 482–489, 2008.
- [64] R. Zhang, G. Jiang, and J. Liang, “The Albedo of Pervious Cement Concrete Linearly Decreases with Porosity”, *Adv. Mater. Sci. Eng.*, vol. 2015, 2015.
- [65] S. R. O. Aletba et al., “Thermal performance of cooling strategies for asphalt pavement: a state-of-the-art review”, *J. Traffic Transp. Eng. (English Edition)*, vol. 8, no. 3, pp. 356–373, 2021.
- [66] J. Gui, P. E. Phelan, K. E. Kaloush, and J. S. Golden, “Impact of pavement thermophysical properties on surface temperatures”, *J. Mater. Civ. Eng.*, vol. 19, no. 8, pp. 683–690, 2007.
- [67] ASTM “D5930-97 standard test method for thermal conductivity of plastics by means of a transient line-source technique”, ASTM International, West Conshohocken, PA, USA, 2001.
- [68] J. Chen, H. Wang, P. Xie, and H. Najm, “Analysis of thermal conductivity of porous concrete using laboratory measurements and microstructure models”, *Constr. Build. Mater.*, vol. 218, pp. 90–98, 2019.
- [69] J.-X. Lu, X. Yan, P. He, and C. S. Poon, “Sustainable design of pervious concrete using waste glass and recycled concrete aggregate”, *J. Clean. Prod.*, vol. 234, pp. 1102–1112, 2019.
- [70] J. Chen, R. Chu, H. Wang, L. Zhang, X. Chen, and Y. Du, “Alleviating urban heat island effect using high-conductivity permeable concrete pavement”, *J. Clean. Prod.*, vol. 237, p. 117722, 2019.
- [71] P. Shen, H. Zheng, S. Liu, J.-X. Lu, and C. S. Poon, “Development of high-strength pervious concrete incorporated with high percentages of waste glass”, *Cem. Concr. Compos.*, vol. 114, p. 103790, 2020.

- [72] S. Nassiri and B. Nantasai, “Thermal conductivity of pervious concrete for various porosities”, *ACI Mater. J.*, vol. 114, no. 2, p. 265, 2017.
- [73] H. Li, J. T. Harvey, T. J. Holland, and M. Kayhanian, “The use of reflective and permeable pavements as a potential practice for heat island mitigation and stormwater management”, *Environ. Res. Lett.*, vol. 8, no. 1, p. 15023, 2013.
- [74] T. R. Oke, *Boundary layer climates*. Routledge, 2002.
- [75] A. Singh, P. V. Sampath, and K. P. Biligiri, “A review of sustainable pervious concrete systems: Emphasis on clogging, material characterization, and environmental aspects”, *Constr. Build. Mater.*, vol. 261, p. 120491, 2020.
- [76] J. Chen, H. Wang, and H. Zhu, “Analytical approach for evaluating temperature field of thermal modified asphalt pavement and urban heat island effect”, *Appl. Therm. Eng.*, vol. 113, pp. 739–748, 2017.
- [77] M. Marceau and M. G. Van Geem, *Solar reflectance of concretes for LEED sustainable sites credit: heat island effect*. Portland Cement Association, 2007.
- [78] P. Cortez and M. J. Embrechts, “Using sensitivity analysis and visualization techniques to open black box data mining models”, *Inf. Sci. (Ny)*, vol. 225, pp. 1–17, 2013, doi: 10.1016/j.ins.2012.10.039.
- [79] J. Sun, J. Zhang, Y. Gu, Y. Huang, Y. Sun, and G. Ma, “Prediction of permeability and unconfined compressive strength of pervious concrete using evolved support vector regression”, *Constr. Build. Mater.*, vol. 207, pp. 440–449, 2019.
- [80] P. Cortez and M. J. Embrechts, “Opening black box data mining models using sensitivity analysis”, in *2011 IEEE Symposium on Computational Intelligence and Data Mining (CIDM)*, 2011, pp. 341–348.

Chapter VI Thermal behavior of pervious concrete in wet conditions

Article soumis au journal : Materials and Structures



Résumé et objectif

Après avoir étudié le comportement thermique du béton drainant (BD) en condition sèche (chapitre 5), ce chapitre présente une étude sur le comportement thermique du BD en condition humide en laboratoire. Dans le chapitre 3, il a été montré que le béton drainant peut-être rafraichissant à condition qu'il soit humide. Cet effet peut durer de 12 à 24 h maximum en raison de ses faibles propriétés d'absorption et de rétention d'eau. Par conséquent, le BD ne peut pas répondre efficacement aux besoins de refroidissement par évaporation. L'étude présentée dans le chapitre 4 a montré que les revêtements perméables à base de pouzzolane présentent un effet de refroidissement par évaporation plus important que à celles à base de gravier. Cette étude a fourni l'idée d'utiliser les granulats de pouzzolane dans le BD dans le but d'améliorer son effet absorbant ce qui pourra améliorer aussi l'effet de refroidissement par rapport au BD conventionnel à base de granulats dense. Le travail présenté dans ce chapitre est la première étude qui étudie le comportement thermique du BD à base des agrégats légers en condition humide. Trois types de BD ont été fabriqués : BD à base de gravier (BDG) et BD à base de pouzzolane (BDP1) ayant presque la même distribution granulométrique, et BD à base de pouzzolane moins grossière avec une distribution granulométrique monodispersée (BDP2).

Les résultats montrent qu'en condition sèche, la température maximale de surface du BDP2 est supérieure à celle du BDP1 et du BDG en raison de la faible conductivité thermique des granulats pouzzolaniques. L'utilisation de granulats légers dans le mélange de béton perméable doit être évitée en conditions sèches.

L'essai d'immersion partielle montre que l'utilisation de granulats légers et moins grossiers peut augmenter la surface spécifique et améliorer les propriétés d'absorption du BD. Le coefficient d'absorption capillaire du BDP2 est largement plus élevé que celui du BDG tandis que sa teneur en eau capillaire est également bien plus élevée que celle du BDG. De plus, L'absorption d'eau capillaire affecte de manière significative le phénomène d'évaporation du BD. L'utilisation de granulats pouzzolaniques moins grossiers améliore la structure de l'interstice capillaire interne et assure la continuité hydraulique sur une longue distance. En condition humide, après 5 jours, la masse totale d'eau évaporée du BDP2 est 40% plus élevée que celle du BDP1 et 77% plus élevée que celle du BDG en raison de sa porosité ouverte élevée et de sa grande capacité d'absorption et de rétention d'eau. Par conséquent, le taux d'évaporation de l'échantillon BDP2 est plus élevé pendant les périodes diurnes et nocturnes tout au long de l'expérience par rapport aux autres revêtements perméables.

La température de surface maximale du BDP2 pendant 5 jours en condition humide est inférieure à celle du BDG, de jour comme de nuit. Ce type de BD est plus efficace pour réduire

les effets des îlots de chaleur urbains diurnes et nocturnes que le BD ordinaire à base de granulats denses.

La différence entre la température de surface à l'état sec et à l'état humide du BDG diminue fortement entre le premier et le dernier jour de l'essai. La différence de température est plus significative pour le BDP2 en raison de son flux d'évaporation plus élevé que celui du BDG. Après 5 jours d'expérience, le BDP2 a ainsi pu réduire sa température de 18% en condition sèche alors que sa teneur en eau était supérieure à 6%, la chaussée n'était pas donc complètement sèche en volume. Cela signifie que la présence d'eau près de la surface est un facteur clé qui contrôle le flux d'évaporation et l'effet de refroidissement dans le BD. De plus, l'arrosage périodique est un facteur essentiel pour assurer un effet de refroidissement plus important sur une plus longue période.

Le vent a un fort impact sur le coefficient de convection thermique et sur l'échange de chaleur sensible entre les chaussées et l'air. Dans cette étude, en raison des limitations de l'équipement expérimental et de l'absence d'un dispositif précis de contrôle de la vitesse du vent, l'étude du comportement thermique a été réalisée dans des conditions climatiques contrôlées en laboratoire, en l'absence de vent (convection naturelle). Cependant, comme les chaussées perméables sont de plus en plus utilisées dans le monde pour atténuer les îlots de chaleur urbains, l'évaluation de l'effet de refroidissement de ces chaussées dans diverses conditions climatiques devrait être étudiée plus en détail. En outre, il est important de se concentrer sur la conception des mélanges du BD afin d'optimiser leurs propriétés d'absorption d'eau et d'améliorer l'effet capillaire pour augmenter le taux d'évaporation et maximiser l'effet de refroidissement.

Khaled Seifeddine ^a, Sofiane Amziane ^a, Evelyne Toussaint ^a

^a Université Clermont Auvergne, CNRS, SIGMA Clermont, Institut Pascal, F-63000 Clermont-Ferrand, France.

Highlights

- The hygrothermal properties of pozzolan and gravel-based pervious concrete (PC) have been studied.
- Factors that influence the cooling effect of PC have been studied.
- The use of pozzolan aggregates can improve the water-absorption properties of PC.
- Pozzolan-based PC has proven to have better cooling performance than gravel-based PC.

Keywords

Urban heat island; Pervious concrete; Lightweight aggregates; Water-absorption properties; Cooling effect.

1 Introduction

The continuous development of urbanization stemming from socio-economic development, and the burgeoning world population, is a significant contributor to climate and environmental change [1]. This urban development has led to the emergence of urban heat islands (UHIs) – a phenomenon characterized by the fact that urban areas are often warmer than the surrounding rural areas, especially during heat waves [2]. Many factors are behind this phenomenon. The most significant ones are the complex geometry of the urban environment, the use of building materials, anthropogenic heat emissions and the reduction of vegetation [3]. In particular, conventional impervious pavements (such as asphalt) have high thermal inertia and relatively low reflectivity [4]. These pavements can be warmer than natural vegetation during both the daytime and nighttime, due to the high absorption of incident solar radiation and their impermeable nature, which suppresses evapotranspiration [5].

There are several solutions to limit the formation of UHIs [6], such as optimizing urban morphology to promote heat dissipation and urban ventilation [7], decreasing anthropogenic heat [8], increasing urban vegetation [9], [10] and installing cool and green roofs, though this technique has little benefit for air temperature at pedestrian height [11]. Since pavements constitute 30-45% of the total surface area of cities [12], the use of cool pavements to mitigate UHIs is an interesting strategy in today's world. There are several types of cool pavements, such as reflective pavements [13], [14], heat storage modifying pavements [15]–[17] and evaporative permeable pavements [18], [19].

Pervious Concrete (PC) is among the most widely used types of permeable pavements. It was first discovered for use in construction 100 years ago in Europe [20]. It has become popular in recent years because of its contribution to stormwater management and sustainable development [21]. It is a special type of pavement with sufficient macro/micro pores that allows water to infiltrate into the soil with purification, and helps replenish natural water sources [22]. Due to its porous structure that allows water retention, this type of pavement has been advocated as a solution to reduce the effects of UHIs through cooling by evaporation [23], [24].

In dry conditions, PC has a higher surface temperature than asphalt during hot summer days [25]. Other studies have found that PC has a higher surface temperature during the day but a lower surface temperature with a higher cooling ratio than ordinary concrete during the night [26]–[28]. On the other hand, in wet conditions, Qin and Hiller [28] show that PC can be cooler than ordinary concrete for 12 to 24 hours. Due to the importance of the presence of water in permeable pavements, water-retentive filler has been used to improve the cooling effect of such pavements. Various materials have been used to improve the water-absorption properties of permeable pavements such as porous geopolymers [29], blast furnace slag [30], [31], steel by-products based on a silica compound [30], and allophane- and vermiculite-based materials [32]. In a recent study, Tan et al. [33] show that the use of 5% pulverized biochar particles as an admixture in the PC mixture increases the capillary water content from $100 \pm 2 \text{ kg/m}^3$ to $117 \pm 8 \text{ kg/m}^3$, and makes its surface temperature up to 6°C lower than that of PC without biochar.

In a previous study [26], the thermal behavior of PC and the influence of thermophysical factors on its surface temperature were investigated in detail, with the objective of decreasing its temperature in dry conditions. In this study, the thermal behavior of pozzolan-based PC was compared to that of conventional dense aggregate-based PC in dry and wet conditions under controlled laboratory weather conditions using an innovative experimental bench. This is the first study to investigate the improvement of the evaporative cooling effect of PC using lightweight pozzolan aggregates. These aggregates are characterized by a high water-absorption coefficient, and will be able to improve the absorption properties and cooling effect of PC. The factors affecting the evaporation rate and evaporative cooling effect were also investigated.

2. Materials and methods

2.1. Materials

Two types of natural aggregates were used in this study to fabricate the PC mixtures: gravel and pozzolan (Fig. 1). The water-absorption coefficient WA (%) of the aggregates was determined according to the procedure described in ASTM C127-15 [34]. The bulk density ρ_d (kg/m^3) was determined according to ASTM C29 [35]. The results of these tests are presented in Fig. 1.

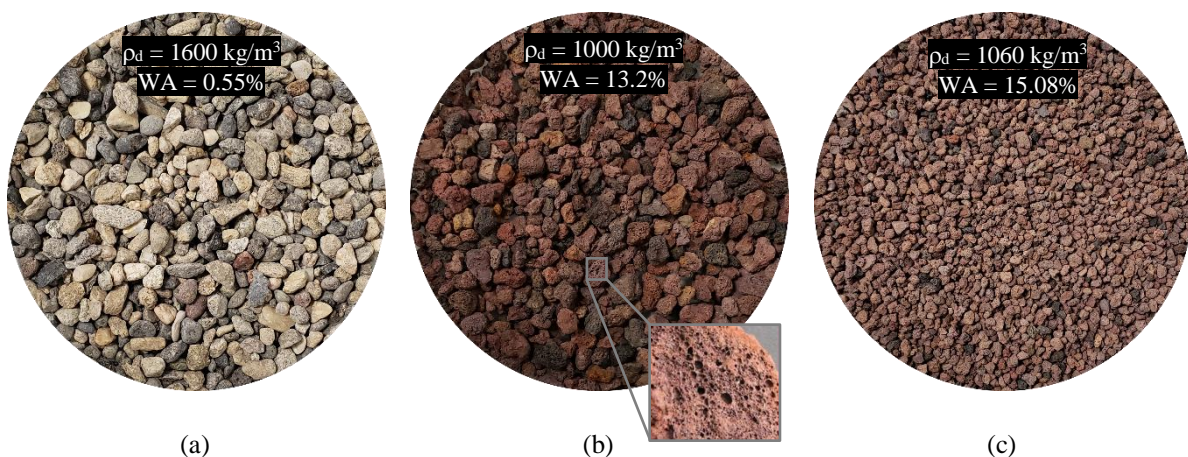


Fig. 1. Aggregates used in PC mixes: (a) gravel 'G', (b) pozzolan 'P1' and (c) pozzolan 'P2'.

The absorption coefficient of pozzolan particles (P1 and P2) is much higher than that of natural gravel (G) due to their high intergranular porosity (Fig. 1b), which allows them to retain a greater amount of water.

2.2. Experimental methods

2.2.1. Dosage and sample preparation

Table 1 shows the dosages of the gravel-based PC (PCG) and pozzolan (PCP1, PCP2) samples. An ordinary Portland cement CEM II/B-LL 32.5 R CE NF was used in all three mixes. The coarse aggregates used in the PCG and PCP1 mixtures have a particle size distribution between 5 and 12.5 mm. Those used in the PCP2 mix have a particle size distribution between 3.15 and 6 mm.

Table 1
Dosage of PC Mixtures.

Sample	Sand (kg/m ³)	Coarse aggregates (kg/m ³)	Cement (C) (kg/m ³)	Water (W) (kg/m ³)	W/C
PCG	0	1600	350	112	0.32
PCP1	0	1000	350	140	0.4
PCP2	0	1065	350	140	0.4

The particle size distributions of the aggregates used in the three mixtures are presented in Fig. 2. This test was performed by sieving (NF EN ISO17892-4 [36]). The selection of this granulometry facilitates the study of the influence of the type of aggregates (case of PCG and PCP1) and the size and specific surface of the aggregates (case of PCP1 and PCP2) on the thermal behavior of PC.

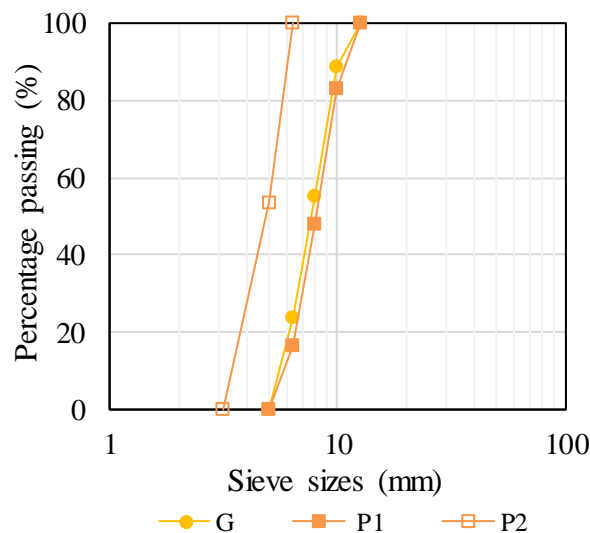


Fig. 2. Particle size distribution of the aggregates used: G, P1 and P2.

The PCG, PCP1 and PCP2 mixes were produced using a standard concrete mixer with a capacity of 300 liters. The coarse aggregates and the required amount of cement as well as a

small amount of water were mixed first. After a quick mixing of these materials, the remaining water was added progressively. Then, these mixtures were mixed for 3 minutes. Once the mixing was complete, they were poured in layers into prepared molds. Each layer was gently compacted with a rubber mallet. The samples were removed from the mold after 24 hours. They were then stored in water until the date of the tests.

3 types of samples were fabricated for each mix: 3 cylindrical samples (diameter = 16 cm and height = 32 cm) to measure compressive strength, density and open porosity; 2 parallelepiped samples (15×15×6 cm³) to measure thermal conductivity; and 1 parallelepiped sample (40×30×5 cm³) to measure permeability and cooling performance. The fabricated samples and their dimensions are shown in Fig. 3.

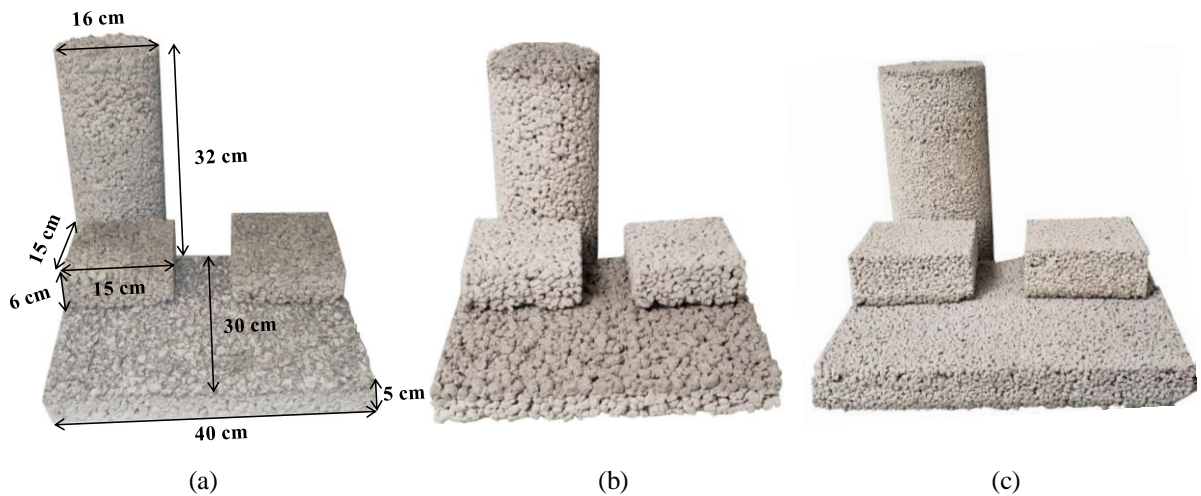


Fig. 3. Prepared samples: (a) PCG, (b) PCP1, (c) PCP2.

2.2.2. Porosity measurement

A methodology matching that of previous studies [37], [38] was used to measure the open porosity P_0 (%) of PC samples. It consists of filling all the interstices of a sample with water to correlate the open porosity with the total volume of water introduced. The cylindrical samples were covered with a PVC film and inserted into non-deformable cylindrical molds to ensure the PVC film did not suffer any deformation. Then, the mold and the sample inside were placed on a balance and water was added to fill the voids of the PC. Knowing the volume of the sample V_s (m³) and the volume of water V_w (m³), the open porosity was calculated using **Eq. (1)**.

$$P_0 = \frac{V_w}{V_s} \times 100 \quad (1)$$

When using this method, it is recommended to perform this test on at least 3 samples to measure open porosity [39], [40]. In this study, three samples of each PC mixture were tested at 28 days of age, which meets the requirements of this method.

2.2.3. Strength and permeability tests

The compressive strength at 28 days (R28d) of the samples was measured with reference to the standard NF EN 12390-3 [41].

The permeability of PC samples was measured using the standard method described in ASTM C 1701 [42]. This method determines the water infiltration rate (mm/h) of PC in the field by recording the time required for a certain volume of water to pass through a defined area of a pavement (**Eq. (2)**). In this study, PC pavers measuring $40 \times 30 \times 5 \text{ cm}^3$ were used to measure permeability.

$$I = \frac{\gamma M}{D^2 t} \quad (2)$$

where I (mm/h) = infiltration rate or permeability; M (kg) = infiltrated water mass; D (mm) = inner diameter of the infiltration ring; t (s) time required for the measured amount of water to infiltrate the pavement; γ (dimensionless) = 4,583,666,000 in SI units.

2.2.4. Tests to determine thermophysical properties

Albedo

The albedo is the reflectivity of a surface, which is the ratio of reflected light energy flux to incident light energy flux. It is a dimensionless. This characteristic was measured using a pyranometer in accordance with ASTM E1918 [43].

The tested pavers (PCG, PCP1 and PCP2) were dried in a ventilated oven at 105°C to obtain a constant mass. They were then cooled to laboratory room temperature. The pyranometer was then placed over the dry pavements to determine the radiative flux reflected from the surface. The incident shortwave radiative flux can be controlled, since the experimental bench (see Appendix A) is equipped with infrared lamps with a power control graduated from 0 to 100% (see [26]). As an example, 100% corresponds to the maximum power of the infrared lamps, which is 2000 W/m^2 (with respect to the position of the pavement under the infrared lamps) and 0% means that the lamps are completely switched off. The values of the radiative flux corresponding to each graduation were provided by the company that designed the experimental bench. These values were verified in the laboratory using a pyranometer. To measure the albedo accurately and avoid any influence by the other surrounding conditions, the bin in which the pavements were placed was covered with a black fabric having high solar absorption, in accordance with the experimental protocol employed by Chen et al. [44].

Emissivity

Emissivity is the ratio of the energy flux emitted by any body to the energy flux emitted by a black body of identical shape and temperature. A pyrgeometer was used to measure the emissivity of the PC pavements. It was placed above the pavements to measure the long-wave radiative flux emitted from the surface L_e (W/m^2) during a 1-hour period. By measuring the surface temperature of the pavements, the change in emissivity during this experiment was calculated by means of **Eq. (3)**.

$$\varepsilon_s = \frac{L_e}{T_s^4 \times \sigma} \quad (3)$$

where T_s (K) = surface temperature; σ ($\text{W}\cdot\text{m}^{-2}\cdot\text{K}^{-4}$) = Stefan–Boltzmann constant equal to 5.67×10^{-8} .

Thermal conductivity

The parallelepiped samples measuring $15 \times 15 \times 6 \text{ cm}^3$ were used to measure the thermal conductivity λ ($\text{W}\cdot\text{m}^{-1}\cdot\text{K}^{-1}$) of the PC pavements using a hot-wire conductivity meter, in line with ASTM D5930-97 [45].

2.2.5. Water absorption test

The water-absorption coefficient is an important property for permeable pavements as it expresses the rate of water absorption due to capillary forces. This coefficient has a significant effect on the heat- and mass-transfer of evaporative pavements. The water-absorption properties of PC pavements were determined by the partial immersion test, in keeping with ISO15148 [46] (Fig. 4).

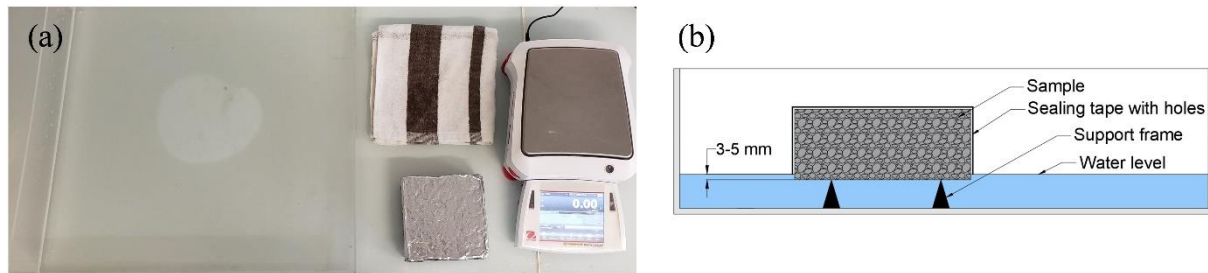


Fig. 4. Partial immersion test: (a) photograph and (b) diagram.

For each mixture, a parallelepipedal paver measuring $15 \times 15 \times 6 \text{ cm}^3$ was used. The pavers were dried in an oven at $110 \pm 5^\circ\text{C}$ until a constant mass was obtained. They were then stored in a room with controlled climatic conditions: $20^\circ\text{C} \geq \text{Ambient temperature} \leq 23^\circ\text{C}$; $35\% \geq \text{Relative humidity} \leq 40\%$. Subsequently, they were sealed with waterproof adhesive tape on all surfaces except the bottom surface. Small holes with a diameter of less than 1 mm and spaced less than 1 cm apart were made in the tape covering the top. The sample was placed in the water bin on supports to ensure a contact height of 3 to 5 mm between the base of the sample and the water, according to ASTM C1585-13 [46].

The specimen was removed from the water at regular time intervals; then its surface was wiped with a wet towel and its weight was determined with an electric balance (accuracy $\pm 0.01 \text{ g}$). Initially, the sampling interval was short (e.g. 5 s) and then a longer interval was chosen (e.g. 30 s, 1 min, 5 min, 30 min, 1 h, etc.). The cumulative capillary water absorption height i (mm) was calculated by means of Eq. (4). At the end of each test, the sample was dried again in the oven and subjected to two further tests.

$$i = \frac{M_{(t)}}{A \times \rho_{\text{water}}} \quad (4)$$

where $M_{(t)}$ (g) = gain in mass due to water absorption as a function of time; A (mm^2) = surface of the sample exposed to water; ρ_{water} (g/mm^3) = density of water.

2.2.6. Experimental setup to study the thermal behavior of pervious concrete

To investigate the thermal behavior of the PC samples, an innovative experimental bench (Appendix A) has been designed to study their thermal behavior in dry and wet conditions. This bench is equipped with several devices: a pyranometer to measure the albedo and the shortwave radiative fluxes; a pyrgeometer to measure the emissivity and the longwave radiative fluxes; temperature sensors to measure the surface temperature and the temperature at depth; infrared lamps to simulate the solar flux; and a balance to measure the mass of evaporated water over time. All these devices are connected to data-acquisition units that automatically record the data. All these devices establish a complete energy balance of a pavement in order to analyze the variation of different energy fluxes (see [26] for more information on the function of the experimental bench).

In order to simulate the real structure of a permeable pavement, the bin (Appendix A) was filled with a layer of sand (0.08–5 mm), representing the reservoir layer on which a PC pavement is laid. The dimensions of each layer are shown in Fig. 5. At the beginning of each experiment, the side walls of the bin were insulated with rockwool thermal insulation ($\lambda = 0.03 \text{ W}\cdot\text{m}^{-1}\cdot\text{K}^{-1}$) to ensure unidirectional heat transfer. The surface temperature at the center of the pavement was measured using an infrared temperature sensor placed on top of the bin. The temperatures at depth: $T_{5 \text{ cm}}$ (bottom side of the pavement) and $T_{15 \text{ cm}}$ (bottom of the bin) were measured by two temperature sensors inside the bin (Fig. 5c). To accurately measure the evaporated water mass through the PC pavements, the empty spaces between the side walls of the pavement and the side walls of the bin were sealed with a transparent silicone seal to eliminate lateral evaporation (Fig. 5a and 5b).



Fig. 5. The placement of PCP1 in the bin: (a) dry condition, (b) wet condition, (c) the dimensions of the complete PC pavement structure.

The experimental bench was placed in a room with controlled climatic conditions: $20^{\circ}\text{C} \geq$ ambient temperature $\leq 23^{\circ}\text{C}$; $35\% \geq$ relative humidity $\leq 40\%$. Table 2 shows the duration of the day phase (infrared lamps turned on) and the night phase (infrared lamps turned off) chosen to study the thermal behavior of the PC pavements in dry and wet conditions. This table also shows the values of the shortwave radiative fluxes (emitted by the infrared lamps) and the incident longwave radiative fluxes (emitted by all the materials surrounding the bin) during these two periods.

Table 2

Characteristics of the day and night phases during the experiment.

	Daytime phase	Nighttime phase
Duration	8 hours	16 hours
Incident radiation I (W/m^2)	520	0
Incident radiation L_{down} (W/m^2)	531	430

The following experimental protocol was adopted to study the thermal behavior of the pavements in dry and wet conditions: the power of the infrared lamps was adjusted at the beginning of each experiment to obtain the desired incident shortwave radiation (Table 2). The recording frequency of all sensors was set to one reading every two minutes. The first data recording was when the lamps were turned off. Immediately afterwards, the lamps were turned on using the switch, and left on for 8 hours, to study the thermal behavior of the pavements during the daytime period. At the end of this period, the lamps were turned off for 16 hours to study the thermal behavior of the pavements during the nighttime period. In wet conditions, the total mass of the sample decreases over time. This decrease corresponds to the mass of water evaporated. After 24 hours, all recordings were stopped and the data were harvested.

3. Results and discussions

3.1. Physical properties

Table 3

Open porosity, density, compressive strength and permeability of PC samples.

Sample	Open porosity (%)	Density (kg/m ³)	Compressive strength (MPa)	Permeability (cm/s)
PCG	21.97 ± 1.67	1951 ± 42.33	11.6 ± 0.460	1.30 ± 0.051
PCP1	22.67 ± 0.21	1592 ± 66.45	10.18 ± 0.580	1.37 ± 0.050
PCP2	27.27 ± 0.25	1584 ± 94.03	8.03 ± 0.369	1.67 ± 0.059

Table 3 shows that the average open porosity of PCP1 is 3.2% higher than that of PCG. The main reason behind this small deviation is that these two mixtures are fabricated using aggregates with almost the same particle size distribution (see Fig. 2). However, the open porosity of PCP2 is 20.3% higher than that of PCP1, the latter being made with coarser pozzolan aggregates. Indeed, the aggregates of the P1 pozzolan (5-12.5 mm) have a more widely dispersed grain size than those of the P2 pozzolan (3.15-6 mm); P2 has a monodisperse formulation, which increases the percentage of pores in the PC structure.

The average compressive strength (3 samples/mix) of the three PC pavements is presented in Table 3. The average compressive strength of PCG is 13.9% greater than that of PCP1 and 44.5% greater than that of PCP2. Indeed, the mechanical strength of PCP1 and PCP2 is affected by the low mechanical strength of pozzolan grains and their low densities. Fig. 6 shows that the compressive strength of the PC samples decreases linearly with increasing open porosity, which is in keeping with the results found by Sahdeo et al. [47] and Kevern et al. [48].

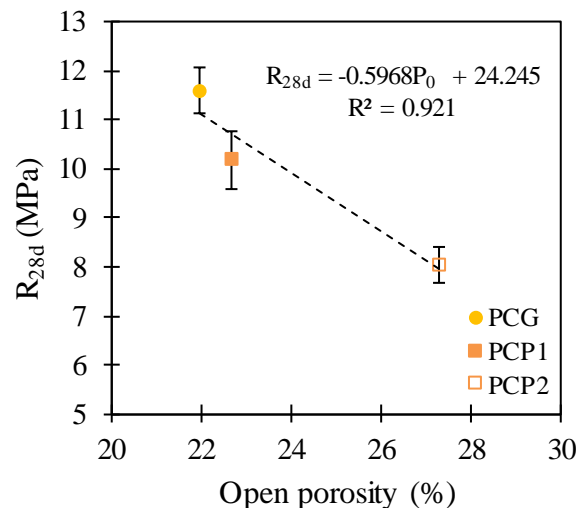


Fig. 6. Variation in compressive strength of PC samples as a function of open porosity.

The permeability results (3 measurements/sample) are presented in Table 3. The permeability of the PC must be higher than 0.054 mm.s⁻¹ which is a critical value, beyond which a concrete can be qualified as pervious [49]. In addition, to avoid the risk of clogging, the minimum permeability must be higher than or equal to 1 mm.s⁻¹ [50]. The results show that PCG, PCP1

and PCP2 all have a permeability well above the critical values. They are therefore able to perform their main function: stormwater management.

The deviation between the permeability of PCG and PCP1 is 0.07 cm/s as they have almost the same open porosity and the aggregates used in these two mixtures have almost the same particle size distribution. Meanwhile, the permeability of PCP2 is 21.9% higher than that of PCP1 and 28.5% higher than that of PCG. The main reasons are the high open porosity of PCP2 and the uniform granulometry of the aggregates used in this mix, leading to a less tortuous pore network which allows faster infiltration of water through the pavement.

Fig. 7 shows that the permeability of PC increases in linear fashion with increasing open porosity, which is in agreement with the results of several prior studies [51]–[53]. The correlation coefficient of the permeability–open porosity curve ($R^2 = 0.997$) is higher than that of the compressive strength–open porosity curve ($R^2 = 0.921$). Indeed, the mechanical strength of PC is more closely related to the total porosity than to the open porosity [54] because the total porosity includes all types of pores: inter-granular porosity + aggregate porosity + cement paste porosity + transition zone porosity [55].

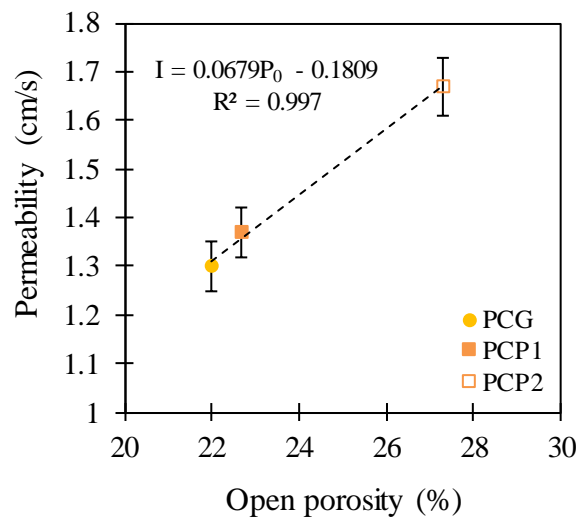


Fig. 7. Variation in permeability of PC pavements as a function of open porosity.

Table 4 shows the average measured albedo values (3 measurements/pavement). Fig. 8 shows that the three pavers have the same gray color, as the cement dominates the color of the pavements, while the results show that the albedo of PCP2 is 5% higher than that of PCG and 8.1% higher than that of PCP1. This increase in albedo is mainly due to the low roughness of PCP2, which is manufactured using less coarse aggregates than those used in the other two pavements. These results contradict those found by Zhang et al. [56] who show that the albedo of PC decreases linearly from 0.39 to 0.26 when the porosity varies from 7 to 32.4%. Indeed, larger porosity do not always lead to larger pore sizes and higher roughness (as in the cases of PCP1 and PCP2). It was deduced that porosity is an insufficient factor to predict the albedo of PC, which is more closely related to pore characteristics such as size, shape and distribution.

Table 4

Albedo, emissivity and thermal conductivity of PC pavements.

Sample	Albedo (dimensionless)	Emissivity (dimensionless)	Thermal conductivity (W.m ⁻¹ .K ⁻¹)
PCG	0.203 ± 0.007	0.877 ± 0.005	0.613 ± 0.018
PCP1	0.197 ± 0.005	0.892 ± 0.004	0.549 ± 0.010
PCP2	0.213 ± 0.007	0.902 ± 0.004	0.452 ± 0.0147

Fig. 8 shows the variation in emissivity of PC pavements as a function of time. 31 emissivity values were calculated. The results show that the average emissivity values of the three pavements are: $\varepsilon_s = 0.877 \pm 0.005$ for PCG, $\varepsilon_s = 0.892 \pm 0.004$ for PCP1 and $\varepsilon_s = 0.902 \pm 0.004$ for PCP2.

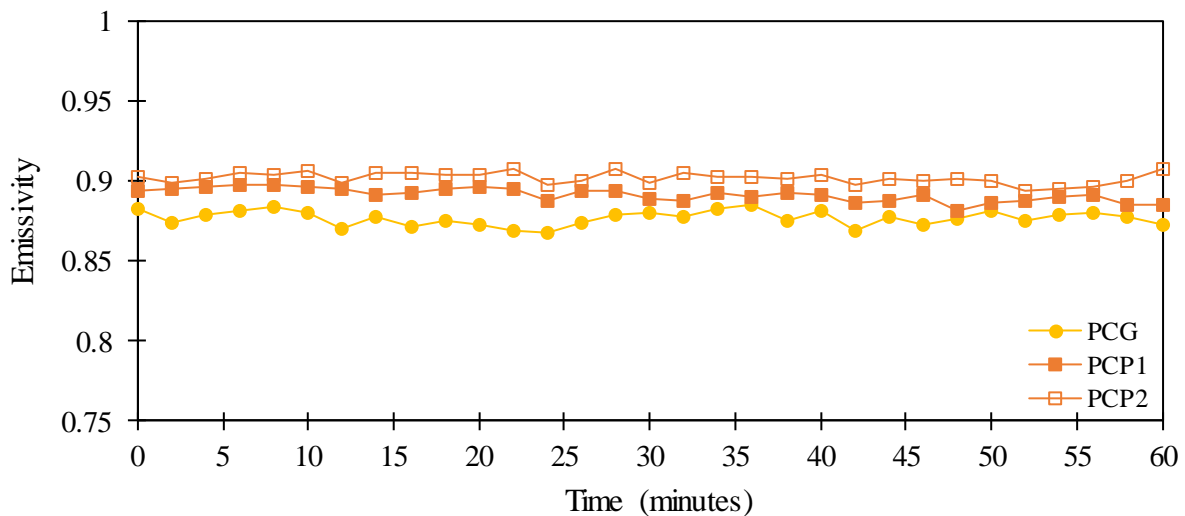


Fig. 8. Variation in emissivity of the pavements (PCG, PCP1 and PCP2) as a function of time.

As regards the thermal conductivity of the PC pavements, 5 measurements were performed for each type of PC in 5 different locations. The results obtained (Table 4) are in agreement with those found by Chen et al. [57], who show that the thermal conductivity of PC decreases with increasing porosity. Moreover, the thermal conductivity of PCP1 is 11.5% lower than that of PCG while its open porosity is slightly lower than that of PCP1. Indeed, this decrease is also attributable to the low thermal conductivity of pozzolanic aggregate ($\lambda = 0.141 \text{ W.m}^{-1}.\text{K}^{-1}$, ASTM C518 [58]), which is a lightweight aggregate with high intragranular porosity compared to gravel which is a denser aggregate with higher thermal conductivity ($\lambda = 0.179 \text{ W.m}^{-1}.\text{K}^{-1}$, ASTM C518). This means that with the same value of open porosity, the thermal conductivity of PC can vary depending on the type of aggregate used in the mix.

3.2. Water-absorption properties

Fig. 9 shows the variation of the cumulative capillary absorption height of PCG, PCP1 and PCP2 samples. This figure shows that the capillary absorption process of each type of sample can be divided into three stages. The first is the capillary absorption stage. During this stage, the absorption is governed by capillary and viscous forces, and the water front gradually approaches the upper surface of the sample. The absorption coefficient A_{cap} (mm/s^{0.5}) can be calculated by linear regression of the slope of this stage [59]. The second stage corresponds to

the transition process, during which water continuously fills the small pores of the sample until the point of capillary saturation. The capillary water content W_{cap} (kg/m^3) corresponds to the mass water content of the samples after the transition stage [60]. The final stage corresponds to the air diffusion process (Fig. 9), when the water reaches the upper surface of the sample. Any slight increase in water content during this period may be caused by the dissolution and removal of air trapped in the water.

Fig. 9 shows that the change in the cumulative capillary absorption height of all PC samples is fast during the first stage and slow during the other two.

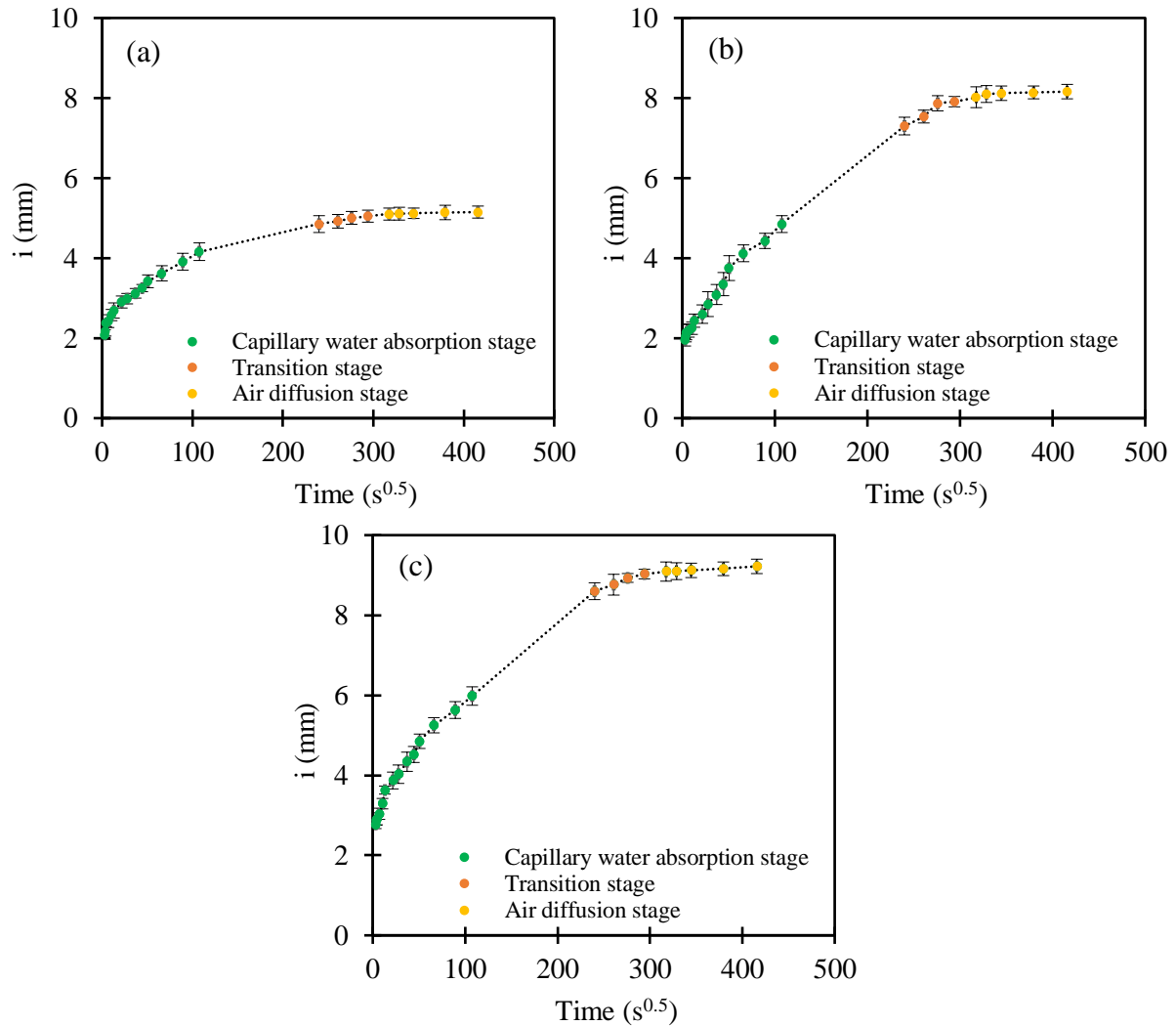


Fig. 9. Variation in cumulative capillary water-absorption height of PC samples as a function of time: (a) for PCG, (b) for PCP1 and (c) for PCP2.

The water-absorption properties of PCG and those obtained in other studies [33], [59] that performed similar tests on PC based on dense aggregates are presented in Table 5. The open porosities of the PC samples tested in these two studies are similar to those obtained in this experiment. This table shows that PC has a low absorption coefficient and low capillary water content. The deviation between the results could be related to several factors: the type of aggregates used, the density of each sample, the cement dosage, the degree of compaction, and the pore characteristics (size, shape and distribution), which have a direct influence on the water-absorption properties of PC.

Table 5

Water absorption properties of dense aggregate-based PC samples.

Study	Aggregate type	Aggregate size (mm)	Open porosity (%)	A_{cap} (mm/s ^{0.5})	W_{cap} (kg/m ³)
Experiment	Gravel	5–12.5	21.97 ± 1.67	0.0186 ± 0.0024	85.17 ± 2.49
Tan et al., 2021 [33]	Gravel and limestone	4.75–9.0	22.05 ± 0.11	0.0199 ± 0.0025	100.58 ± 6.62
Wang et al., 2019 [59]	-	5–10	22.86 ± 0.004	0.010 ± 0.007	97.33 ± 2.74

The absorption coefficient A_{cap} (mm/s^{0.5}) and capillary water content W_{cap} (kg/m³) of pozzolan-based PC samples are presented in Table 6. The PCP2 sample has the highest water-absorption coefficient which is 10% higher than PCP1 and 67% higher than PCG. Similarly, PCP2 has the highest capillary water content which is 13.38% higher than PCP1 and 78% higher than PCG. It is evident from these results that PCP2 can hold more water than the other two pavements in a shorter time. It was found that this sample is capable of a higher evaporation rate compared to the others and a more potent cooling effect as a consequence.

Table 6

Propriétés d'absorption d'eau des échantillons de béton drainant à base de pouzzolane.

Sample	A_{cap} (mm/s ^{0.5})	W_{cap} (kg/m ³)
PCP1	0.0283 ± 0.0036	133.61 ± 4.25
PCP2	0.0311 ± 0.0019	151.50 ± 4.02

The main factors that cause the differences in the water-absorption properties of these pavements studied are the type of aggregates used and the pore size. PCP2 is manufactured with less coarse aggregates which increases the contact surface between aggregates and water. Moreover, when the aggregate size decreases, the pore size decreases which increases the capillary suction capacity. The open porosity of PCP2 is also higher compared to the other two samples which contributed to a higher capillary water content. It should be noted that the micropores that are present in the pozzolan aggregate structure improved the absorption coefficient and capillary water content of PCP1 and PCP2 compared to PCG. On the other hand, the main factor ensuring water absorption for PCG was the hydrophilicity of the cement which explains why it has the lowest water-absorption coefficient.

3.3. Thermal behavior of PC pavements in dry conditions

Fig. 10 shows the variation in surface temperature of PC pavements as a function of time. The results show that in dry conditions, the surface temperature of PC pavements increases from: 23.5°C to 59°C for PCG, to 61.1°C for PCP1 and to 63°C for PCP2. The temperature of pozzolan-based PC pavements is higher than that of gravel-based PC. Since the difference between the albedo of these pavements is small, the main reason for this temperature increase is the low thermal conductivity of PCP1 and PCP2 compared to that of PCG (Table 4). Indeed, the lower the thermal conductivity, the less heat will be transferred to the interior of the pavement which leads to an increase in surface temperature during the diurnal period. On the other hand, during the nocturnal period, the difference between the surface temperature of these three pavements is not significant.

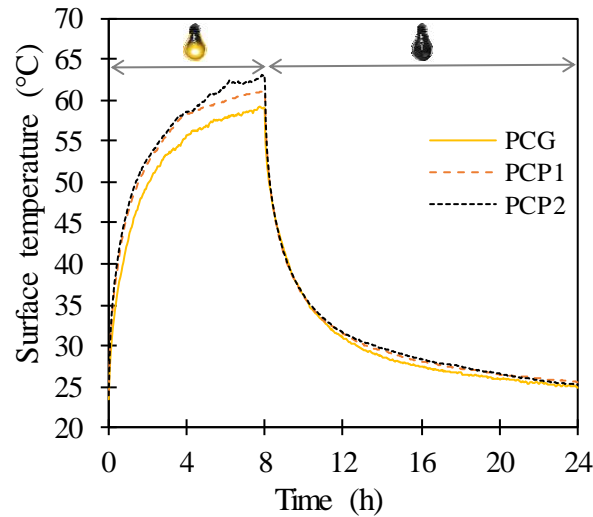


Fig. 10. Variation in surface temperature of PC pavements as a function of time.

It was deduced that in dry conditions the use of lightweight aggregates should be avoided. These results are consistent with those obtained by Chen et al. [61] who showed that increasing the thermal conductivity of PC from $0.59 \text{ W.m}^{-1}.\text{K}^{-1}$ to $0.85 \text{ W.m}^{-1}.\text{K}^{-1}$ by adding steel fibers to the mix reduces its surface temperature by 1 to 3°C .

3.4. Thermal behavior of PC pavements in wet conditions

3.4.1. Variation in albedo and evaporation rate

The thermal behavior of PC pavements in wet conditions was studied according to the same experimental protocol adopted in dry conditions. The only difference was that the experiment was carried out for 5 days while recording the variation of the total mass of the bin and the albedo of the pavement over time (pyranometer placed above the pavement). Fig. 11 shows the variation in cumulative evaporated water mass (Fig. 11a), evaporation rate (Fig. 11b), and albedo (Fig. 11c) over 5 days. By monitoring the mass of evaporated water during the 5 days of the experiment, the researchers were able to calculate the variation of the evaporation rate by means of **Eq. (5)** [23].

$$\text{ER} = \frac{m_{t1} - m_{t2}}{A (t_2 - t_1)} \quad (12)$$

where ER ($\text{kg.m}^{-2}.\text{h}^{-1}$) = evaporation rate; $m_{t1} - m_{t2}$ (kg) = difference between the total mass of the sample at time t_1 (s) and the total mass of the sample at time t_2 (s); A (m^2) = top surface of the pavement exposed to the exterior.

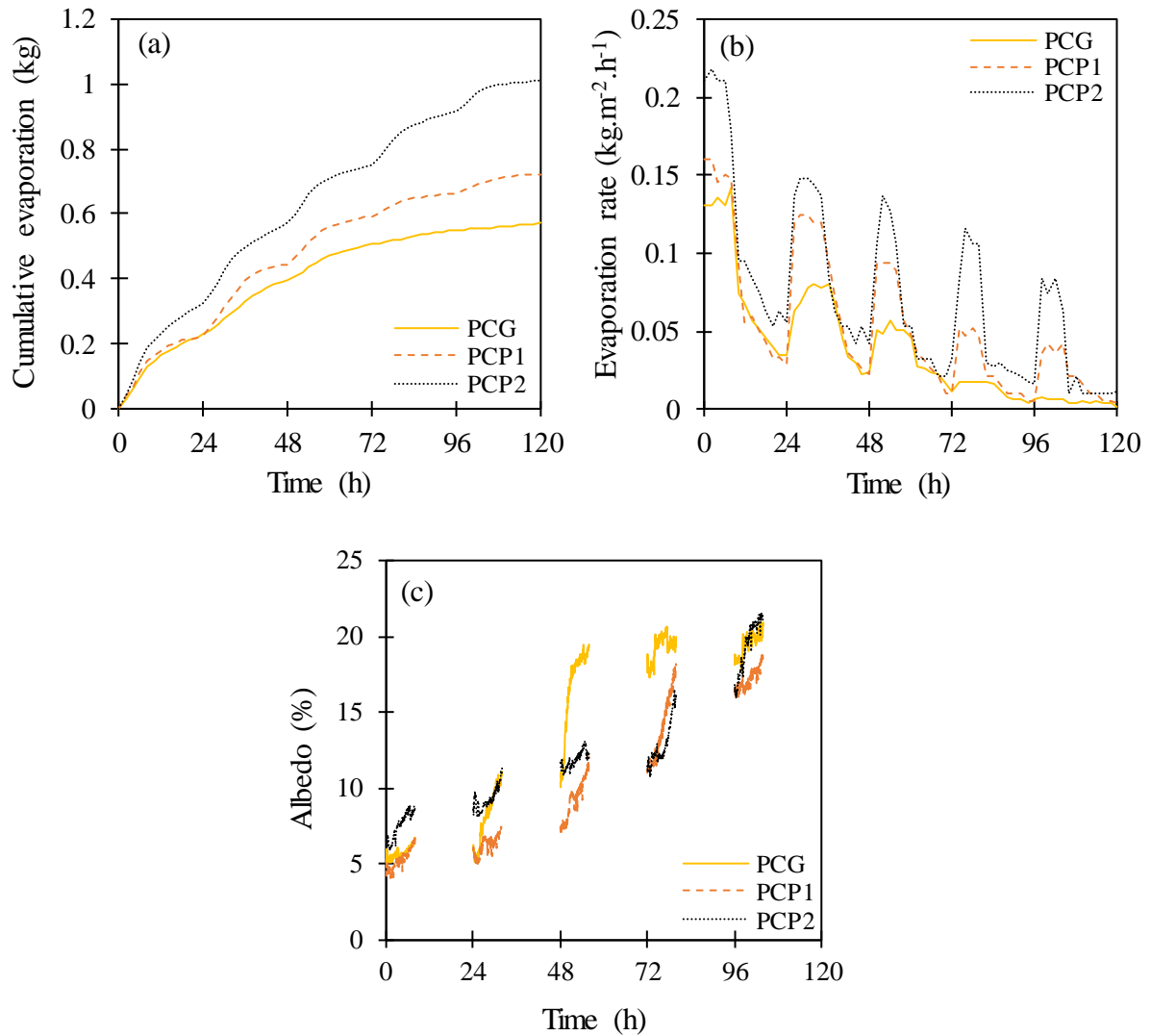


Fig. 11. Variation in: (a) cumulative evaporated water mass, (b) evaporation rate, and (c) albedo, as a function of time.

Fig. 11a shows that the cumulative evaporated water mass in sample PCP2 increases from 0 to 1.01 kg. The total evaporated water mass in this sample is 40% higher than that in PCP1 and 0.77% higher than that in PCG. In addition, the slope of the curve is steepest for PCP2, followed by PCP1, while the curve for PCG has the least slope (Fig. 11a). The change in the slope of the evaporated water mass curve over time is an important indicator of the evaporation process, because it can be used to calculate the change in the evaporation rate for each sample. Fig. 11b shows that the evaporation rate of the PCP2 sample is greater than that of the PCP1 during both the daytime and nighttime phases. The lowest evaporation rate is that of the PCG sample, which becomes insignificant from the third day ($ER < 0.0173 \text{ kg.m}^{-2}.\text{h}^{-1}$).

The maximum evaporation rate of each sample was observed on the first day of each experiment when the samples were saturated with water. At saturation, free water is retained by capillary forces and ready to evaporate. Then, as the water content decreases, the gap between the saturated zone and the evaporation plane increases, preventing the water in the pores from reaching the evaporation plane. The plane recedes to a lower level and a new evaporation plane is formed. Evaporation continues within the pavements at the new evaporation plane, by

diffusion of vapor through the pores present at the upper surface. As the water content decreases, the global resistance to evaporation becomes high [62], which explains the decrease in evaporation rate after the first day.

The albedo variation of wet PC was ignored in a previous study [33], looking at the thermal behavior of different types of PC in wet conditions. In that study [33], the authors relied on the albedo of pavements in dry conditions. This assumption may affect the accuracy of the energy balance analyses of the pavements, to study the variation of the shortwave energy flux absorbed by the pavements over time. In this experiment, the albedo of the pavements in wet conditions was measured during the 5 days of the experiment during the daytime phases of each day. The results are shown in Fig. 11c: at the beginning of each experiment, the wet-to-dry albedo ratio of the pavements varies from 22.8% to 30.7%. The main reason for the decrease in albedo is the color of the cement, which becomes darker when it is wet; this finding is in agreement with the results of Lekner and Dorf [63]. Fig. 11c shows that the albedo of PCG increases rapidly during the third day to 19.5%, which represents 96% of its albedo in dry conditions. This shows that the water on the surface of the PCG has evaporated and its surface has become dry, which explains the sharp decrease in the evaporation rate of PCG from the third day. Furthermore, Fig. 11c shows that the albedo of the pavements at the beginning of each diurnal phase is slightly lower than that corresponding to the end of the diurnal period of the previous day. This decrease is caused by the capillary absorption of water during the night period, which brings moisture to the pavement surface.

3.4.2. Variation in surface temperature

Fig. 12 shows the variation in surface temperature (Fig. 12a) and the variation in water content (Fig. 12b) of PC pavements as a function of time. It has been shown previously that the surface temperature of pozzolan-based PC pavements is higher than that of PCG during the day. However, in wet conditions, the results show that the maximum surface temperature of PCG is 2.8°C to 5.8°C higher than that of PCP1 and 3.2°C to 11.7°C higher than that of PCP2. Furthermore, during the night, the surface temperature of PCG is 0.9°C to 2.3°C higher than that of PCP1 and 1.3°C to 3.3°C higher than that of PCP2 at the end of the night phases. These results show that the use of the pozzolanic aggregate P2 in the PC mix improves the cooling effect and results in a surface temperature up to 11.7°C lower during the day and up to 3.3°C lower at night compared to dense aggregate PC pavements.

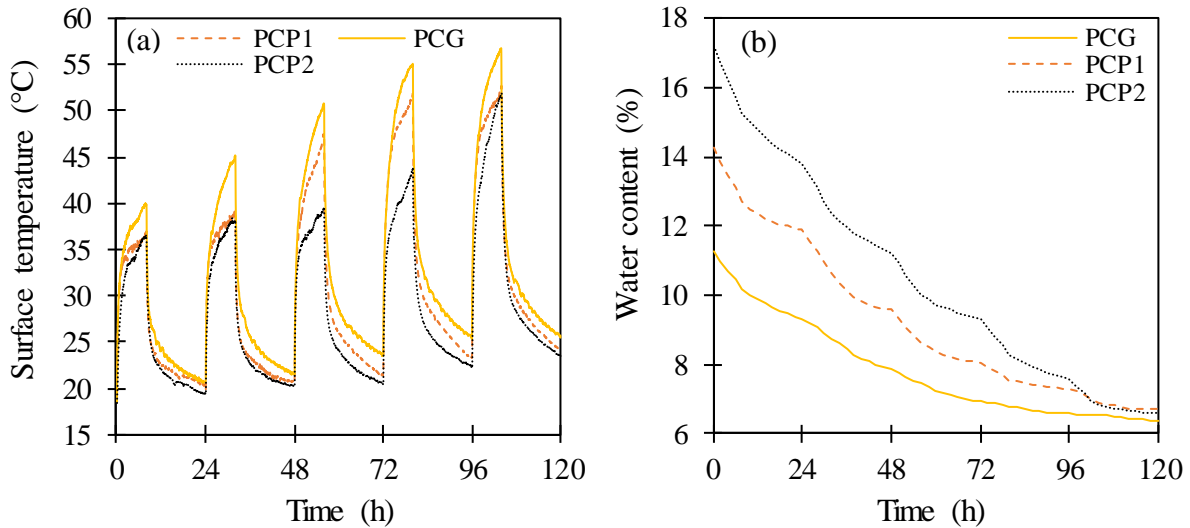


Fig. 12. Variation in: (a) surface temperature and (b) moisture content of PC pavements in wet conditions over the course of 5 days.

The deviations between the maximum surface temperature ΔT_{\max} of PC pavements in wet conditions and that in dry conditions at the end of the diurnal periods of each day are presented in Table 7. This table shows that PCP2 has the highest evaporative cooling performance compared to PCP1 and PCG. At saturation, the maximum surface temperature of PCP2 is up to 26.4°C lower than that in dry conditions. This gap decreased to 11.1°C after 5 days, which represents 42% of initial cooling performance, while the cooling performance at the end of the experiment represents 22.4% for PCP1 and 12% for PCG compared to their cooling performance during the first day. PCP2 exhibits the best cooling performance due to its high open porosity, the porous nature of the pozzolan aggregate and the high specific surface area of the P2 aggregate, which allows a larger amount of water to be retained near the surface compared to PCP1 and PCG. In addition, the high capillarity (Table 6) of the PCP2 pavement compared to the other pavements allows for the transfer of a greater amount of free water to its surface, which can effectively prolong the first stage of evaporation and ensure a greater cooling effect.

It was found that the cooling performance is strongly related to the evaporation rate in these pavements. As the evaporation rate increases (Fig. 11b), the pavement temperature decreases due to the latent heat absorbed during the phase change of water (from liquid to gas).

Table 7

Difference between the maximum surface temperature in wet and dry conditions.

Sample	ΔT_{\max} (day 1)	ΔT_{\max} (day 2)	ΔT_{\max} (day 3)	ΔT_{\max} (day 4)	ΔT_{\max} (day 5)
PCG	19.2	13.9	8.2	3.9	2.3
PCP1	24.1	21.8	13.5	9.2	5.4
PCP2	26.4	24.8	23.5	19.3	11.1

Fig. 12b shows that at the end of the experiment, the water contents of all pavements were above 6%. The cooling performance of PCG pavement was negligible on the last day (2.3°C decrease in temperature), though this pavement was not completely dry. It was found that it is not sufficient for the permeable pavement to be wet to have a significant cooling effect; the

effect is strongly dependent on the presence of water near the surface. In order to ensure a greater cooling effect over a longer period of time, PC pavements should be watered periodically. For example, the PCG pavement should be saturated after 5 days to increase its water content from 6.4% to 11.3% (saturation state); this would achieve a powerful cooling effect, decreasing its surface temperature by 19.2°C. Periodic watering of PC pavements is essential to maximize the cooling effect and to increase the effectiveness of these pavements in mitigating the formation of UHIs.

3.4.3. Energy distribution

Heat exchange occurs between pavements and their environment. When permeable pavements are exposed to solar radiation, their surface temperatures gradually increase until they become higher than the air temperature. This increase causes a significant release of convective heat flux (sensible heat flux), which increases the air temperature and affects the thermal comfort of residents. However, when water is present within the permeable pavement, the latent heat flux (evaporation flux) releases the absorbed energy and lowers the surface temperature.

The shortwave radiative flux absorbed by the permeable pavements I_{abs} (W/m^2) was calculated according to **Eq. (6)**. The convective heat flux (sensible heat flux) H (W/m^2) was calculated according to **Eq. (7)**. The theoretical maximum latent heat flux lost by evaporation E (W/m^2) was calculated according to **Eq. (8)** [23]. This equation shows that the latent heat loss by evaporation is proportional to the evaporation rate ER ($kg.m^{-2}.h^{-1}$).

$$I_{abs} = (1 - \alpha) I \quad (6)$$

$$H = h_c (T_s - T_a) \quad (7)$$

$$E = \frac{ER \cdot L}{3.6} \quad (8)$$

where α = albedo (dimensionless); h_c ($W.m^{-1}.^{\circ}C^{-1}$) = convection heat transfer coefficient [64]; T_s ($^{\circ}C$) = surface temperature ($^{\circ}C$); T_a ($^{\circ}C$) = air temperature near the surface; L (kJ/kg) = heat of vaporization of water.

Figs. 13a, 13b and 13c show that the sensible heat flux (H) which is responsible for UHIs development and the latent heat flux (E) vary inversely. The results show that PCG has the highest sensible heat flux during the 5 days of the experiment compared to that of the other permeable pavements. The sensible heat flux for the PCG sample exceeded 60 W/m^2 on the second day, while the sensible heat flux exceeded this value on the third day for PCP1 and on the fifth day for PCP2, which has the highest evaporative flux. Indeed, the convective heat flux is converted into latent heat in wet conditions by evaporation, leading to a decrease in surface temperature. Moreover, during the night, the significant latent heat flux released by the PCP2 sample allowed it to have a surface temperature lower than that of the air, which led to the negative sensible heat flux observed during the first four days of the experiment. On the other hand, the sensible heat flux of the PCG at night was higher than 20 W/m^2 from the fourth day onwards, which intensifies the nocturnal UHI effect.

Fig. 13d shows that the shortwave radiative flux absorbed by the PCP2 sample was up to 43 W/m^2 higher than that of the PCG during the third and fourth days. The main reason is the high capillary absorption coefficient and large open porosity of PCP2 compared to PCG, which made its surface wetter (lower albedo) over a longer time. In contrast, the PCP2 sample has the lowest surface temperature and sensible heat flux over the 5 days of the experiment. Indeed, the additional absorption of shortwave radiation by PCP2 compared to PCG that was observed during the third and fourth day was compensated by higher water evaporation. It was deduced that in order to achieve a greater cooling effect, the permeable pavement must provide a greater evaporative flux over a longer period of time.

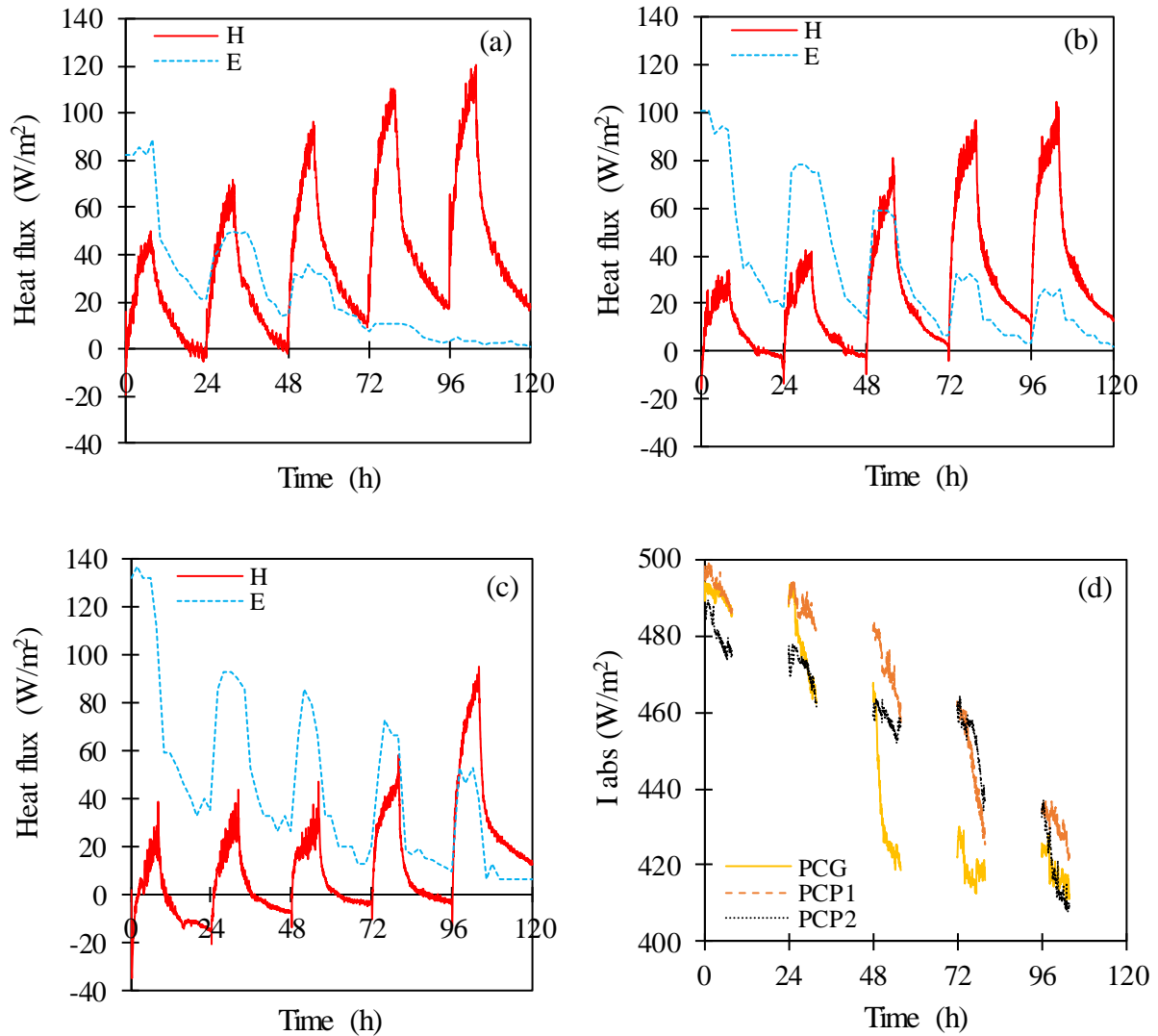


Fig. 13. Variation in latent and sensible heat fluxes for (a) PCG, (b) PCP1 and (c) PCP2 pavements as well as the (d) variation in absorbed shortwave heat flux as a function of time.

4. Conclusion

In this study, the thermal behavior of three types of pervious concrete was investigated under controlled climatic conditions in the laboratory in dry and wet conditions using an innovative experimental bench. The factors that influence the cooling effect of these pavements were identified. The main conclusions of this study can be summarized as follows:

(1) In dry conditions, the maximum surface temperature of PCP2 is 1.9°C higher than that of PCP1 and 4°C higher than that of PCG, due to the low thermal conductivity of pozzolan aggregates. The use of lightweight aggregates in the pervious concrete mix should be avoided in dry conditions.

(2) The partial immersion test shows that the use of lightweight and less coarse aggregates can increase the specific surface and improve the absorption properties of pervious concrete. The capillary absorption coefficient of PCP2 is 67% higher than that of PCG, while its capillary water content is 78% higher than that of PCG.

(3) Capillary water absorption significantly affects evaporation in permeable pavements. The use of less coarse pozzolan aggregates improves the structure of the internal capillary interstices and ensures hydraulic continuity over a long distance. In wet conditions, after 5 days, the total evaporated water mass of PCP2 is 40% higher than PCP1 and 77% higher than PCG due to its high open porosity and high water-absorption and retention capacity. Therefore, the evaporation rate of the PCP2 sample is higher during both daytime and nighttime periods throughout the experiment, compared to other permeable pavements.

(4) The maximum surface temperature of PCP2 over the course of 5 days in wet conditions is 3.2°C to 11.7°C lower than that of PCG. During the night, its surface temperature is up to 3°C lower than that of PCG. This type of pervious concrete is more effective in reducing urban heat islands during the daytime and nighttime than ordinary pervious concrete based on dense aggregates.

(5) The difference between the surface temperature of PCG in dry and wet conditions varied from 19.2°C (first day) to 2.3°C (last day). That of PCP2 varied from 26.4°C to 11.1°C due to its higher evaporation flux compared to PCG. After 5 days of the experiment, PCP2 was able to reduce its temperature by 18% in dry conditions; its water content was over 6% and the pavement was not completely dry in volume. This means that the presence of water near the surface is a key factor that controls the evaporation flux and the cooling effect. In addition, periodic watering is an essential factor to ensure a greater cooling effect over a longer period.

Wind has a major impact on the thermal convection coefficient and on the sensible heat exchange between pavements and air. In this study, due to limitations in experimental equipment and the lack of an accurate wind-speed control device, the thermal behavior study was performed under controlled laboratory weather conditions in the absence of wind (natural convection). However, as permeable pavements are being used increasingly worldwide to mitigate urban heat islands, the cooling effect of these pavements under various climatic conditions needs to be studied in more detail. In addition, it is important to focus on designing pervious concrete mixtures to optimize their water-absorption properties and improve the capillary effect to increase the evaporation rate and maximize the cooling effect.

Acknowledgements

The authors would like to thank the Auvergne Regional Council (France) and the European Regional Development Fund (ERDF) for their financial support of this work through the CPER ECOMAT program.

Appendix A. Experimental bench

Fig. A1 shows the experimental bench used to study the thermal behavior of pervious concrete pavement in dry and wet conditions.

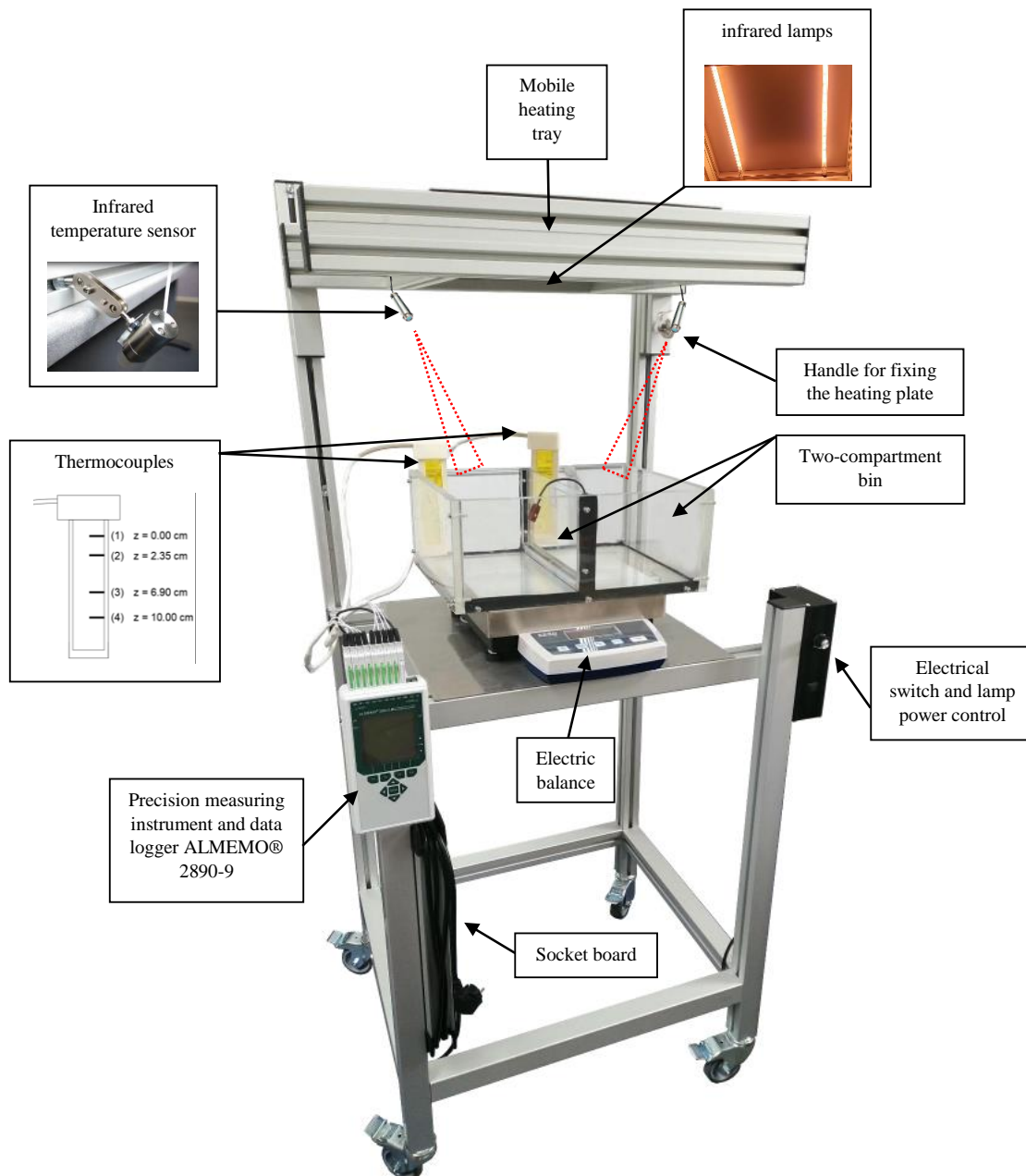


Fig. A1. Presentation of the experimental bench.

Bibliography

- [1] C. Wang, Z.-H. Wang, K. E. Kaloush, and J. Shacat, "Cool pavements for urban heat island mitigation: A synthetic review", *Renew. Sustain. Energy Rev.*, vol. 146, p. 111171, 2021.
- [2] H. Li, Y. Zhou, G. Jia, K. Zhao, and J. Dong, "Quantifying the response of surface urban heat island to urbanization using the annual temperature cycle model", *Geosci. Front.*, vol. 13, no. 1, p. 101141, 2022.
- [3] A. Mohajerani, J. Bakaric, and T. Jeffrey-Bailey, "The urban heat island effect, its causes, and mitigation, with reference to the thermal properties of asphalt concrete", *J. Environ. Manage.*, vol. 197, pp. 522–538, 2017, doi: 10.1016/j.jenvman.2017.03.095.

- [4] K. Seifeddine, E. Toussaint, and S. Amziane, “Experimental Investigation on Evaporation Rate for Enhancing Evaporative Cooling of Pervious Pavement Containing Recycled Rubber”, in *Construction Technologies and Architecture*, 2022, vol. 1, pp. 847–854.
- [5] S. Parison, M. Hendel, A. Grados, and L. Royon, “Analysis of the heat budget of standard, cool and watered pavements under lab heat-wave conditions”, *Energy Build.*, vol. 228, p. 110455, 2020.
- [6] T. Susca, F. Zanghirella, L. Colasuonno, and V. Del Fatto, “Effect of green wall installation on urban heat island and building energy use: A climate-informed systematic literature review”, *Renew. Sustain. Energy Rev.*, vol. 159, p. 112100, 2022.
- [7] E. L. Krüger, F. O. Minella, and F. Rasia, “Impact of urban geometry on outdoor thermal comfort and air quality from field measurements in Curitiba, Brazil”, *Build. Environ.*, vol. 46, no. 3, pp. 621–634, 2011.
- [8] C. Wang et al., “Efficient cooling of cities at global scale using urban green space to mitigate urban heat island effects in different climatic regions”, *Urban For. Urban Green.*, p. 127635, 2022.
- [9] F. Marando, E. Salvatori, A. Sebastiani, L. Fusaro, and F. Manes, “Regulating ecosystem services and green infrastructure: Assessment of urban heat island effect mitigation in the municipality of Rome, Italy”, *Ecol. Modell.*, vol. 392, pp. 92–102, 2019.
- [10] H. Herath, R. U. Halwatura, and G. Y. Jayasinghe, “Evaluation of green infrastructure effects on tropical Sri Lankan urban context as an urban heat island adaptation strategy”, *Urban For. Urban Green.*, vol. 29, pp. 212–222, 2018.
- [11] T. Susca, “Green roofs to reduce building energy use? A review on key structural factors of green roofs and their effects on urban climate”, *Build. Environ.*, vol. 162, p. 106273, 2019.
- [12] M. Carpio, Á. González, M. González, and K. Verichev, “Influence of pavements on the urban heat island phenomenon: A scientific evolution analysis”, *Energy Build.*, vol. 226, p. 110379, 2020.
- [13] C. Miao et al., “A super-cooling solar reflective coating with waterborne polyurethane for asphalt pavement”, *Prog. Org. Coatings*, vol. 165, p. 106741, 2022.
- [14] C. Zhu et al., “Dark, heat-reflective, anti-ice rain and superhydrophobic cement concrete surfaces”, *Constr. Build. Mater.*, vol. 220, pp. 21–28, 2019.
- [15] A. Sha, J. Zhang, M. Jia, W. Jiang, and W. Jiao, “Development of polyurethane-based solid-solid phase change materials for cooling asphalt pavements”, *Energy Build.*, p. 111873, 2022.
- [16] Q. Liu et al., “A novel functional coating with 2DMts/SA phase change material as filler and its pavement temperature regulation performance”, *Mater. Lett.*, vol. 306, p. 130905, 2022.
- [17] J. H. Park, Y. U. Kim, J. Jeon, S. Wi, S. J. Chang, and S. Kim, “Effect of eco-friendly pervious concrete with amorphous metallic fiber on evaporative cooling performance”, *J. Environ. Manage.*, vol. 297, p. 113269, 2021.
- [18] Y. Shimazaki, M. Aoki, K. Karaki, and A. Yoshida, “Improving outdoor human-thermal environment by optimizing the reflectance of water-retaining pavement through subjective field-based measurements”, *Build. Environ.*, vol. 210, p. 108695, 2022.
- [19] Y. Shimazaki, M. Aoki, J. Nitta, H. Okajima, and A. Yoshida, “Experimental Determination of Pedestrian Thermal Comfort on Water-Retaining Pavement for UHI Adaptation Strategy”, *Atmosphere (Basel)*, vol. 12, no. 2, p. 127, 2021.
- [20] B. Huang, H. Wu, X. Shu, and E. G. Burdette, “Laboratory evaluation of permeability and strength of polymer-modified pervious concrete”, *Constr. Build. Mater.*, vol. 24, no. 5, pp. 818–823, 2010, doi: 10.1016/j.conbuildmat.2009.10.025.
- [21] X. Wang et al., “The quantitative assessment of clogging and cleaning effects on the permeability of pervious concrete”, *Constr. Build. Mater.*, vol. 335, p. 127455, 2022.
- [22] C. Xie, L. Yuan, H. Tan, Y. Zhang, M. Zhao, and Y. Jia, “Experimental study on the water purification performance of biochar-modified pervious concrete”, *Constr. Build. Mater.*, vol. 285, p. 122767, 2021, doi: 10.1016/j.conbuildmat.2021.122767.
- [23] H. Li, J. Harvey, and Z. Ge, “Experimental investigation on evaporation rate for enhancing evaporative cooling effect of permeable pavement materials”, *Constr. Build. Mater.*, vol. 65, pp. 367–375, 2014, doi: 10.1016/j.conbuildmat.2014.05.004.
- [24] J. Wang, Q. Meng, K. Tan, and M. Santamouris, “Evaporative cooling performance estimation of pervious pavement based on evaporation resistance”, *Build. Environ.*, vol. 217, no. November 2021, p. 109083, 2022, doi: 10.1016/j.buildenv.2022.109083.
- [25] B. H. Lynn et al., “A modification to the NOAA LSM to simulate heat mitigation strategies in the New York City metropolitan area”, *J. Appl. Meteorol. Climatol.*, vol. 48, no. 2, pp. 199–216, 2009.
- [26] K. Seifeddine, S. Amziane, and E. Toussaint, “Thermal behavior of pervious concrete in dry conditions”, *Constr. Build. Mater.*, 2022. doi: 10.1016/j.conbuildmat.2022.128300
- [27] J. T. Kevern, V. R. Schaefer, and K. Wang, “Temperature behavior of pervious concrete systems”, *Transp. Res. Rec.*, vol. 2098, no. 1, pp. 94–101, 2009.

- [28] Y. Qin and J. E. Hiller, “Water availability near the surface dominates the evaporation of pervious concrete”, *Constr. Build. Mater.*, vol. 111, pp. 77–84, 2016.
- [29] K. Okada, A. Ooyama, T. Isobe, Y. Kameshima, A. Nakajima, and K. J. D. MacKenzie, “Water retention properties of porous geopolymers for use in cooling applications”, *J. Eur. Ceram. Soc.*, vol. 29, no. 10, pp. 1917–1923, 2009.
- [30] T. Nakayama and T. Fujita, “Cooling effect of water-holding pavements made of new materials on water and heat budgets in urban areas”, *Landsc. Urban Plan.*, vol. 96, no. 2, pp. 57–67, 2010.
- [31] K. Takahashi and K. Yabuta, “Road temperature mitigation effect of ‘road cool,’ a Water-retentive material using blast furnace slag”, *JFE Tech. Rep.*, vol. 19, pp. 58–62, 2009.
- [32] K. Okada, S. Matsui, T. Isobe, Y. Kameshima, and A. Nakajima, “Water-retention properties of porous ceramics prepared from mixtures of allophane and vermiculite for materials to counteract heat island effects”, *Ceram. Int.*, vol. 34, no. 2, pp. 345–350, 2008.
- [33] K. Tan, Y. Qin, T. Du, L. Li, L. Zhang, and J. Wang, “Biochar from waste biomass as hygroscopic filler for pervious concrete to improve evaporative cooling performance”, *Constr. Build. Mater.*, vol. 287, p. 123078, 2021.
- [34] A. ASTM, “Standard test method for relative density (specific gravity) and absorption of coarse aggregate”, ASTM West Conshohocken, PA, 2015.
- [35] A. ASTM, “C29 standard test method for bulk density (‘Unit Weight’) and voids in aggregate”, *Am. Soc. Test. Mater. Annu. Book*, Pennsylvania, USA, 2009.
- [36] P. NF, “94-056. Sols: reconnaissance et essais”, *Anal. granulométrique. Méthode par tamisage à sec après lavage*. AFNOR, 1996.
- [37] N. Neithalath, M. S. Sumanasooriya, and O. Deo, “Characterizing pore volume, sizes, and connectivity in pervious concretes for permeability prediction”, *Mater. Charact.*, vol. 61, no. 8, pp. 802–813, 2010.
- [38] G. F. B. Sandoval, I. Galobardes, R. S. Teixeira, and B. M. Toralles, “Comparison between the falling head and the constant head permeability tests to assess the permeability coefficient of sustainable Pervious Concretes”, *Case Stud. Constr. Mater.*, vol. 7, pp. 317–328, 2017.
- [39] A. C. I., (American C. Institute), “Report on pervious concrete”, 2010.
- [40] P. D. Tennis, M. L. Leming, and D. J. Akers, “Pervious concrete pavements”, no. PCA Serial No. 2828. Portland Cement Association Skokie, IL, 2004.
- [41] N. F. EN, “12390-3, 2012”, *Norme. Essais pour Bét. durci-Partie*, vol. 3.
- [42] ASTM C1701, “Standard Test Method for Infiltration Rate of In Place Pervious Concrete”, *Annual Book of ASTM Standards*, ASTM International, West Conshohocken, PA.
- [43] “ASTM-E1918-06; 2015. “Standard Test Method for Measuring Solar Reflectance of Horizontal and Low-Sloped Surfaces in the Field”, ASTM International; ASTM; West Conshohocken; PA; pp. 1–3.
- [44] J. Chen, Z. Zhou, J. Wu, S. Hou, and M. Liu, “Field and laboratory measurement of albedo and heat transfer for pavement materials”, *Constr. Build. Mater.*, vol. 202, pp. 46–57, 2019.
- [45] ASTM, “D5930-97 Standard test method for thermal conductivity of plastics by means of a transient line-source technique”, ASTM International, West Conshohocken, PA, USA, 2001.
- [46] C. Astm, “Standard test method for measurement of rate of absorption of water by hydraulic-cement concretes,” West Conshohocken, PA, 2013.
- [47] S. Kant Sahdeo, G. D. Ransinchung, K. L. Rahul, and S. Debbarma, “Effect of mix proportion on the structural and functional properties of pervious concrete paving mixtures”, *Constr. Build. Mater.*, vol. 255, p. 119260, 2020, doi: 10.1016/j.conbuildmat.2020.119260.
- [48] V. R. Schaefer and K. Wang, “Mix design development for pervious concrete in cold weather climates”, Iowa. Dept. of Transportation. Highway Division, 2006.
- [49] Probeton, PTV 122, “Prescriptions techniques pour les pavés et dalles en béton perméables à l’eau”, 3rd edition, 12 p., 2009
- [50] G. F. B. Sandoval, I. Galobardes, A. Campos, and B. M. Toralles, “Assessing the phenomenon of clogging of pervious concrete (Pc): Experimental test and model proposition”, *J. Build. Eng.*, vol. 29, p. 101203, 2020.
- [51] Y. Zhang, H. Li, A. Abdelhady, and J. Yang, “Comparative laboratory measurement of pervious concrete permeability using constant-head and falling-head permeameter methods”, *Constr. Build. Mater.*, vol. 263, p. 120614, 2020.
- [52] G. F. B. Sandoval, I. Galobardes, C. Dias, A. Campos, and B. M. Toralles, “Pervious concrete made with electric furnace slag (FEA): mechanical and hydraulic properties”, *Rev. IBRACON Estruturas e Mater.*, vol. 12, pp. 590–607, 2019.
- [53] R. Zhong and K. Wille, “Material design and characterization of high performance pervious concrete”, *Constr. Build. Mater.*, vol. 98, pp. 51–60, 2015, doi: 10.1016/j.conbuildmat.2015.08.027.
- [54] R. Zhong and K. Wille, “Compression response of normal and high strength pervious concrete”, *Constr. Build. Mater.*, vol. 109, pp. 177–187, 2016.

- [55] D. H. Nguyen, N. Sebaibi, M. Boutouil, L. Leleyter, and F. Baraud, “A modified method for the design of pervious concrete mix”, *Constr. Build. Mater.*, vol. 73, pp. 271–282, 2014.
- [56] R. Zhang, G. Jiang, and J. Liang, “The Albedo of Pervious Cement Concrete Linearly Decreases with Porosity”, *Adv. Mater. Sci. Eng.*, vol. 2015, 2015, doi: 10.1155/2015/746592.
- [57] J. Chen, H. Wang, P. Xie, and H. Najm, “Analysis of thermal conductivity of porous concrete using laboratory measurements and microstructure models”, *Constr. Build. Mater.*, vol. 218, pp. 90–98, 2019, doi: 10.1016/j.conbuildmat.2019.05.120.
- [58] ASTM, “Standard Test Method for Steady-State Thermal Transmission Properties by Means of the Heat Flow Meter Apparatus (C 518)”, West Conshohocken, PA 19428-2959, United States; 2010, p. 152-166.”.
- [59] J. Wang et al., “Impacts of the water absorption capability on the evaporative cooling effect of pervious paving materials”, *Build. Environ.*, vol. 151, pp. 187–197, 2019.
- [60] S. Roels et al., “Interlaboratory comparison of hygric properties of porous building materials”, *J. Therm. Envel. Build. Sci.*, vol. 27, no. 4, pp. 307–325, 2004.
- [61] J. Chen, R. Chu, H. Wang, L. Zhang, X. Chen, and Y. Du, “Alleviating urban heat island effect using high-conductivity permeable concrete pavement”, *J. Clean. Prod.*, vol. 237, p. 117722, 2019, doi: 10.1016/j.jclepro.2019.117722.
- [62] C. Syrrakou and G. F. Pinder, “Experimentally determined evaporation rates in pervious concrete systems”, *J. Irrig. Drain. Eng.*, vol. 140, no. 1, p. 4013003, 2014.
- [63] J. Lekner and M. C. Dorf, “Why some things are darker when wet”, *Appl. Opt.*, vol. 27, no. 7, pp. 1278–1280, 1988.
- [64] Y. Qin and J. E. Hiller, “Ways of formulating wind speed in heat convection significantly influencing pavement temperature prediction”, *Heat Mass Transf. und Stoffuebertragung*, vol. 49, no. 5, pp. 745–752, 2013, doi: 10.1007/s00231-013-1116-0.

CONCLUSIONS GÉNÉRALES ET PERSPECTIVES

Les chaussées imperméables conventionnelles ont une surface sombre et une grande inertie thermique. En été, elles ont tendance à absorber et à stocker le rayonnement solaire et annulent le refroidissement par évaporation ce qui contribue au développement de l'îlot de chaleur urbain. L'idée d'utiliser des chaussées rafraichissantes pour atténuer les îlots de chaleur urbains a récemment pris de l'ampleur. La chaussée en béton drainant (BD) fait partie des chaussées évaporatives rafraichissantes. Ce type de chaussée est caractérisé par une grande porosité interconnectée qui permet à l'eau de s'écouler à travers sa structure. De plus, elle peut retenir l'eau dans les pores de sorte que la température de la surface de la chaussée peut être réduite par évaporation. Ce type de chaussées peut donc résoudre les problèmes liés aux développements des îlots de chaleur urbains et à la gestion des eaux pluviales.

L'objectif principal de ce travail de thèse consistait à étudier le comportement thermique du BD en condition sèche et humide et d'identifier les facteurs qui influent sur la température de surface afin de proposer des solutions permettant d'améliorer l'effet rafraichissant de ce type de chaussée. Un banc expérimental innovant a été conçu pour réaliser cette étude thermique dans des conditions climatiques contrôlées en laboratoire. Ce banc a également été utilisé pour valider les résultats du modèle analytique. Les principaux résultats obtenus dans ce travail sont les suivants :

(i) La densité du BD diminue linéairement avec l'augmentation de la porosité ouverte tandis que la résistance à la compression diminue d'une façon exponentielle. Ce facteur n'est pas suffisant pour prédire avec précision les caractéristiques mécaniques du BD qui dépendent aussi d'autres facteurs tels que les rapports eau/ciment et agrégats/ciment, la teneur en pâte de ciment, ainsi que le type et les propriétés mécaniques, physiques et géométriques des granulats. Il existe certaines techniques permettant d'augmenter la résistance mécanique du BD en optimisant la conception du mélange en ajoutant une quantité de sable limité à 10% de la masse des agrégats, en augmentant le degré de compactage et en assurant un rapport eau/ciment variant 0,3 à 0,36 et un rapport agrégats/ciment variant de 4,2 à 5. Le modèle de prédiction de la résistance à la traction du béton conventionnel ne peut pas être appliqué au BD. En revanche, le modèle pour le béton conventionnel peut être utilisé pour prédire la résistance à la flexion des mélanges de BD à partir de leur résistance à la compression.

(ii) La perméabilité du BD diminue exponentiellement avec l'augmentation de la porosité ouverte, elle dépend également des propriétés physiques et géométriques des granulats utilisés, du rapport massique agrégats/ciment, de la teneur en pâte de ciment et de la quantité de sable utilisée. La valeur de perméabilité du BD est fortement dépendante de la méthode de mesure. Le perméamètre à charge constante présente moins d'incertitude dans la mesure de la perméabilité comparée au perméamètre à charge variable. La perméabilité du BD augmente avec la taille des granulats, diminue avec l'augmentation de l'épaisseur de la pâte de ciment et du rapport eau/ciment, et augmente avec l'augmentation du rapport agrégats/ciment. Les modèles de prédiction de la perméabilité les plus précis sont ceux qui tiennent compte des paramètres de la structure des pores.

(iii) Tous les types de chaussées rafraichissantes : chaussées évaporatives, chaussées réfléchissantes et chaussées qui modifient leur stockage de chaleur sont efficaces pour atténuer les effets d'îlots de chaleur urbain. Cependant, il existe des limitations concernant la mise en œuvre de ces chaussées. Par exemple, le vieillissement des chaussées réfléchissantes peut diminuer leurs réflectivités et affecte leurs pouvoirs de refroidissement. De plus les performances de réflexion de ces chaussées doivent être évaluées plus en détail pour garantir le confort thermique et la sécurité de conduite. La performance de refroidissement des chaussées évaporatives perméables est conditionnée par la présence de l'eau dans le revêtement. En condition sèche ces derniers peuvent avoir une température plus élevée que celle des chaussées conventionnelles durant les périodes de canicule. L'augmentation de la conductivité thermique des chaussées assure une diminution de leur température de surface durant la journée mais cette technique aggrave la problématique des îlots de chaleur urbains nocturnes.

(vi) L'augmentation du taux d'évaporation des revêtements perméables entraîne une augmentation de l'effet de refroidissement par évaporation. Le taux d'évaporation augmente avec l'augmentation de la porosité ouverte et la perméabilité. De plus, le phénomène d'évaporation est contrôlé par la présence de l'eau proche de la surface ce qui met en valeur l'importance du phénomène de remontée capillaire qui peut remonter l'eau à la surface en assurant un effet de refroidissement plus important sur une durée plus longue. L'arrosage périodique est un facteur essentiel pour assurer un effet de refroidissement plus important sur une plus longue période. Pendant la nuit, la température de surface de tous les revêtements perméables est inférieure à celle de l'asphalte, même après la fin de l'effet de refroidissement par évaporation, en raison de leur nature poreuse et de leur faible conductivité thermique.

(v) Le BD est globalement plus chaud que le béton ordinaire pendant la journée, et globalement plus froid la nuit. L'augmentation de la conductivité thermique du BD diminue sa température de surface pendant la journée, par contre, cette augmentation rend sa température plus élevée pendant la nuit. Au contraire, L'augmentation de l'albédo du BD diminue sa température de surface pendant la journée et la nuit. L'étude de sensibilité montre que ce dernier facteur a plus d'influence sur la température de surface maximale du BD que la conductivité thermique. L'albédo est donc le facteur à privilégier dans la conception de chaussées en BD. Afin de diminuer la température de surface du BD en condition sèche, il est possible d'optimiser la conception du mélange du BD en utilisant un liant et des agrégats de couleur claire, des agrégats moins grossiers et ayant une conductivité thermique élevée

(vi) En condition humide, l'utilisation des agrégats légers de pouzzolane améliore les propriétés d'absorption du BD. Le coefficient d'absorption capillaire et la teneur en eau capillaire des BD à base de pouzzolane peuvent être beaucoup plus élevés que ceux des BD à base de gravier respectivement. L'utilisation des granulats de pouzzolane dans le mélange du BD améliore l'effet de refroidissement par évaporation et assure une température de surface largement inférieure à celle du BD à base du gravier durant les périodes diurnes tandis que sa température de surface est toujours inférieure à celle du BDG pendant la nuit.

Le comportement mécanique, hydraulique et thermique dans des conditions sèches et humides du béton drainant ont été étudiés en détail. Néanmoins, plusieurs perspectives peuvent être proposées :

(i) Le vent a un fort impact sur le coefficient de convection thermique et sur l'échange de chaleur sensible entre les chaussées et l'air. Durant cette thèse, en raison des limitations de l'équipement expérimental et de l'absence d'un dispositif précis de contrôle de la vitesse du vent, l'étude du comportement thermique du béton drainant en condition sèche et humide a été réalisée dans des conditions climatiques contrôlées en laboratoire, en l'absence de vent (convection naturelle). Cependant, comme les chaussées en béton drainant sont de plus en plus utilisées dans le monde pour atténuer les îlots de chaleur urbains, l'évaluation de l'effet de refroidissement de ces chaussées dans diverses conditions climatiques devrait être étudiée plus en détail. En outre, il est important de se concentrer sur la conception des mélanges de béton drainant afin d'optimiser leurs propriétés d'absorption d'eau et d'améliorer l'effet capillaire pour augmenter le taux d'évaporation et maximiser l'effet de refroidissement.

(ii) L'utilisation des agrégats légers de pouzzolane améliore l'effet de refroidissement par évaporation. Cependant l'utilisation des agrégats légers peut affecter la résistance mécanique du béton drainant ce qui peut limiter son utilisation. Il faut donc prévoir des mélanges de béton drainant à base d'agrégats légers ayant une résistance à la compression supérieure à 17 MPa et une perméabilité supérieure à 1 mm/s. Il faut aussi étudier l'influence de cette optimisation sur le comportement thermique et sur l'effet de refroidissement.

(iii) L'influence des caractéristiques des pores sur le comportement mécanique et hydraulique du BD a été largement étudiée dans la littérature. Les études futures devraient se concentrer sur les effets des caractéristiques des pores telles que leur taille, leur distribution, leur forme et leur tortuosité sur le comportement thermique de la BD. Ces études conduiront à la conception de chaussées présentant de bonnes performances mécaniques et hydrauliques et un effet rafraichissant important. De plus, il est nécessaire de concevoir des chaussées qui combinent plusieurs technologies de chaussées rafraichissantes telles qu'une chaussée réfléchissante et perméable avec une conductivité thermique élevée afin de maximiser l'effet rafraichissant.

VALORISATION DES TRAVAUX

Articles journal publié

K. Seifeddine, S. Amziane, E. Toussaint. "State of the art on the mechanical properties of pervious concrete", *European Journal of Environmental and Civil Engineering* (2021), 1-29. Doi: 10.1080/19648189.2021.2008511.

K. Seifeddine, S. Amziane, E. Toussaint. "Thermal behavior of pervious concrete in dry conditions", *Construction and Building Materials*. Doi: 10.1016/j.conbuildmat.2022.128300.

K. Seifeddine, S. Amziane, E. Toussaint. "Experimental investigation on physical characteristics to improve the cooling effect of permeable pavements", *Construction and Building Materials*. Doi : 10.1016/j.conbuildmat.2022.128342.

Articles journal soumis

K. Seifeddine, S. Amziane, E. Toussaint. "State of the art on the hydraulic properties of pervious concrete", (submitted to Road Materials and Pavement Design journal).

K. Seifeddine, S. Amziane, E. Toussaint. "Review on thermal behavior of cool pavements", (submitted to Building And Environment journal).

K. Seifeddine, S. Amziane, E. Toussaint. "Thermal behavior of pervious concrete in wet conditions", (submitted to Construction and Building Materials journal).

Communication dans des congrès internationaux

K. Seifeddine, S. Amziane, E. Toussaint, "Thermal behaviour of pervious concrete in dry conditions", The 16th ICAST2021, International student conference on advanced science and technology, online conference, Kumamoto University, Japan, 2-3 December 2021.

K. Seifeddine, S. Amziane, E. Toussaint. "Experimental investigation on ivaporation rate for enhancing evaporative cooling of pervious pavement containing recycled rubber", *Construction Technologies and Architecture*. Trans Tech Publications Ltd, 2022. p. 847-854. Doi : 10.4028/www.scientific.net/CTA.1.847.

Communication dans des congrès nationaux à comité de lecture

K. Seifeddine, S. Amziane, E. Toussaint. "Etat de l'art sur les propriétés mécaniques du béton drainant. *Academic Journal of Civil Engineering*, 2021, vol. 39, no 1, p. 43-46. Doi : 10.26168/ajce.39.1.9.

K. Seifeddine, S. Amziane, E. Toussaint. "Étude de l'effet rafraichissant du béton drainant en condition sèche et humide". *Academic Journal of Civil Engineering*, 2022.

Prix.

1^{er} prix vidéo RUGC : <https://www.youtube.com/watch?v=9bhqtyYvawg&t=86s>

Bibliography (introduction générale)

- [1] U. N. PUBLICATIONS., “Sustainable development goals report 2018”. United Nations Pubns, 2018.
- [2] T. R. Oke, G. Mills, A. Christen, and J. A. Voogt, “Urban climates”, Cambridge University Press, 2017.
- [3] G. Mills, “Luke Howard and the climate of London”, *Weather*, vol. 63, no. 6, pp. 153–157, 2008.
- [4] P. E. Phelan *et al.*, “Urban heat island: mechanisms, implications, and possible remedies”, *Annu. Rev. Environ. Resour.*, vol. 40, pp. 285–307, 2015.
- [5] H. Akbari and D. Kolokotsa, “Three decades of urban heat islands and mitigation technologies research”, *Energy Build.*, vol. 133, pp. 834–842, 2016.
- [6] A. Mohajerani, J. Bakaric, and T. Jeffrey-Bailey, “The urban heat island effect, its causes, and mitigation, with reference to the thermal properties of asphalt concrete”, *J. Environ. Manage.*, vol. 197, pp. 522–538, 2017.
- [7] M. Kolokotroni, X. Ren, M. Davies, and A. Mavrogianni, “London’s urban heat island: Impact on current and future energy consumption in office buildings”, *Energy Build.*, vol. 47, pp. 302–311, 2012.
- [8] S. Guhathakurta and P. Gober, “The impact of the Phoenix urban heat island on residential water use”, *J. Am. Plan. Assoc.*, vol. 73, no. 3, pp. 317–329, 2007.
- [9] H. Akbari, M. Pomerantz, and H. Taha, “Cool surfaces and shade trees to reduce energy use and improve air quality in urban areas”, *Sol. energy*, vol. 70, no. 3, pp. 295–310, 2001.
- [10] C. Sarrat, A. Lemonsu, V. Masson, and D. Guédalia, “Impact of urban heat island on regional atmospheric pollution”, *Atmos. Environ.*, vol. 40, no. 10, pp. 1743–1758, 2006.
- [11] G. B. Anderson and M. L. Bell, “Heat waves in the United States: mortality risk during heat waves and effect modification by heat wave characteristics in 43 US communities”, *Environ. Health Perspect.*, vol. 119, no. 2, pp. 210–218, 2011.
- [12] J. Tan *et al.*, “The urban heat island and its impact on heat waves and human health in Shanghai”, *Int. J. Biometeorol.*, vol. 54, no. 1, pp. 75–84, 2010.
- [13] J. Yang, L. Hu, and C. Wang, “Population dynamics modify urban residents’ exposure to extreme temperatures across the United States”, *Sci. Adv.*, vol. 5, no. 12, p. eaay3452, 2019.
- [14] D. E. Bowler, L. Buyung-Ali, T. M. Knight, and A. S. Pullin, “Urban greening to cool towns and cities: A systematic review of the empirical evidence”, *Landsc. Urban Plan.*, vol. 97, no. 3, pp. 147–155, 2010.
- [15] H. Saaroni, J. H. Amorim, J. A. Hiemstra, and D. Pearlmutter, “Urban Green Infrastructure as a tool for urban heat mitigation: Survey of research methodologies and findings across different climatic regions”, *Urban Clim.*, vol. 24, pp. 94–110, 2018.
- [16] Z.-H. Wang, X. Zhao, J. Yang, and J. Song, “Cooling and energy saving potentials of shade trees and urban lawns in a desert city”, *Appl. Energy*, vol. 161, pp. 437–444, 2016.
- [17] J. Yang, Z.-H. Wang, and K. E. Kaloush, “Environmental impacts of reflective materials: Is high albedo a ‘silver bullet’ for mitigating urban heat island?”, *Renew. Sustain. Energy Rev.*, vol. 47, pp. 830–843, 2015.
- [18] H. Akbari, R. Levinson, and L. Rainer, “Monitoring the energy-use effects of cool roofs on California commercial buildings”, *Energy Build.*, vol. 37, no. 10, pp. 1007–1016, 2005.
- [19] R. Levinson and H. Akbari, “Potential benefits of cool roofs on commercial buildings: conserving energy, saving money, and reducing emission of greenhouse gases and air pollutants”, *Energy Effic.*, vol. 3, no. 1, p. 53, 2010.
- [20] Y. Qin, “A review on the development of cool pavements to mitigate urban heat island effect”, *Renew. Sustain. Energy Rev.*, vol. 52, pp. 445–459, 2015.
- [21] M. Santamouris, “Using cool pavements as a mitigation strategy to fight urban heat island—A review of the actual developments”, *Renew. Sustain. Energy Rev.*, vol. 26, pp. 224–240, 2013.
- [22] T. Nakayama and T. Fujita, “Cooling effect of water-holding pavements made of new materials on water and heat budgets in urban areas”, *Landsc. Urban Plan.*, vol. 96, no. 2, pp. 57–67, 2010.
- [23] H. E. Gilbert *et al.*, “Energy and environmental consequences of a cool pavement campaign”, *Energy Build.*, vol. 157, pp. 53–77, 2017.
- [24] M. Žuvela-Aloise, R. Koch, S. Buchholz, and B. Früh, “Modelling the potential of green and blue infrastructure to reduce urban heat load in the city of Vienna”, *Clim. Change*, vol. 135, no. 3, pp. 425–438, 2016.
- [25] C. Van Mechelen, T. Dutoit, and M. Hermy, “Adapting green roof irrigation practices for a sustainable future: A review”, *Sustain. Cities Soc.*, vol. 19, pp. 74–90, 2015.
- [26] C. Wang, Z.-H. Wang, and J. Yang, “Urban water capacity: Irrigation for heat mitigation”, *Comput. Environ. Urban Syst.*, vol. 78, p. 101397, 2019.
- [27] P. Rode, C. Keim, G. Robazza, P. Viejo, and J. Schofield, “Cities and energy: urban morphology and residential heat-energy demand”, *Environ. Plan. B Plan. Des.*, vol. 41, no. 1, pp. 138–162, 2014.
- [28] F. Sher, A. Kawai, F. Güleç, and H. Sadiq, “Sustainable energy saving alternatives in small buildings”, *Sustain. Energy Technol. Assessments*, vol. 32, pp. 92–99, 2019.

- [29] E. Cuce, F. Sher, H. Sadiq, P. M. Cuce, T. Guclu, and A. B. Besir, “Sustainable ventilation strategies in buildings: CFD research”, *Sustain. Energy Technol. Assessments*, vol. 36, p. 100540, 2019.
- [30] M. Santamouris, A. Synnefa, and T. Karlessi, “Using advanced cool materials in the urban built environment to mitigate heat islands and improve thermal comfort conditions”, *Sol. Energy*, vol. 85, no. 12, pp. 3085–3102, 2011.
- [31] A. E. P. EPA, “Reducing urban heat islands: compendium of strategies”, *Heat Isl. Reduct. Act.*, pp. 1–23, 2008.
- [32] M. Carpio, Á. González, M. González, and K. Verichev, “Influence of pavements on the urban heat island phenomenon: A scientific evolution analysis”, *Energy Build.*, vol. 226, p. 110379, 2020.
- [33] C. Miao *et al.*, “A super-cooling solar reflective coating with waterborne polyurethane for asphalt pavement”, *Prog. Org. Coatings*, vol. 165, p. 106741, 2022.
- [34] C. Zhu *et al.*, “Dark, heat-reflective, anti-ice rain and superhydrophobic cement concrete surfaces”, *Constr. Build. Mater.*, vol. 220, pp. 21–28, 2019.
- [35] A. Sha, J. Zhang, M. Jia, W. Jiang, and W. Jiao, “Development of polyurethane-based solid-solid phase change materials for cooling asphalt pavements”, *Energy Build.*, p. 111873, 2022.
- [36] Q. Liu *et al.*, “A novel functional coating with 2DMts/SA phase change material as filler and its pavement temperature regulation performance”, *Mater. Lett.*, vol. 306, p. 130905, 2022.
- [37] J. H. Park, Y. U. Kim, J. Jeon, S. Wi, S. J. Chang, and S. Kim, “Effect of eco-friendly pervious concrete with amorphous metallic fiber on evaporative cooling performance”, *J. Environ. Manage.*, vol. 297, p. 113269, 2021.
- [38] Y. Shimazaki, M. Aoki, K. Karaki, and A. Yoshida, “Improving outdoor human-thermal environment by optimizing the reflectance of water-retaining pavement through subjective field-based measurements”, *Build. Environ.*, vol. 210, p. 108695, 2022.
- [39] Y. Shimazaki, M. Aoki, J. Nitta, H. Okajima, and A. Yoshida, “Experimental Determination of Pedestrian Thermal Comfort on Water-Retaining Pavement for UHI Adaptation Strategy”, *Atmosphere (Basel)*, vol. 12, no. 2, p. 127, 2021.
- [40] H. M. Imran, S. Akib, and M. R. Karim, “Permeable pavement and stormwater management systems: a review”, *Environ. Technol.*, vol. 34, no. 18, pp. 2649–2656, 2013.
- [41] M. Kayhanian, H. Li, J. T. Harvey, and X. Liang, “Application of permeable pavements in highways for stormwater runoff management and pollution prevention: California research experiences”, *Int. J. Transp. Sci. Technol.*, vol. 8, no. 4, pp. 358–372, 2019.
- [42] X. Liang, S. Cui, H. Li, A. Abdelhady, H. Wang, and H. Zhou, “Removal effect on stormwater runoff pollution of porous concrete treated with nanometer titanium dioxide”, *Transp. Res. Part D Transp. Environ.*, vol. 73, pp. 34–45, 2019.
- [43] H. Wang, H. Li, X. Liang, H. Zhou, N. Xie, and Z. Dai, “Investigation on the mechanical properties and environmental impacts of pervious concrete containing fly ash based on the cement-aggregate ratio”, *Constr. Build. Mater.*, vol. 202, pp. 387–395, 2019.
- [44] Y. Zhang, H. Li, A. Abdelhady, and J. Yang, “Effect of different factors on sound absorption property of porous concrete”, *Transp. Res. Part D Transp. Environ.*, vol. 87, p. 102532, 2020.
- [45] Y. Zhang, H. Li, A. Abdelhady, and H. Du, “Laboratorial investigation on sound absorption property of porous concrete with different mixtures”, *Constr. Build. Mater.*, vol. 259, p. 120414, 2020.